Error Corrections

Page	Line	Error	Correction
11	19	exmained	examined
67	15	dioxide	monoxide
115	24	sunction	suction
121	3	distribution	distributions
135	15	assess	assist
137	17	auxillary	auxilary
216	24	restuls	results
231	25	is	was
245	7	basics	bases
251	2	transistor	transistor.The transistor

A STUDY OF NATURAL GAS AND PULVERIZED COAL DIFFUSION FLAMES

by

Mohammed Mahmoud Aly Hassan

THESIS SUBMITTED FOR THE DEGREE
OF DOCTOR OF PHILOSOPHY
IN THE FACULTY OF ENGINEERING
UNIVERSITY OF LONDON
AND
FOR THE DIPLOMA OF MEMBERSHIP
OF IMPERIAL COLLEGE

Fluids Section
Mechanical Engineering Department
Imperial College of Science and Technology
London SW7

1983

TO

my wife MONA

ABSTRACT

The research leading to this thesis had two aims. The first was to obtain data for scalar quantities in well defined turbulent gaseous diffusion flames. Data of this kind are relatively few. They are needed to enhance the physical understanding of turbulence and for the development of improved combustion models for engineering prediction procedures. The second objective was to develop and obtain data from a research cylindrical pulverized coal-fired furnace of a size large enough to be representative of industrial practice. Combustion data for pulverized coal are needed to develop and verify the mathematical models currently used in prediction procedures and to provide new information of immediate practical value which could result in improving coal utilization.

Measurements of the mean species concentration and of mean and fluctuating axial velocities have been performed in vertical turbulent round free jet natural gas diffusion flames burning in stagnant air. The data was obtained with the aid of a quartz microprobe for the concentration measurements and a laser-Doppler anemometer for the velocity measurements. Both lifted and burner stabilized flames have been studied. Data have been obtained for several Reynolds numbers and for varying the amount of nitrogen added to the fuel gas.

A new cylindrical, axisymmetrical, vertical furnace composed of water-cooled and refractory segments has been constructed and commissioned. The furnace is 0.6 m in diameter and is axially fired from its top end with a variable swirl double concentric burner. The exhaust gases exit via an axial port at its bottom

end so that axial symmetry of the flow is preserved throughout the combustor. Special care was given to ensure safe ignition and operation of the experimental arrangement.

To assist the validation of the combustor prediction methods and as a part of the run up to coal firing, measurements were made in the new furnace for natural gas firing situation. Results have been obtained for two excess air levels and two swirl numbers. Very fine wire thermocouples have been deployed to map gas temperatures. For species concentration, comparative measurements have been made using a quartz microprobe, a water-cooled probe and a direct water-quench probe. Incident radiation fluxes to the walls were measured with an ellipsoidal radiometer.

Particular attention has been paid to the coal feed system. The coal feed rate is held within close tolerances around a set feed rate by a microprocessor feedback control system, relying on the "loss-in-weight" principle. United Kingdom bituminous pulverized coal was studied and characterized. Measurements have been obtained for local gas composition, flame temperature and local char burnout in a pulverized coal diffusion flame. These measurements were again performed, in the furnace, using a fine wire thermocouple probe coupled with an automatic data logging system for in-flame temperature measurements and a water-cooled shower probe for gas concentration and char sample collection.

ACKNOWLEDGEMENTS

It gives me great pleasure to express gratitude to all those who provided me with assistance and guidance during my study.

First and foremost, I wish to acknowledge with gratitude the guidance, suggestions and encouragement provided by my supervisor, Dr. F.C. Lockwood, whose help greatly aided the progress and completion of this work.

Dr. H.A. Moneib and Dr. Y. El-banhawy gave generously of their time and knowledge. I gratefully acknowledge their contribution to this work.

The support of the Fluids Section technical staff was vital to the research programme. Thanks are due to Messrs. W. Crew, P. Trowell, M. Tennison, P. Woodward, J. Laker, M. Roper, T. Thomas and A. Solomon. The precision and quality of their work is appreciated.

My thanks to Cathy Maxwell who had the patience to go through every typing detail with great skill.

I wish to acknowledge the UK Science and Engineering Research Council for their financial support of this work under grant GR/A/8737.1.

Many thanks are due to all my colleagues for sharing college life. My thanks are due to, in particular, Dr. A. Abbas, Dr. A. Attya, Mr. G. Sauba, Mr. K. Hirji, Mr. A. Ahmed, Mr. K. Beshay and Mr. P. Stolakis.

Finally, my appreciation and deepest gratitude are extended to my wife, Mona and my fine son, Asem for their patience, support and ever-enhancing love which accompanied me throughout this effort.

CONTENTS

		Page
ABSTRACT		i
ACKNOWLEDGEMENTS		iii
CONTENTS		iv
NOMENCLATURE		vii
CHAPTER 1	INTRODUCTION	1
1.1	Background	1
1.2	A Brief History of the Previous Laboratory Gaseous and Pulverized Coal Turbulent Diffusion Flame Experiments	3
	1.2.1 Free Jet Gaseous Diffusion Flames	3
	1.2.2 Confined Gaseous Diffusion Flames	6
	1.2.3 Coal Firing Experiments	10
1.3	Objectives and Scope of the Present Work	14
1.4	Outline of the Thesis	17
CHAPTER 2	MEASUREMENTS IN FREE-JET TURBULENT DIFFUSION FLAMES	19
2.1	Introduction	19
2.2	Experimental Details	21
	2.2.1 Flow Arrangement	21
	2.2.2 The Burner	24
2.3	Characterization of the Flames Studied	24
2.4	Measuring Techniques	27
	2.4.1 Velocity Measurement	27
	2.4.2 Concentration Measurement	32
2.5	Presentation and Discussion of the Experimental Results	42
	2.5.1 Concentration Measurements	49
	2.5.2 Velocity Measurements	81

		Page
CHAPTER 3	MEASUREMENTS IN A GAS-FIRED CYLINDRICAL FURNACE	88
3.1	Introduction	88
3.2	Experimental Arrangement	89
	3.2.1 The Furnace	89
	3.2.2 The Burner	99
	3.2.3 Controlled Ignition and Safety Precautions	108
3.4	Measuring Instrumentation	115
	3.4.1 Mean Temperature Measurement	115
	3.4.2 Radiation Flux Measurement	123
	3.4.3 Concentration Measurement	128
3.5	Presentation and Discussion of the Experimental Results	137
	3.5.1 Probe Type	140
	3.5.2 Incident Radiation Flux Measurements	143
	3.5.3 Concentration and Temperature Measurements	148
CHAPTER 4	A FURNACE FOR RESEARCH INTO COMBUSTION OF PULVERIZED COAL	160
4.1	Introduction	160
4.2	The Preliminary Experiment and the Analytical Consideration of the Particle Diffusion	162
	4.2.1 The Preliminary Experiment	162
	4.2.2 Turbulent Diffusion of Particles: Fundamental Consideration of Particle/Turbulence Interaction	168
4.3	Extension of the Gas-Fired Furnace for Coal Firing	174
4.4	Microprocessor Control of the Pulverized Coal Feed Rate	190

		Page
4.4.1	The "Loss-In-Weight" Technique	192
4.4.2	Design Features of the Weighing Bridge	195
4.4.3	The Microprocessor Control	201
4.4.4	Computing, Control Theory and Performance	207
CHAPTER 5	MEASUREMENTS IN THE COAL-FIRED FURNACE	215
5.1	Introduction	215
5.2	Coal Characterization	217
5.2.1	Particle Size Distribution	217
5.2.2	Proximate Analysis	219
5.2.3	Ultimate Analysis	222
5.3	Measurements and Instrumentation	226
5.3.1	Concentration Measurement	228
5.3.2	Burnout Measurement	234
5.3.3	Flame Temperature Measurement	237
5.3.4	An Automatic Data Logging System	242
5.4	Representation of the Experimental Results	251
CHAPTER 6	SUMMARY AND CONCLUSIONS	265
6.1	Summary	265
6.2	Conclusions	268
6.2.1	Experimental Results in Free Jet Diffusion Flames	268
6.2.2	Experimental Results in Gas-Fired Cylindrical Furnace	270
6.2.3	Coal Firing Experiment	272
6.3	Recommendations for Future Work	274
REFERENCES		276
APPENDIX I		299

NOMENCLATURE

A	area, surface area
C	volume concentration
C_d	drag coefficient
C_i	mass concentration of species i
C_p	specific heat under constant pressure
CV	calorific value of fuel
d, d_o	diameter, exit diameter of jet
d_s	jet source diameter = $d(\rho_o/\rho_\infty)^{1/2}$
D	internal diameter of combustor
E	error in coal feed rate
f_{st}	stoichiometric fuel/air ratio
F	force
Fr	Froude number
g	gravitational acceleration
G	axial flux of momentum
$\dot{G}_o$	input momentum flux
G_k	turbulence kinetic energy source term
h	convection heat transfer coefficient
H	enthalpy
k	kinetic energy of turbulence, thermal conductivity
K	gain factor
L	thermocouple fine wire length, visible flame length
L_T	thermal length of vertical flame (measured from the burner port to the point of maximum mean temperature on the flame axis)

L_l	lifted distance (measured from the burner port to the mean location of the stabilizing base of lifted flame)
m	mass
$\dot{m}$	mass flow rate
$\dot{m}_o$	input mass flow rate through the jet port
M_l	mean molecular weight of combustion products of a stoichiometric air/fuel mixture at the adiabatic combustion temperature
M_∞	molecular weight of ambient gas (air)
Nu	Nusselt number
p	pressure
p'	pressure-correction
Pr	Prandtl number
$\dot{q}$	volume flow rate
Q	heat transfer rate
r	radius, radial distance measured from the jet axis
R	radius, radial distance measured from the combustor axis
Re	Reynolds number
Re_L	flame tip Reynolds number
Ri_L	overall flame zone Richardson number
S	swirl number
t	time
T	instantaneous value of temperature
T_l	adiabatic combustion temperaure of a stoichiometric air/fuel mixture
T_∞	surrounding gas(air) temperature
u	axial velocity component
U_g	gas flow velocity

U_o axial component of mean velocity at jet exit port

U_s suction velocity

v radial velocity component

V velocity

w weight of coal in feed hopper

$\dot{w}$ desired coal feed rate

w_o initial weight of coal in feed hopper

W_1 mass fraction of source stream material in a stoichiometric mixture with the ambient gas (normally air)

x distance, axial distance from jet axis

X axial distance from furnace quarl exit

Greek Symbols

Γ exchange or transport coefficient

ε dissipation rate of turbulence kinetic energy, emissivity

μ viscosity

γ measured angle of adjustment of swirl block generator (angle between radial and tangential stream lines)

ρ density

ρ_∞ surrounding gas density

σ Stefan-Boltzman constant = 4.93×10^{-8} Kcal/hr m^2 $^oK^4$

ω weight fraction

ψ burnout (weight fraction), the ratio τ_d/λ

β $= (M_\infty T_1 / M_1 T_\infty)^{1/2}$

ν kinematic viscosity

α volume fraction

τ_d particle dynamic relaxation time

λ the integral time scale of turbulence

ξ_L $= (\pi g \rho_\infty / 4\dot{G}_o)^{1/3} L$

Subscripts

a ambient

av average

bf burnt fuel

CO carbon monoxide

cond conduction

conv vonection

e,o burner exit

eff effective

g gas

H2 hydrogen

i species

j thermocouple junction

k coal

i,j,k components in Cartesian tensor notation

m maximum, sample analysis point

p particle, primary

rad radiation

s stored

t thermocouple, probe tip

th theoretical (calculated)

w wall

x axial, char sample

α ash

ϕ angular

Superscripts

$\bar{}$	time averaged
$'$	fluctuating component
$\vec{}$	vector

CHAPTER 1

INTRODUCTION

1.1 Background

With the development of the world oil crisis there has been an ever increasing demand for alternative energy sources which are cheap, plentiful and free from harmful side effects. There have been a number of responses to this demand with the result of detailed studies being undertaken in the fields of atomic, solar, wind and wave energy sources. However, one of the most promising alternatives is that of coal. Coal resources are projected to last well into the future and this coupled with the dramatic rises in the prices of gas and oil in recent years, has resulted in coal experiencing a considerable revival of interest.

Basic or fundamental research in pulverized coal combustion processes has only received significant emphasis during the last few years. The trial and error methods, prevailed prior to that time and used in most of the design work, did not provide a basic understanding of the principles, mechanisms, and processes involved. Trial and error approaches were used simply because of the extremely complex nature of the processes associated with coal combustion. A basic and better understanding of such processes is nevertheless important.

Therefore the primary objective of the present effort was to design and develop a coal combustion facility which could generate controlled coal combustion data in practical circumstances. Such data would enhance furnace performance understanding and further establish the data base for prediction procedures validation.

Chemically reacting turbulent flows occur over a wide range of engineering practice. Fuel and air issue into the combustion chambers of most large industrial furnaces in a round jet and in a mainly unpremixed state. The scale of these furnaces is normally large enough for the jet flow to be fully turbulent and for the chemical kinetics to exert no significant influence on the overall rate of combination of fuel and oxidant molecules. Important examples of such turbulent diffusion flames can be found in the steel and other metal producing industries, the glass-making industry, oil refineries and a wide variety of chemical process plants and central electricity generating plants.

Computer prediction procedures capable in principle of handling practically interesting combustion flows now exist, see for example, Patankar and Spalding (1973) and Gosman and Lockwood (1973). It is necessary to incorporate in these procedures realistic models of the complex physical and chemical processes, which characterize such flows, in order to obtain accurate predictions. These predictions, which perform well when tested against data procured in laboratory conditions on simple, gaseous-fired, round jet, free or confined, turbulent diffusion flames, can be of immediate and considerable value to furnace designers. Particulate matter in the form of soot or pulverized coal particles is of significance in many furnaces, and modelling for this further complication can be introduced once a predictive method for largely soot free gaseous diffusion flame is established. Local data for velocity, temperature and species concentration are therefore required to facilitate the prescription of realistic models as well as for the validation of the existing predictive methods.

Therefore the secondary objective of the present effort was to provide a considerable number of data for natural gas turbulent diffusion flames, free and enclosed, mainly to assist the prediction procedures. Firstly, axisymmetric free jet diffusion flames have been studied. Secondly, as a logical step in the procedure to develop the coal combustion experiment, data have been collected for axisymmetric confined diffusion flames.

1.2 A Brief History of the Previous Laboratory Gaseous and Pulverized Coal Turbulent Diffusion Flame Experiments

This section reviews relevant literature and is included to provide the background necessary for formulating and assessing the aims and purposes of the present contribution.

In subsection (1.2.1), the previous work on free jet diffusion flames is considered, followed by that in confined flames in subsection (1.2.2). The present section then ends by considering the experiment carried out on pulverized coal flames in subsection (1.2.3).

1.2.1 Free Jet Gaseous Diffusion Flames

Becker and Brown (1969) and Günther and Simon (1969) described measurements of turbulence intensity in diffusion flames. Velocity fluctuation measurements were reported in propane-air flame using simple probes and in town gas-air flames using an

optical method. They compared their results with those of isothermal jets.

Measurements of mean and fluctuating temperature and of ion concentration in methane diffusion flames were reported by Lockwood and Odidi (1975). Quantitative information about the intermittent nature of turbulent combustion was provided by the data.

Ebrahimi and Kleine (1977) used a light scattering technique to measure the nozzle fluid concentration field in isothermal free jets, and stabilized as well as lifted natural gas diffusion flames.

Becker and Liang (1978) and Becker and Yamazaki (1978) studied visible flame length, jet spread rate, mass entrainment rate and momentum growth rate in vertical free diffusion flames and general correlations were given for predicting these quantities.

Kennedy and Kent (1979) measured the statistics of mixture fraction in a hydrogen jet diffusion flame using a light scattering technique. Measurements were made for flames at two nozzle velocities and two diameters and the results were presented as conventional and Favre quantities.

Mean velocity and turbulence were measured by Eickhoff and Schodl (1980) in hydrogen-air and propane-air free jet flames under different input conditions. The optically measured values were compared with pitot-tube and hot wire data. Wittmer and Günther (1980) and Lenz and Günther (1980) studied velocity and temperature fields in free jet diffusion flames burning natural gas. With a laser-Doppler anemometry, the mean and fluctuating velocities were measured. The local mean and fluctuating

temperatures were measured using a thermocouple whose frequency response was determined and compensated at each point. Fluctuating temperature measurements were also reported by Ballantyne and Moss (1977).

Roberts and Moss (1981) and Dibble and Hollenbach (1981) reported temperature measurements in diffusion flames. The former used fine wire thermocouples in methane flame while the latter authors used a mixture of hydrogen and methane as fuel and laser Rayleigh scattering thermometry as the measuring technique. Günther and Wittmer (1981) reported a detailed study of the time mean and fluctuating properties and of some correlations in a concentric methane-air diffusion flame with a slight oxygen stabilization. Ventura et al (1981) used ionization probes to measure mean ionization current and frequency spectra in propane-air jet flames with variation in the initial Reynolds number and equivalence ratios. Rawe and Kremer (1981) studied flame stabilization in natural gas flames using various degrees of swirl. Blow-off data and measurements of temperature, concentration, velocity and flow direction under flame and non-flame conditions were reported.

Jeng et al (1982) reported measurements of the structure of methane diffusion flames, with significantly buoyancy effects. These included characterization of initial conditions and total radiative heat losses. Ventura et al (1982) provided ionization and concentration measurements in the transition region of stabilized propane-air flames. Schoenung and Hanson (1982) made local measurements of carbon monoxide mole fraction in a CO diffusion flame and a cold jet using two types of optical probes combined with laser spectroscopy. You and Faeth (1982)

described measurements in natural gas flames. Measurements included profiles of velocity, temperature, and concentration for two flames having different heat release rates. Flame shape and the variation of flame radiation along the axis were also measured. Godoy (1982) reported mean concentration measurements in propane-air diffusion flames. Three different high Reynolds number flames were studied. Measurements of the fluctuating temperature were reported by Lockwood and Moneib (1982) for a range of burner stabilized, lifted and nitrogen diluted methane diffusion flames. The measurements were performed with fine wire thermocouples, its time constant being determined by a pulsing technique.

One can conclude that the previously reported results for free natural gas diffusion flames are remarkably few. The data has been confined to somewhat restricted flame conditions and are not extensive enough to allow the exploration of the effect of Reynolds number and fuel type on concentration and velocity fields in both stabilized and lifted flames. Non of those previous investigators has reported a complete set of temperature, velocity and concentration data for a wide range of natural gas diffusion flames. Moneib (1980) partly fulfilled that gap but he reported only results for temperature field.

1.2.2 Confined Gaseous Diffusion Flames

Hubbard (1957) investigated the effects of preheating combustion air on flame properties in a furnace burning coke oven gas. Probe measurements were made for radiation, flame temperature,

gas composition, velocity and carbon concentration. Becker et al (1963, 1967) studied furnace mixing patterns for cold, co-flowing streams in a cylindrical duct with emphasis on the regime where recirculation occurs. The performance of natural gas flames and oil flames was compared by Wu (1969) in a cylindrical water-cooled furnace under identical aerodynamic flow conditions. The effect of swirl on the emissivity, temperature, concentration and heat fluxes was considered.

Beltagui and MacCallum (1973) described the application of vane generated swirl to premixed town gas-air flames in a furnace. Results were compared with corresponding free flames and isothermal jets. Lockwood et al (1974) investigated turbulent mixing in a cylindrical furnace axially fired with a gaseous fuel (town gas) from a concentric tube burner. Measurements of mixture fraction were obtained for four fuel/air ratios,two burner geometries, two Reynolds numbers, and four swirl numbers imparted to the incoming air stream.

Kent and Bilger (1973a) provided gas species concentration and temperature measurements for diffusion flame of a jet of hydrogen in a co-flowing stream of air. That work was extended by Bilger and Beck (1975) to investigate nitric oxide formation in that flame. Also, the effect of the probe size and construction on sample accuracy was considered. Experiments were also conducted for a vertical jet hydrogen diffusion flame into still air.

Cernasky and Sawyer(1975) studied nitric oxide in diffusion flames of propane in a co-flowing swirled stream of air. A similar investigation was carried out by Takagi et al (1975) in hydrogen and propane jet in air. Gupta et al (1975) discussed the mechanism

of noise generation in swirl stabilized natural gas flames, varying flow rate, air-fuel ratio and for different modes of fuel injection. Baker et al (1975) reported mean velocities and normal stresses in the flow within a small-scale furnace. The measurements were obtained in isothermal air flow and in a combusting mixture of air and natural gas, effect of swirl was investigated. Elgobashi and Pun (1975) reported a study of diffusion flames in a small axisymmetrical cylindrical furnace using town gas. Results of the probability of reaction made by an ionization probe were reported.

Leuckel and Fricker (1976) investigated the characteristics of swirl-stabilized natural gas flames. Flow patterns and flame types were related to burner geometry, swirl intensity and gas/air velocities. Wu and Fricker (1976) studied the influence of the furnace shape and dimensions on swirling natural gas flames. The study included the effects on flame shape, flow pattern, stability and heat flux distribution. Fricker and Leuckel (1976) investigated the effects of swirl and burner mouth geometry on the stability of industrial-scale natural gas flames. Khalil (1976) reported measurements of velocities and the rms of the corresponding fluctuations, of mean temperature $\bar{T}$ and wall heat flux in a natural gas-fired model furnace for a range of burner arrangements and initial flow conditions. The results were compared with those of an isothermal furnace.

Onuma and Ogasawara (1977) and Glass and Bilger (1978) provided data for combustion of two co-axial jet diffusion flames of hydrogen and propane in air. The experimental study included flame shape, temperature, co-existence of reactants, velocity, turbulence and shear stress.

Starner and Bilger (1981) made simultaneous measurements of scattered light intensity and velocity in a hydrogen flame in a co-flowing stream with accelerating and decelerating pressure gradients. The nitric oxide production in flames of H_2, CH_4, C_3H_8, natural gas and a CO/H_2 mixture in a co-flowing stream of air was measured by Peters and Donnerhack (1981). Instantaneous temperature and major concentrations were measured simultaneously by Drake et al (1981) using pulsed Raman spectroscopy in hydrogen-air diffusion flames of low turbulence produced in a combustion tunnel. Mixture fraction and concentration measurements in natural gas diffusion flames were reported by Lewis and Smoot (1981). The experiments were performed in a combustor with co-axial feed of fuel and air. The test variables included type and arrangement of sample probe, combustor wall temperature and air feed temperature. Claypole and Syred (1981) studied the effect of the levels of swirl on the aerodynamic and No_x emission. Measurements were taken in a combustor burning natural gas and for a variable swirl level.

Axial and radial mass fluxes were measured by Driscoll et al (1982) throughout a high Reynolds number flame burning mixture of argon and hydrogen in a co-axial stream of air. Lenze(1982) investigated the influence of recirculation and excess air on enclosed diffusion flames. The experiments were performed in a vertical model of a furnace with single jet and concentric jet, natural gas flames.

As a conclusion, it can be said that the effect of excess air and combustion air swirl on natural gas diffusion flames in vertical axisymmetrical furnaces had received little

emphasis by the previous investigators. Most of the existing previous work was performed either in small scale furnaces or in a co-flowing flow configurations. Temperature, concentration fields and heat flux measurements were not extensively reported for large size furnaces which use industrial type of burners. In respect of the measuring instrumentation used in large size furnaces, the suction pyrometer dominated the temperature measurements while comparative concentration measurements using different types of small size sampling probes have received very little attention.

1.2.3 Coal Firing Experiments

Recent interest in pulverized coal research is evidenced by the significant extent of investigative work and effort now being conducted in this area. Theoretical and experimental studies are being made of several different aspects of the pulverized coal combustion process. Some of the critical areas of interest are: (1) pyrolysis of the coal particles, (2) combustion of the volatiles products, (3) char oxidation and reaction, (4) pollutant formation, and (5) computer modelling of these processes. All of these areas can and in some cases are being studied in relation to certain flow characteristics such as recirculation and relative to such parameter variations as particle size, operating temperature and coal type, etc. Since the primary thrust on this research is experimental and not theoretical, experimental work is only reviewed and it is concentrated on the related work pertinent and of immediate interest to the present work.

The first significant investigation dealing with mixing and combustion of pulverized coal was conducted by Hubbard (1960). He described a performance trial on a pulverized coal flame in which the effect of primary and secondary air, coal fineness and thermal load were studied. The furnace used in that work was described by Mayer (1957). Several additional articles relating to Hubbard's study which provide further information on operating conditions, test variables and results of coal/air combustion tests, include Tissandier (1960), Thurlow (1960), Alpern et al (1960) and Loison and Kissel (1962). Beér et al (1962) studied the mixing in a cold model and in a tunnel furnace burning pulverized coal and coke oven gas. With the aid of tracer technique, measurements of gas concentrations and velocity distributions were determined for the primary, the secondary and the recirculating fluids.

Sunavala (1968 and 1973) compared theoretical prediction and experimental results on mixing and combustion in non-swirling, swirling and impinging jet pulverized coal flames. Ramsden (1968) described a probe and a sampling technique for collecting particles from pulverized coal flame. The samples were exmained by an electron microscopy to study the combustion of coal particles and fly ash formation. Baker et al (1969) described a coal-fired furnace arrangement and provided some basic information concerning flame stability, reproducibility and symmetry. Beér and Chigier (1969) studied the application of swirl to primary and secondary air streams, impingement of secondary air jets and the use of a divergent extension to the burner on the stability and combustion intensity of pulverized coal flames.

Bandyopadhyay and Bhaduri (1971) and Leesley and Hedley (1972) studied the effect of particle size distribution on combustion rate of pulverized coal. Abbott et al (1974) conducted a study of particle mixing and combustion efficiency in a ducted, particle laden jets while Hedman and Smoot (1975) gave results of non-reacting, gas-particle dispersion effects in confined, co-axial jets. Their work was continued by Memmott (1977) and Tice (1977) who investigated mixing rates and effects of recirculation in these confined co-axial jets.

Michel and Payne (1980) reported detailed measurements in long pulverized coal flames for the characterization of pollutant formation. The data were obtained in a refractory tunnel furnace with a double concentric parallel flow burner system. Several long coal flames were studied varying air to fuel input velocities and temperatures. Their measurements included the determination of local gas and solid composition and concentration, temperature and radiative and aerodynamic characteristics. Thurgood et al (1980) reported rate measurements in a laboratory scale pulverized coal combustor with the aid of a water quench probe. Mixture fraction, gaseous species, particle flux and coal burnout measurements were provided for varied secondary air velocity and injection angle and initial coal size. Rees (1980) and Rees et al (1981), used the same combustor and investigated the effect of stoichiometric ratio on nitric oxide formation. Harding (1980) extended that investigation to study the effect of swirl, primary velocity and solid loading, coal size and secondary temperature on coal burnout and nitrogen pollutants. Data were reported for pollutants, gas species concentration and char composition.

A 15 kg/hr pulverized coal furnace was used by Floris (1981) to determine combustion efficiency, ignition stability and species concentration profiles of experimental combustors under oxygen-lean and variable excess air conditions for applications to gas turbine/steam turbine combined engines. Ragland et al (1981) studied the burning rate and the characteristic combustion times of a bituminous coal. The measurements were conducted in a jet of heated gas, the variables being the gas temperature, Reynolds number and excess oxygen.

Chen et al (1982) burned several coal types in a 21 kW, refractory-lined tunnel furnace to determine the influence of coal composition on the volatile and char nitrogen during combustion. Flow pattern, mixing and combustion within and near the quarl of a swirled, pulverized-coal burner were studied on a cold air model by Truelove et al (1982). Glass and Wendt (1982) and Wendt et al (1979) used a 2 kg/hr pulverized fuel one-dimensional downflow combustor to study No_x formation mechanism during fuel rich and staged combustion.

In spite of current interest, there are, with notable exceptions (e.g. Michel and Payne (1980)), few combustion data for pulverized coal firing in large furnace chambers which are large enough to represent practical circumstances. Control on the uniformity of the coal feed rate, which is a primary requirement for reliable data, has received very little attention by the previous investigators. Conventional suction pyrometer with its blockage problem and severe flow disturbances is commonly used for temperature data collection in combustors. For particle char burnout, solid samples were normally collected from

reactors, with some exceptions (e.g. Thurgood et al (1980) and Harding (1980)), using a filter located at the sampling probe tip where the lack of rapid quenching is obvious.

1.3 Objectives and Scope of the Present Work

At the beginning of the present research project, measurements were obtained in turbulent axisymmetric free jet diffusion flames. These experiments, representing the first objective of the present research work, were intended to enhance the understanding of turbulent combustion and to provide new data facilitating the prescription of appropriate mathematical models. An axisymmetric, free vertical jet geometry was utilized because it is simple and well defined and simulates, provided the Reynolds number is large enough, most of the phenomena of the engineering flames. The experimental programme was arranged to provide measurements of mean species concentrations, mean and fluctuating velocity components.

A wide range of practical flame types are considered including both stabilized and lifted flames. As part of the stabilized flames investigation, different fuel types have been simulated by adding inert gas (nitrogen) to the combustible gas (natural gas) while keeping the input Reynolds number constant. For both the stabilized and lifted flames cases (excluding the nitrogen diluted cases) the experimental study covers the influence of the jet input Reynolds number on the measured

quantities. The lifted flames can be viewed as partially premixed flames as the developed flames are not attached to the burner port. The progress in addition of nitrogen to the fuel streams simulates fuels of decreasing calorific values.

The major and second objective of this research effort was to construct and develop a research combustor facility capable of studying the physical and chemical processes associated with pulverized coal combustion. A new segmented, cylindrical, axisymmetric, vertical laboratory furnace has been designed, built and commissioned to obtain a well-defined data for the experimental circumstances of coal firing.

The furnace chamber is 0.6 m in diameter, large enough to represent adequately the essential phenomena occurring in full-scale furnaces. The furnace is vertically orientated with the result that the flame is axisymmetrical offering the possibility of economic computer simulation. The burner is an industrial type concentric device with a calibrated variable swirl generator and a quarl. A great deal of concern and priority was given to safety aspects in the layout of the experimental arrangement.

Prior to coal firing, data was collected for natural gas firing. These data were intended to assist the validation of combustion prediction procedures in furnaces. These experiments were also conducted to check the proper operation of the present combustion facility. Also those experiments gave an opportunity to test the measuring techniques and evaluate their performance before using them in coal combustion experiments. The experiments in these confined turbulent diffusion flames cover the effects of excess air level and swirl number and results were obtained for

gas temperatures, comparative concentration measurements and incident radiation flux.

The physical properties of fine pulverized coal are such that considerable technical difficulties are encountered in attempting to control its flow behaviour. Apart from the problem of the local density variations causing fluctuations in the output feed, the main mean bulk density tends to reduce as the level in the feed hopper falls. For these reasons, a microprocessor-based feedback control system, relying on the "loss-in-weight" principle, was designed and incorporated in the coal feeding system. It controlled accurately the mass flow rate of the pulverized coal fed to the combustor. A considerable amount of time and effort was devoted to establishing the measuring techniques which were used in the coal firing experiment. Data was collected for the mean flame temperature, concentrations of CO_2, CO and O_2 and for the char particle burnout. The results covered restricted range of operating conditions and they were for a typical British bituminous coal. The primary value for that data was for the prediction procedure validation. At the same time, it proved the successful commissioning of the coal combustion data producing facility.

1.4 Outline of the Thesis

The remainder of the thesis is contained in five chapters.

Chapter 2 describes the details of the experiments performed in turbulent axisymmetric free-jet diffusion flames. The experimental method is described and includes a detailed description of the measuring instrumentation together with an estimate of errors incurred in the measurements. The results are then presented and discussed with particular reference to the influence of flame type and Reynolds number.

Chapter 3 is concerned with the experiments conducted in a gas-fired cylindrical furnace. This chapter provides the details of the test rig and the experimental arrangement. Measurement techniques are presented together with an assessment of their accuracy. Results are presented and the effects of swirl number and air/fuel ratio are discussed.

Chapter 4 is mainly devoted to the development of the furnace for research into combustion of pulverized coal. It describes the extension of the gas-fired furnace for coal firing. This includes details of the design features of a microprocessor feedback control system for coal feeding together with the auxiliary equipment needed for coal combustion.

Chapter 5 reports the measurements conducted in the coal-fired furnace. It includes the measuring techniques and the uncertainties associated with the measurements.

Chapter 6 presents the concluding remarks of the present work. Its purpose is to summarize the achievements of the thesis and to suggest the direction in which further work may be required.

In addition to the six chapters, the thesis also includes an appendix giving the derivation of the gaseous and particles turbulence kinetic energy equations.

CHAPTER 2

MEASUREMENTS IN FREE-JET TURBULENT DIFFUSION FLAMES

2.1 Introduction

A number of prediction procedures for turbulent combustion now exist. By contrast the number of good and detailed data for well-defined laboratory turbulent hydrocarbon flames are relatively few. This is remarkable since the physical modelling contained by the prediction procedures can only be verified by reference to a sufficient number of reliable and controlled data. So one concludes that the physical models have received insufficient systematic testing. More fundamentally, combustion models can in the first instant only be formulated on a base of sufficient understanding of the physical nature of the turbulent flame which can only be realized with the assistance of an adequate number of data.

Now, while it is easy to lament the lack of measurements, the provision of new and useful data is quite another matter, combustion experiments are notoriously difficult. And because of the number of quantities which one wants to measure are very large, the total experimental task is exceedingly large. It is hoped that the set of measurements reported in this chapter will offer a very small, but useful, contribution to the whole.

The present experiment is confined to the velocity and mean concentration measurements in turbulent axisymmetric free jet diffusion flames. Velocity and mean values of carbon dioxide, carbon monoxide, oxygen and unburnt hydrocarbon have been obtained. These results together with the mean and fluctuating values of the

temperature reported in full, for the same flames, by Moneib (1980) form a more complete picture.

Three flame types were studied: (1) burner stabilized, (2) burner stabilized but with nitrogen dilution of fuel and (3) lifted flames. The experiments carried out in case (2) were aimed at investigating the effect of fuels of lower calorific values on the measured quantities. The lifted flames are partially premixed cases because the entrained air premixes with the fuel gas before combustion takes place. The fuel used was natural gas (94% methane), chosen because it avoids the complication of significant soot formation.

The present chapter describes the details of the experiments performed in those turbulent diffusion flames. In section (2.2) the experimental details of the test rig are provided. These include the experimental set up, a full description of the burner, the measures taken to minimize aerodynamic disturbances of the flames and the properties and composition of fuel gas utilized. In section (2.3) some aerodynamic parameters characterizing free flames are presented. In section (2.4) various measuring techniques are discussed. It contains the description of the concentration sampling system and velocity laser-Doppler anemometer (LDA). The influences of the suction rate, the probe type and probe tip diameter on the concentration values are discussed. The errors associated with the velocity measurements are quantified. Section (2.5) presents and discusses the experimental results. The flames studied are tabulated in terms of input conditions, flame geometry and aerodynamic parameters. Measurements of carbon dioxide, carbon monoxide, oxygen

and unburnt hydrocarbon (as methane) are presented and discussed for all the flames studied, while velocity results are reported for a sample of them.

2.2 Experimental Details

2.2.1 Flow Arrangement

In the experiments carried out in turbulent jet diffusion flames, the fuel was British North Sea natural gas having the composition and particulars as shown in Table (2.1). In order to characterize fuels of lower calorific values, in some experiments, nitrogen was premixed with natural gas.

The flow diagram of the experiment is shwon in Fig. (2.1). Because of the low pressure of the natural gas mains, a compressor (Rotary Compressor Ltd., type 163 CWD) was necessary to achieve Reynolds numbers up to 30,000. Flow rates of the gases were controlled by rotameters. A small mixing chamber was used, in nitrogen diluted flame cases, to mix natural gas with nitrogen. The mixing of the gases was enhanced by fine wire meshes placed inside the mixing chamber and the mixture of the two gases was fed to the central tube of the burner. The stabilized flames were retained at the burner by an annular pilot hydrogen flame.

Table (2.1)

Physical properties and chemical composition of North Sea natural gas*

Physical Properties

Density Kg/m^3	0.7283
Molecular weight Kg/Kmol	17.18
Specific heat $MJ/Kmol/^oK$	0.03634
Net calorific value MJ/m^3	35.05

Volumetric Composition

Gas	% Volume
Methane	93.63
Ethane	3.25
Nitrogen	1.78
Propane	0.69
Butane	0.27
Carbon Dioxide	0.13
Pentanes	0.09
Helium	0.05
Hexanes	0.03
Benzene	0.02
Toluene	0.01
Octanes	0.01

*These data have been provided by the Research and Development Division of the British Gas Corporation.

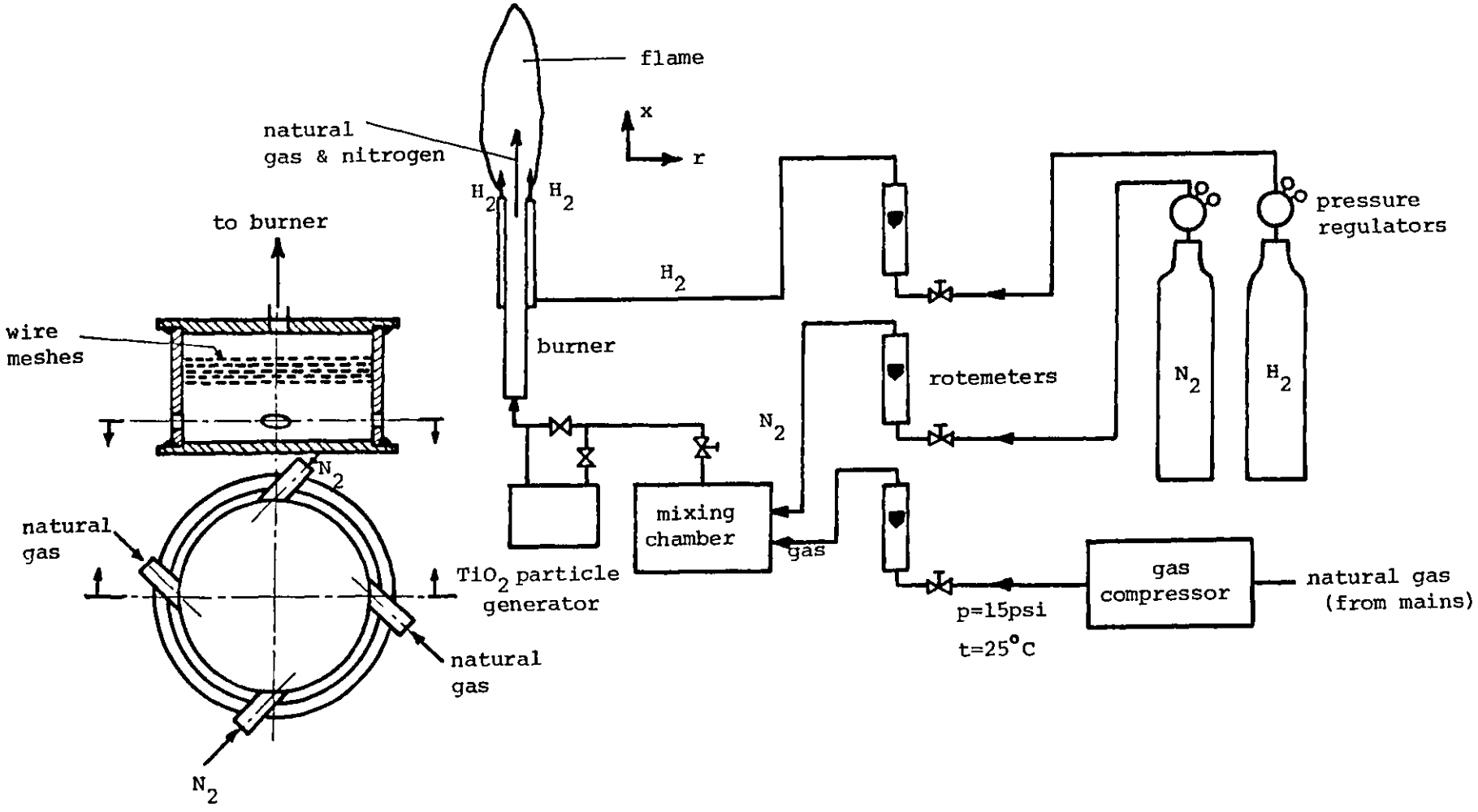

Fig.(2.1) Schematic diagram for free jet flow arrangements

2.2.2 The Burner

The details of the exit section of the burner pipe is shown in Fig. (2.2). The burner was thin walled, vertically aligned, comprised of two concentric tubes of 7.74 and 8.5 mm internal diameters. Collets were arranged along the outer surface of the inner tube to ensure a uniform inflow of the stabilizing gas and to provide a symmetrical pilot flame at the burner exit. The exit wall thickness of the burner was very small, 0.25 mm, to minimize the effect of the wall disturbance on the exit profiles. The length/diameter ratio of the burner pipe was nearly 100 to ensure fully developed velocity profiles. Relative positioning of the central and pilot tubes was possible to achieve maximum stability of the developed flames, see Shet et al (1978). The burner was vertically aligned using three-dimensional movement frame, its design and the alignment procedure are detailed by Moneib (1980). Disturbances in the surroundings were minimized by wire mesh screens contained in an open-topped cloth tent. The combustion products were carried away by the laboratory forced-draught hood positioned symmetrically, about 2 m above the maximum visible flame tip.

2.3 Characterization of the Flames Studied

In order to ensure fully turbulent conditions, the stabilized, nitrogen-diluted and lifted flames studied were operated at burner pipe exit Reynolds numbers, $Re = \frac{\rho_o U_o d_o}{\mu_o}$, in the range 10,000 to 30,000.

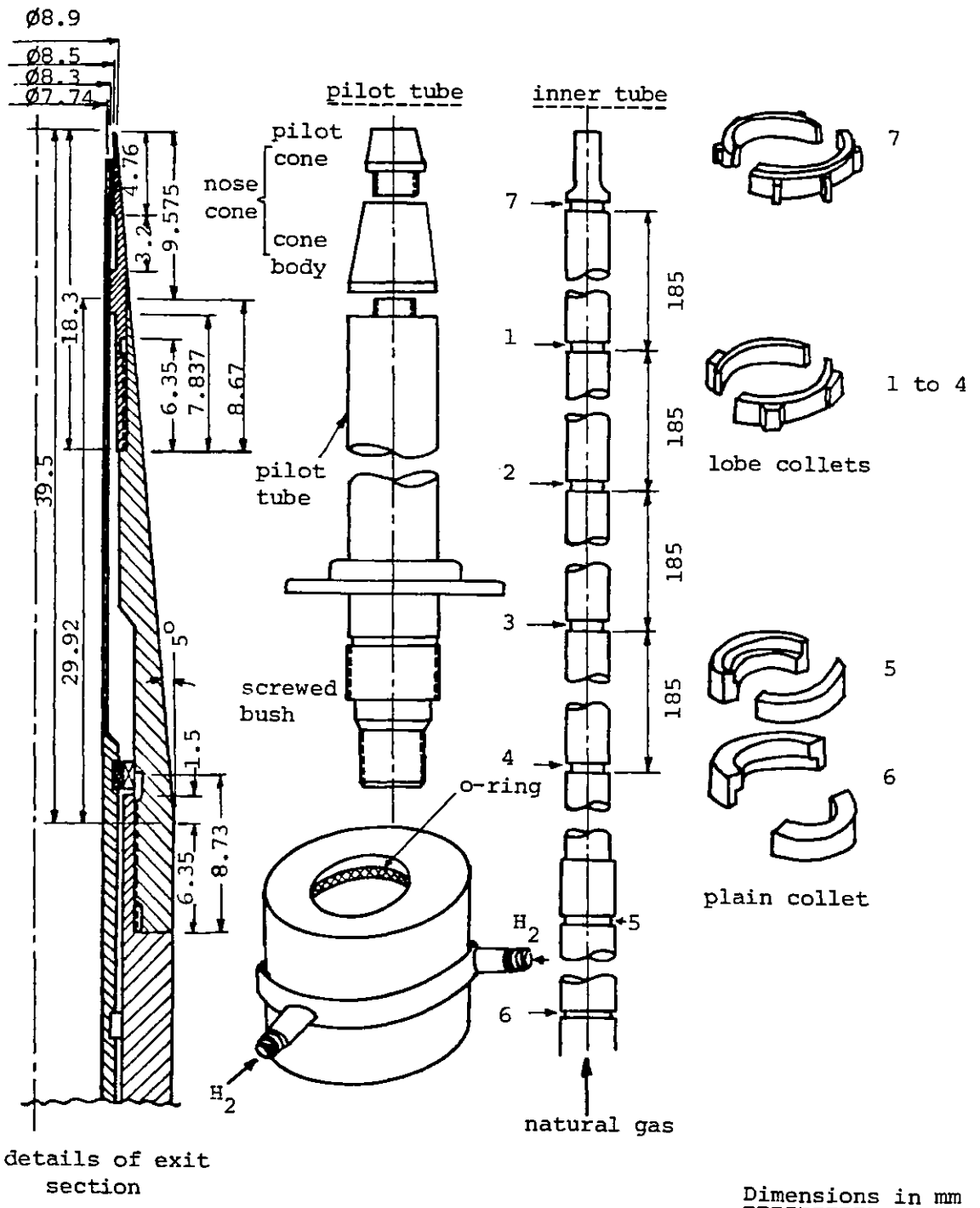

Fig.(2.2) Burner design

These are high values relative to the transitional Reynolds number of about 3200 for a free jet flame, see Gaydon and Wolfhard (1970), and it is, also, to be noted relative to the values of many previous flame experiments, see Chapter (1).

Combustion diminishes the Reynolds number based on local conditions through its direct effect on the density and viscosity and enhances it indirectly through buoyancy. The flame tip Reynolds number, Re_L, proposed by Becker and Liang (1978) and based on approximated conditions of the visually observed flame tip would seem to offer the best guidance for characterizing the overall downstream state of the flow. It is defined as:

$$Re_L = \frac{14\dot{m}_o\beta}{\mu_\infty W_1 L}$$

where μ_∞ is the surrounding gas viscosity (kg/msec), L is the visible flame length (m) and $\dot{m}_o$ is the input mass flow rate (kg/sec). These authors concluded that the visual turbulent character of the flame is established for Re_L value of about 8000. This value is well below those for the present flames, see Tables (2.3), (2.4) and (2.5).

Dynamic similarity is not assured for high Reynolds number as it is for non-reacting jets because the ratio of the buoyancy forces to the jet momentum as characterized by the Richardson number is also important. Becker and Liang (1978), following the work done by Becker and Yamazaki (1978), usefully classified the flames of their survey with reference to a Richardson number, Ri_L, in which the buoyancy is scaled by the visible flame length. It is expressed as:

$$Ri_L = \left(\frac{\pi g \rho_\infty}{4\dot{G}_o}\right) L^3$$

where $\dot{G}_o = \dot{m}_o U_o$ is the input momentum flux with $\dot{m}_o$ being the input mass flow rate. These authors preferred to work with $\xi_L \equiv Ri_L^{1/3}$, a dimensionless representation of the flame length. By reference to the surveyed data, they established that natural convection effects dominate for ξ_L greater than 15, while the forced convection limit is of course achieved as $\xi_L \to o$. Referring to Tables (2.3), (2.4) and (2.5), it is noted that the overall characters of the present flames are influenced by both forced and natural convection effects.

2.4 Meausring Techniques

2.4.1 Velocity Measurement

Mean and fluctuating axial velocities were obtained with a laser-Doppler anemometer (LDA) operating in the fringe mode. Figure (2.3) presents a line diagram of the geometrical arrangement and block diagram of the laser-Doppler instrumentation.

The laser-Doppler anemometer comprised an argon laser (Spectra Physics model 164), operated at wave length 515.5 nm and around 400 mW power. The laser beam passed through a water-filled acousto-optic cell which provided zero and first order beams with frequency difference 21 MHz, see Durão and Whitelaw (1975). The beams were separated to a distance 71.5 mm, made parallel and focussed to their intersection by a 300 mm focal length lens. The forward scattered light was collected with 200 mm focal length lens and

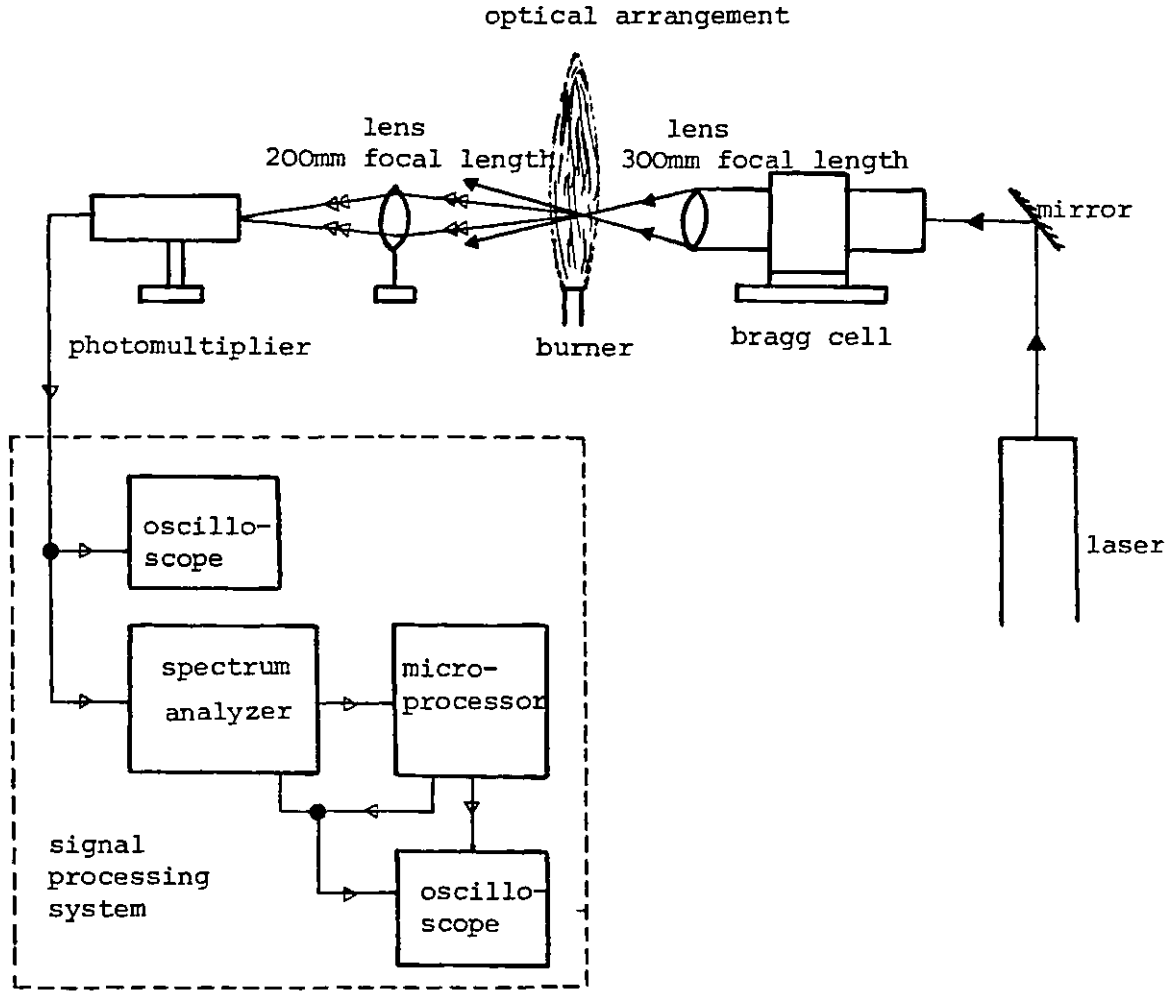

Fig.(2.3) Optical and signal processing arrangements for laser-Doppler anemometry

focussed to a pin-hole in front of a photomultiplier cathode (EMI 9815 B).

All the optical components were secured to an optical bench located on a three-dimensional traversing arrangement having a positioning precision of better than 1 mm. The more important characteristics of the optical arrangement are indicated in Table (2.2).

The signal from the photomultiplier was passed to an oscilloscope (Hewlett Packard 180A/1801A/1821A) and analysed by a spectrum analyzer (Hewlett Packard Model 8553B/8552A/141T) interfaced to an Intersil IM6101 Microprocesser which controlled the frequency analyzer, see Durão (1976) and Durão et al (1973).

The seeding particles were necessary for seeding the flame for laser-Doppler anemometry. It is difficult to ensure an equal seeding rate of the internal nozzle flow and the surrounding air. In the present set of velocity measurements, Titanium dixoide (TiO_2) particles, generated by a mechanically improved version of across flow-particle generator, developed by Asalor and Whitelaw (1974), was used to seed only the nozzle flow. So, for that reason, all the velocity measurements reported in section (2.5) were carried out on the centreline in the initial flame region and up to 130 nozzle diameters downstream. At locations away from the centreline or faraway downstream, it was not possible to measure the velocity correctly due to significantly reduced number of particles and non-uniformity of seeding due to intermittency.

Laser-Doppler anemometers with signal processing based on the averaging of a number of individual frequency measurements may be subjected to errors due: to gradient and particle broadening,

Table (2.2)

Optical characteristics of the laser-Doppler anemometer arrangement

Half angle between the incident beams	6.7 degrees
Transformation relationship without frequency shift	2.23 $msec^{-1}/MHz$
Length of intersection volume at e^{-2} location	0.337 mm
Diameter of part of intersection volume observed by photodetector	0.039 mm
The fringe distance	2.2 μm
Magnification of light collection arrangement	1.5

to the number of signals used to form the average, to the method of averaging, to the photo-detector averaging and to non-zero correlation between number of particles and flow velocity.

The dimensions of the present scattering volume are small and gradient effects can be neglected. The number of signals used to form the averages ranges from 2500 to 73,700 and, in accordance with the calculations of Yanta (1973), implies uncertainties of up to 1.7% in the mean velocity and 2.8% in the rms values at the maximum turbulence intensity recorded. The dispersion of the laser light and movement of the local region, due to the variations in the refractive index with position and time in turbulent reacting flows, reduce the signal quality and the number of signals per unit time resulting in an effective control volume of larger size. These effects were considered by removing the receiving optical components and the two laser beams were projected onto a screen positioned at a long distance from the control volume. Observation of the two beam movements indicated negligible effect of the refractive index variations, probably because of the small dimensions of the flame. Durão et al (1980) indicated that the averaging characteristics of the photomultiplier can lead to a variation of the signal amplitude with velocity and tend to bias the velocity probability density function towards lower velocities. An opposite bias effect can also stem from the greater probability of detecting particles whose velocity exceeds the average fluid velocity, see for example Dimotakis (1976) and MacLaughin and Tiederman (1973). The magnitude of the error in mean velocity due to both biasing effects depends largely, as

indicated by Durão et al (1980), on the signal processing arrangement. If the sampling time of the signal processing equipment is greater than the time scale of the particle arrival rate, the magnitude of the correction to the measured values reduces to a negligible level. The signal processing arrangement used in this work operate with a low sampling rate, therefore bias effects are expected to be very small. The average uncertainties in measured mean and rms velocities are estimated to be of the order of 2% and 5% respectively.

2.4.2 Concentration Measurement

Samples for the measurements of carbon dioxide (CO_2), carbon monoxide (CO), oxygen (O_2) and unburned hydrocarbon (UHC) were withdrawn from different points within the present flames using an uncooled quartz microprobe. The samples were fed continuously to infrared analyzers, Analytic Development Co. types 483 and 336, for CO_2 and CO measurements respectively, a paramagnetic analyzer (Beckman, model E2) for O_2 concentration measurements and a high temperature flame ionization detector (Analysis Automation Ltd., model S23II) for UHC concentrations. All the sampling lines were of Teflon, so the absorption of sample by the wall is minimized; also Teflon is known to have no catalytic activities. The CO, CO_2 and O_2 sampling system is sketched in Fig. (2.4a). The sample was taken by suction, using a Teflon-diaphram suction pump capable of giving a sample flow rate of between 0.5 and 2 litre/min as required

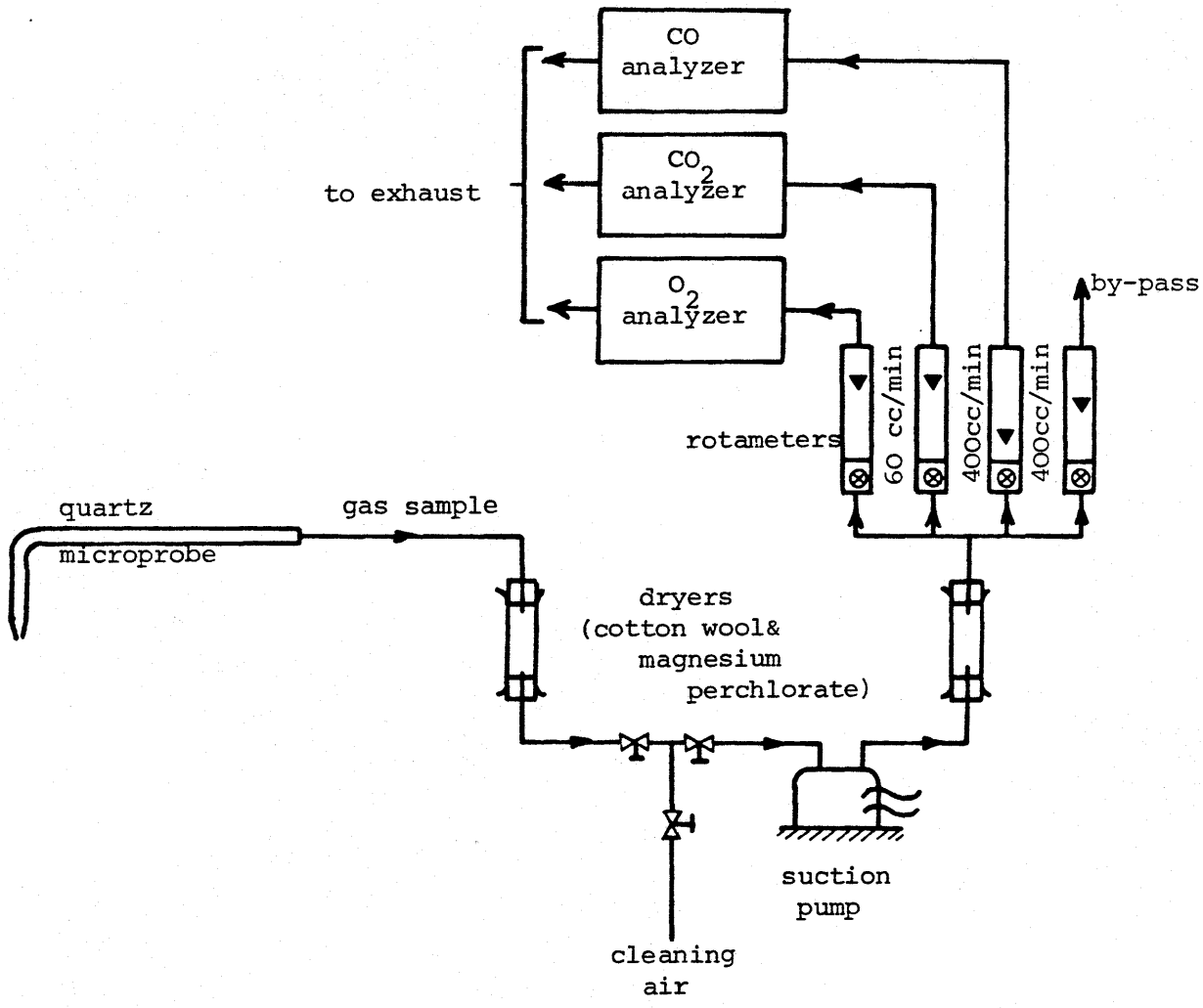

Fig.(2.4a) Sampling System(dry analysis)

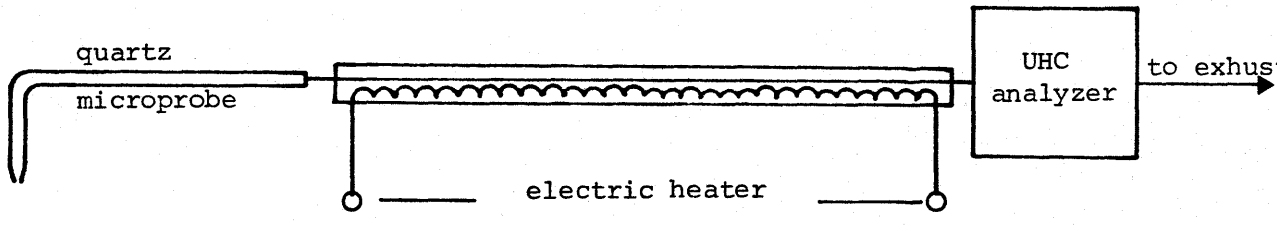

Fig.(2.4b) Sampling System(wet analysis)

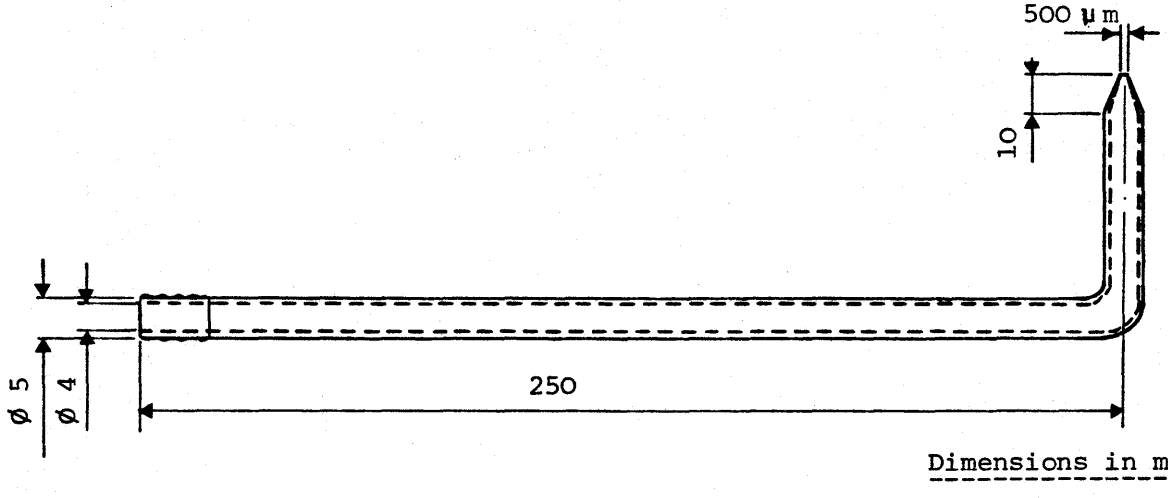

Fig.(2.4c) Quartz Microprobe

by the infrared analyzers. The unburned hydrocarbon vapours and H_2O were condensed and removed chemically from the sample line, using a magnesium perchlorate dryer and cotton wool, before entering the CO, CO_2 and O_2 analyzers. Consequently the reported CO, CO_2 and O_2 concentrations are based on a dry analysis. On the other hand, in Fig. (2.4b) which shows the UHC sampling arrangement, the flame ionization detector has a sampling pump incorporated. The unburned hydrocarbon samples were electrically heated to 150°C before entering the UHC analyser and the UHC results are based on a wet analysis.

Tine (1961) has discussed in some detail three methods that can be used to quench the chemical reaction occuring in samples extracted from a flame. These methods are (1) quenching by diluting the sample with cold suitable fluid as for example in the water-quench probes, (2) quenching the sample by convective heat transfer from the sample to a coolant by using water-cooled probes and (3) quenching by rapid expansion of the sample as in the quartz microprobes. The third method is also known as aerodynamic quenching and it is of a particular interest due to the exceptionally high quenching rates that may be achieved, see Fristrom et al (1957). For the present measurements in turbulent free diffusion flames, an uncooled quartz microprobe relying on sonic expansion was chosen.

The quartz probe, sketched in Fig. (2.4c), was selected because the interference effects caused by the probe body were minimal due to the small size of the probe (probe diameter/flame diameter ≃ 0.008 maximum) compared to the bulkier alternative of

a water-cooled stainless steel probe. The right angle bend minimizes the physical impact of the probe on the combustion processes when it is introduced along the direction of the streamlines. Quartz has the ability to withstand high temperatures and has minimal catalytic effect on the sample gases, as indicated by Fristrom and Westenberg (1965). Since the probe was uncooled the question of it being a heat sink does not arise and the amount of heat transferred to the probe, which its outer walls at nearly the same temperature as that of the flame, was negligible, so it provided minimal thermal disturbances. The probe, Fig. (2.4c), was made of fused quartz and has inside and outside diameters of 4 to 5 mm respectively. To obtain the manufacturers recommended flow rates for the gas analyzers, an orifice of 500 μm was necessary, which, although somewhat large, nonetheless gave an expansion ratio of 64. A similar decision was taken by Schoenung and Hanson (1981).

Typical results illustrating the effect of using quartz microprobes of different orifice sizes (400 μm 500 μm and 1000 μm) on the measured volumetric concentration of O_2, CO_2 and CO across the flames are shown in Fig. (2.5). In the core of the flame ($r < 20$ mm) the spread of the results is typically less than 0.5% volume fraction. This spread approaches an average of 1.0% volume fraction in the intermittent and outer regions. The reason for this difference is difficult to identify because of the multiplicity of influential parameters such as: spatial resolution, suction rate, repeatability, intermittency, segregation, quenching etc. The 500 μm probe was preferred in the present measurements to the 400 μm one because the latter does not quite provide the necessary minimum instrumentation flow rate.

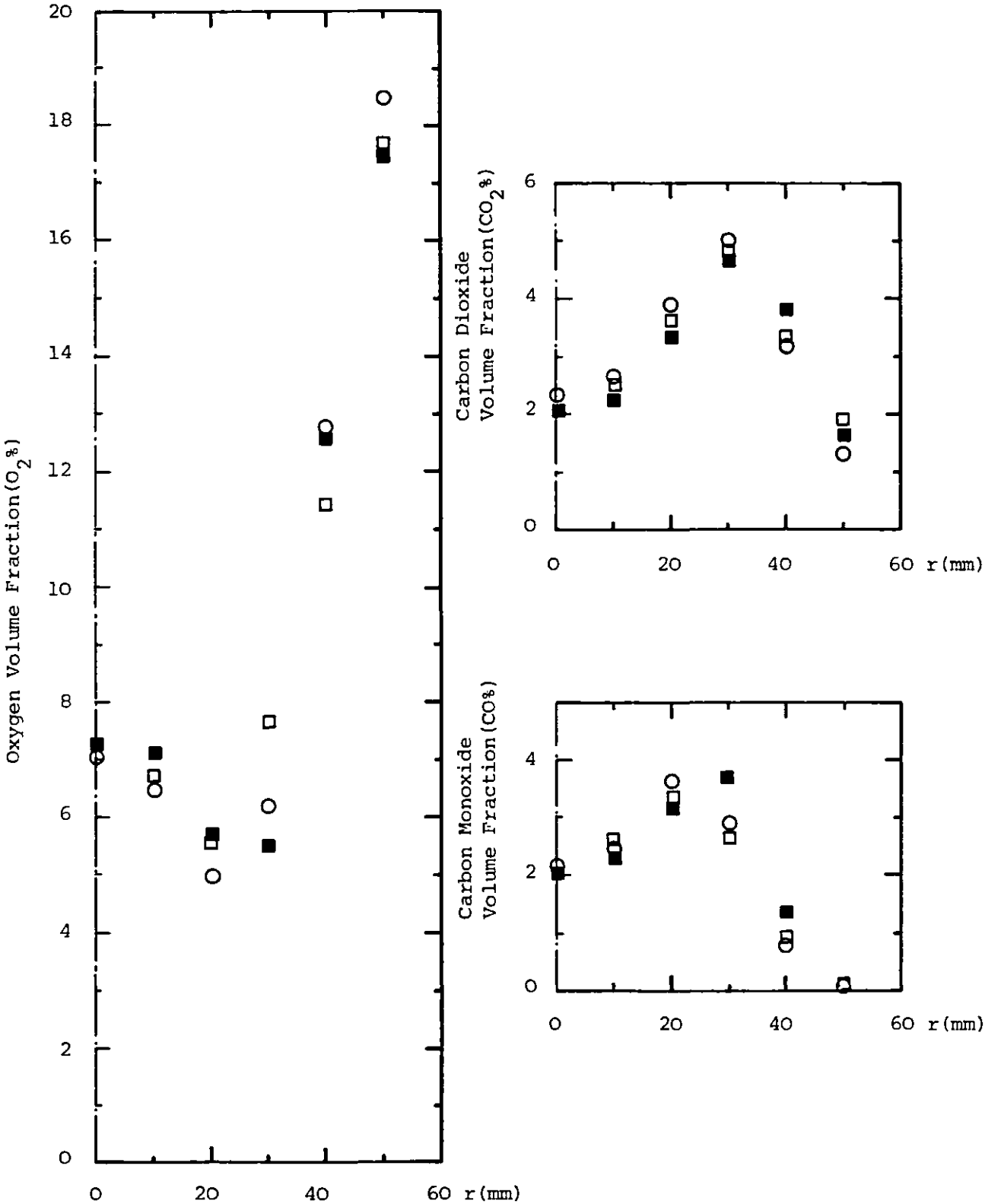

Fig.(2.5) Comparison between three different orifice diameter quartz microprobes.Lifted flame,run LAo,Re=10,000,x/d=39.

■ 400 μm*

○ 500 μm

□ 1000μm

* Regarding the quenching efficiency, the 400 μm is more efficient than the others because of its greater expansion ratio and therefore, the measured concentration values by the 400 μm probe are considered herein as the reference values against which the comparison should be made.

The factors influencing the accuracy of the concentration measurements can be normally grouped into two categories: the first includes those resulting from probe-gas interference and quenching of the chemical reaction within the probe, while the second includes factors associated with the sample handling and analysis. Non-isokinetic sampling and insufficient quenching are the possible sources of significant error for quartz microprobes, all of which are little explored and very difficult to estimate for a turbulent flow. These will be separately considered as follows:

i. Non-isokinetic Sampling

Probe measurements in combusting flows are usually associated with uncertainties in the measured quantities due to expected thermal and aerodynamic interference between the probe and the surrounding gases. The degree of interference also increases with probes which use suction of gases through the probe · Fristrom and Westenberg (1965), Yanagi (1977) and Tine (1961) considered, both experimentally and theoretically the problem of probe effects on the concentration profiles in laminar flames, where the effects are likely to be greatest. Probe effects, for simplified conditions, were mainly related to the probe size, geometry and operating conditions. For example, the distortion of profiles decreased with the probe size and with the application of isokinetic sampling (suction velocity equals gas velocity). In turbulent combustion flows, however, probe-gas interference effects are more difficult to quantify due to the fluctuating nature of the measured quantities and the large variations in flow conditions

from point to point within a turbulent flame. Attempts to use probe with isokinetic sampling in turbulent combustion were described by Kent and Bilger (1973b),Vranos et al (1969) and Bowman (1977) but errors associated with departures from isokinetic conditions were not quantified in detail. As indicated by Tine (1961), it is difficult to guarantee isokinetic sampling in turbulent combustion. Unfortunately, with quartz probes, the orifice velocities necessary to ensure rapid quenching through sonic sampling withdrawal exceed those corresponding to time average isokinetic sampling over much of the flow region. The suction rate from the present probe was progressively decreased,to the ultimate minimum flow rate imposed by analysers at different points in the flame, in order to estimate its effect. Figure (2.6) shows the results of test performed to study the influence of the suction velocity on the measurements. The results correspond to points within the present flames which were selected to coincide with regions of different concentration gradients. In general, the results show a small increase of both CO and CO_2 (less than 0.5%) and also a small decrease in O_2 concentration (around 0.5%) correspond to a variation of the suction velocity from around 30 m/sec to 110 m/sec. This increase is unlikely to have resulted due to the probe sampling from a finite region surrounding the point of measurements. This can be interpreted from the results obtained at points which are surrounded by comparatively lower concentrations. Bearing in mind that deviation from the maximum suction velocity, reduces quenching efficiency and consequently an opposite effect would be expected, it is however,

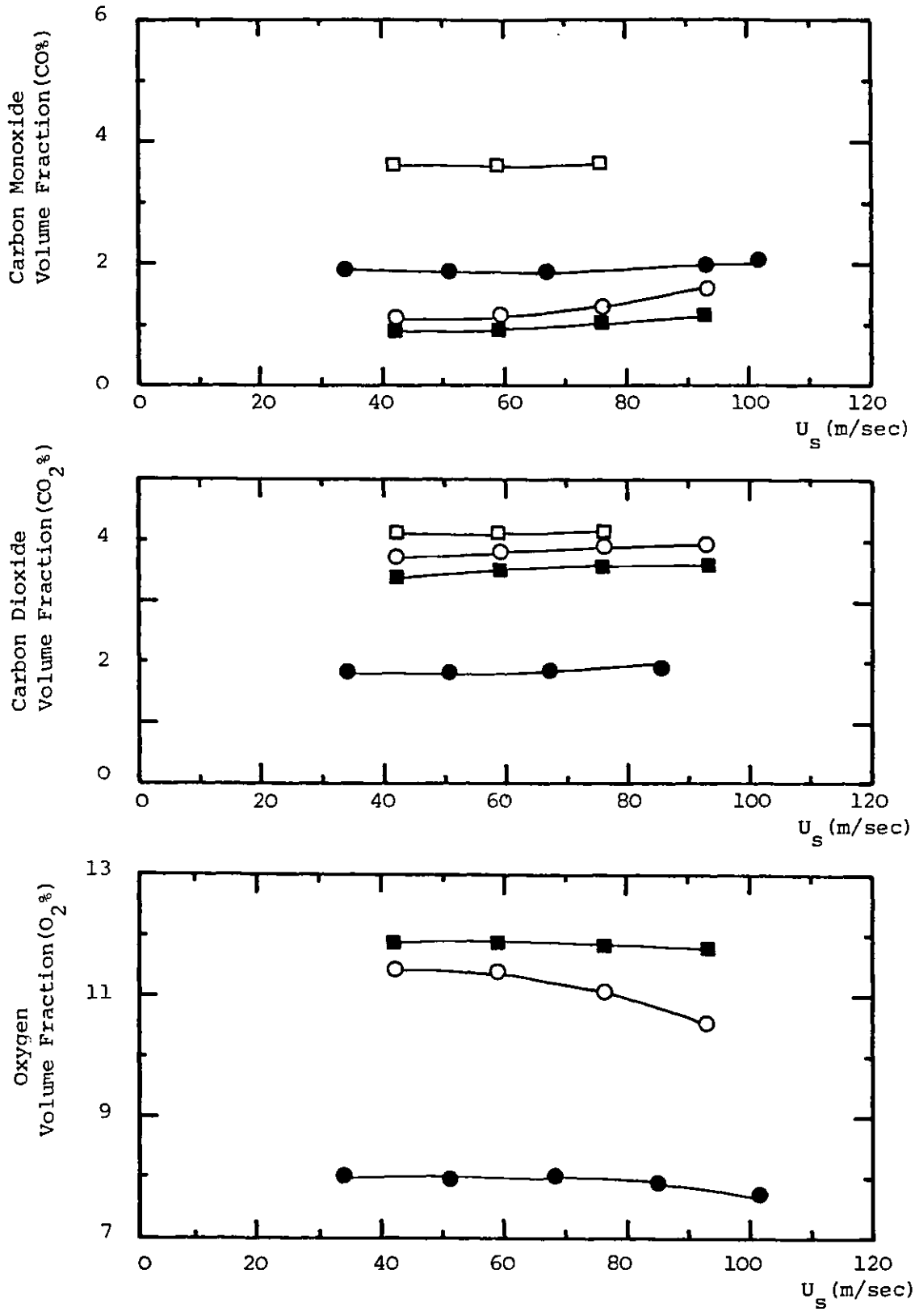

Fig.(2.6) Effect of suction velocity on the volumetric concentration measurements

- ● Stable flame,Run SA1,x/d=39,r=0
- ■ Stable flame,Run SA1,x/d=39,r=35mm
- ○ Lifted flame,Run LAo,x/d=39,r=0
- □ Lifted flame,Run LAo,x/d=39,r=35mm

probable that the increase of CO_2 and CO and decrease of O_2 are either a segregation effect of the type described, for example, by Bilger (1977) or enhancement of chemical reaction at the point of measurement as a result of the higher suction velocities. Bilger (1977) indicated that the suction of gases at velocities different from the local gas velocities introduces the possibility that the probe segregates between gas pockets of low and high density especially at regions where large density fluctuations exist. Higher suction velocities may thus be associated with a bias towards lower density components. As gas pockets of low density (high temperature) are expected to be associated with high concentrations of combustion products, it is, therefore, likely that the observed increase in CO, CO_2 and decrease of O_2 can be related to this effect.

ii. Insufficient rapid quenching

An aerodynamic quench in a gas sampling probe is defined as a rapid reduction in static temperature and static pressure achieved by quickly accelerating the flow to supersonic speed. Supersonic flow is maintained until the stagnation temperature of the sample is reduced to a low value by convective heat transfer, naturally or to a coolant, within the probe such that upon return to subsonic conditions through a shock system, the static temperature and pressure are sufficiently low to minimize chemical reaction. A rapid reduction in static temperature is needed to reduce the rates of initiation and chain branching reactions which in general have medium to high activation energies (> 15 Kcal).

The reduction in static pressure is necessary to enhance the relative importance of recombination of radicals on the walls at the expense of chain propagation reactions. In general, the temperature and pressure below which chemical reactions are unimportant are dependent upon the appropriate homogeneous and heterogeneous chemical kinetics. While the present experiments are relying on aerodynamic quenching to suppress chemical reactions in the gas samples, it is usually very difficult to prove that aerodynamic quenching has been achieved. Fristrom and Westenberg (1965) have argued that, since a supersonic flow may be maintained in a large scale area-ratio nozzles, a supersonic flow may also be maintained in small-scale, large area-ratio passages such as those found in the tip region of microprobes and concluded that a microprobe having a large area ratio tip will produce an aerodynamic quenching of flame gases provided that the pressure ratio across the probe is large enough. Bilger (1977) and Bowman (1977),however, have questioned whether an aerodynamic quench can be achieved using a small-scale probe. Colket et al (1982) raised doubts about the capabilities of microprobes to achieve aerodynamic quenching of flame gases, although they stated that quenching rates in microprobes may be sufficient under many conditions even in the absence of an aerodynamic quench.

For turbulent diffusion flames, where the rate of reaction is controlled by diffusion rather than by kinetics, the problem of quenching is considered relatively unimportant. Bilger (1977) stated that the net result of insufficient quenching will tend to give concentrations at the analyzers corresponding to a position

some 5 to 10 probe orifice diameters downstream of the measuring point which appears to be acceptable in the presence of small spatial concentration gradients in this direction.

In Fig. (2.7) a comparison is shown between the results of 500 μm quartz microprobe and two water-cooled stainless steel probes of 1 mm orifice diameter with different construction, see Toral and Whitelaw (1982) and Attya (1983), a maximum spread of 1% volume fraction in the flame intermittent region is encouraging. Finally, on the basis of the previous discussion, it is estimated that the overall error in the present concentration measurements (including the experimental repeatability shown in Fig. (2.8)) is within ±1% volume fraction.

2.5 Presentation and Discussion of the Experimental Results

The experimental results of the mean species concentration of CO_2, CO, O_2 and unburnt hydrocarbon (as CH_4 equivalent) in turbulent diffusion flames are presented and discussed in the present section. These cover the three flame types under investigation; namely:

i. Stabilized Natural Gas Diffusion Flames

Table (2.3) specifies the runs made for the burner stabilized flames. The Reynolds number was varied between 10,000 and 30,000. A complete set of measurements (i.e. CO_2, CO, O_2 and UHC volume concentrations; mean, rms and turbulence intensity of velocity) was obtained for only one of these runs,

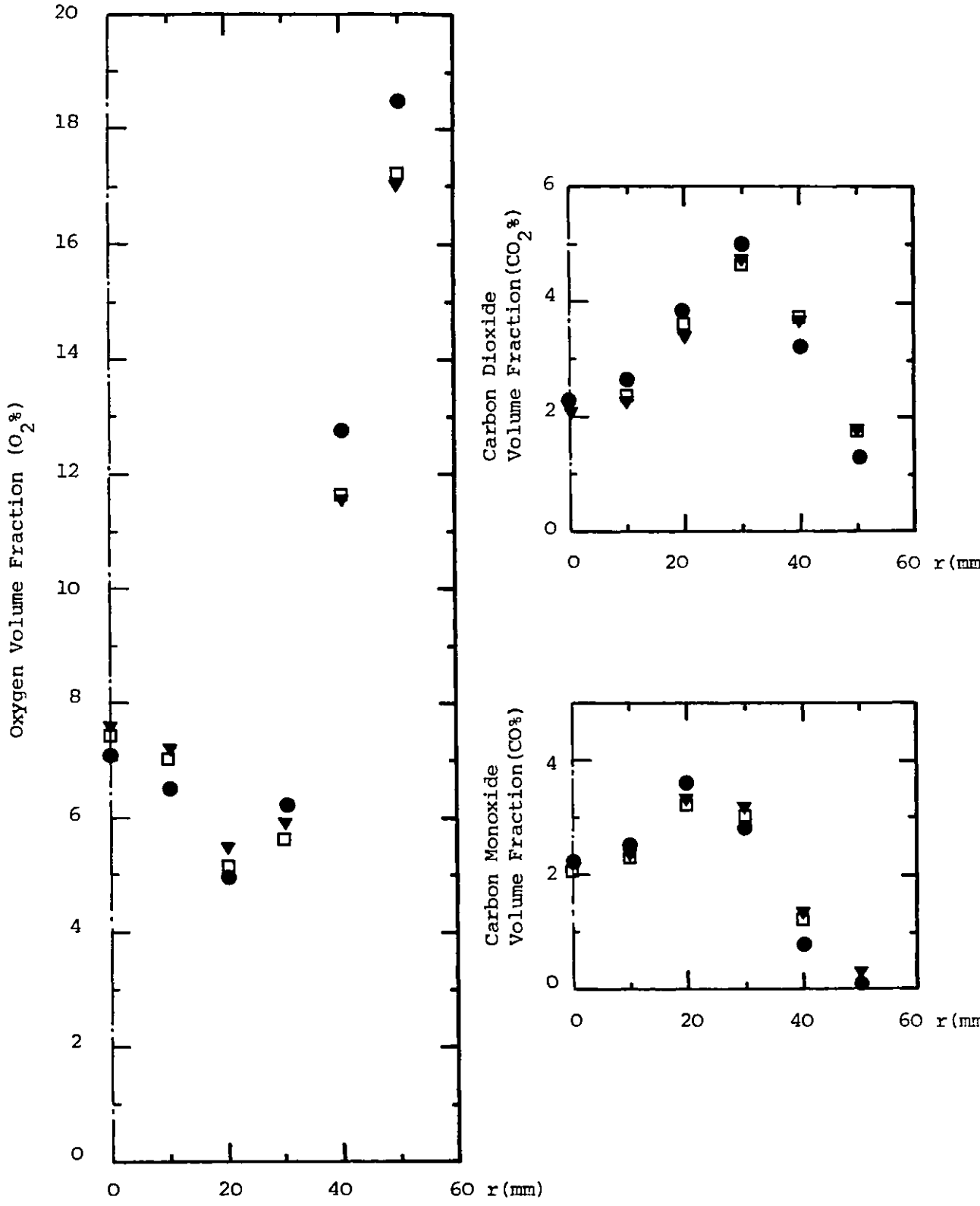

Fig.(2.7) Comparison between 500 μm quartz microprobe and 1 mm tip stianless steel water-cooled probes.Lifted flame,Run LAo, Re=10,000,x/d=39.
● 500 μm quartz microprobe .
O Horizontal 1 mm tip stainless steel water-cooled probe.*
▼ Right angle 1 mm tip stainless steel water-cooled probe.**

* See Attya(1983)
** See Toral and Whitelaw(1982)

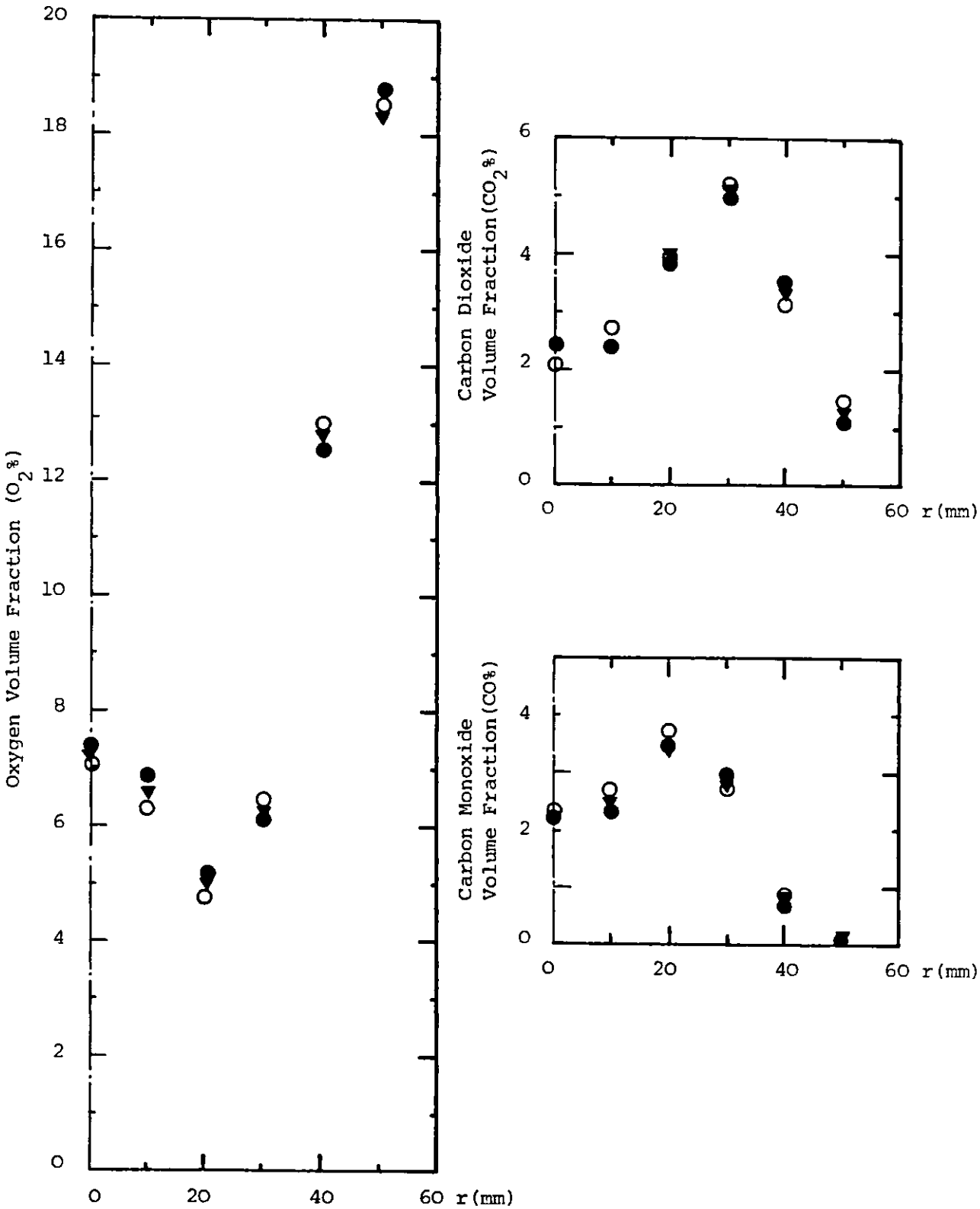

Fig.(2.8) Repeatability of the measured volumetric concentration. Lifted flame,Run LAo,Re=10,000,x/d=39.

● Run 1
○ Run 2
▼ Run 3

run SA2. For this run, the axial distributions for each quantity as well as radial distributions, except for velocity, (at x/d = 36.2, 75, 113.7 and 204) were obtained. For the remaining runs only the axial distributions of CO_2, CO, O_2 and UHC are reported and compared.

ii. Stabilized Natural Gas/Nitrogen Diluted Flames

In this case, nitrogen was mixed with the natural gas while keeping the input Reynolds number at 15,000 to allow comparison with the pure natural gas case, run SA2. Four runs were performed varying the nitrogen concentrations. These appear in Table (2.4) designated as NA1 to NA4. Similar to the previous case (i), a complete set of measurements was obtained for only one of these runs, run NA2, axial distributions as well as radial distributions (at x/d = 36.2 and 75). For the remaining runs, only the axial distributions of CO_2, CO, O_2 and UHC volume concentrations were obtained and are compared.

iii. Lifted Natural Gas Flames

Three flames have been studied. These are designated as runs LA1 to LA3 in Table (2.5). The Reynolds number was varied between 15,000 and 30,000. A complete set of measurements was obtained in only one of these runs, run LA1. The axial distributions at x/d = 18, 36.2, 75 and 152.5) have been obtained in this case. In all three flames the effect of Reynolds number on the axial distributions of CO_2, CO, O_2 and UHC volume concentrations is explored.

Table (2.3)

Stabilized natural gas diffusion flames, (d = 7.74)

Run	Mass flow rate		Burner Velocity U_o (m/sec)	Re	$Fr = \frac{U_o^2}{gd}$	Re_L	L/d	L_T/d	$\xi_L \equiv (\frac{\pi g \rho_\infty}{4\dot{G}_o})^{1/3} L$
	Natural gas (kg/hr)	H_2 (kg/hr)							
SA1	3.283	0.0227	26.6	10,000	9.4×10^3	27.5×10^3	182	94	10.21
SA2	4.924	0.1545	39.9	15,000	21×10^3	35.7×10^3	210	115	8.98
SA3	8.207	0.307	66.5	25,000	58.4×10^3	51.5×10^3	243	140	7.4
SA4	9.848	0.3347	79.8	30,000	84×10^3	56.6×10^3	265	160	7.14

Table (2.4)

Stabilized (natural gas/nitrogen) diluted flames, (d = 7.74)

Run	Mass flow rate			Average density ρ_{av} (kg/m^3)	Burner velocity U_o (m/sec)	Re	$Fr = \frac{U_o^2}{gd}$	Re_L	L/d	L_T/d	$\xi_L \equiv (\frac{\pi g \rho_\infty}{4\dot{G}_o})^{1/3} L$
	Natural gas (kg/hr)	N_2 (kg/hr)	H_2 (kg/hr)								
NA1	3.06	1.865	0.169	0.9076	32.05	15,000	13.54×10^3	27.6×10^3	172	91	7.91
NA2	2.185	2.74	0.1545	0.9917	29.3	15,000	11.33×10^3	23.86×10^3	145	80	6.88
NA3	1.311	3.613	0.1545	1.0756	27.03	15,000	9.63×10^3	20.45×10^3	106	65	5.17
NA4	0.874	4.05	0.144	1.1177	26.01	15,000	8.92×10^3	14.89×10^3	95	57	4.69

Table (2.5)

Lifted natural gas diffusion flames, (d = 7.74)

Run	Mass flow rate Natural gas (kg/hr)	Burner velocity U_o (m/sec)	Re	$Fr = \frac{U_o^2}{gd}$	Re_L	Lifted distance L_l/d	L/d	L_T/d	$\xi_L \equiv (\frac{\pi g \rho_\infty}{4\dot{G}_o})^{1/3} L$
LAo	3.283	26.6	10,000	9.4×10^3	27.5×10^3	-	182	94	10.21
LA1	4.924	39.9	15,000	21×10^3	36.6×10^3	16.8	205	109	8.774
LA2	6.565	53.2	20,000	37.4×10^3	41.67×10^3	20.7	224	129	7.91
LA3	9.848	79.8	30,000	84×10^3	61.76×10^3	29.8	243	130	6.552

The measured quantities are presented separately in the remaining part of the present chapter. The CO_2, CO, O_2 and UHC concentrations are presented in section (2.5.1) while the mean velocity ($\overline{u}$), velocity fluctuation ($\sqrt{\overline{u'^2}}$) and its turbulence intensity ($\sqrt{\overline{u'^2}}/\overline{u}$) are presented in section (2.5.2). All the axial distances are normalized with the burner diameter, d(=7.74 mm). Carbon dioxide, carbon monoxide and oxygen concentrations are shown on a dry basis, whereas unburnt hydrocarbon volume fractions are shown on a wet basis as they were measured.

2.5.1 Concentration Measurements

i. Burner Stabilized Flames

Data for stabilized flame at Reynolds number 15,000 (run SA2) is shown in Fig. (2.9). The data comprises CO, CO_2, O_2 and UHC volume concentrations. They reveal a typical diffusion flame behaviour. Perhaps the most noteworthy feature is the finite O_2 concentration upstream of the main flame region ($x/d < 80$). The same finding was reported by Günther and Simon (1969) for town gas jet flames. Some possible and not necessarily independent explanations which may be advanced are: partial extinction due to the very rapid mixing in the strongly sheared flow near the burner; finite intermittency on the jet axis; turbulent diffusion of oxygen "packets" to the axis; oxygen penetration between ring vortices shed from the burner; and extinction because a limiting equivalence ratio is exceeded.

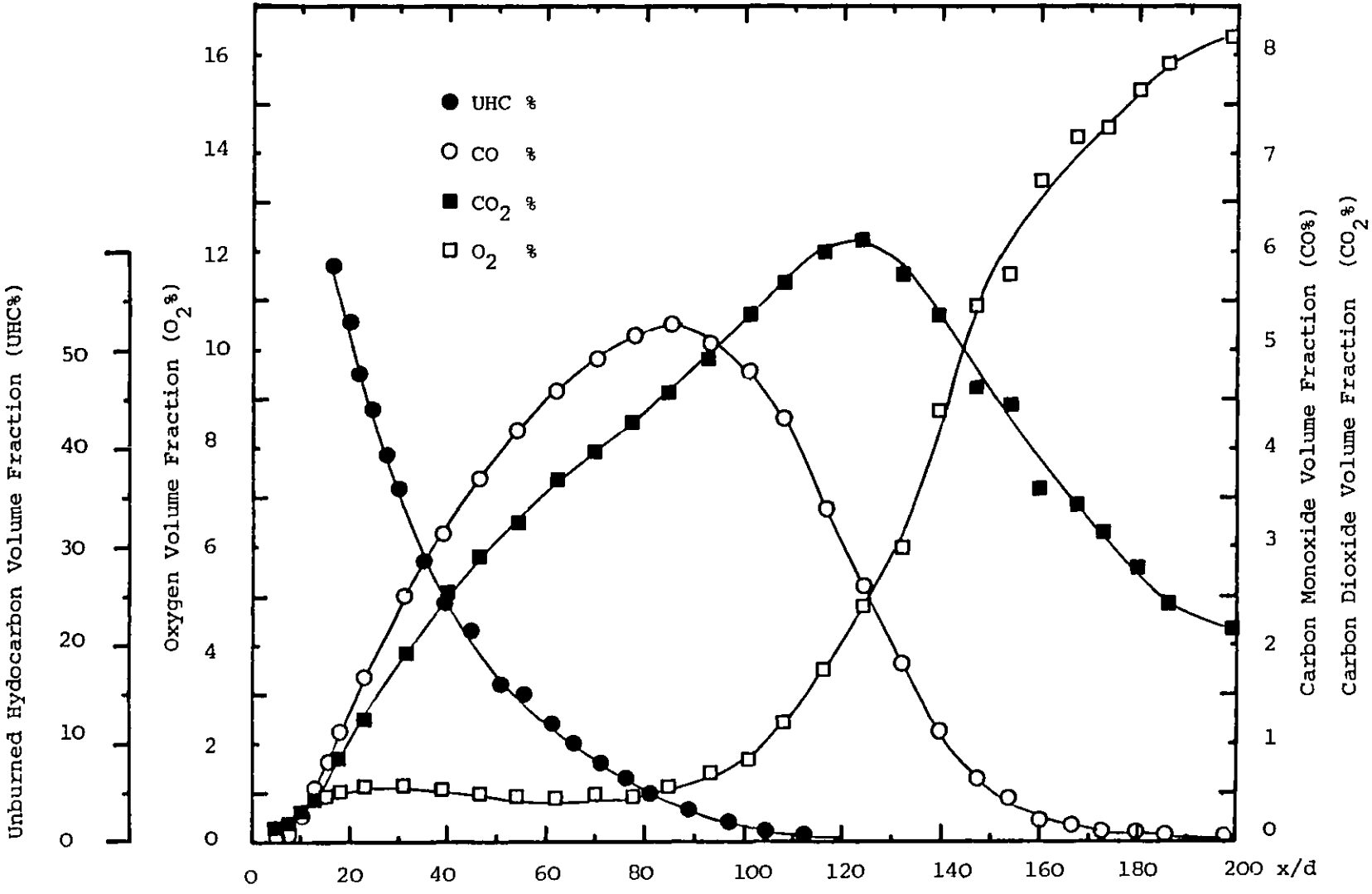

Fig.(2.9) On-axis distributions of volumetric concentration measurements (stabilized flame,run SA2)

Because the CO producing reactions are fast relative to the kinetics of the conversion to CO_2, fast mixing might be expected to result in increased CO with, since the velocity decay is rapid, this effect being confined to the near burner region. Because of the presence of the hydrogen pilot flame in this region, one hestiates to admit the possibility of extinction due to very fast mixing. However, Figs. (2.10) to (2.13) which show the effect of increasing Reynolds number, suggest a tendency towards total extinction very near the burner with possible delayed conversion further downstream. The on-axis picture of such phenomena will be "stretched" by the time scale of diffusion from the surrounding reaction zone.

The intermittency is signalled by the occurrence of fluid possessing the ambient temperature. The temperature probability density functions reported by Moneib (1980) for the same present flames, do not reveal any intermittency for $x/d < 80$, rather they suggest that, if oxygen is indeed present on the axis, mixing has already taken place. Its presence there must be the result of turbulent diffusion. With the aid of an ionization probe, Ahlheim and Günther (1980) in natural gas flames and also Lockwood and Odidi (1975) in town gas flames detected a small amount of reaction on the axis in the early part of the flame. But since the concentration of O_2 is finite even though the mixing would appear to be complete, it must be concluded that reaction is incomplete. This possibility is not catered for by the equilibrium assumption normally contained by combustor prediction procedures.

The ring vortex shedding phenomenon described by Chigier and Yule (1979) might result in an on-axis intermittency, but only

very near the burner. No visual or experimental supporting evidence of this has been found, see temperature probability density functions reported by Moneib (1980) but his measurements are not sufficiently detailed in this upstream region. In any case, if such an effect does exist the consequences downstream will be mixed fuel and oxygen in the absence of sufficient hot products to promote complete combustion.

The possibility of exceeding the flammability limits is usually excluded from physical models of diffusion flames because the reaction rate is presumed to be much greater than the mixing rate, so excluding premixing. However premixing will occur in the absence of sufficient hot product material to initiate reaction. One can imagine that the intermittency phenomena is a mechanism by which fresh fuel and air may be brought into contact without products, which have to diffuse from a neighbouring reaction zone, necessarily being present as well. Paauw et al (1979) have drawn attention to a paper by Bulau and Kaskan (1975) in which it is suggested that in very rich methane/air flames unreacted methane persists in the burned gases due to a paucity of the free radicals necessary for combustion. Further mention of this will be made in the discussion of the nitrogen-diluted flames.

Figures (2.10) to (2.13) show the axial distributions of the mean species concentrations for the stabilized diffusion flames. Increasing the Reynolds number, in addition to apparently causing some extinction in the near burner region, it also lengthens the flame because the role of buoyancy (as characterized by ξ_L of Table (2.3)), and so the entrainment rate which is linked

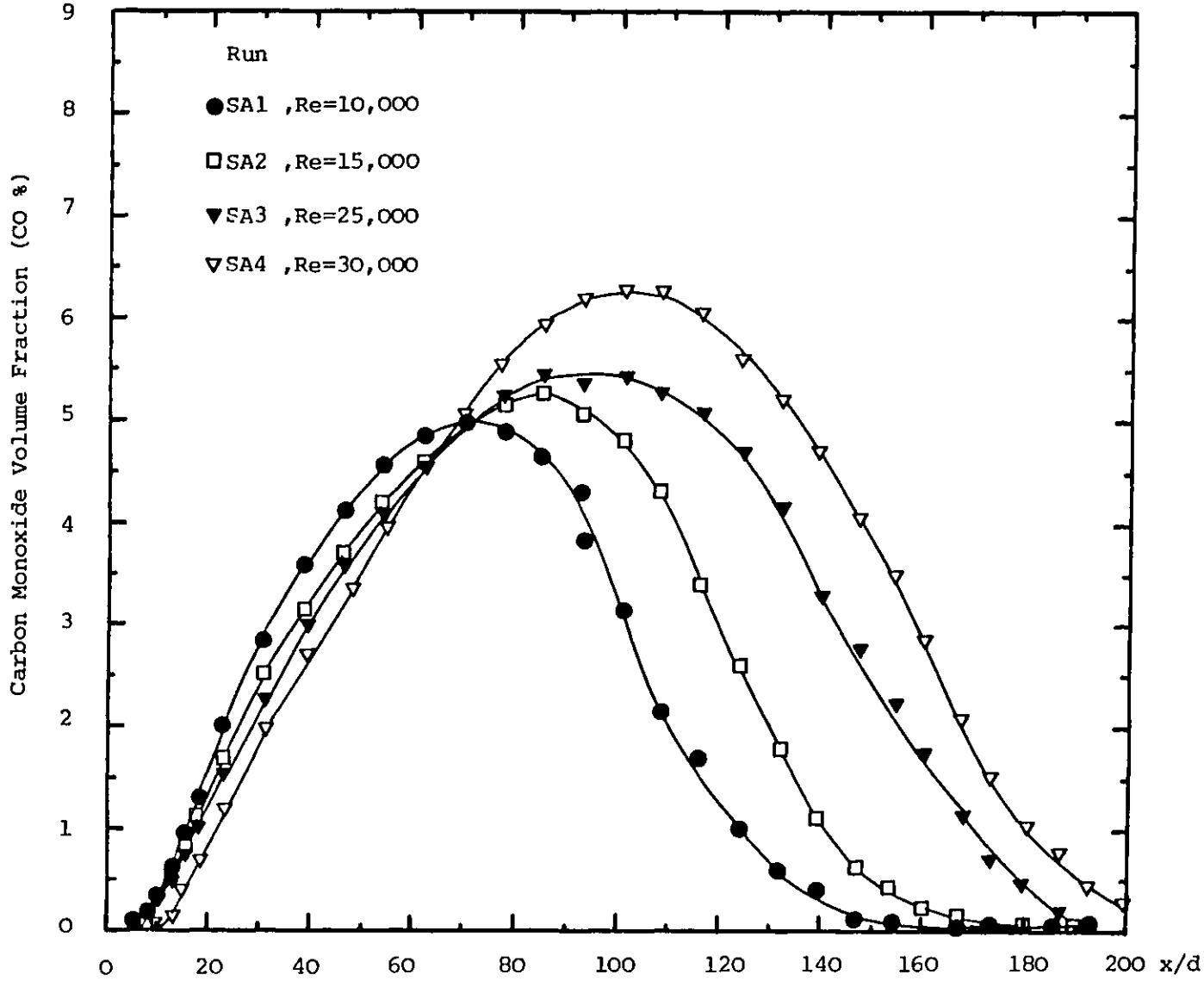

Fig.(2.10) Axial distributions of volumetric concentration measurements of carbon monoxide in stabilized flames for varying REYNOLDS number

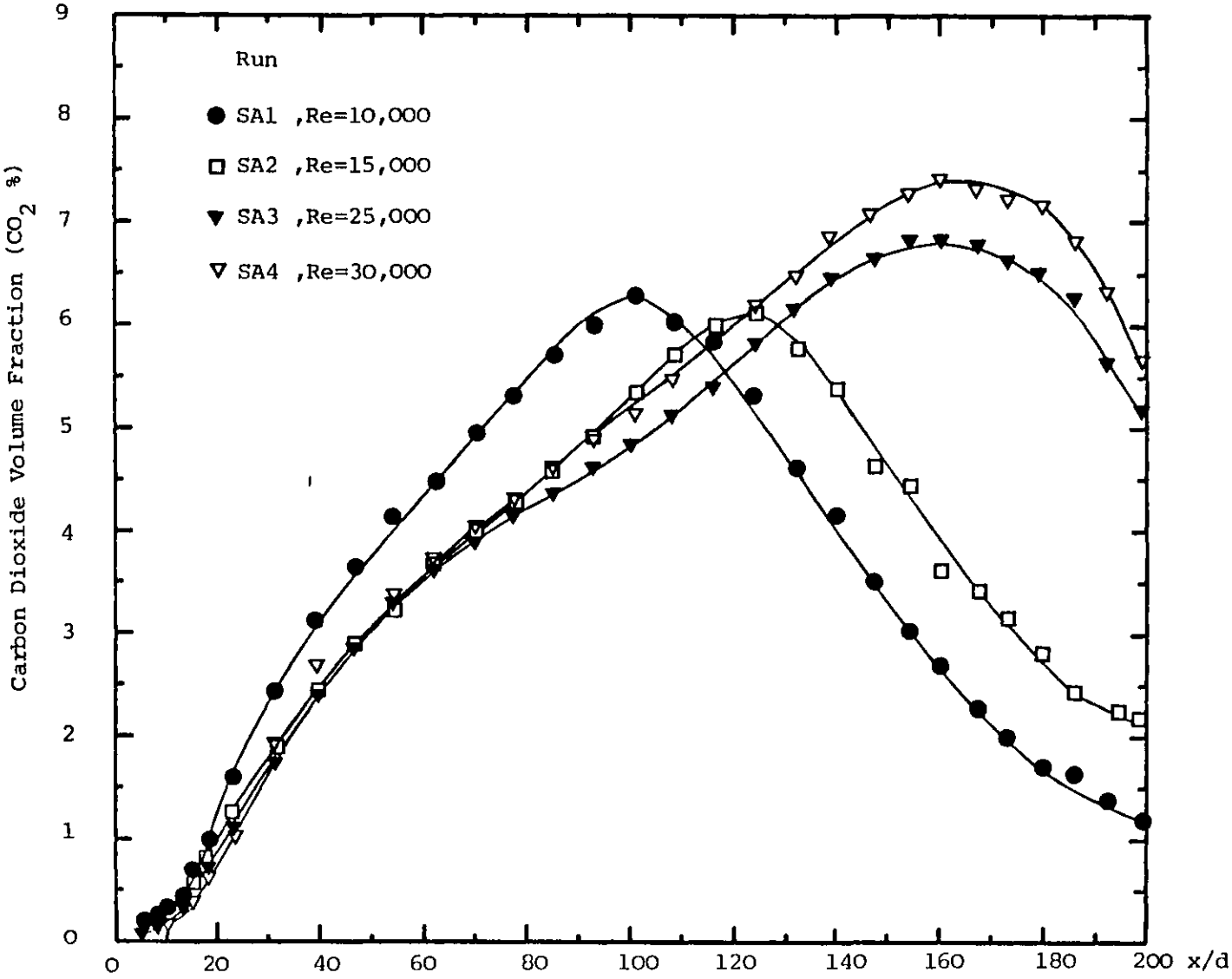

Fig.(2.11) Axial distributions of volumetric concentration measurements of carbon dioxide in stabilized flames for varying REYNOLDS number

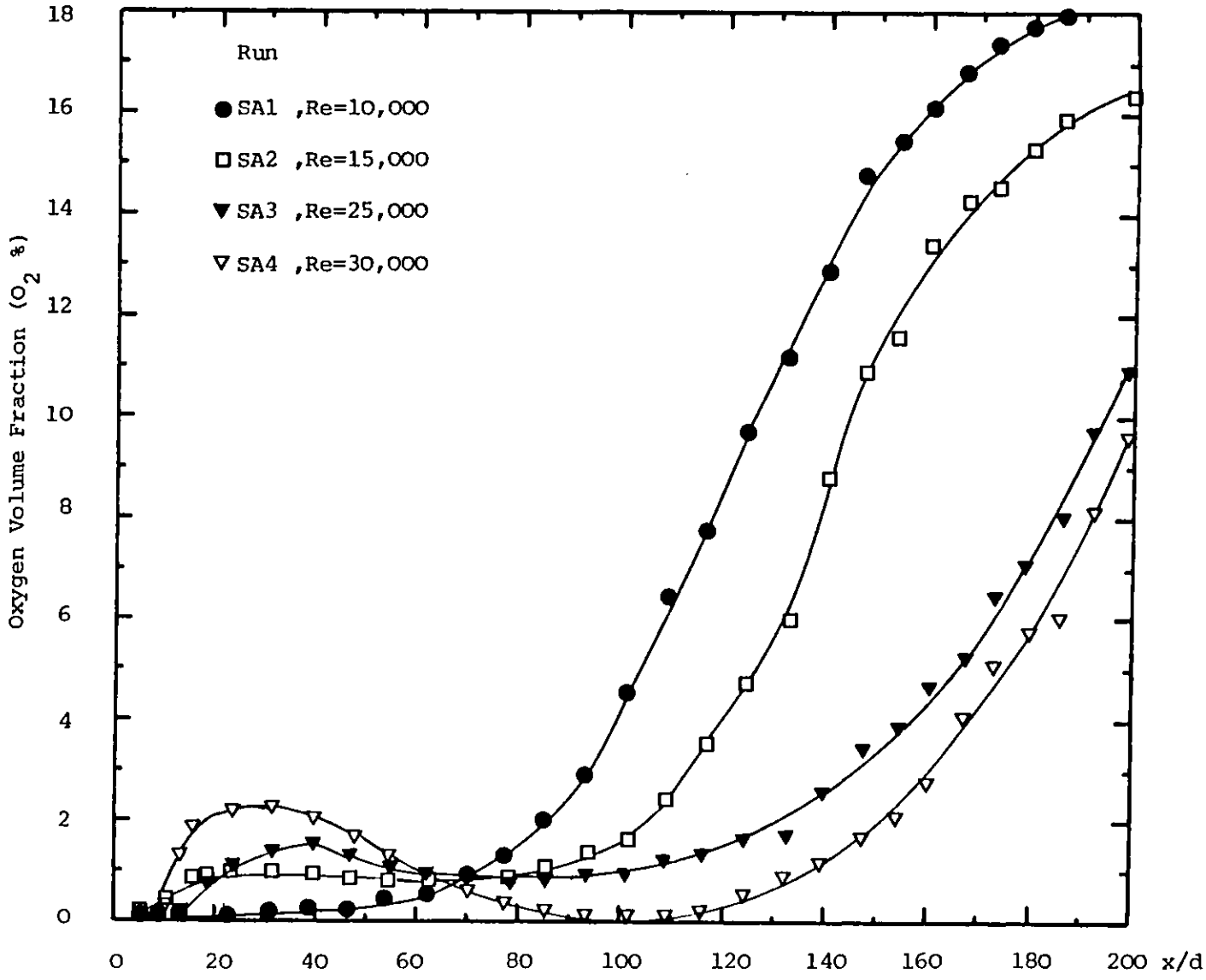

Fig.(2.12) Axial distributions of volumetric concentration measurements of oxygen in stabilized flames for varying REYNOLDS number

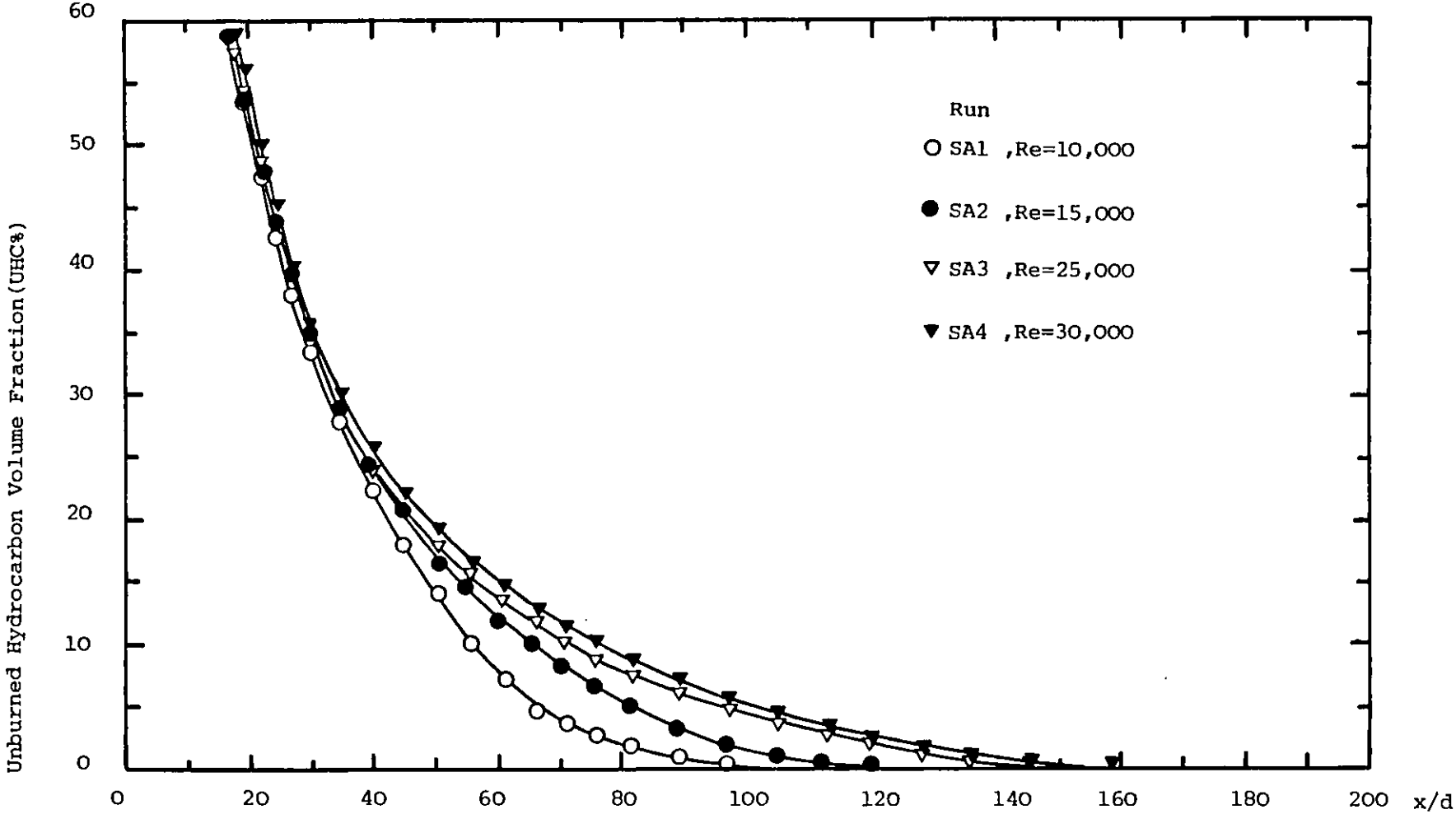

Fig.(2.13) Axial disributions of volumetric concentration measurements of unburned hydrocarbon in stabilized flames for varying REYNOLDS number

to the intensity of large scale motion, is reduced (see Ricou and Spalding (1961) for example). The reduced entrainment (a concept closely linked with that of intermittency) also causes the peak mean concentration of CO and CO_2 to augment with the Reynolds number. Comparison with the temperature results reported in Lockwood and Moneib (1982) shows reasonably that the UHC concentrations reach zero at nearly the same x/d for which the CO_2 concentrations attain maxima and slighly downstream (because CO is present) of the temperature peaks. It is also interesting to note that the maximum CO_2 and CO peaks are flatter as the role of buoyancy decreases with the increase of Reynolds number which means that the volume occupied by the main reaction zone increases; this is simply the result of the larger turbulence scales further downstream and thicker region of the jet, serving to spread the reaction over a greater distance.

Some radial profiles for a Reynolds number 15,000 (run SA2), at four axial positions, are presented in Fig. (2.14) and Fig. (2.15). These show no unexpected tendencies. The location of maximum concentration of CO and CO_2 at 75 d with respect to the location at 36.2 d shows the spreading of the jet flame. A large concentration of the unburnt fuel (28% and 8% respectively) on the centre line is observed. Further downstream, a typical behaviour of a diffusion flame can be observed: as axial distance increases to 113.7 d, the mean species concentration radial profiles become wider showing a thicker flame zone, with an increase in oxygen and decrease in the unburnt fuel levels on the centreline. In the far downstream region, where mean concentration radial profiles at 204 d are shown,

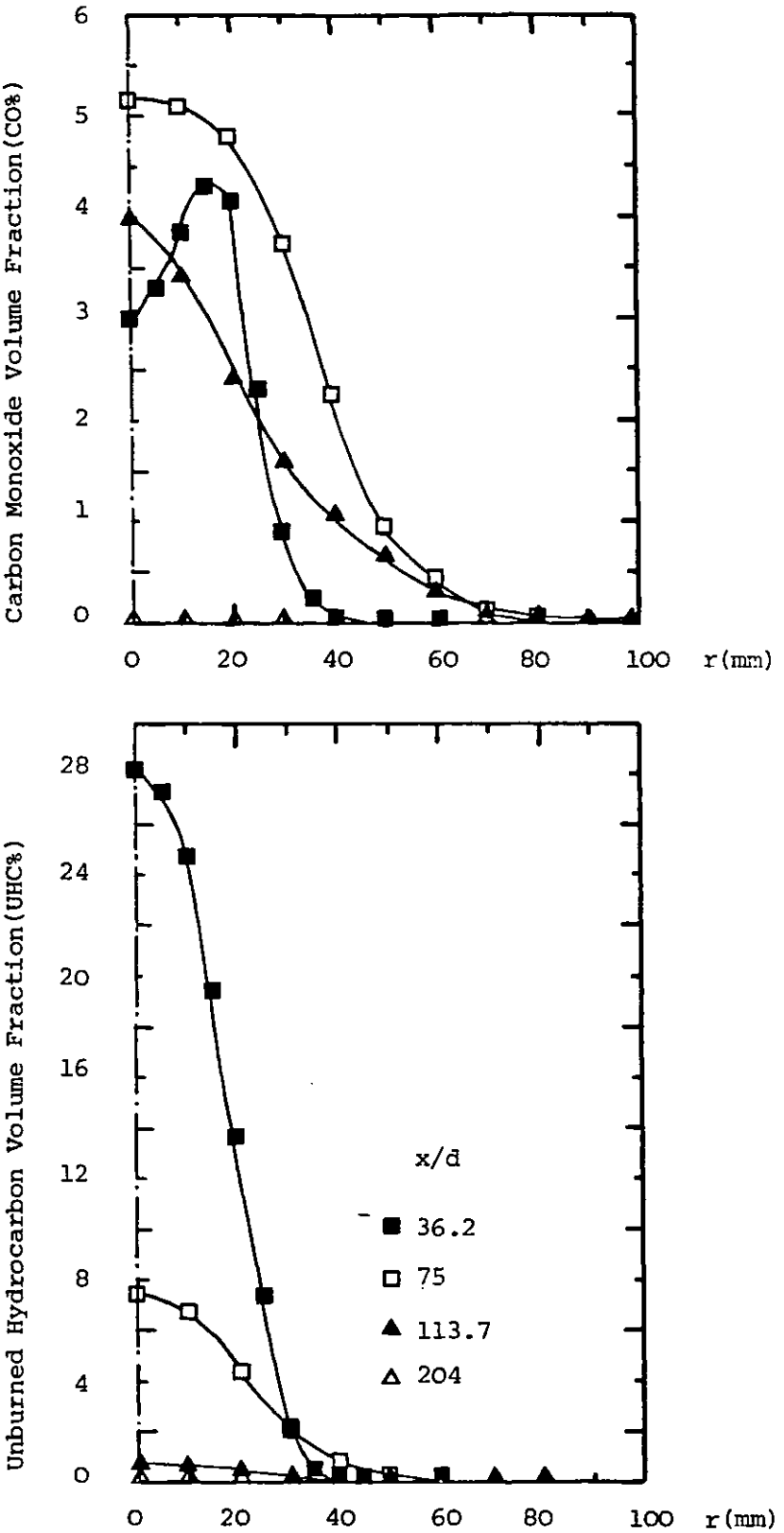

Fig.(2.14) Radial distributions of volumetric concentration measurements at several axial stations.
Stabilized flame,run SA2

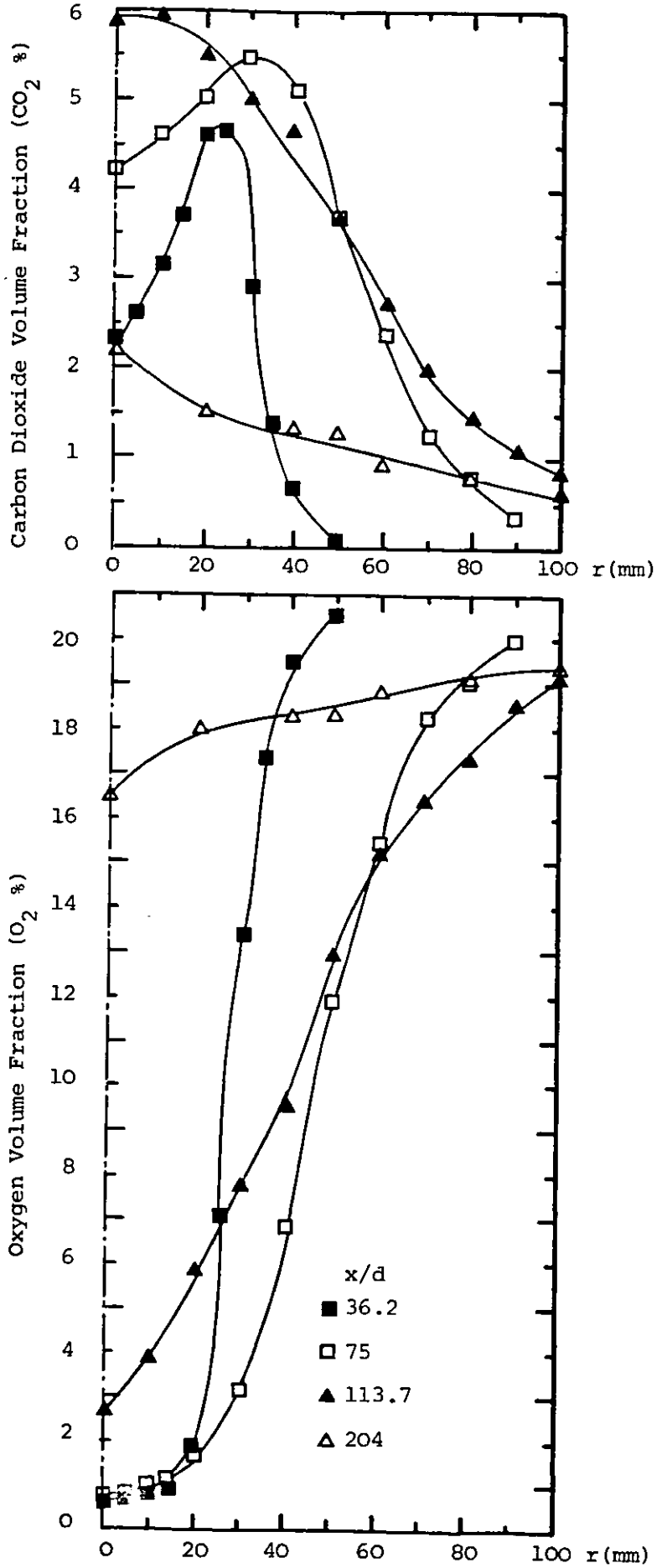

Fig.(2.15) Radial distributions of volumetric concentration measurements at several axial stations.
Stabilized flame, run SA2

all the fuel has been burnt; the CO has decreased being oxidized to CO_2 until only CO_2 (H_2O as well but this has not been measured) and air can be detected.

On the balance of all of the evidence it is probable that the equilibrium concentrations of CO is locally exceeded in the very near burner region, see Fig. (2.10), especially for the higher Reynolds numbers. Given some knowledge of the probability density function for this species it would be possible to suggest whether this is so by comparing calculated with the measured mean concentrations, but such knowledge is essentially non-existant.

ii. Lifted flames

Data for the lifted flame which resulted when the pilot flame (H_2 flame) was extinguished at a Reynolds number of 15,000 (flame LA1) are shown in Fig. (2.16). In the lifted flame cases the flame appears to be divided into two main zones: a premixed zone at the base of the flame and a diffusion zone which follows the former. The entrainment of air in the non-burning lifted zone (between the burner exit and the flame base) results in premixed combustion in the early part of the flame which gives way to diffusion combustion further downstream as the premixed air is depleted. In general terms, the flame stabilizes at the location where the gas and flame propagation velocities match. Descriptions of the stabilization mechanism of lifted diffusion flames have been provided by several authors; see Vanquickenborne and Tiggelen (1966) and Lockwood and Megahed (1978) for example.

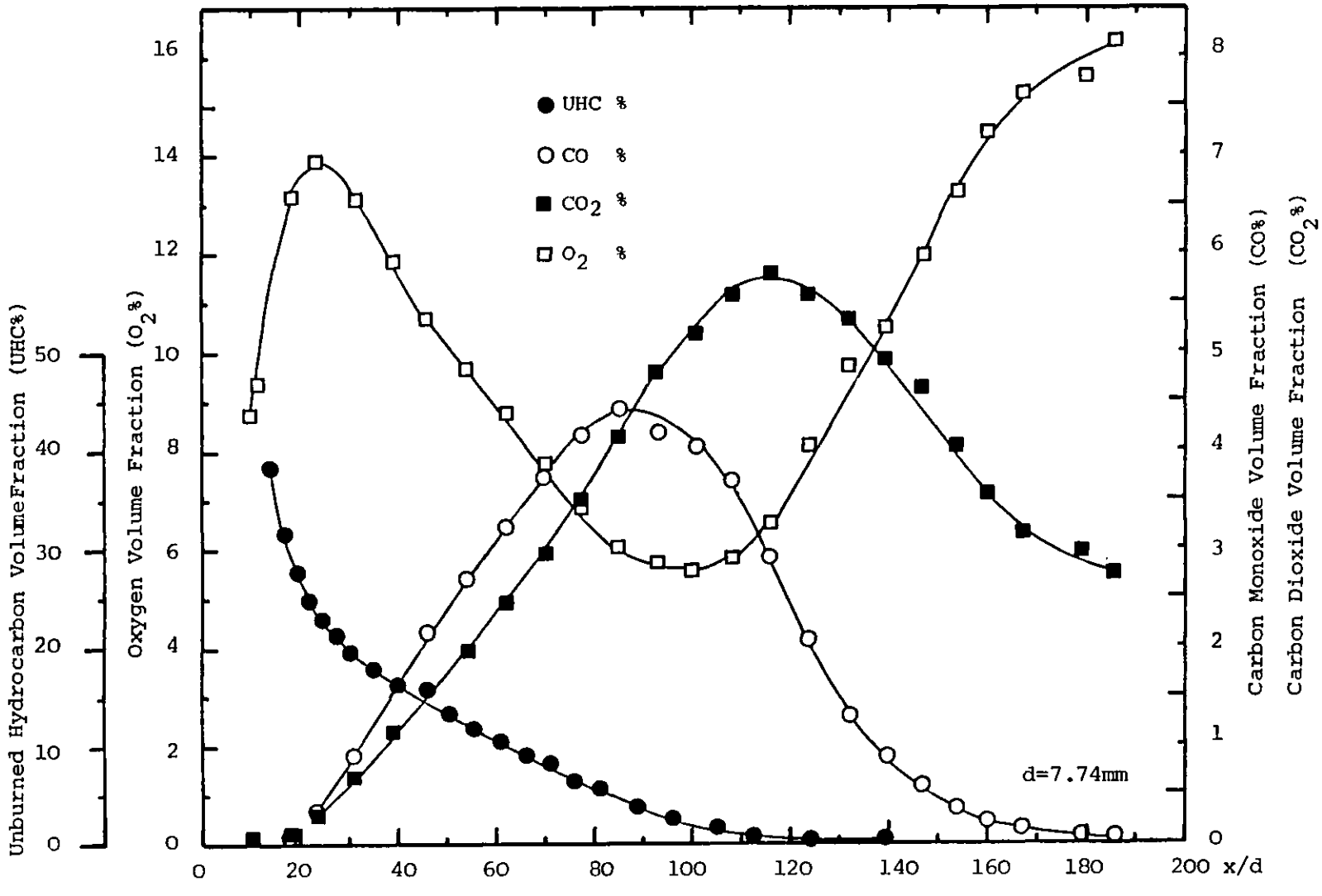

Fig.(2.16) On-axis disributions of volumetric concentration measurements (lifted flame,run LA1)

The overall effect of flame lifting, as can be seen from comparison between the results of run LA1, Fig. (2.16), with those of run SA2, Fig. (2.9), both of which have nearly the same value of ξ_L, is not major, a fact which every combustion engineer knows. The data show that beyond about 80 burner diameter downstream the characters of the lifted and burner stabilized flames are not too different, and indeed it has often been noted that the overall appearances of corresponding lifted and stabilized flames are very similar. The O_2 values drop very low once combustion is established which suggests that the arrival of air by entrainment from the surroundings rather than by diffusion from axis dictates the nature of the diffusion flame downstream.

The axial distributions of the mean CO, CO_2, O_2 and UHC for the lifted flames plotted against x/d are shown in Fig. (2.17) to (2.20). The increase in Reynolds number is shown to be associated with an increase in the length of the premixed region and in the on-axis concentration of CO_2 and CO reached at the end of this zone. The former is due to the increase in the burner injection velocity. The latter is explained by the greater amount of premixing due to the greater lift-off distance. Also increasing the Reynolds number augments the peak oxygen concentrations because the lift height increases. The minimum O_2, however, decreases; the same behaviour is observed for the stabilized flames, Fig. (2.10) to (2.13). This must be due to the reduced role of buoyancy, and so the turbulent mixing with ambient air (note that the flame length increases with Reynolds number), enhancing the role of that oxidant available from the core of the flow. Some radial profiles are presented for flame LA1 at four axial locations,

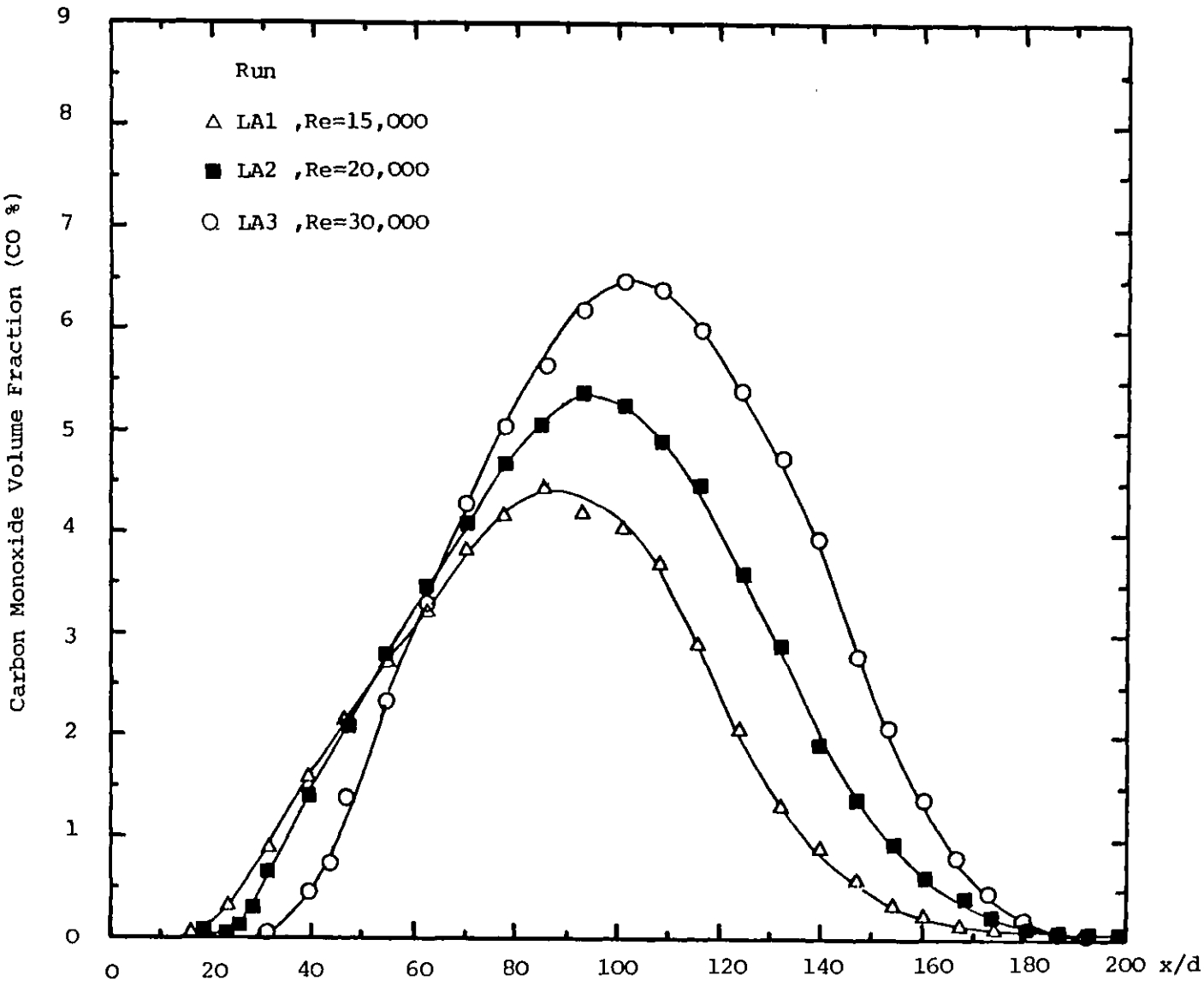

Fig.(2.17) Axial distributions of volumetric concentration measurements of carbon monoxide in lifted flames for varying REYNOLDS number

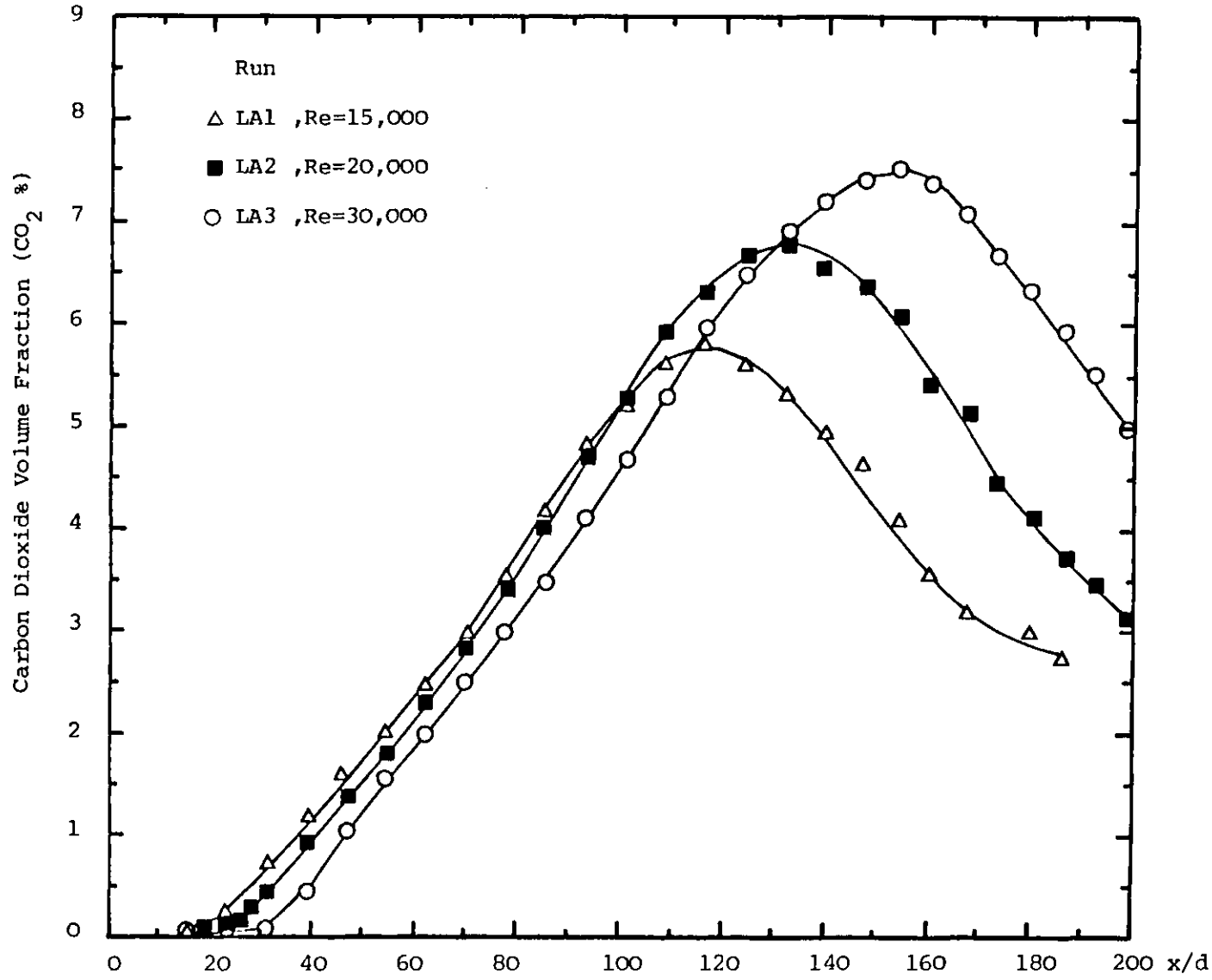

Fig.(2.18) Axial distributions of volumetric concentration measurements of carbon dioxide in lifted flames for varying REYNOLDS number

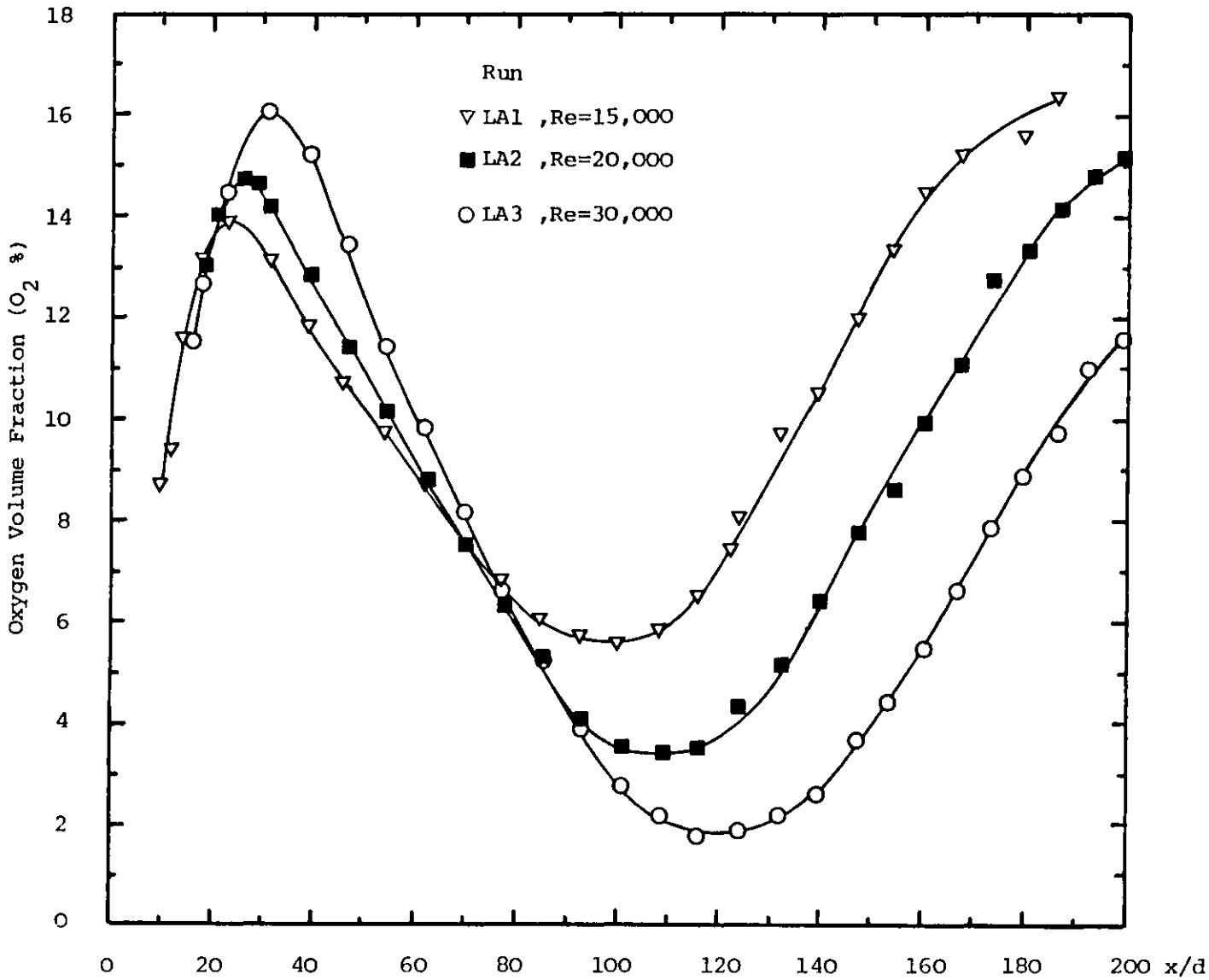

Fig.(2.19) Axial distributions of volumetric concentration measurements of oxygen in lifted flames for varying REYNOLDS number

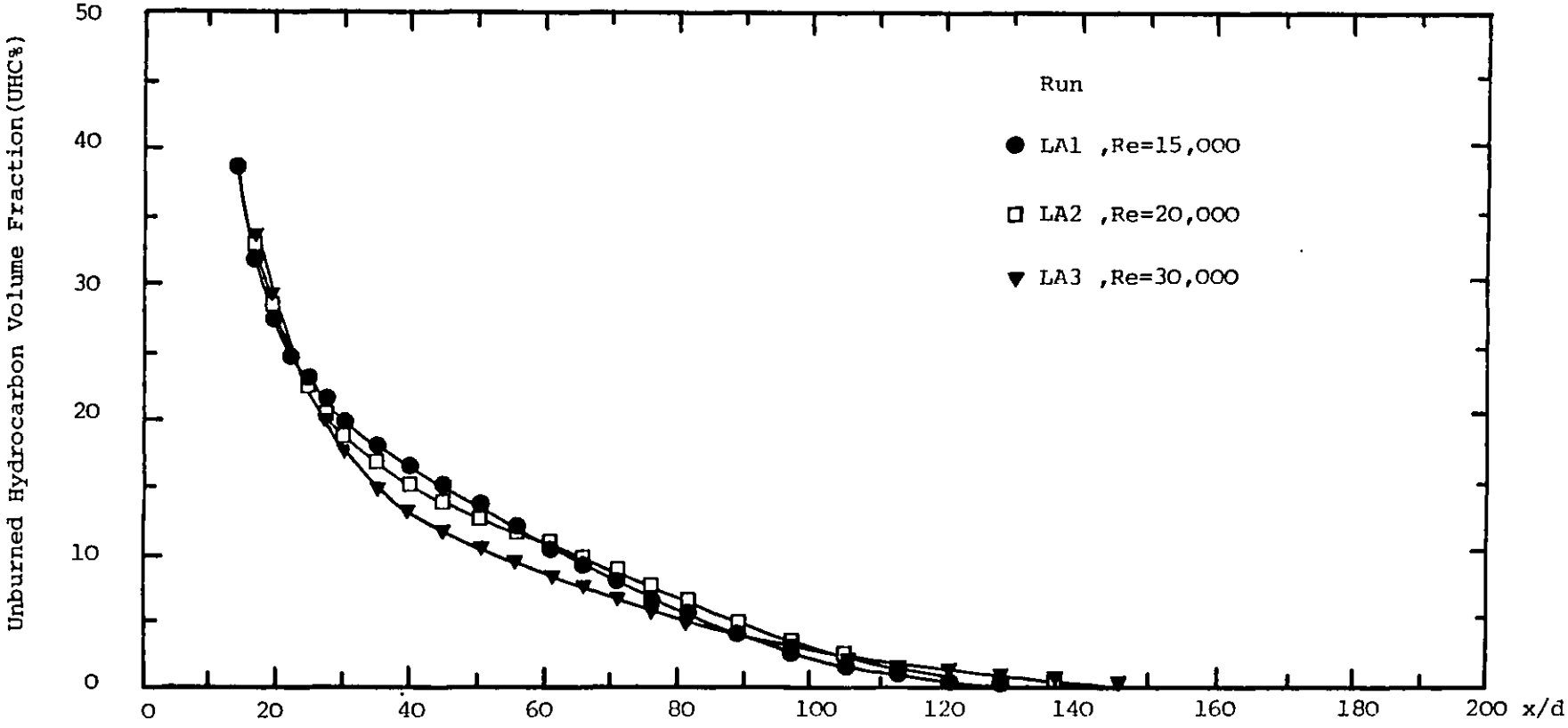

Fig.(2.20) Axial distributions of volumetric concentration measurements of unburned hydrocarbon in lifted flames for varying REYNOLDS number

Fig. (2.21) and Fig. (2.22). These downstream exhibit features similar to those for the stabilized flame, see Fig. (2.14) and Fig. (2.15).

A chemical balance was performed for the lifted flame (run LA1), Fig. (2.18), based on the assumption that all of the fuel injected was methane (CH_4) and that the unburnt hydrocarbon exists in the form CH_4. The water concentration was calculated from the conservation of hydrogen atoms and knowledge of carbon/hydrogen ratio, see Clifford et al (1977). Since all the carbon containing components (CO_2, CO and UHC) were analysed, together with the hydrogen in the UHC, the remaining hydrogen (since hydrogen was not measured) was assigned to the water and free hydrogen estimated by an empirical correlation, see Lyon et al (1975):

$$C_{H2} = C_{CO} \left[0.2(100\ C_{CO})^{0.16}\right]$$

where C_{CO} is the carbon dioxide volume concentration (Kmol). The nitrogen volume fraction was calculated from the known oxygen concentration knowing the nitrogen/oxygen ratio in air.

Knowing the H_2O water concentration, it was possible to convert the CO, CO_2 and O_2 and consequently the N_2 and H_2 concentrations, which were based on a dry analysis, to a wet basis analysis. This method of calculation implies uncertainties of around 10% in the overall wet basis results, see table (2.6).

The theoretical mean temperature, using the wet analysis of the gas species concentrations, was calculated from the heat balance equation:

$$C_{bf}.CV = \sum_i C_i H_i$$

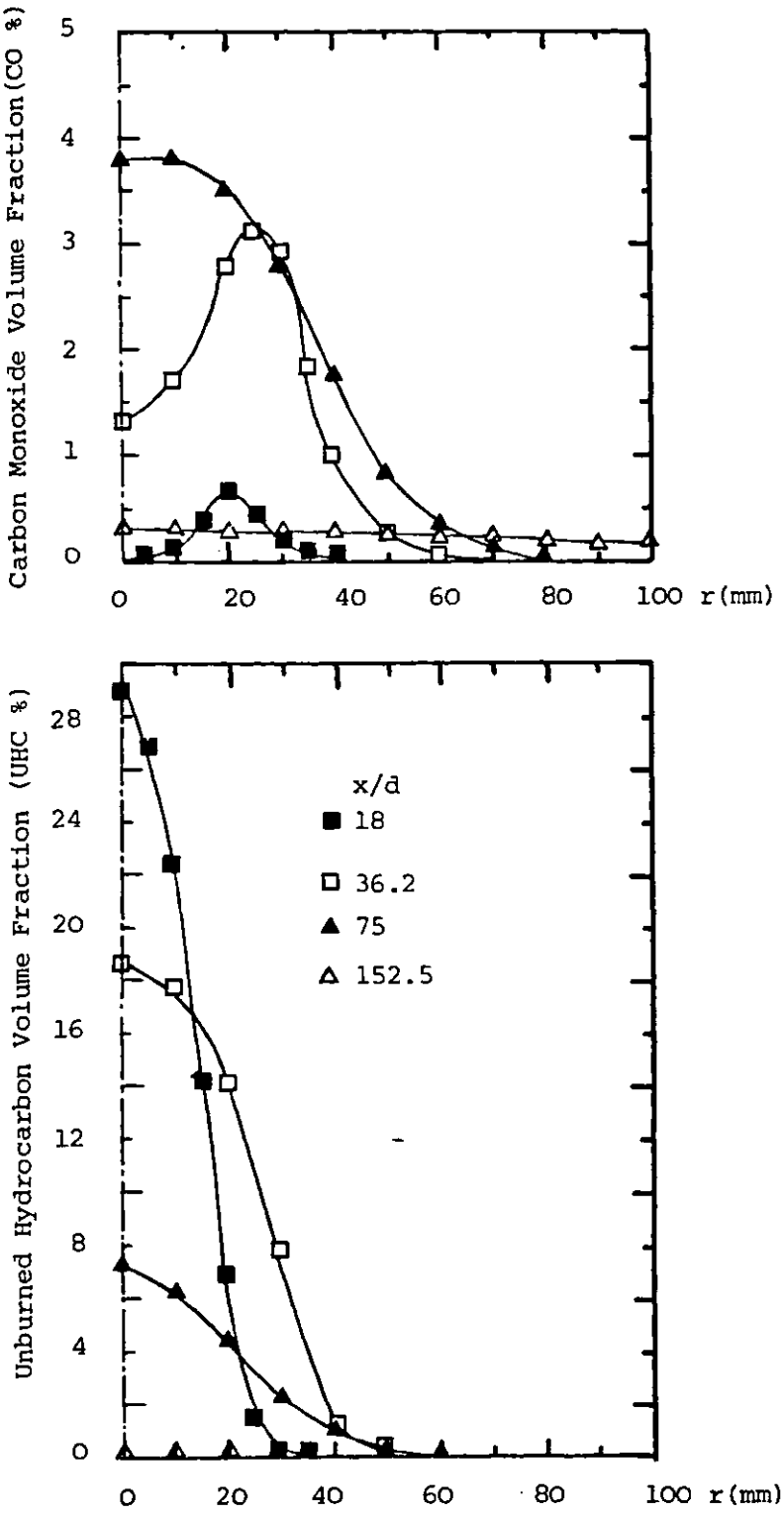

Fig.(2.21) Radial distributions of volumetric concentration measurements at several axial stations.
Lifted flame,run LA1

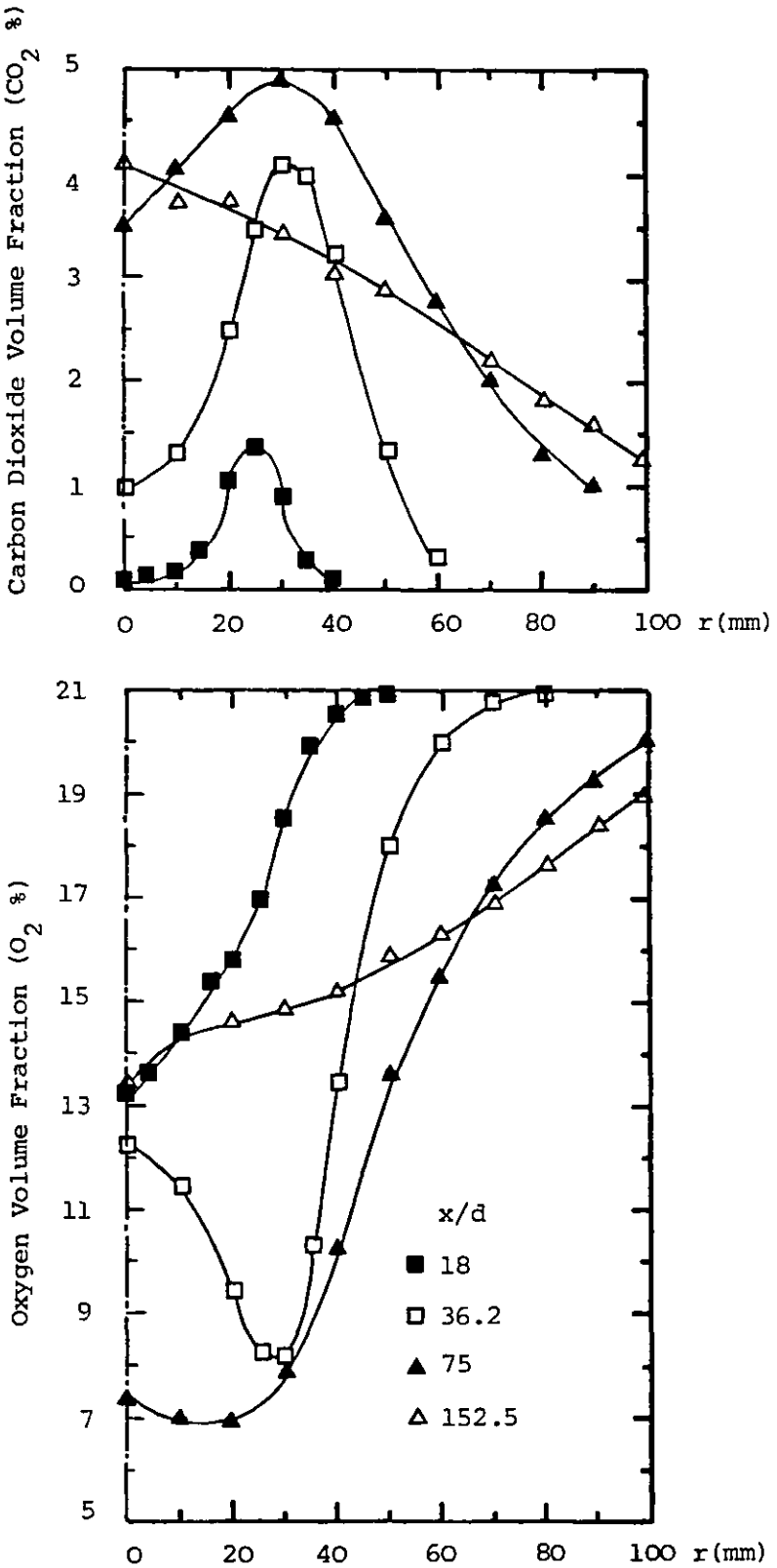

Fig.(2.22) Radial distributions of volumetric concentration measurements at several axial stations.
Lifted flame,run LA1

Table(2.6)

On-axis volume concentrations (wet analysis)*

x/d	CO%	CO2%	O2%	N2%	H2%	H2O%	UHC%	SUM%
5.0	0	0	0	0	0	0	0	0
10.0	0	0	0	0	0	0	0	0
15.0	0	.0	11.9	45.3	0	.0	35.0	92.4
20.0	.0	.1	13.5	52.3	.0	.3	26.5	92.9
25.0	.4	.3	13.6	56.4	.0	1.5	22.0	94.5
30.0	.8	.5	12.9	57.6	.1	2.6	19.5	94.3
35.0	1.2	.8	12.0	57.6	.2	3.7	18.0	93.7
40.0	1.5	1.0	11.0	57.6	.3	4.9	16.0	92.5
45.0	1.9	1.4	10.1	58.6	.4	6.2	15.0	93.8
50.0	2.2	1.5	9.4	59.1	.5	7.1	13.5	93.5
55.0	2.5	1.8	8.8	60.1	.5	8.1	12.0	94.0
60.0	2.8	2.1	8.0	61.0	.6	9.2	10.5	94.4
65.0	3.0	2.3	7.4	61.7	.7	10.1	9.0	94.5
70.0	3.2	2.6	6.7	62.2	.8	11.0	8.0	94.7
75.0	3.6	2.9	6.1	63.8	.9	12.1	6.7	96.3
80.0	3.7	3.2	5.5	64.7	.9	13.0	5.5	96.8
85.0	3.8	3.5	5.1	66.1	.9	13.8	4.5	98.0
90.0	3.7	3.9	4.9	67.2	.9	14.3	3.5	98.6
95.0	3.6	4.1	4.7	68.2	.9	14.7	2.5	99.0
100.0	3.5	4.4	4.7	69.3	.8	15.0	2.0	99.9
105.0	3.3	4.6	4.8	70.4	.8	15.1	1.5	100.6
110.0	2.9	4.8	5.0	70.7	.7	14.9	1.0	100.2
115.0	2.5	4.9	5.4	71.0	.6	14.4	.7	99.7
120.0	2.1	4.9	6.0	71.0	.4	13.6	.5	98.8
125.0	1.6	4.8	6.9	71.6	.3	12.7	.2	98.5
130.0	1.2	4.7	7.8	71.8	.2	11.8	0	97.7
135.0	.9	4.5	8.6	72.1	.2	10.9	0	97.4
140.0	.7	4.3	9.5	72.6	.1	10.1	0	97.5
145.0	.5	4.0	10.4	73.0	.1	9.2	0	97.5
150.0	.4	3.8	11.4	74.1	.0	8.4	0	98.3
155.0	.3	3.6	12.4	75.5	.0	7.7	0	99.7
160.0	.2	3.3	13.2	76.0	.0	7.0	0	99.9
165.0	.1	3.0	13.9	76.6	.0	6.4	0	100.4
170.0	.1	2.9	14.4	76.7	.0	6.0	0	100.3
175.0	.0	2.7	14.8	77.0	.0	5.7	0	100.4
180.0	.0	2.6	15.1	77.4	.0	5.5	0	100.9
185.0	.0	2.6	15.3	77.7	.0	5.3	0	101.0

* For lifted flame,run LA1

where C_{bf} is the burnt fuel (Kmol of CH_4), CV is the gross calorific value of the fuel (MJ/Kmol), C_i is the concentration (Kmol) and H_i is the enthalpy (MJ/Kmol) respectively for the six species; CO, CO_2, O_2, N_2, H_2O and H_2. The data for both the enthalpies and the calorific value were detected from thermodynamic tables by Haywood (1972). Figure (2.23) shows the calculated temperatures together with those measured by Moneib (1980) for the lifted flame case LA1 (Re = 15,000). The difference between the calculated and the measured values is of the order of 300°C at most. It should be noted that the thermocouple radiation error in the measured temperature was estimated to be about 40°C, see Moneib (1980).

The reasons for the discrepancies between the measured and the calculated temperatures are: (i) the radiation heat loss by the flame to the surroundings which was estimated by Stolakis (1983) to be of the order of 200°C, (ii) the energy consumed by atoms and free radicals and more important (iii) any attempt to calculate the properties of a flame without consideration of the fluctuations in the temperature and species concentration is unlikely to provide accurate answers, see Jones and Whitelaw (1981). The results of the analysis reported in Fig. (2.23) are surprisingly good in view of the omission of information of fluctuations.

iii. Nitrogen-Diluted Flames

The effect of diluting the fuel jet with nitrogen on the on-axis concentration is presented in Fig. (2.24) for flame NA2 (Reynolds number 15,000). Also the axial distributions of the mean species concentrations as a function of x/d for all the nitrogen

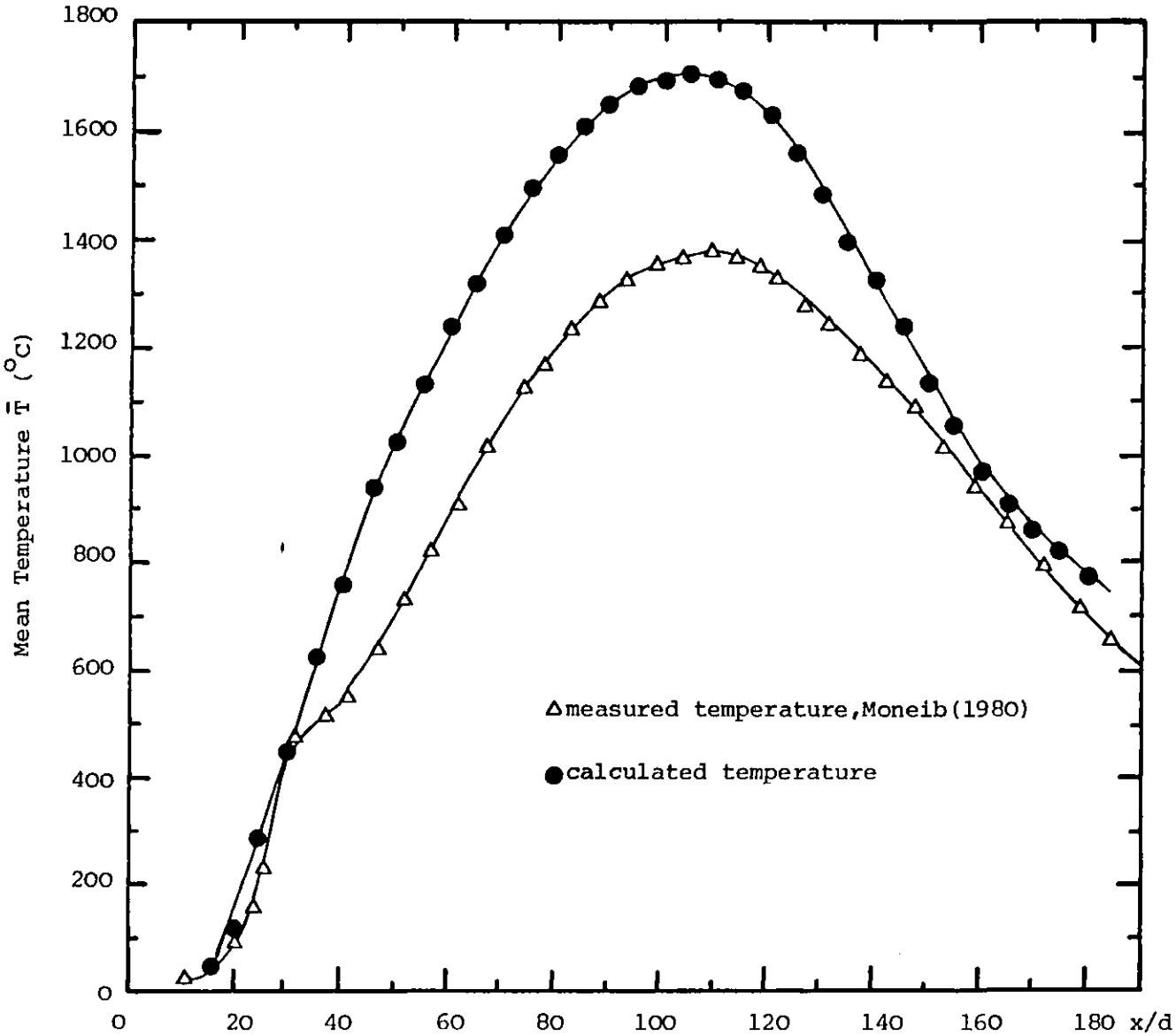

Fig.(2.23) Axial distribution of mean temperature.Lifted flame,run LA1

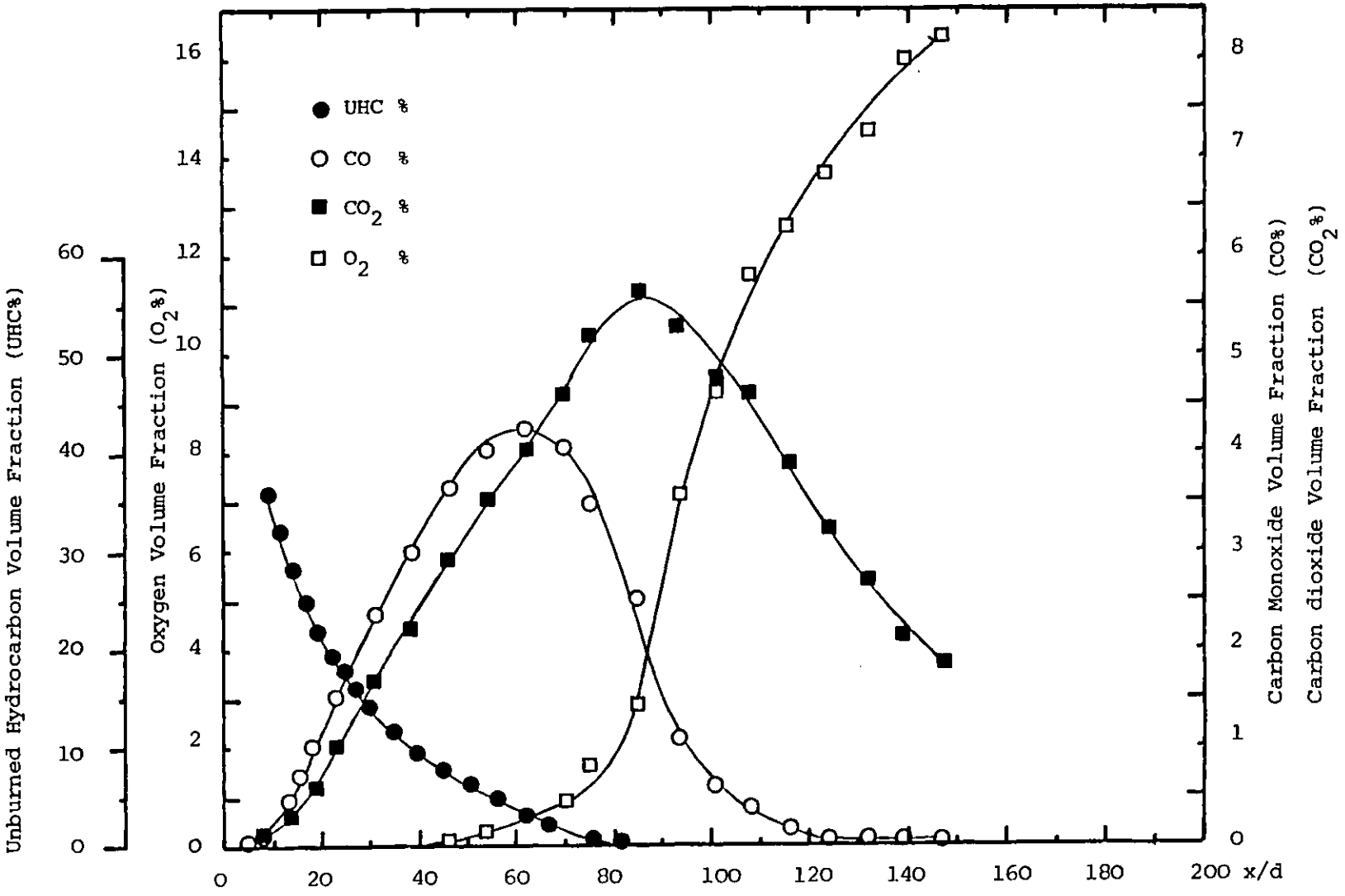

Fig.(2.24) On-axis distributions of volumetric concentration measurements
(stabilized nitrogen-diluted flame,run NA2)

diluted flames are displayed in Fig. (2.25) to Fig. (2.28). All these flames have the same Reynolds number of 15,000, as that of the reference undiluted flame SA2.

The flame is shortened in inverse proportion to the increasing stoichiometric mixture fraction due to the dilution, as expected from conventional jet theory. Both the visible flame length (L) and the thermal length (L_T) when normalized by the input source diameter; $d_s = d_0\sqrt{\rho_0/\rho_\infty}$, see Thring and Newby (1953), show linear variation with respect to the reciprocal of the stoichiometric fuel/air ratio ($1/f_{st}$) as shown in Fig. (2.34a).

Perhaps the most noteworthy feature in Fig. (2.24) is the reduction, compared to the undiluted flame, Fig. (2.9), of the on-axis oxygen concentration in the pre-flame region. That may be because there is less turbulent diffusion associated with these less buoyant flames. This argument is not supported by Fig. (2.12) where increasing the Reynolds number (and so diminishing the role of buoyancy) has the opposite effect. Nor can the results be explained by obvious kinetic arguments since the addition of nitrogen should increase the tendency towards extinction near the burner and so increase the on-axis oxygen content. It is tempting to advance again the kinetically-based argument used to explain the presence of the on-axis oxygen for the undiluted flames. Here the effect of nitrogen dilution of the fuel stream is to weaken the fuel mixture strength, suppressing the retardation of reaction and so the oxygen concentration.

Two radial distributions of the mean species concentration (at x/d = 36.2 and 75) for the nitrogen diluted case (run NA2) are shown in Fig.(2.29) and Fig. (2.30). They show that the spread rate

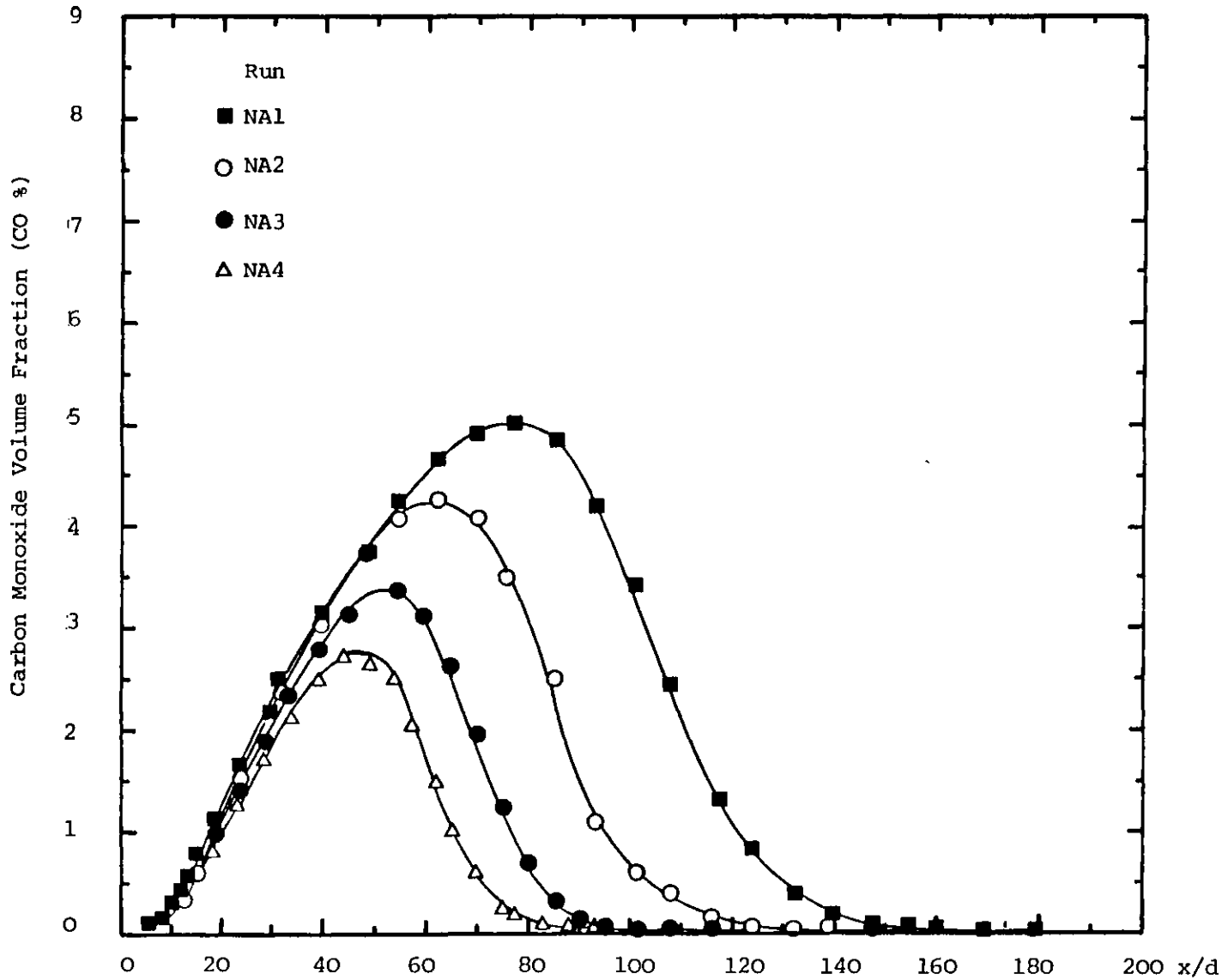

Fig.(2.25) Axial distributions of volumetric concentration measurements for carbon monoxide in stabilized nitrogen-diluted flames(Re=15,000)

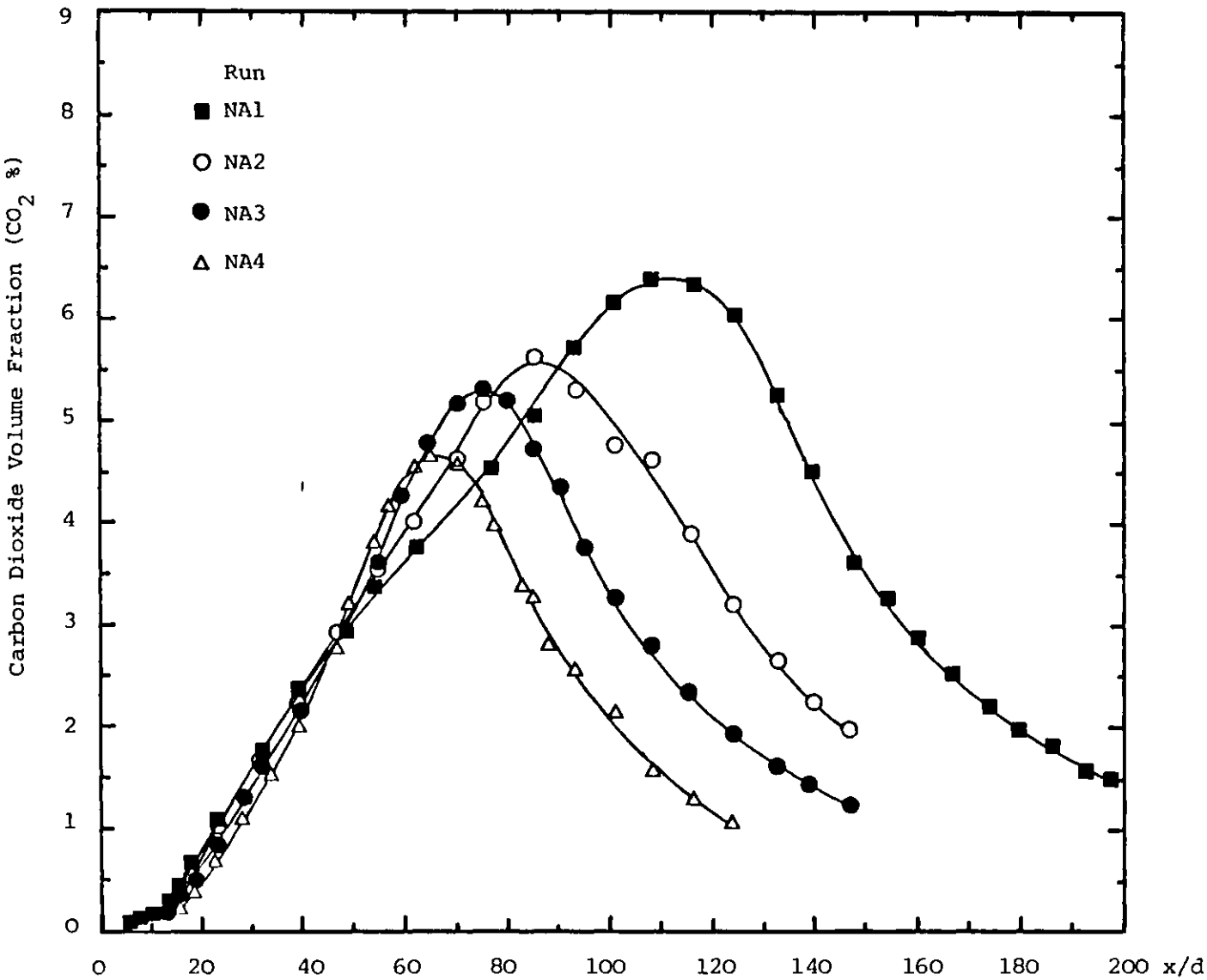

Fig.(2.26) Axial distributions of volumetric concentration measurements of carbon dioxide in stabilized nitrogen-diluted flames(Re=15,000)

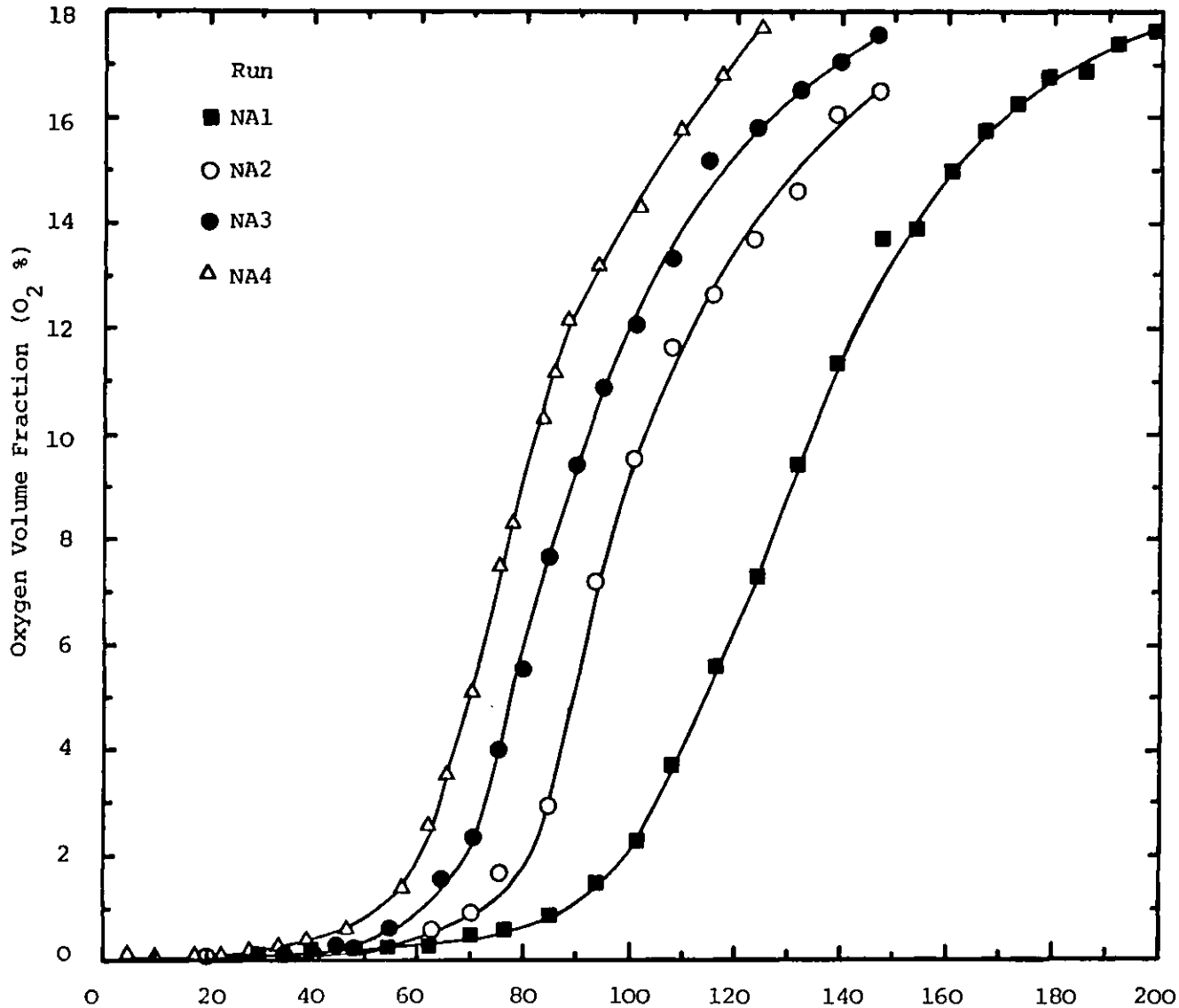

Fig.(2.27) Axial distributions of volumetric concentration measurements of oxygen in stabilized nitrogen-diluted flames (Re=15,000)

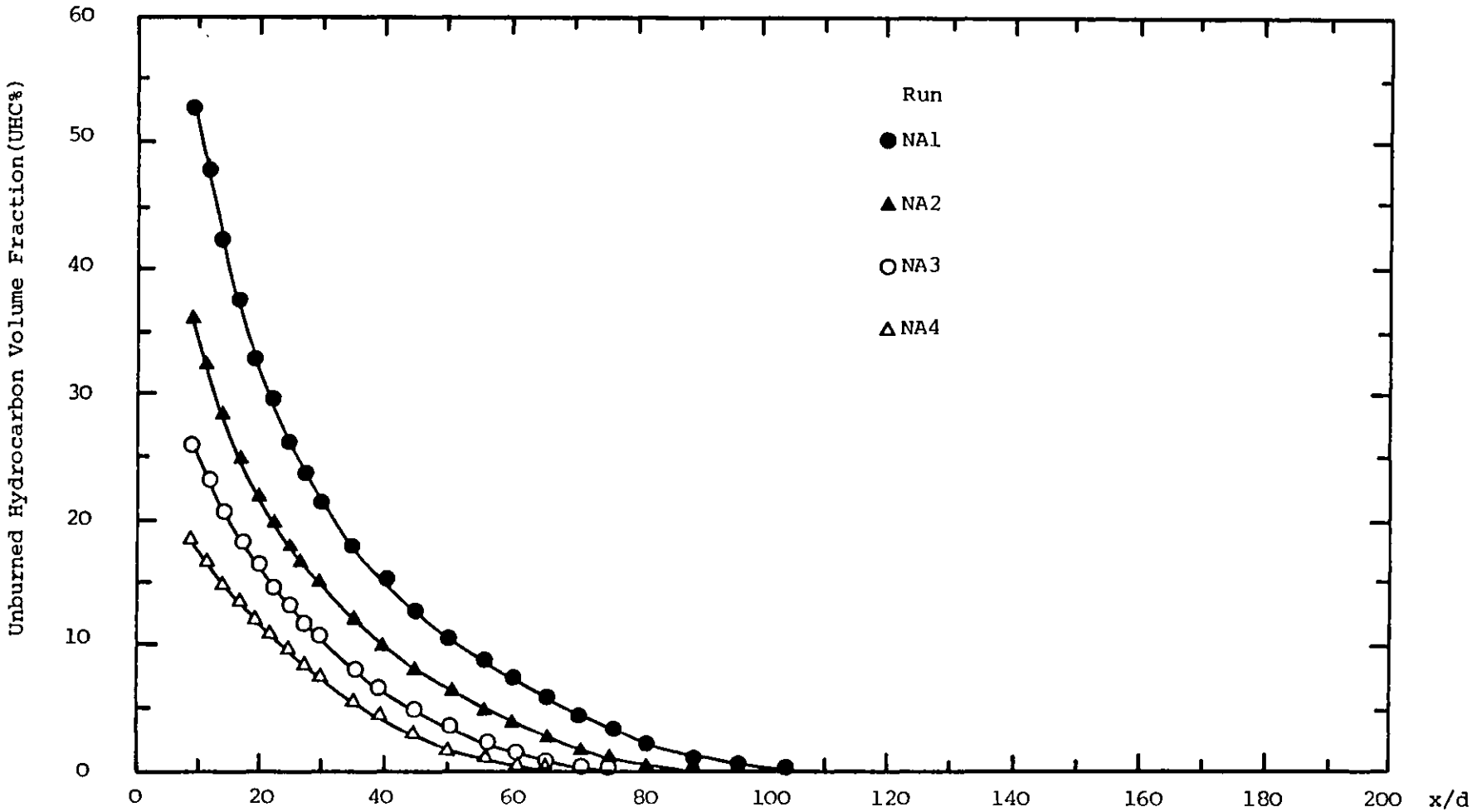

Fig.(2.28) Axial distributions of volumetric concentration measurements of unburned hydrocarbon in stabilized nitrogen-diluted flames(Re=15,000)

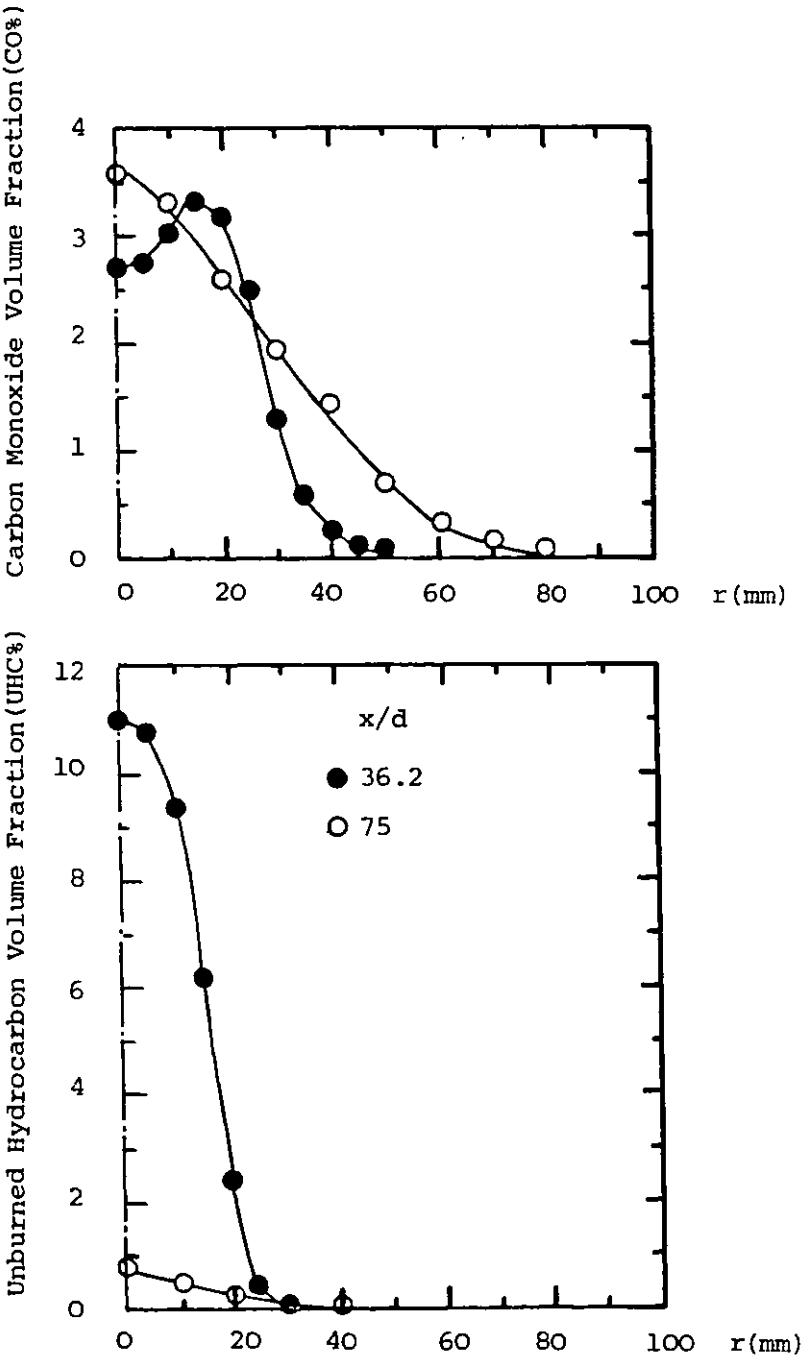

Fig.(2.29) Radial distributions of volumetric concentration measurements at several axial stations.
Stabilized nitrogen-diluted flame, run NA2

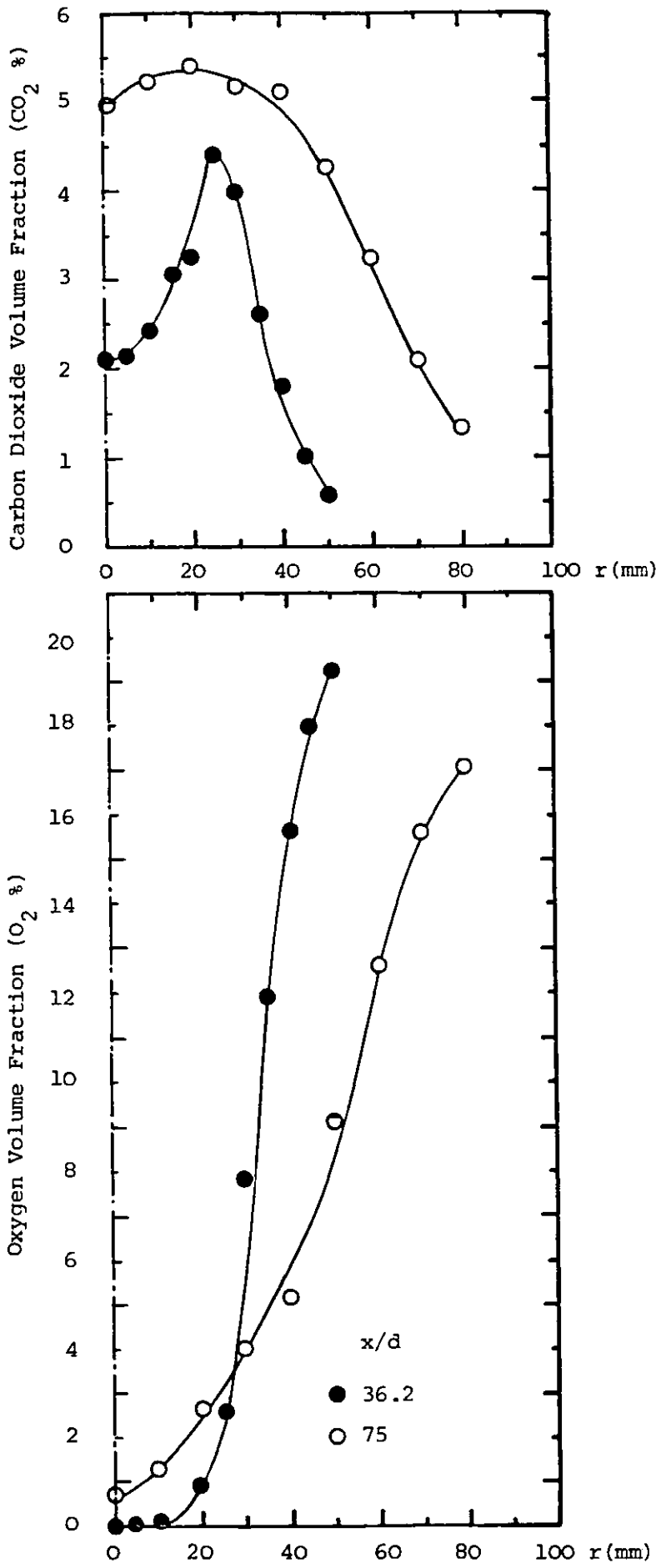

Fig.(2.30) Radial distributions of volumetric concentration measurements at several axial stations.
Stabilized nitrogen-diluted flame, run NA2

of the nitrogen diluted flame case is smaller than both the stabilized, Fig. (2.14) and Fig. (2.15), and the lifted, Fig. (2.21) and Fig. (2.22), flame cases because its stoichiometric oxygen requirement is smaller and so the reaction zone is confined to a smaller volume.

2.5.2 Velocity Measurements

The axial distribution of the axial mean velocity ($\overline{u}$), the fluctuating velocity ($\sqrt{\overline{u'^2}}$) and the turbulence intensity ($\frac{\sqrt{\overline{u'^2}}}{\overline{u}}$) calculated from the former two, for flames: SA2 (burner stabilized), NA2 (nitrogen diluted) and LA1 (lifted flame), all for a Reynolds number of 15,000, are in Fig. (2.31), Fig. (2.32) and Fig. (3.33) respectively. Both the stabilized flames, with and without nitrogen, show nearly the same behaviour. Figure (2.34b), in which the optically measured axial mean velocities ($\overline{u}$ m/sec) which are referred to the mean velocity ($\overline{u}_0$ m/sec) at the nozzle exit are plotted against x/d, shows a comparison between the mean velocity for the three flames with the results reported by Eickhoff and Schodl (1980) and Wittimer and Günther (1980). The qualitative agreement with these measurements is evident.

In Fig. (2.31), the decay of the mean velocity along the flame axis is typical for a jet. The axial fluctuating velocity ($\sqrt{\overline{u'^2}}$) shows a similar distribution to that of the mean velocity. The maxima occur at x/d = 20. Further downstream the fluctuating velocity decreases. In cross sections of the flame near the burner

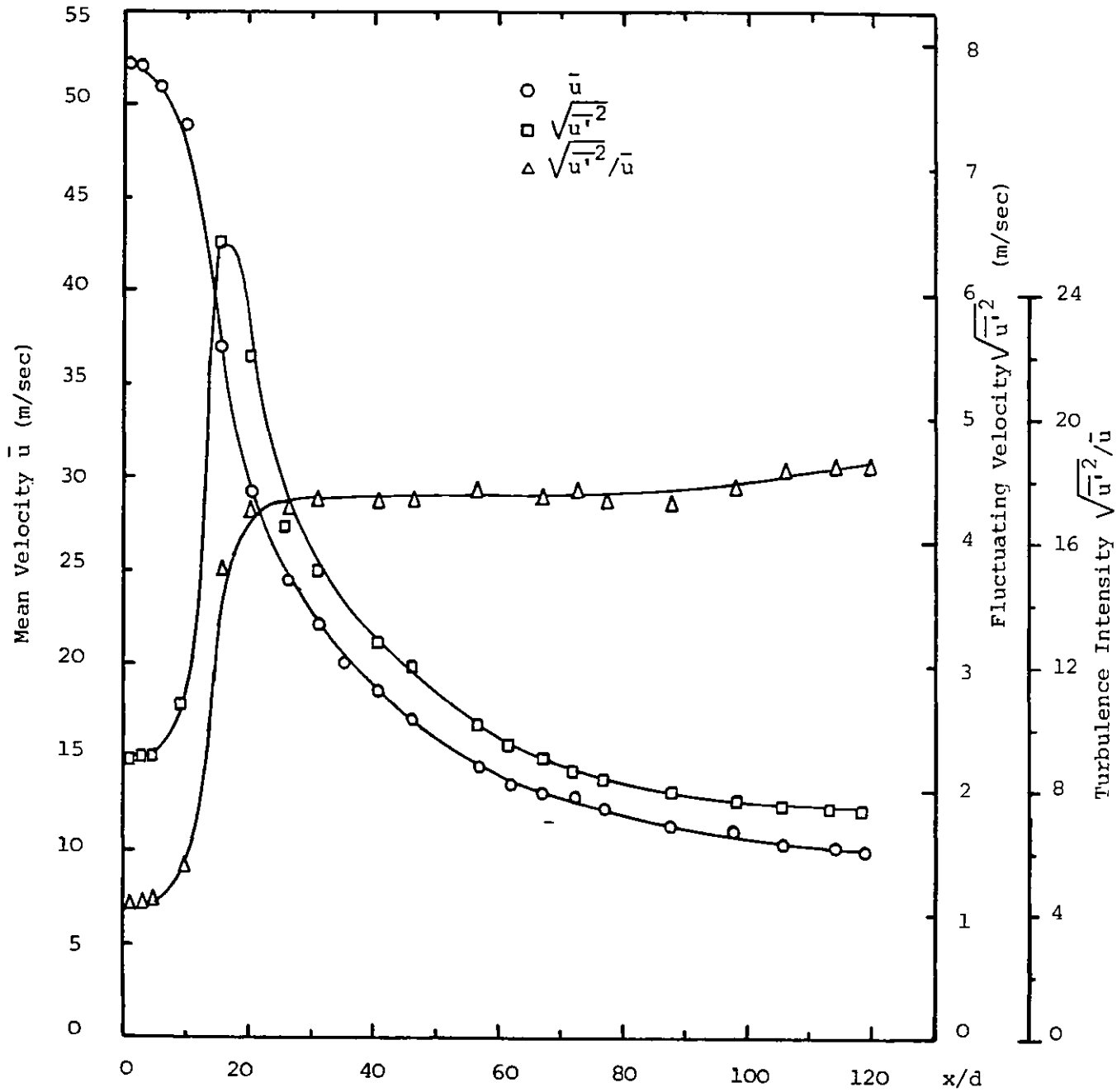

Fig.(2.31) Axial distributions of mean, fluctuation and turbulence intensity of the axial velocity. Stabilized flame, run SA2

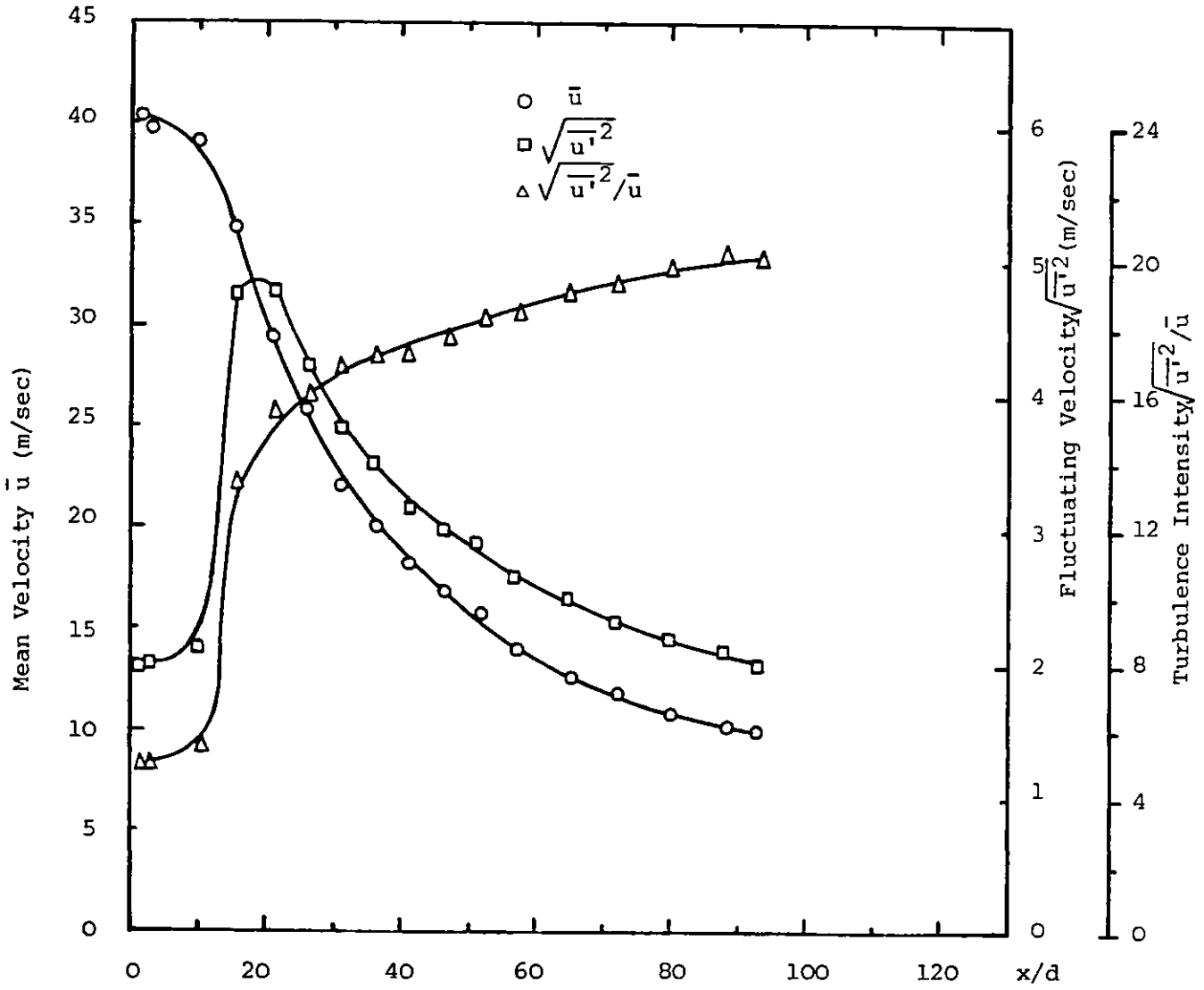

Fig.(2.32) Axial distributions of mean,fluctuation and turbulence intensity of the axial velocity.Stabilized nitrogen-diluted flame,run NA2

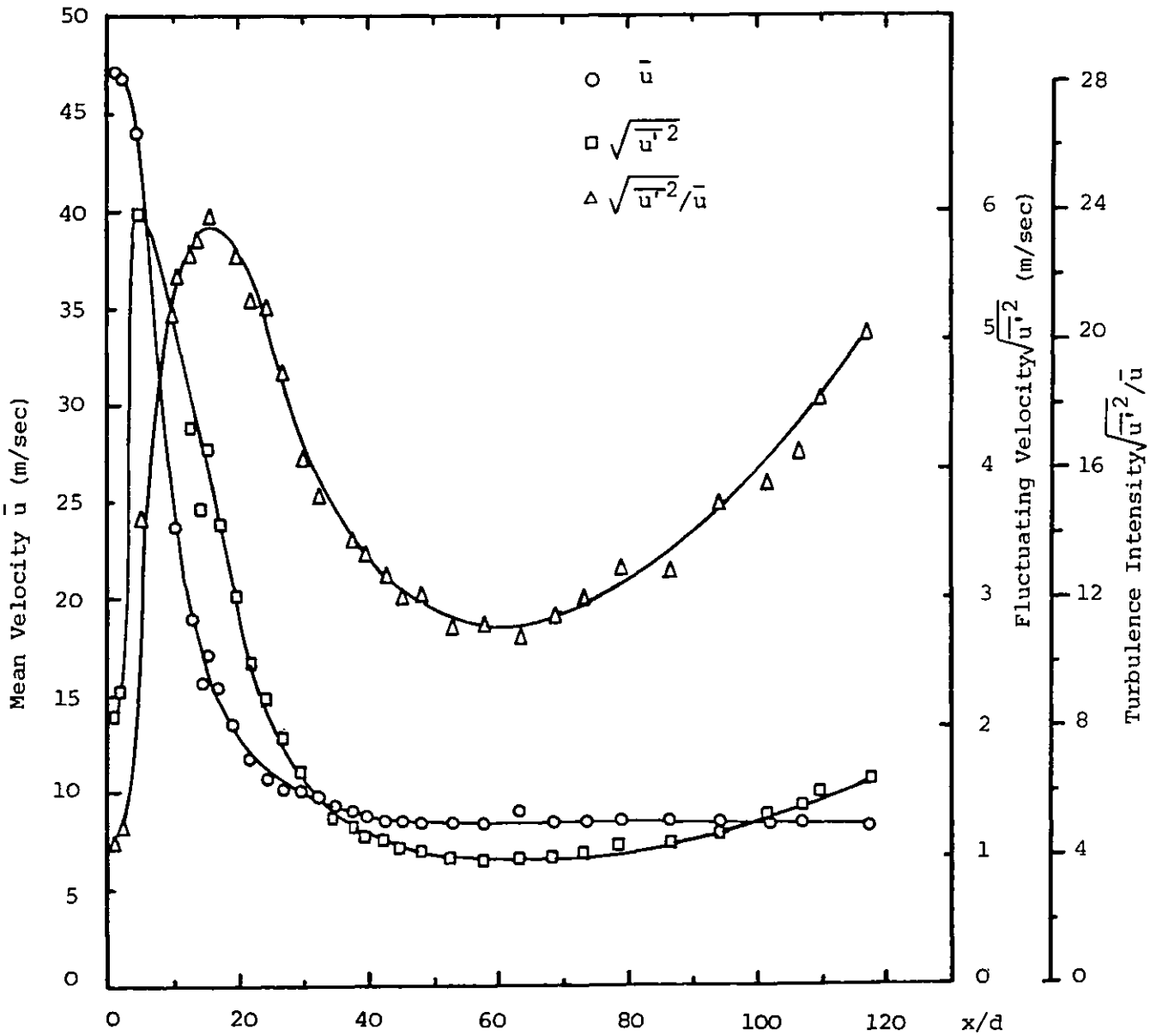

Fig.(2.33) Axial distributions of mean, fluctuation and turbulence intensity of the axial velocity. Lifted flame, run LA1

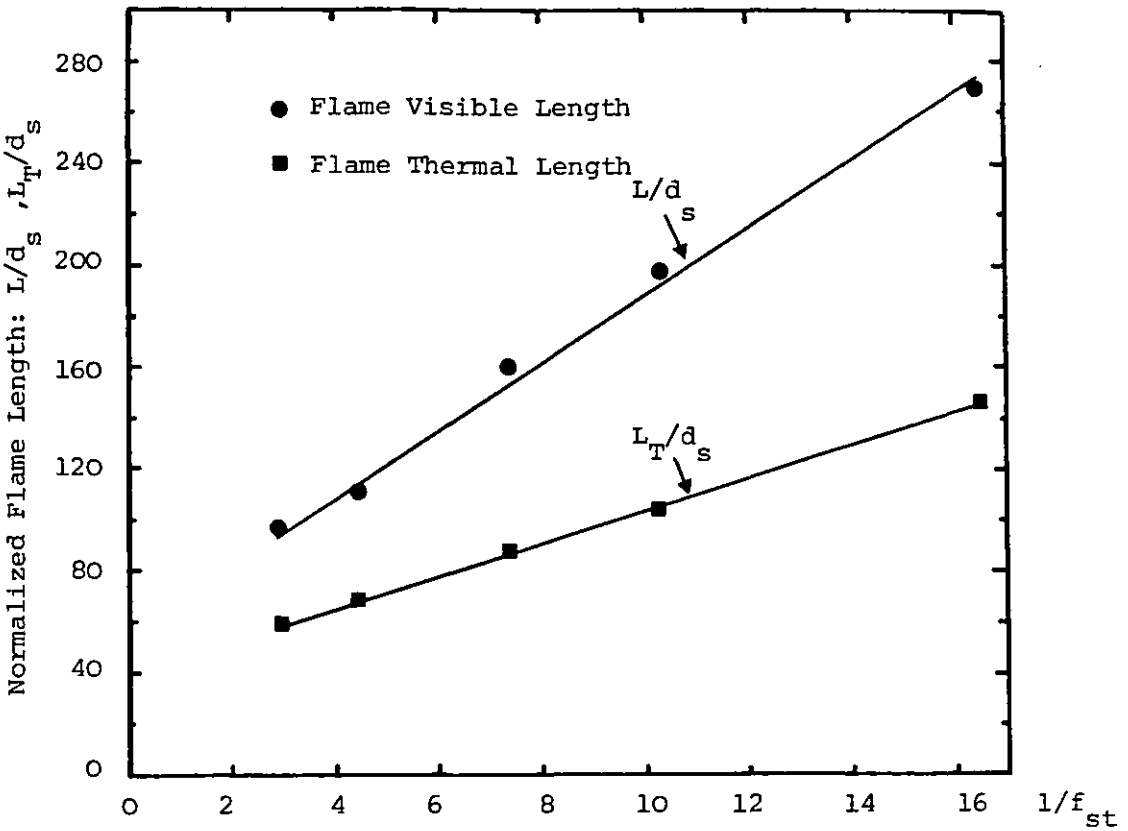

Fig.(2.34a) Effect of stoichiometric fuel/air ratio on flame length

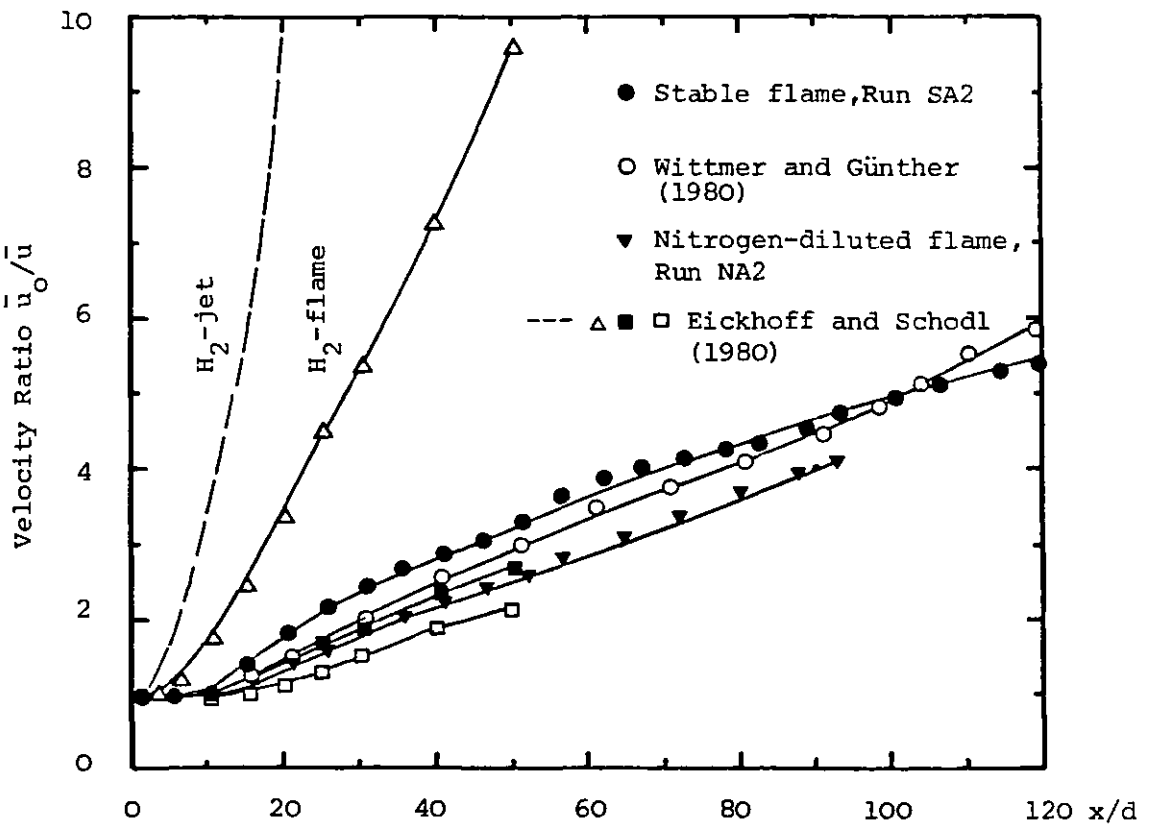

Fig.(2.34b) Comparison between the velocity ratio($\bar{u}_o/\bar{u}$) obtained by different authers along the axis of stabilized flames

exit, a steep peak in turbulence intenstiy exits, caused by extremely high velocity gradients prevailing in this area. Further downstream, the distribution shows comparatively small increases in turbulence intensity.

The results of the lifted flame, Fig. (2.33), show that both the mean velocity and fluctuating velocity behave in the same manner as those of the stabilized flames but from the point of ignition, the turbulence intensity decreases to a minimum and increases again further downstream, an effect opposite to that found in the stabilizing flames in the corresponding part in which the turbulence intensity increases. The onset of reaction is the reason for the difference between the two flame types, i.e. stabilized and lifted. The same phenomenon has been reported by Becker and Brown (1969) and Günther (1970) and was also pointed out by Bray (1974).

For the stabilized flame (run SA2), Fig. (2.31), the axial turbulence intensities are 16 to 18% which are distinctly less than those for an inert jet (30% is typical),see Wygnanski and Fiedler (1969) for example. Similar results have been obtained by Becker and Brown (1969) and Eickhoff (1982). A definite explanation of the damping effect of combustion on the development of turbulence is difficult. But one can assume that the principal combustion induced factors which could alter the turbulence intensity significantly in this case are: the mean buoyancy, the density fluctuations and the mean dilatation due to heat release. The first two are also features of buoyant non-reacting plumes and serve to augment the turbulence when the plume is vertically orientated, see Rodi (1978). The suppression of turbulence by

combustion must therefore be due to the dilatation effects. This may be easily seen, Jones (1982), by reference to the production term of the balance equation for turbulence kinetic energy k:

$$- (\overline{u'^2} \frac{\partial \bar{u}}{\partial x} + \overline{v'^2} \frac{\partial \bar{v}}{\partial y} + \overline{u'v'} \frac{\partial \bar{u}}{\partial y}) \sim \frac{dk}{dt}$$

Further evidence of the effect is offered by Fig. (2.32) which suggests that turbulence intensity is slightly higher in the cooler nitrogen-diluted flames and particularly by Fig. (2.33) where the onset of the partially premixed combustion in the lifted flame causes a dramatic reduction in the turbulence intensity.

CHAPTER 3

MEASUREMENTS IN A GAS-FIRED CYLINDRICAL FURNACE

3.1 Introduction

A new cylindrical, axisymmetrical and vertically oriented laboratory furnace has been designed, built and commissioned to obtain data for the experimental circumstances of coal firing. The data can be used first to play a significant part in a concentrated effort to develop models of combustion/heat transfer systems and second to provide, wherever possible, immediately applicable results whether these be in the field of engineering design (burner applications for example), of methods of measurements or in any relevant field of activity. As a logical step in the run up to the coal firing experiment, a considerable amount of data has been collected for gas firing. This is mainly intended to assist the validation of combustion prediction procedures.

The furnace is 0.6 m diameter and about 4 m long, its size is sufficient to render significant the role of thermal radiation of the walls and also to ensure fully developed turbulent flow. Particular care has been taken to ensure axisymmetrical flow conditions. The burner is an industrial type concentric device with variable swirl and quarl. Results have been obtained for two excess air levels and for zero swirl and swirl number of 0.56. The fuel used is British North Sea natural gas which contains about 94% methane (CH_4). Very fine wire thermocouple has been deployed to map the gas temperatures. For species concentrations, comparative measurements have been made using a quartz microprobe,

a water-cooled probe and a direct-quench probe. Incident radiation fluxes to the walls have been obtained with an ellipsoidal radiometer.

The present chapter describes the details of the experiments performed in the gas-fired furnace. The measurements within three turbulent diffusion flames comprised carbon dioxide, carbon monoxide and oxygen concentrations, radiation flux to the furnace walls and temperature distributions. In section (3.2) the experimental details of the test rig are provided. These include the experimental set up, a full description of the furnace, its auxiliary equipments and its burner. The details of the ignition system used to light up the furnace and precautions taken to ensure safe operation of different parts of the test facility are given in section (3.3). Section (3.4) contains the measuring techniques used for concentration, temperature and radiation measurements, including the description of the probes and instrumentation together with an assessment of the accuracy of each technique. The description of the experimental programme is given in section (3.5) together with the presentation and discussion of the concentration, temperature and radiation results.

3.2 Experimental Arrangement

3.2.1 The Furnace

A diagram of the furnace and its auxiliary equipments (cooling water, fuel gas and combustion air supplies, exhaust gas scrubbing system, etc.) is shown in Fig. (3.1) and Panel (3.1).

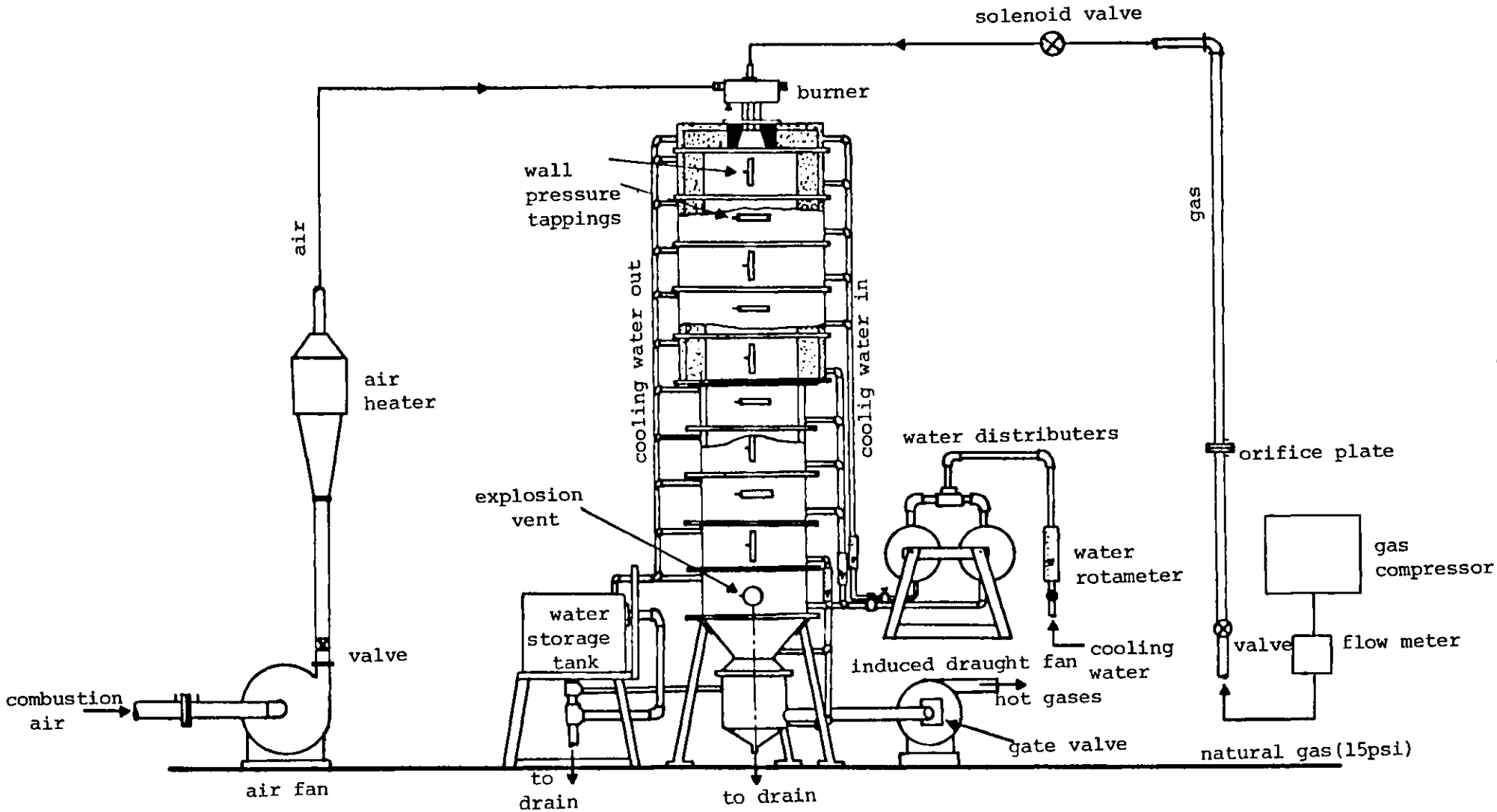

Fig(3.1) Details of furnace arrangement
(gas firing)

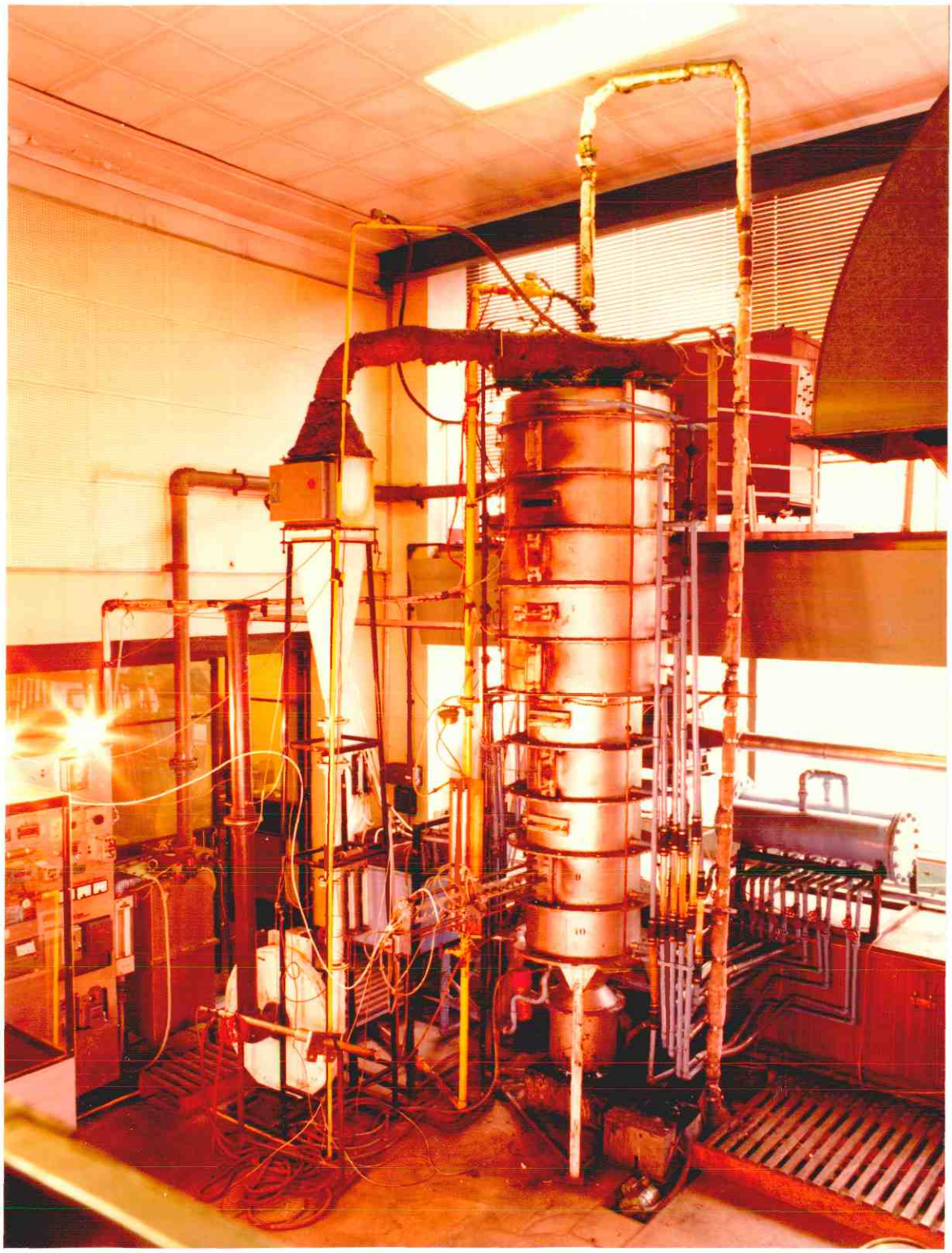

Panel(3.1) Photograph of the furnace arrangements

The furnace was manufactured by the International Flame Research Foundation (IFRF), Ijmuiden, Netherlands. The principal dimensions and design details of the furnace are illustrated in Fig. (3.2). It is cylindrical, oriented vertically to minimize the asymmetric effects due to particle settling and natural convection, and fired from its top end to facilitate particulate and ash removal.

The furnace has a uniform inside diameter of 60 cm and consists of ten interchangeable water-cooled, 30 cm long, segments. As it is presently arranged, Fig. (3.2), the upper five segments, Fig. (3.3), and the furnace roof, Fig. (3.4), are water-cooled and lined with 14 cm thick high quality castable refractory bricks of composition: 24.2% SiO_2, 72.6% Al_2O_3, 0.3%Fe_2O_3, 0.7% TiO_2 and a 0.5% Alkali, and having a maximum operating temperature of 1600^{o}C. Their function is, however, to stabilize pulverized coal flames. The bottom five segments are only cooled by water jackets, Fig. (3.5).

Platinum/platinum - 10% rhodium thermocouples are installed along the walls of the first five segments of the furnace, two in each segment, to measure the wall temperatures. To reduce conduction error their beads, with 2 cm length of wires, are buried in approximately 0.2 cm deep in the walls. Wall temperatures are displayed on a digital voltmeter (type Advance DPM 300 series) using a selector switch (Croydon Precision Instrument Co.) and are used to determine the steady state condition when the data collection can begin. High temperature gaskets interface the furnace segments and completely eliminate all the leakage from/to the furnace.

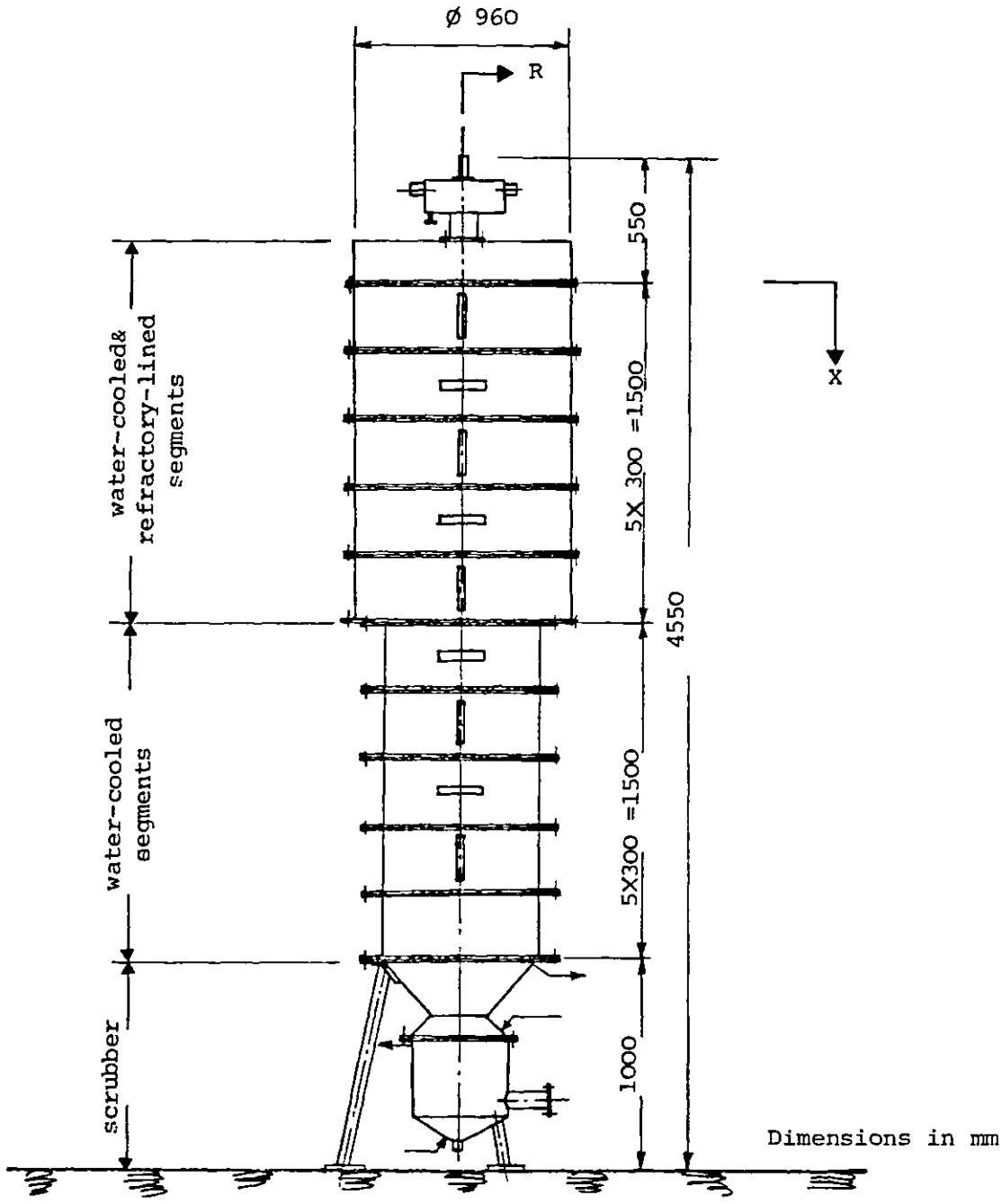

Fig.(3.2) The furnace

Dimensions in mm

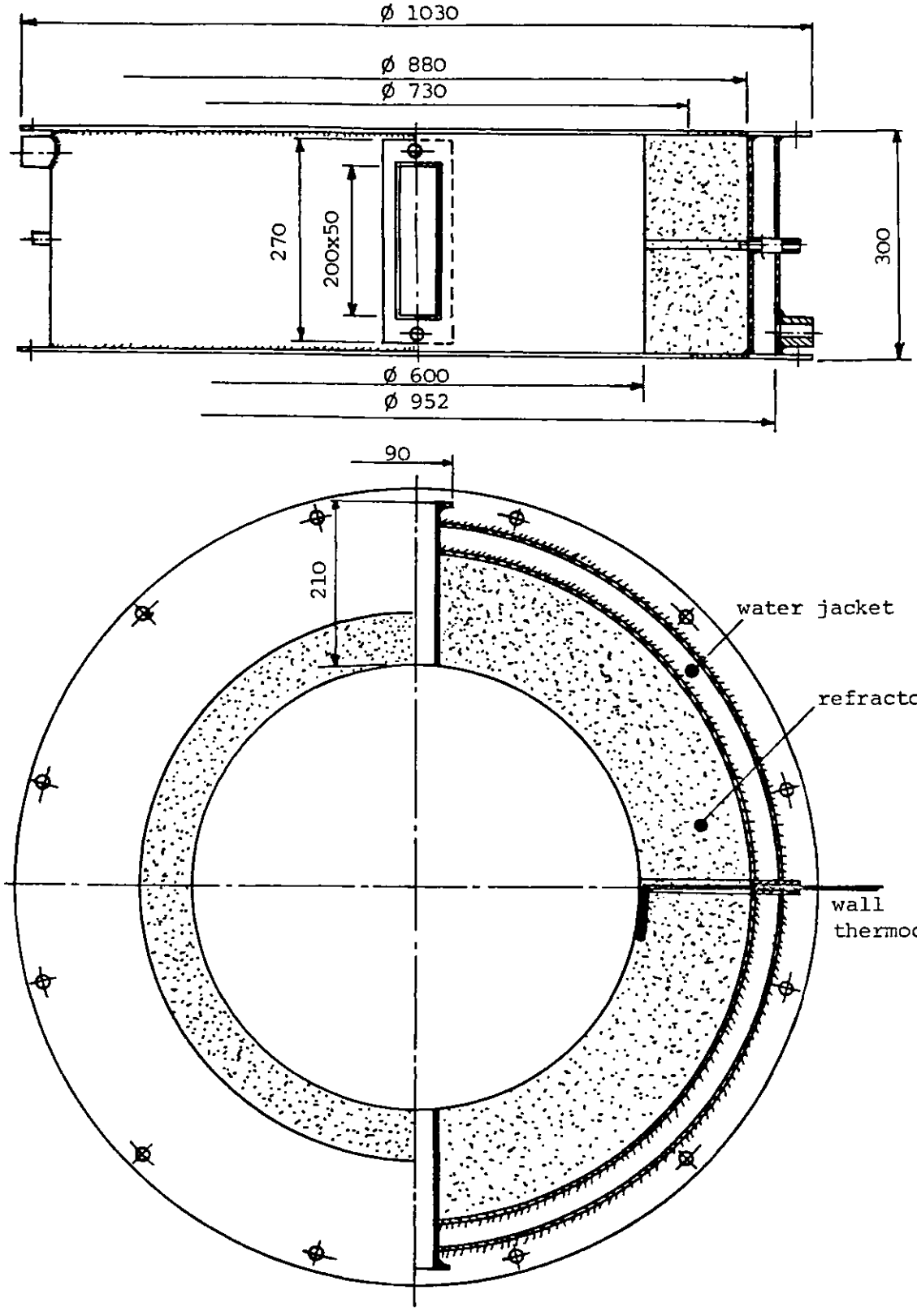

Fig.(3.3) Details of the refractory-lined and water-cooled segment(segments 1 to 5)

Dimensions in mm

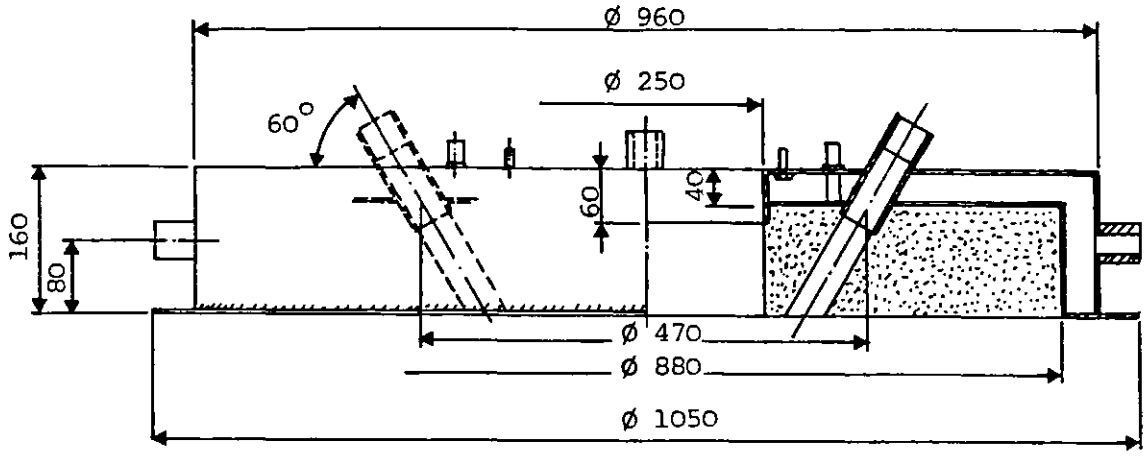

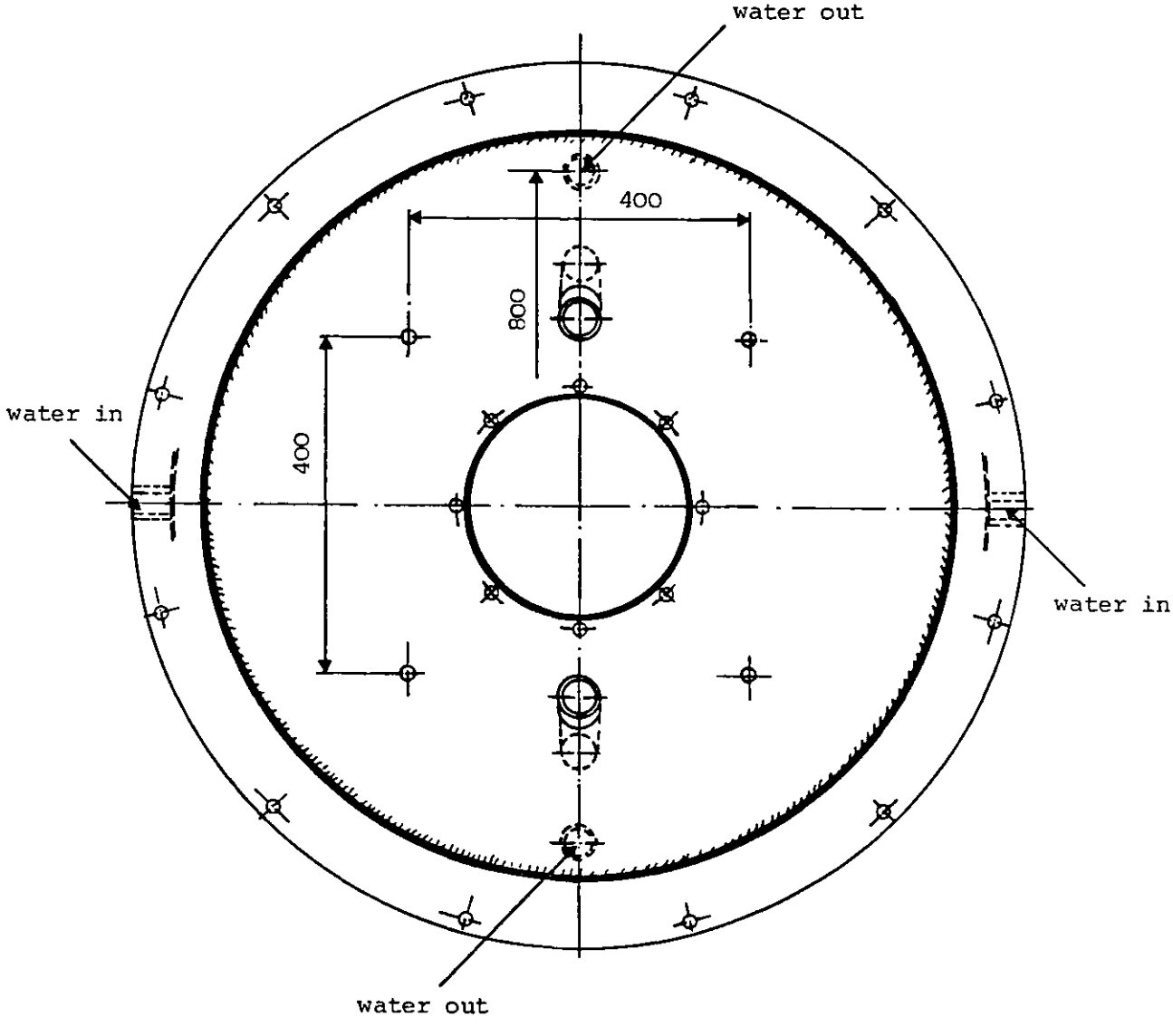

Fig.(3.4) Details of furnace roof

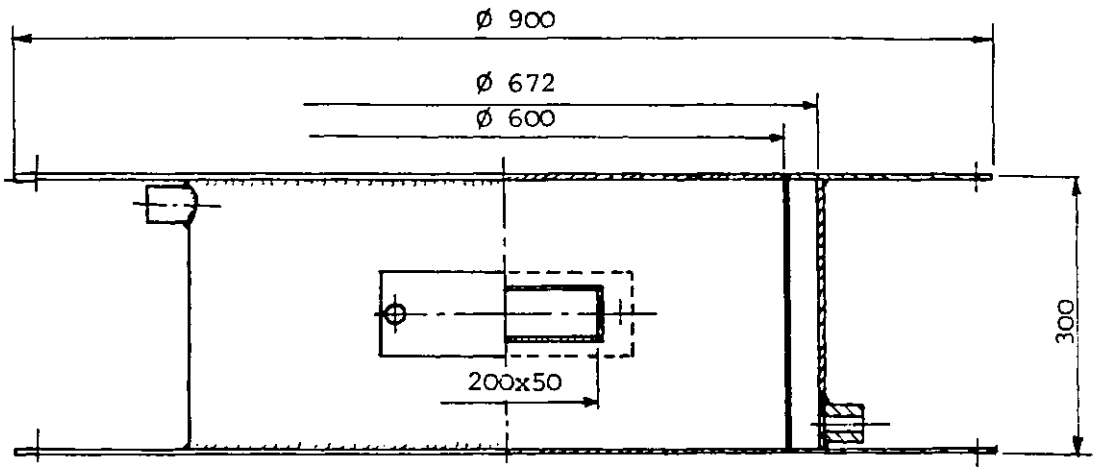

Dimensions in mm

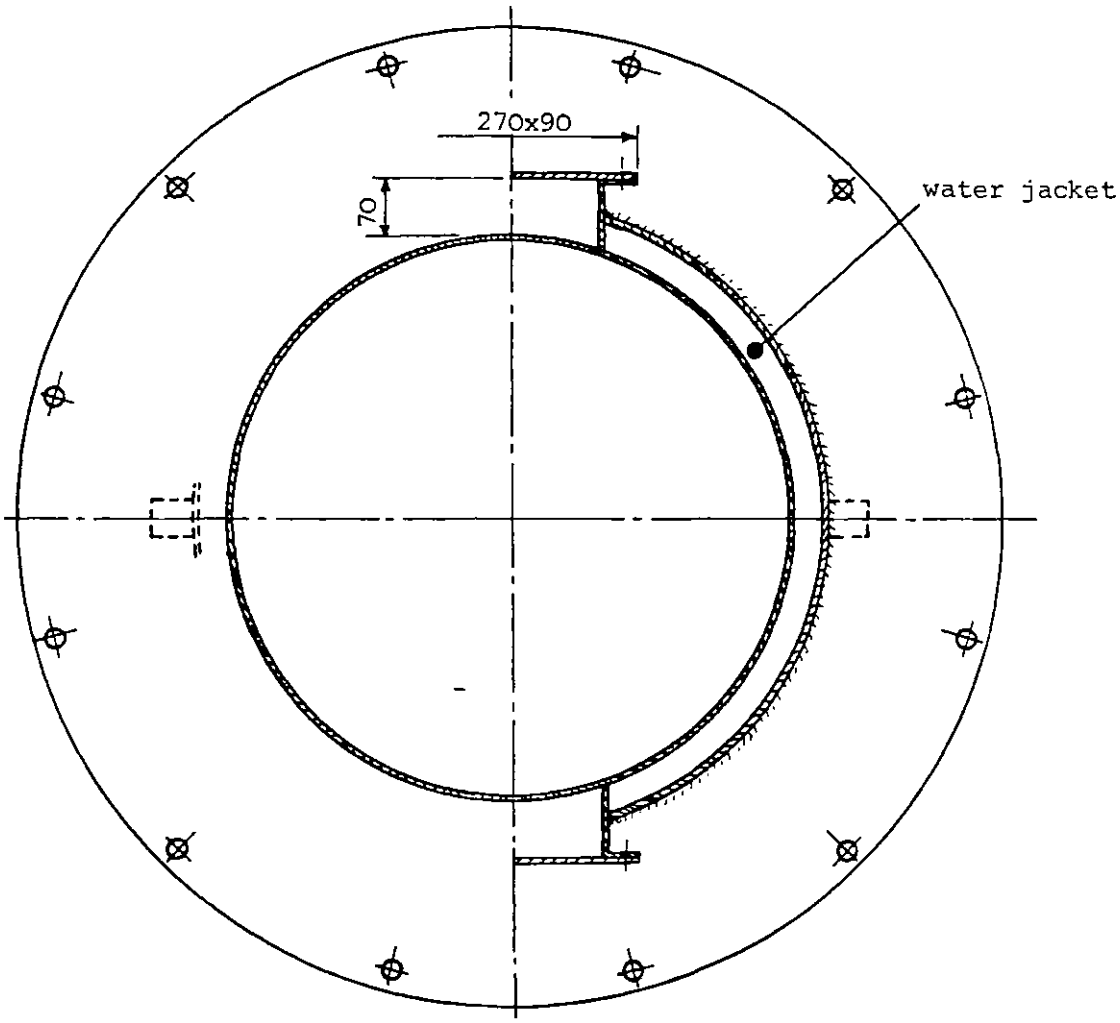

Fig.(3.5) Details of the water-cooled segment
(segments 6 to 9)

The waste gases exit after a convergent section which maintains the flow symmetry. A water spray at the exit of the combustor reduces the temperature of the combustion gases considerably prior to entering the exhaust scrubber. The scrubbing system, which was mainly designed and constructed for coal firing is described in Chapter (4). The flue gases are discharged via an induced draught fan to the laboratory extraction system.

Pairs of diametrically opposite rectangular (5 cm x 15 cm) observation ports (windows) orientated both vertically and horizontally, Fig. (3.2), in the middle of each of the first nine segments of the furnace permit visual observation of the flame and enable direct access for probe measurements. All these ports are normally closed, when not in use, by uncooled sealing covers. The tenth segment is fitted on one side with an explosion vent.

The induced draught fan, fitted with an inlet gate valve, enables the internal furnace pressure to be controlled. The furnace pressure is monitored from wall pressure tappings situated at the side of each window on one side only of the furnace, Fig. (3.1). The pressure is measured by a digital micromanometer (type DMDC Model 4) connected to a 10 pair scanning box (FC 091-2), both manufactured by the Furness Controls Ltd.

The cooling water is distributed to the individual segments at constant rates through two high pressure cylindrical water distributors, Fig. (3.1). The total flowrate is metered, prior to the water distributors by a calibrated water rotameter (Fisher Controls Ltd., type 2000 - TM65 x FMS) fitted with a photo-electric alarm system (Fisher Controls Ltd.), to shut down the fuel supplies (gas and/or

coal) if the water supply drops below the pre-set flow rate. The flow of the cooling water input to the individual segments, which is controlled by manually operated valves, is measured by calibrated rotameters (type 101-24E, Fisher Controls Ltd.) while carefully positioned copper/constantan thermocouples record its temperature immediately at the exit of each segment. The water exit from all the segments is collected in an open tank which drains into the main laboratory drain system.

The combustion air or secondary air is supplied, as it is shown in Fig. (3.1), by a 7.5 kW forced draught fan (type MC - Alldays, Peacock Co. Ltd.) fed to an electric heater via an 8^{o} half angle diffuser. To enhance flow symmetry, a ring of square cross section ducted manifold surrounds the burner and the air is admitted at four spaced radial locations through cylindrical exits to the burner ports, this is shown in Fig. (4.8). The combustion air is metered by a calibrated orifice plate situated at the fan inlet.

United Kingdom North Sea natural gas with composition and properties shown in Table (2.1) is supplied from the low pressure mains to the burner central pipe via a water-cooled compressor (Rotary Compressor Ltd., type 163 CWD) of a maximum exit pressure of 15 psi. A normally closed solenoid valve (Dewraswitch Ltd.) is placed prior to the burner entery to shut down the gas supply in case of flame failure. The gas flow rate is metered by standard (British Gas Corporation) but very precise, displacement meter, and the flow rate is double checked by a calibrated orifice plate.

3.2.2 The Burner

Figure (3.6) shows the assembly drawing of the furnace roof and the burner. Swirl is imparted to the combustion air by a moveable block swirl generator, see Beér and Chigier (1972). The swirl generator is followed by an interchangeable cylindrical duct (inside diameter = 56mm)which leads the combustion air into the burner quarl. The latter is interchangeable and made of castable ceramic. The quarl used for the present tests has a half angle of 24^{0}. The effect of the quarl angle, diameter and length on flame stability was discussed in detail by Fricker and Leuckel (1976). The choice of the inner diameter of quarl and outer diameter of gas nozzle has important consequences on combustion since it controls both the combustion air velocity and the bluff body effect of the fuel nozzle.

Gas is introduced through a central gas injector which has ten holes each 8 mm in diameter arranged symmetrically on the periphery of the injector which has an inside and outside diameters of 25 mm and 30 mm respectively. The injection holes are located at the throat of the quarl. Positioning the gas nozzle at the quarl exit exposes the gas nozzle to the hot gases recirculating within the quarl and may become red hot under some conditions. However, at the burner throat, the gas nozzle lies upstream of the ignition front and is effectively cooled by the gas and air flows. Radial gas injection through a large number of jets at high velocity was found to be very favourable, see Wu (1969). In this situation there is no axial component of the gas momentum which might destroy a weak internal reverse flow zone formed behind

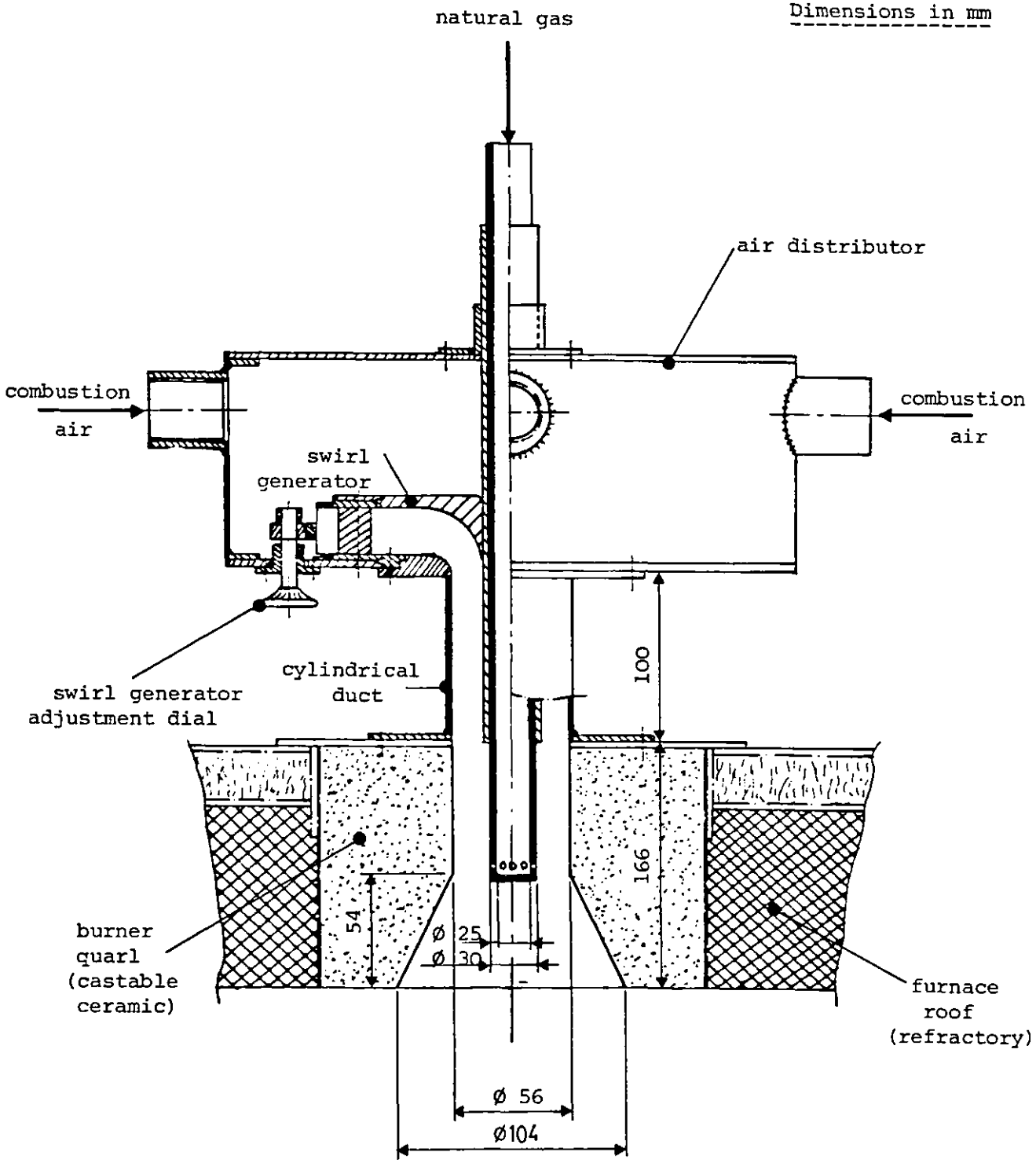

Fig.(3.6) Schematic diagram of gas burner assembly

the gas nozzle at the burner throat with low or zero swirl and the radial gas jets assure rapid and well mixing of fuel and air and seem to add a type of aerodynamic bluff body effect to that of the gas nozzle. Wu (1969), however, argued that concentric or radial injection of the gas has little influence on the flame performance.

As shown in Fig. (3.7), the furnace is lit by an electrically sparked premixed natural gas/air igniter placed in the furnace roof. It is withdrawn after successful ignition to avoid any disturbances to the main flame. The main flame is monitored by two air-cooled ultraviolet flame scanners which are connected with an interlock circuit (see section (3.2.3)) and interrupt the fuel supply on the flame absence. The cross-sectional areas of the igniter and scanners inlets relative to the cross-sectional area of the furnace are negligible. Also the air flow rate, which is used to keep each scanner clean and cool, is less than 1.5 litre/min which is negligible compared to the amount of air used for combustion.

It is a well known fact that one of the most important effects of swirl in combustion is the internal reverse flow zone in the burner quarl region. This region of reverse flow carries hot combusted gases back upstream into the flame root before they lose heat to the surroundings so that an efficient self-stabilizing mechanism for ignition occurs. In addition, the high velocity gradients found near the edge of the internal reverse flow zone improve turbulent mixing between the fuel and air, see Wu and Fricker (1976). The swirl generator, its schematic diagram is shown in Fig. (3.8), consists of two annular plates and two sets of interlocking blocks, one set is fixed in position (triangular blocks) and the other set (wedge-shaped blocks) is moveable, each set being attached to one of the plates.

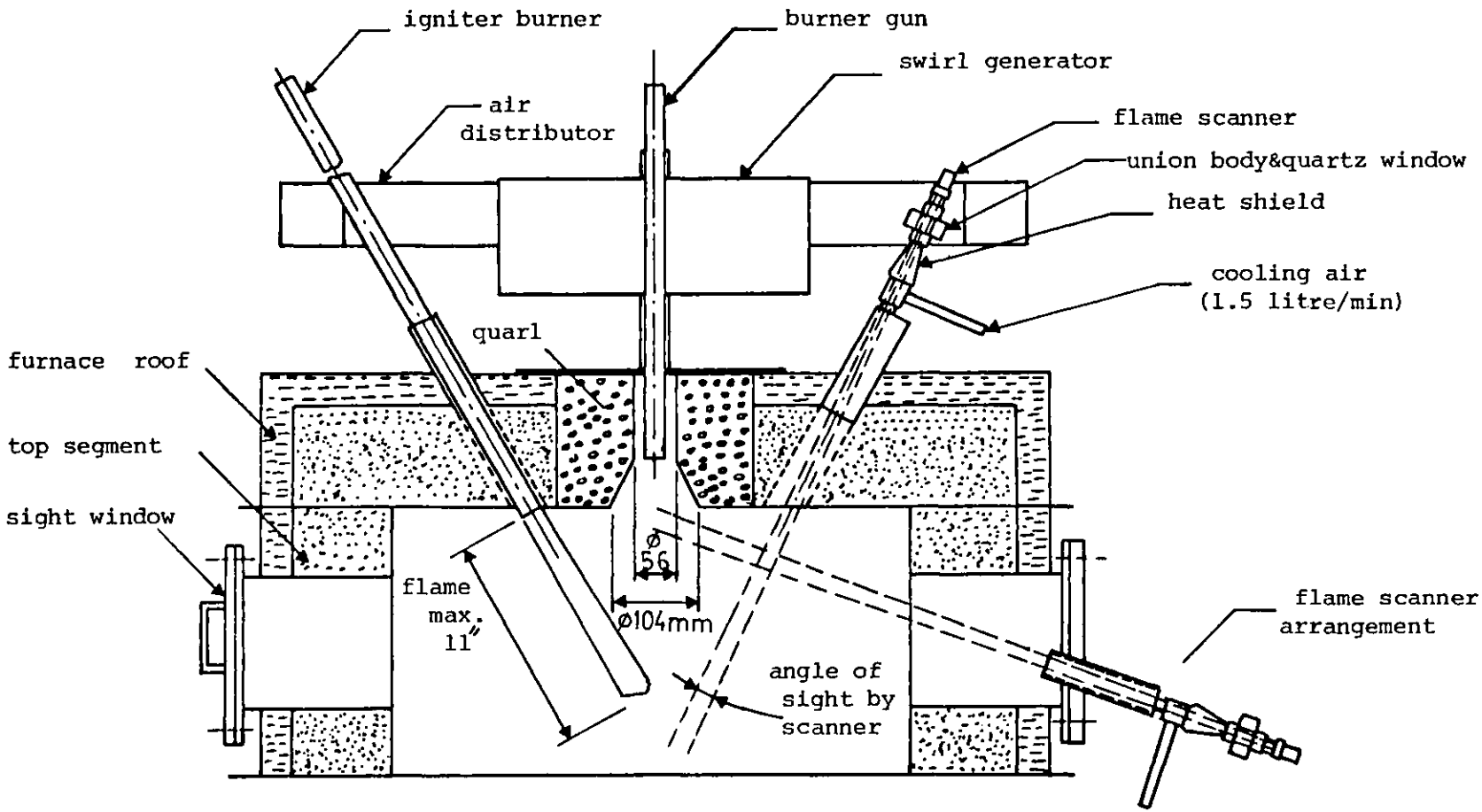

Fig.(3.7) Details of furnace top firing end

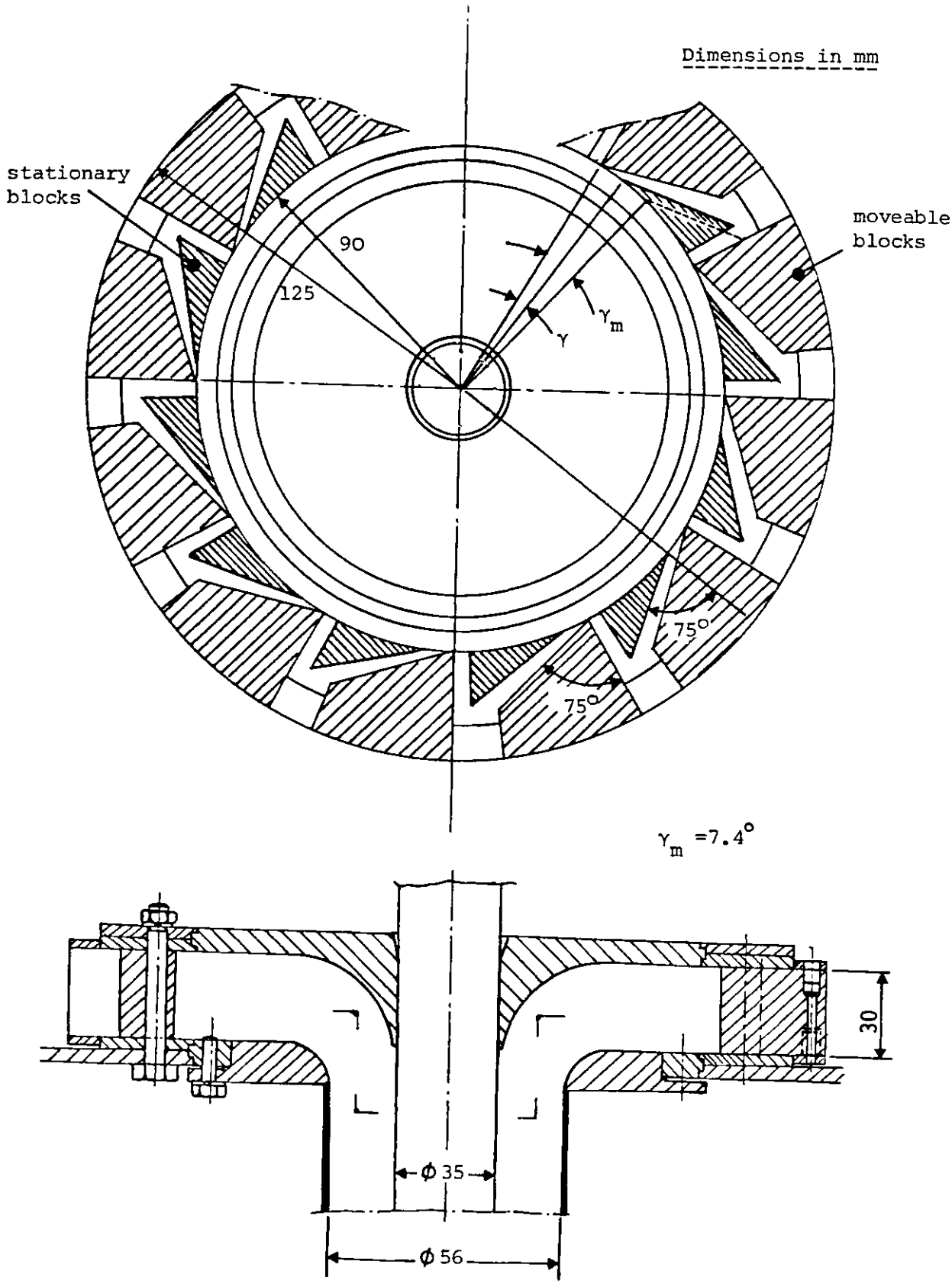

Fig.(3.8) Schematic of swirl generator

The blocks form alternate radial and tangential flow channels, such that the air flow splits into radial and tangential streams which combine further downstream into one swirling flow. By simply rotating the back plate, the front plate being fixed to the burner, radial channels are progressively closed and tangential channels opened or vice versa so that the resulting flux of angular momentum increases continuously, between zero and a maximum value, the latter depending on the geometry of the swirl generator. The swirl generator was constructed entirely of stainless steel to prevent corrosion and warping when heated. The main advantages of such a swirl generator are that it makes changes of swirl intensity during burner operation possible, that the air pressures required for producing a certain swirl level are relatively low, and that it enables high swirl numbers to be obtained. Similar generators were used by Shaffstall and Larson (1973), Leuckel and Fricker (1976) and Harding (1980).

The swirl generator was calibrated with the aid of a honeycomb device (swirl meter), which is shown schematically in Fig. (3.9). The torque on the honeycomb caused by the swirling flow was balanced and measured by a sensitive load cell (Sanganso Schlumberger type D97). This arrangement allowed the force and hence the torque to be measured directly and accurately. Using the torque, and hence the angular momentum together with the axial momentum, a secondary swirl number, S, was calculated using the equation

$$S = \frac{G_\phi}{G_x R_e}$$

where G_ϕ is the axial flux of the angular momentum while G_x is the axial flux of the axial momentum. G_ϕ was taken equal to the

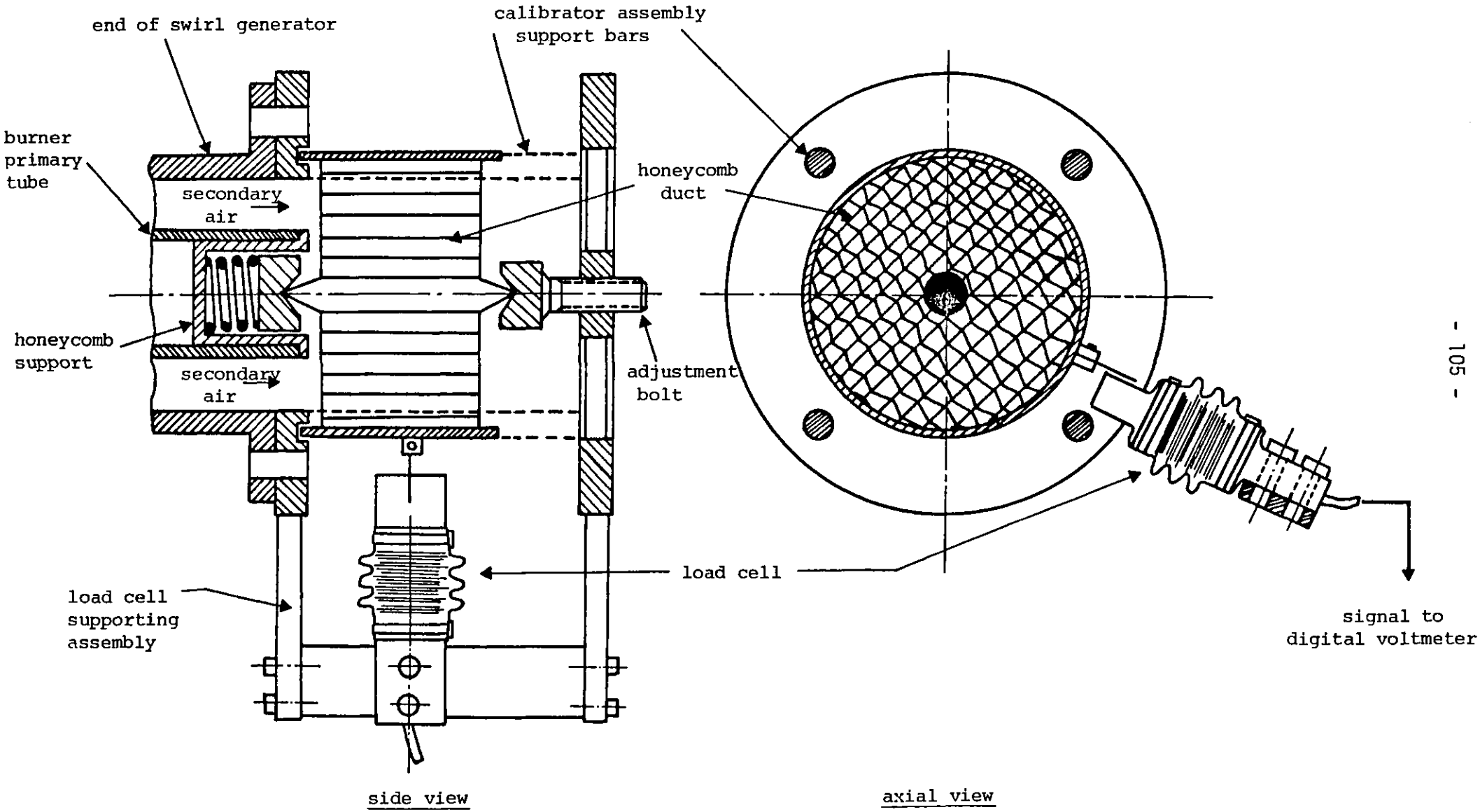

Fig.(3.9) Diagrams of the swirl meter

measured torque on the honeycomb swirl meter and G_x was calculated from the expression:

$$G_x = \rho \dot{q}^2 / A_e$$

where ρ is the air density, $\dot{q}$ is the air flow rate and A_e is the burner throat area expressed as:

$$A_e = \pi(R_e^2 - r_p^2)$$

where R_e is the exit radius of the burner nozzle and r_p is the primary tube radius.

The measured swirl number, for different secondary air flow rates, is shown in Fig. (3.10) as a function of dimensionless adjustment γ/γ_m, see also Fig. (3.8), where γ is the measured angle of adjustment ($0 \leqslant \gamma \leqslant \gamma_m$). As it can be seen, in the air flow range covered by the experiments, the swirl number control curve proved to be independent of the secondary air flow rate. A similar conclusion was obtained by Beér and Chigier (1972). Harding (1980) studied the effect of the secondary air temperature on the calibration of the swirl generator. According to his analysis and with the fact that the swirl number is independent of secondary air flow, Fig. (3.10), the calibration curve for the swirl number will be valid whatever the secondary air temperature.

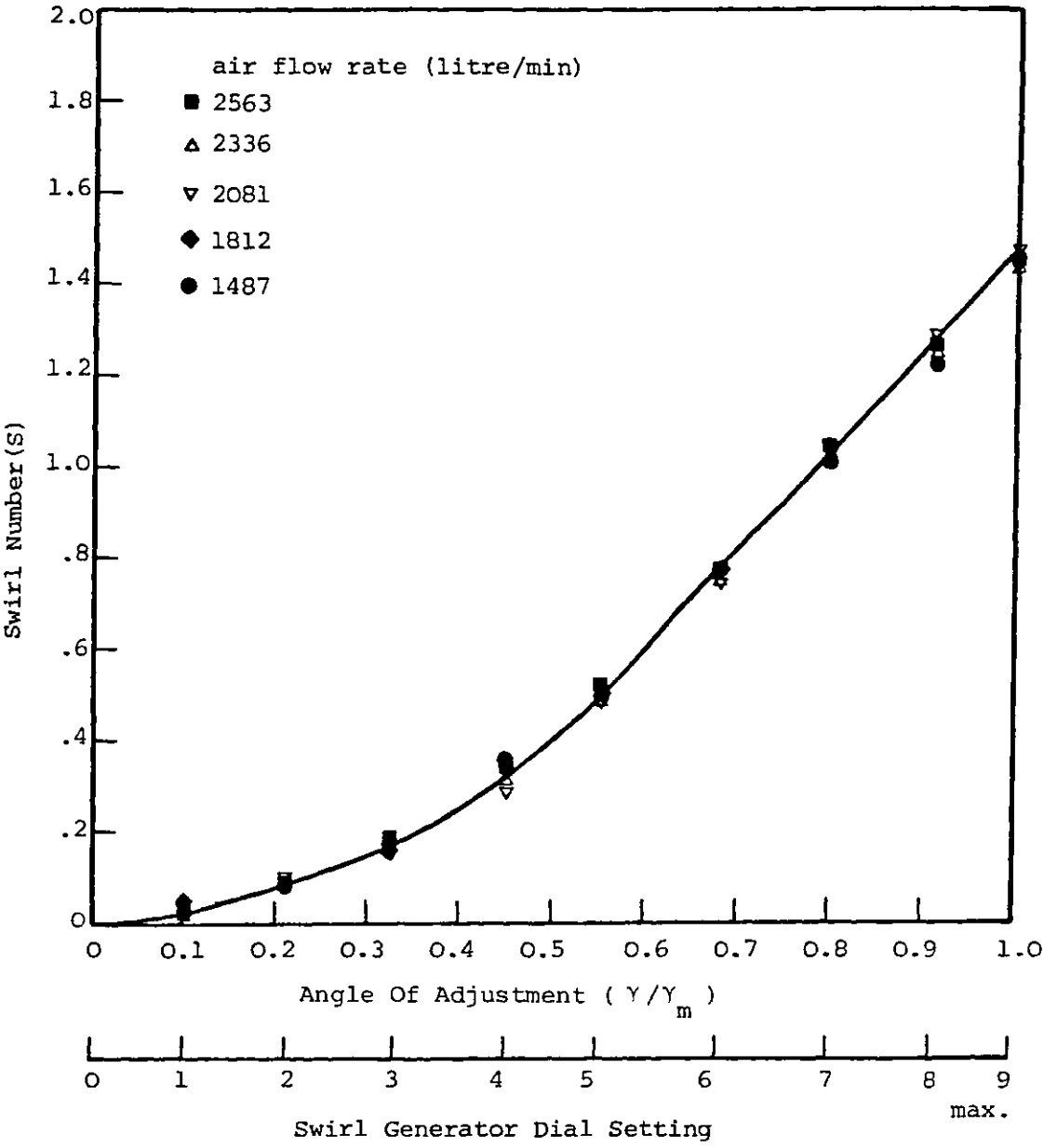

Fig.(3.10) Calibration curve for the swirl generator

3.2.3 Controlled Ignition and Safety Precautions

The ignition system developed by the Industrial Automated Systems Limited (IAS) is used to light up the furnace. It consists of a pilot igniter and a flame supervision system. Safety aspects are given considerable attention. Electric signals are provided for flame on or off, poor cooling water supply, failure of the induced draught fan and exceedingly high temperature in the coal storage hopper. In addition, an interlock system controls the start up and shut down procedures. In the present subsection, the ignition system inclusive of the safety features are explained in detail.

1. Pilot Ignition System

i. Torch igniter

Figure (3.11) shows the details of the P44 Pulse Energy torch igniter construction. It is one meter long approximately with a high quality steel tube housing a concentric conductor rod supported on special insulators. Attached to the firing end is a stainless steel burner head. An ignition coil is supported in gun metal casting at the out board end. The conductor rod performs simultaneously two functions: (1) conveying a voltage from ignition coil to a heat-resistance spark electrode, and (2) serving as the return path for the flame current via a secondary winding of the coil to the flame current amplifier.

ii. Air/gas premixing unit

A mixture of air and gas is provided by the premix unit (type MK6) through a flexible hose to the torch, see Fig. (3.11).

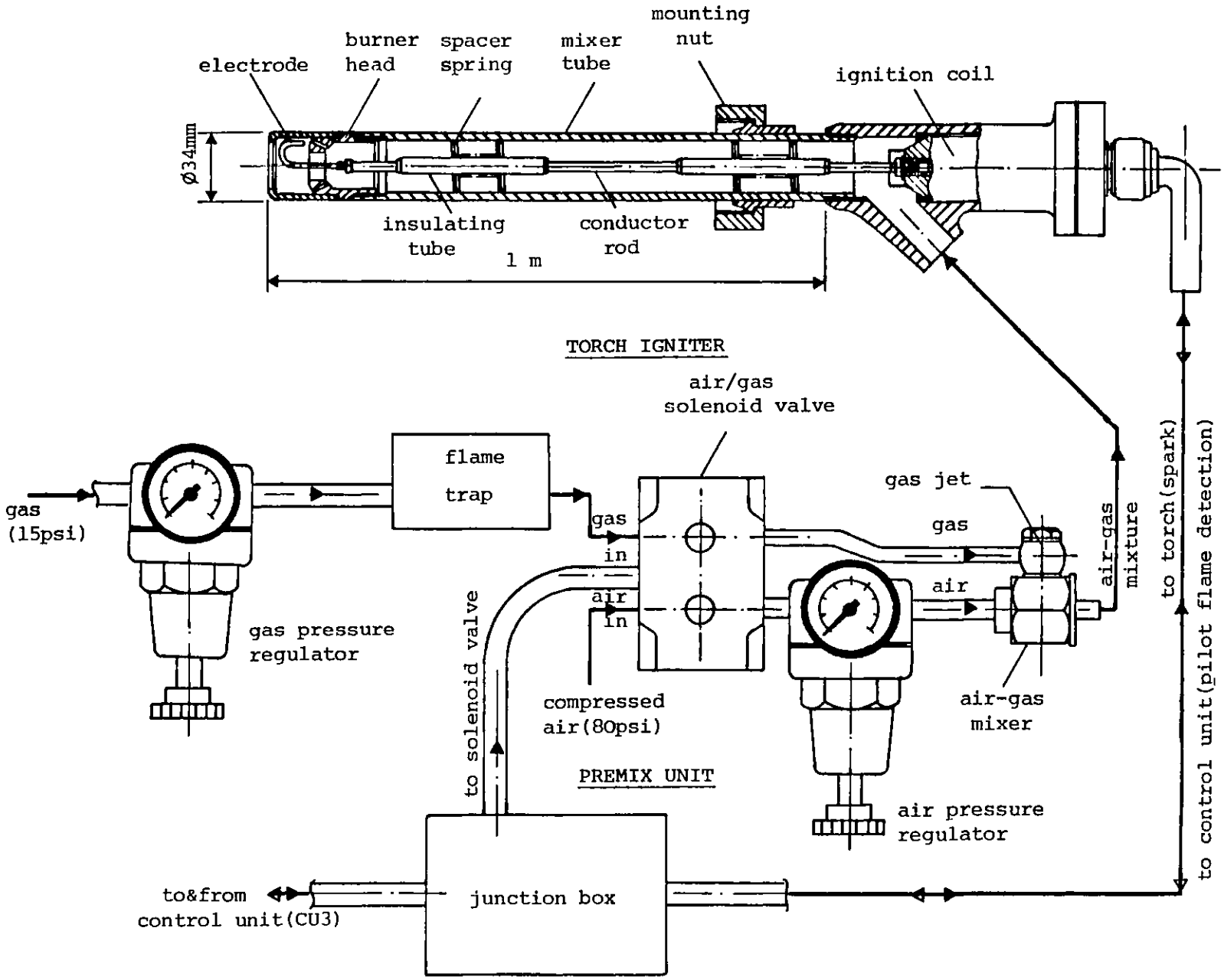

Fig.(3.11) Pilot ignition system

Compressed air is used for combustion to achieve a hard stable flame of maximum heat release. An electrically operated spool valve permits air at pressure of 80 psi to flow to the mixture, while the air pressure operates a normally closed spring valve and allows gas to flow to the mixture at the same time. By interlocking the operation of the gas valve with combustion air pressure, a fail-safe feature is built in, which automatically closes the gas valve in the event of a failure of either the air or electrical supply. The air pressure is dropped to 40 psi through a jet and nozzle mixing arrangement, which controls the size of the pilot flame, and the resulting high velocity flow entrains a regulated amount of gas as air passes on its way to the torch.

iii. The electronic ignition and control unit

An ignition and detection device for providing spark and detection of the pilot flame is used (IAS, type CU3). The CU3 provides a continuous low voltage, low current oscillating pulse signal which when applied to the ignition coil, produces in turn a high voltage to produce a continuous spark for ignition. The unit is energized by a manual push button. At all times the start button is depressed, the unit provides an output which opens a gas/air mixture normally closed solenoid valve (Dewraswitch Limited) prior to the torch. In case of failure to achieve immediate pilot ignition, the button is released and sufficient time is allowed for purging before attempting re-ignition.

Flame rectification is the principle by which the pilot flame is detected by the CU3 device, which uses the ability of a flame to

act as a rectifier when an alternating potential is applied to electrodes having unequal flame contact areas. The pilot detection circuit utilizes part of the spark generation circuit and a common probe (torch electrode) is used for spark and pilot flame detection. It should be noted that the detection circuit functions only when the start push button is released.

2. Main Flame Supervision System

i. Flame scanners

Flame scanners are used for monitoring the main burner flame, i.e. to terminate the fuel supplies on loss of ultraviolet signals from the flame using normally closed solenoid valves (Dewraswitch Ltd.). Two ultraviolet scanners (Type UA1A6) are sited in such a manner, see Fig. (3.7), that at no time can they see the pilot flame. Also, they view two areas in the first one third of the flame,taken from the point where the flame begins, for maximum radiation ultraviolet signal from the flame. This arrangement ensures reliable and sensible detection of the main burner flame.

Because it was necessary to keep the scanners cool (temperature below $52^{o}C$) and clean, in order to avoid nuisance shut-downs, a special mounting arrangement is employed, Fig. (3.7). It comprises: (i) an insulating union to reduce conduction heat, (ii) a quartz window union to seal off the furnace pressure, (iii) cooling air (1.5 litre/min max. flow rate) to reduce the

site pipe temperature and to push the combustion gases out of the scanner arrangement and (iv) nickel-chromium/nickel-aluminium thermocouple to monitor the scanner temperature.

ii. Control unit

The Fireye Burner Management Control Series D41 is used to provide ignition and flame failure protection for the manually ignited gas, gas/coal, or coal flames. The flame failure response time of this unit is four seconds but this time was reduced to one second by using an amplifier (Type 72 DUV1). Additionally, it accommodates momentary power loss of approximately two seconds, and permits the burner to continue to fire provided the flame remains normal.

Finally the sequence of flame ignition operation can be summarized as: (1) pilot flame ignited, (2) a manual push button is pressed. This immediately energizes the main fuel valves, an indication lamp lights when the scanners see the flame, the button is released, and the flame relay then holds the fuel valves open. It must be noted that the fuel valves are open when the button is depressed. If failure to achieve ignition occurs, then safe purging is performed before a repeat start is made.

The electronic circuits of both igniter and that of the main flame supervision system were combined together and modified to incorporate many safety features, see Fig. (3.12) for the complete circuit diagram. Using a relay switch (RS Components Ltd.) the igniter burner and the main flame ignition systems were linked together in order to avoid any attempt to light up the burner flame

1.limit switch on igniter burner
2.photo-electric cell on water supply
3.limit switch on main burner
4.pressure switch on exhaust pipe
5.selector switch
6.gas solenoid valve
7.primary air solenoid valve
8.screw feeder
9.primary air heater
10.vibrators
11.relay switch

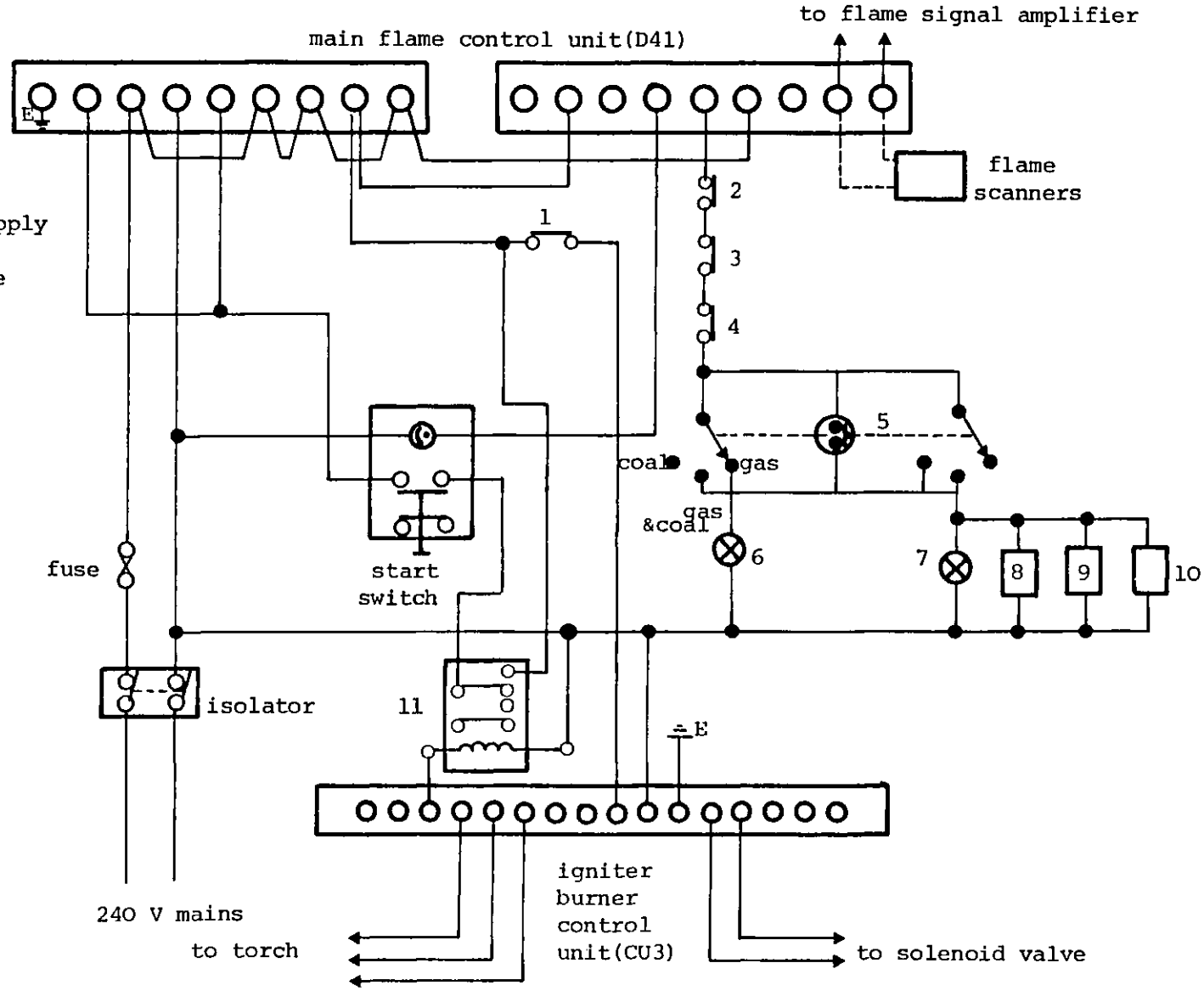

Fig.(3.12) Circuit diagram for furnace control

while the pilot flame is not "on". A limit switch (Mini Switch type MN-E2 by Craig and Derricoll Ltd.); an electric lever device which only will pass power when the lever is depressed, was fixed in its "on" position on the igniter burner tube to make sure that unless the pilot burner is in position inside the furnace, the pilot flame ignition procedure will not succeed. Another limit switch was fixed in the "on" position, to the burner fuel pipe such that the main flame will not ignite if the burner tube is not in its place. A pressure switch (ACTU type LDH/1) activated by a small pressure difference in the range of 0.63 to 3.24 mbar was fitted on the exhaust pipe prior to the induced draught fan to shut down the main flame in case of induced fan failure. An adjustable photo-electric alarm (Fisher Controls Ltd.) was mounted on the main water supply rotameter to close the fuel solenoid valves if the cooling water flow rate drops under a certain minimum value. A flame trap, shown in Fig. (3.11), was fitted to the gas line prior to the igniter burner premix unit to prevent any possibility of flame flash back through the igniter air/gas mixture supply into the premix unit gas supply line. The two scanners, used to supervise the presence of the main flame, were electrically connected in parallel and were used to shut down the fuel supplies if both failed to detect a flame.

3.4 Measuring Instrumentation

3.4.1 Mean Temperature Measurement

Thermocouples are widely recognized as a very useful direct method of measuring local mean temperature in reacting and non-reacting, laminar or turbulent flows. Numerous publications, describing the use of different wire materials, sizes and configurations of the thermocouple probe, are available in the literature. The choice of a thermocouple for flame measurements is dictated by the maximum temperature levels and the melting point of the thermocouple wires. Considerations of the mechanical strength of the wire and its applicability of use in particular situations, such as oxidizing surroundings, have been discussed by Bradley and Mathews (1968).

The mean temperature of a flow can also be measured using water-cooled suction pyrometers, see Khalil et al (1976), El-banhawy (1979) and Attya and Whitelaw (1981) for example . In suction pyrometer probes the thermocouple element is shielded and gases are sucked past it. Shielding the thermocouple significantly reduces the radiant heat transfer (by increasing the temperature of the surroundings seen by the junction) and the suction of gases through the pyrometer increases the convective heat transfer to a level which, in a properly designed probe, renders negligible any radiation loss. The extent to which the true temperature is measured by a sunction pryometer depends on the geometrical details and operating conditions, see Chedaille and Braud (1972) and Khalil (1975). These can be summarized as: the number of shields,

their material and geometry, the suction velocity, the bead position inside the shield and the flow conditions. An estimate of the sources of error associated with the suction pyrometer has been presented by Attya (1983) for example. The suction pyrometer is extremely bulky due to the shields and the presence of the cooling passage. This and the influence of suction, increases the aerodynamic and thermal disturbance to the flow field. The use of the fine thermocouple wires greatly increases the convective heat transfer relative to the radiation transfer. Of particular importance is the minimal aerodynamic and thermal disturbance of the flow offered by the fine thermocouples.

Temperature in combustion systems can also be obtained using optical techniques. Examples of these diagnostic techniques include Raman scattering, Rayleigh scattering, laser flourescence, coherent anti-stokes Raman spectroscopy (CARS) and multichannel pulsed Raman spectroscopy. Some examples of recent applications of these optical techniques to flame studies include the work of Lapp and Hartley(1976), Biarski et al (1978), Hall (1979), Kowalik and Kruger (1979), Sochet et al (1979) and Schoenung and Mitchell (1979). Optical techniques would appear to hold-out the prospect of obtaining, with fairly good spatial resolution, comprehensive time-resolved temperature in combustion systems and because of this great effort is presently being devoted towards their development. Particular stress is being placed on the reduction of background interference, the enhancement of laser intensity impinging on the sample volume, the improvement of electronic detection systems and the devising of good data processing.

Because sophisticated and expensive equipment is required, including a high power laser, spectrometer, optical components and fast on-line minicomputer and because their development is incomplete, optical techniques were not of interest as a diagnostic tool for the present study.

In the present work, temperature measurements were obtained with a fine wire thermocouple probe. Its basic design has been previously used by most investigators, see Odidi (1974), Ballantyne et al (1976), Lenz and Günther (1980) and Moneib (1980) for example. The thermocouple was made of platinum and platinum - 13% rhodium wires of 40 μm diameter and had a hot junction of approximate diameter 50 μm which was formed by electric welding, utilizing a capacitor discharge technique, in the manner explained in detail by Moneib (1980). The hot junction was unshielded and was installed and supported on wires of 500 μm diameter of the same material (platinum/platinum - 13% rhodium) as those of the junction, these wires were supported in a twin-bore alumina sheath with an external diameter of 4 mm. Figure (3.13a) shows the probe details. The fine wire thermocouple was designed so that the wire length between the junction and supporting wire ensures negligible temperature gradient along the wire and consequently minimal conduction heat loss.

The thermocouple indicates its own temperature which generally differs from the actual gas temperature. This difference is due to three principal error sources: (1) conduction in the wires, (2) thermal radiation exchange with the surroundings and in turbulent flows, (3) the thermal inertia of the probe, which because of the finite mass of the thermocouple bead, requires

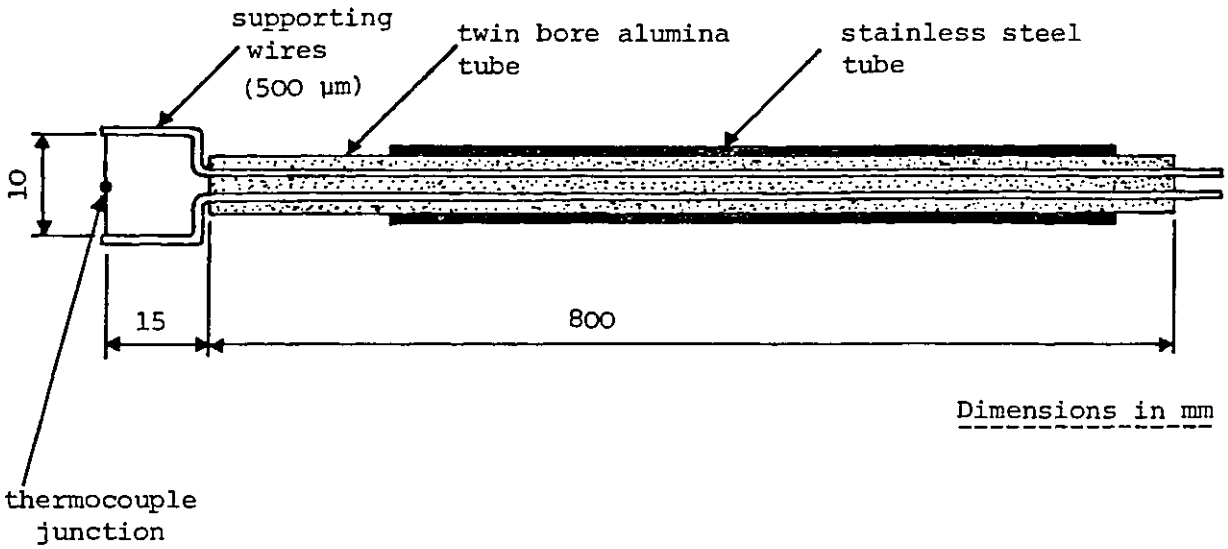

Fig.(3.13a) Design of fine wire thermocouple

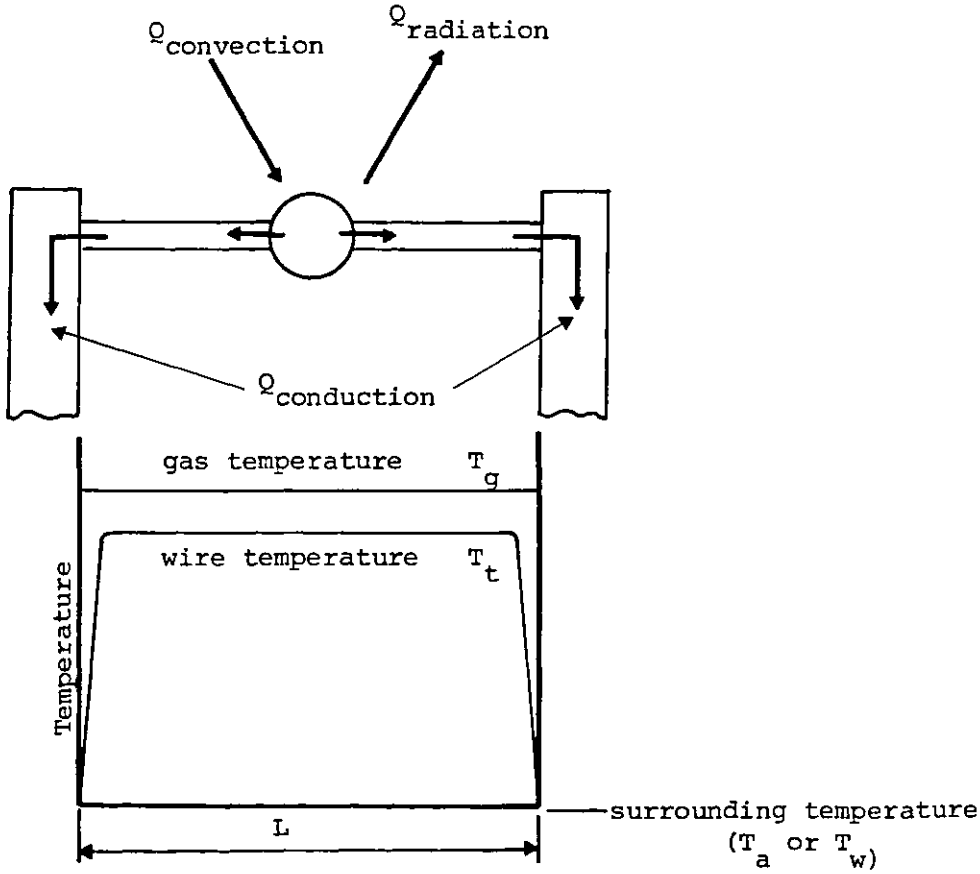

Fig.(3.13b) Modes of heat exchange and
resultant temperature distribution
along the simple supported thermocouple

a finite time to change its temperature. The former sources have been extensively studied by many investigators. Bradley and Mathews (1968) and Sato et al (1975) for example, have obtained numerical solutions of the equations describing the heat transfer modes between the thermocouple and the surroundings. The radiation correction may alternatively be accounted for by experimental methods, see Odidi (1974). The effect of probe thermal inertia was investigated very closely, by Moneib (1980) for example. Catalytic action on the bare wire surface is also a potential source of error, it may be eliminated by coating the wires with non-catalytic materials, see for example Bradley and Mathews (1968), Kent (1970) and Odidi (1974).

Figure (3.13b) is a sketch of the geometry of the simply supported thermocouple employed in the present work on which the principal modes of heat exchange and the resultant temperature distribution along the wire are indicated. The derivation of the general equation that describes the energy exchange between the thermocouple element and the surrounding gas is deduced from the balance of the rate of heat storage and the sum of the rates of energy transfer by conduction, convection and radiation. This energy balance can be written as follows:

$$Q_{conv} + Q_{rad} + Q_{cond} = Q_s \qquad (3.1)$$

where the subscripts conv, rad, cond and s refer respectively to the convection, radiation, conduction and stored energy. For fine wire thermocouples, it can be assumed that the gas surrounding the wire is at constant temperature, and hence the rate of stored energy equals zero, equation (3.1) then becomes:

$$Q_{conv} + Q_{rad} + Q_{cond} = 0 \qquad (3.2)$$

where $Q_{conv} = hA_j(T_g - T_t)$

$$Q_{rad} = -\sigma A_j \varepsilon_t (T_t^4 - T_w^4)$$

$$Q_{cond} = -A_j k_t \frac{\partial^2 T_t}{\partial x^2}$$

So

$$h(T_g - T_t) - \sigma\varepsilon_t(T_t^4 - T_w^4) - \text{conduction} = 0 \qquad (3.3)$$

In turbulent flow, it is evident that h, T_g and hence T_t fluctuate and so $h \equiv \overline{h} + h'$, $T_g \equiv \overline{T}_g + T_g'$, $T_t \equiv \overline{T}_t + T_t'$ where $\overline{h}$, $\overline{T}_g$, $\overline{T}_t$ are the time averaging quantities and h', T_g', T' are the fluctuating quantities. By time averaging and rearranging of equation (3.3), the expression relating the wire and gas mean temperatures can be written as follows:

$$\overline{T}_t = \overline{T}_g \underbrace{- \frac{\sigma\varepsilon_t}{\overline{h}}(\overline{T}_t^4 - \overline{T}_w^4)}_{\text{radiation term}} \underbrace{- \frac{\sigma\varepsilon_t \overline{T}_t^4}{\overline{h}} \left[6 \frac{\overline{(T_t')^2}}{\overline{T}^2} + 4 \frac{\overline{(T_t')^3}}{\overline{T}^3} + \frac{\overline{(T_t')^4}}{\overline{T}^4}\right]}_{\text{temperature fluctuation term}}$$

$$\underbrace{- \left(\frac{\overline{h'T_t'}}{\overline{h}} - \frac{\overline{h'T_g'}}{\overline{h}}\right)}_{\text{correlation term}} - \text{conduction} \qquad (3.4)$$

This equation indicates the contribution of the fluctuating quantities to the temperature measured by the fine wire thermocouple, including radiation and conduction heat transfers, and reveals a further source of possible imprecision. It is clear that the correlation and temperature fluctuation terms in equation (3.4) are difficult to quantify exactly but their order of magnitude can be estimated by close inspection of the temperature results reported by Moneib (1980).

Some of Moneib's (1980) results for temperature measurements in a gaseous diffusion flame are reproduced in Fig. (3.14) and show the axial distribution of the mean temperatures for stabilized flame SA2, see Table (2.3), with 40 μm and 20 μm as well as 15 μm diameter thermocouples of a similar design to the present probe, are identical. A maximum spread of 30°C gives a fair indication of the experimental repeatability. The terms on the right hand side of equation (3.4) are all dependent on the wire diameter and, to achieve the result of Fig. (3.14), the values of the terms involving correlations and temperature fluctuations must be of a similar magnitude to the radiation and conduction heat losses and with positive sign. For wires diameter 40 μm or less, the conduction error is negligible and that due to radiation is less than 40°C, as reported by Moneib (1980). Also it is clear from equation (3.4) that an increase in the wire diameter will be associated with a reduction in the temperature fluctuation term and increase in the correlation term $(\frac{\overline{h'T_g'}}{\bar{h}} - \frac{\overline{h'T_t'}}{\bar{h}})$; however the difference between them will be balanced by an increase in the radiation heat losses.

Although there is insufficient direct evidence of the magnitudes of the correlation terms in equation (3.4), it can be concluded that the use of 40 μm fine wire thermocouple will allow measurement of the true time averaged gas temperature with an expected uncertainty of not more than 40°C.

The catalytic error is ignored in the present measurements. There is perhaps reason to suspect that this is not justifiable for a hydrocarbon fuel. A few experiments, using bare and non-catalytic ceramic coated 120 μm thermocouple probes, have been performed by Odidi (1974)

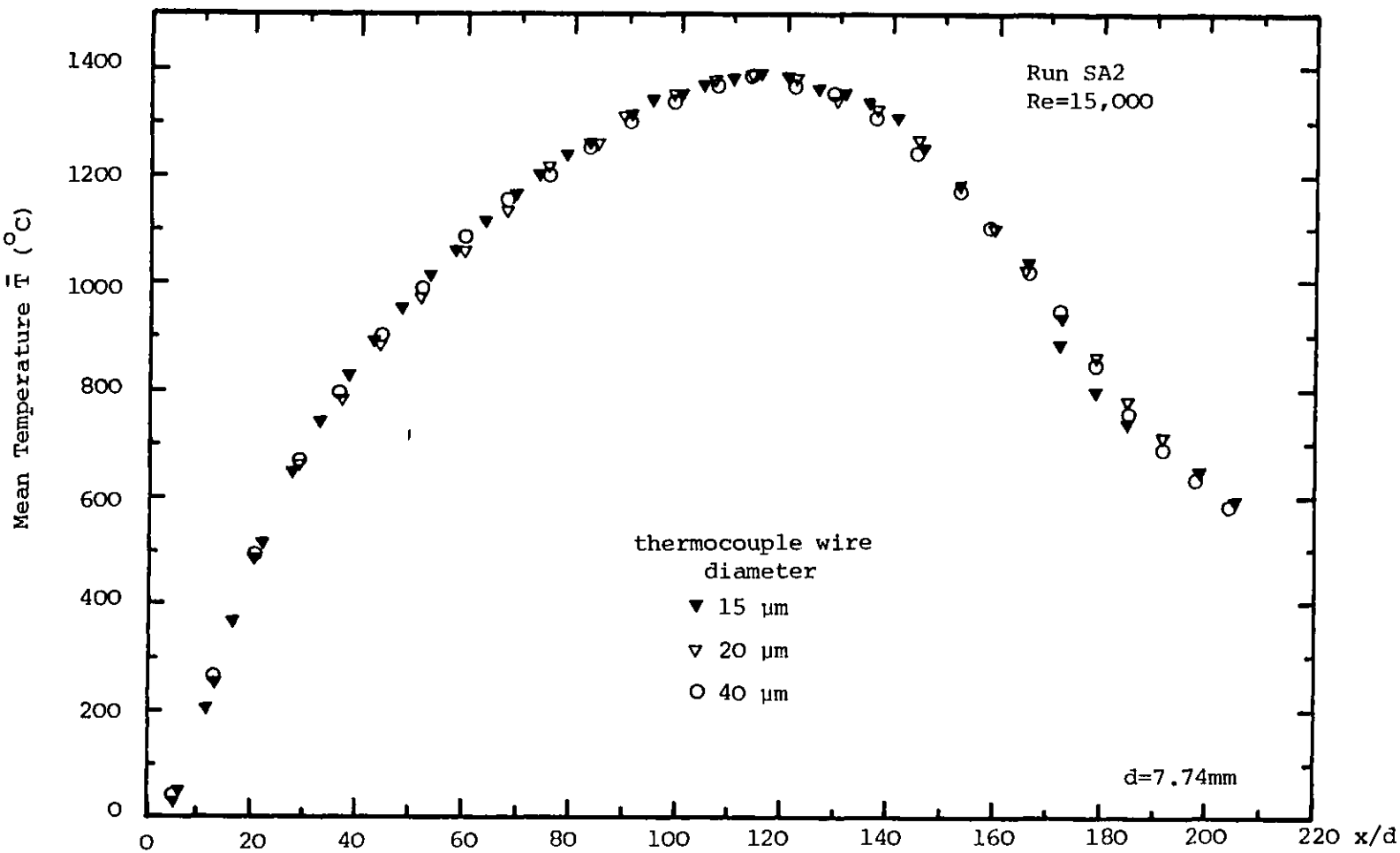

Fig.(3.14) Effect of thermocouple wire diameter on the mean temperature.(Axial distribution of mean temperature-Moneib(1980)-stabilized flame,run SA2,see table(2.2))

These suggested that the effect of catalytic coating on the mean temperature is smaller than the magnitude of radiation correction, but the evidence is hardly conclusive.

Figure (3.15) shows the temperature measurement instrumentation. At each measurement location, the thermocouple signal, after being filtered by a low pass filter, was multiplied by a factor of 100 using a differential amplifier OP-07 giving an e.m.f. in the range of 0-2 volts. The signal was then integrated by a true integrator (DISA type 52B30) over a period of 50 seconds and the integrator output was displayed on a digital voltmeter (Solartron DVM). An ensembled average of at least ten readings was obtained at each point.

3.4.2 Radiation Flux Measurement

The knowledge of the radiation characteristics is important for the prediction procedures concerning the total combustion systems. A calibrated stainless steel water-cooled hollow ellipsoidal total radiation pyrometer, see Chedaille and Braud (1972), was used for measuring the total radiation flux (kW/m^2) incident on the furnace walls. An enlarged section of the ellipsoidal measuring head is shown in Fig. (3.16) together with a detailed drawing of the radiometer. All the radiation falling on a small thin-rimmed circular orifice "O", see Fig. (3.16), which allows all the radiation to enter whatever the angle of incidence, is focussed by the ellipsoidal mirror onto a thermopile which gives a potential difference as a linear function of the energy received.

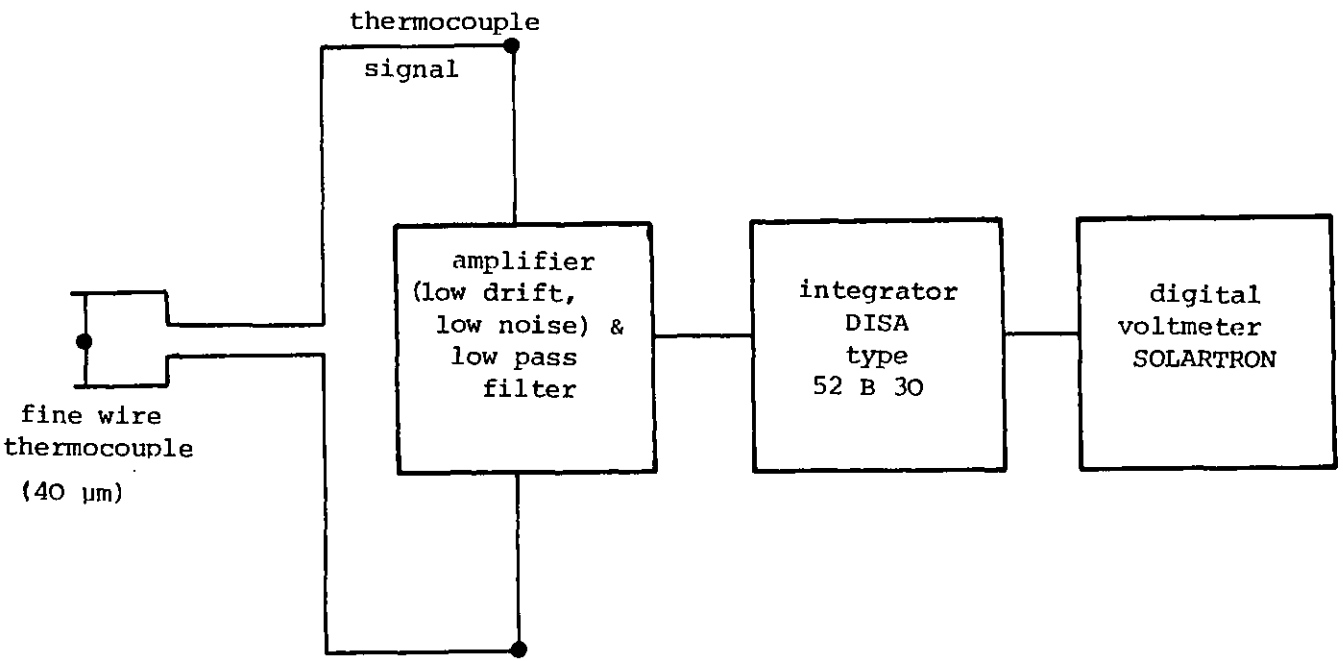

Fig.(3.15) Temperature instrumentation

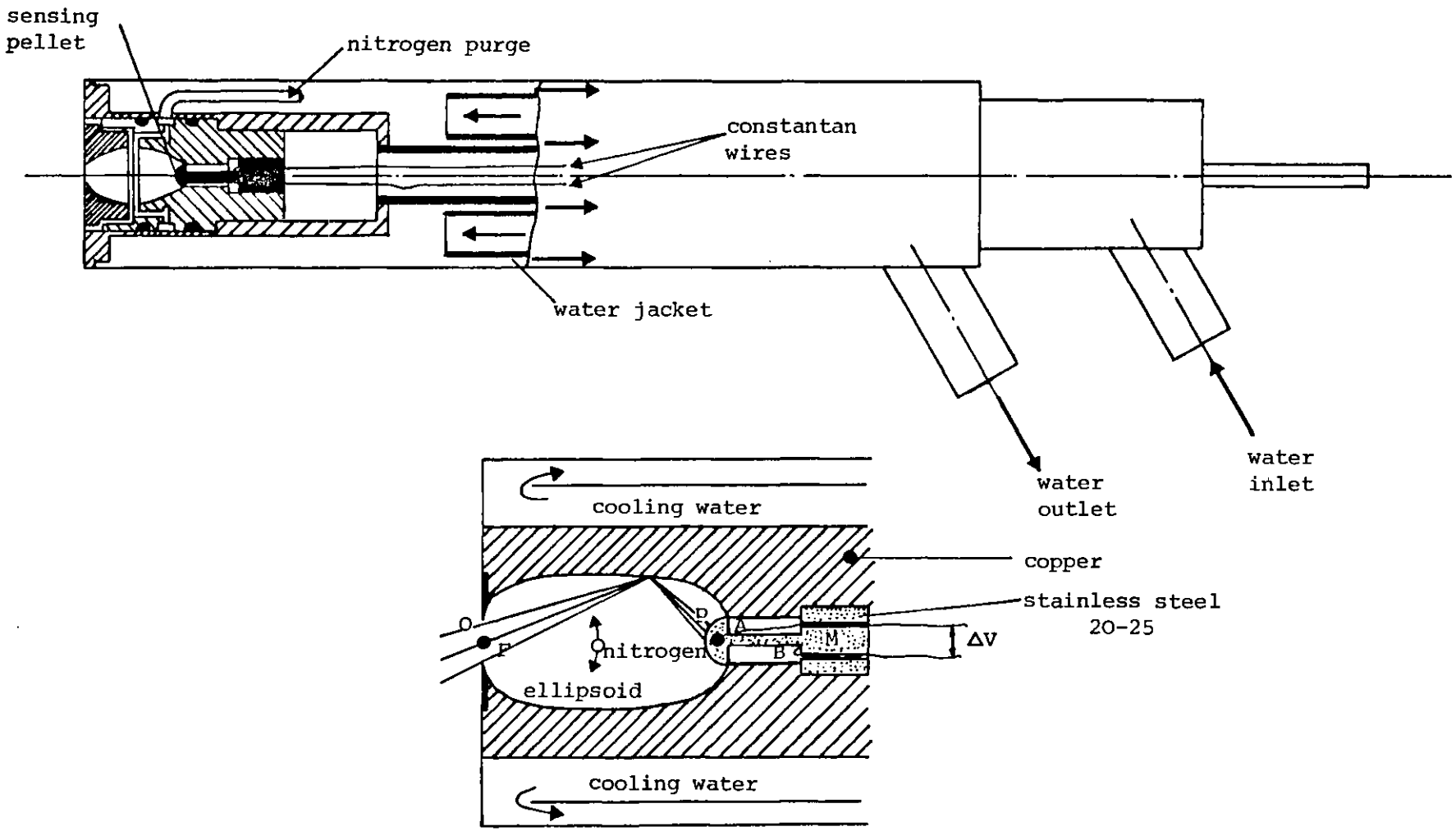

Fig.(3.16) Schematic diagram of the ellipsoidal radiometer

The therompile consists of a hemispherical receiving pellet "P", a 20-25 stainless steel cylinder "AB" and a cooled metal mass "M", the three parts being combined in a common stainless steel block (25% nickel, 25% chromium), in order to obtain a regular flow of heat. The heat sensitive pellet absorbs virtually all the radiation (from 95% to 98%) intercepted by its blackened and oxidized surface. Under steady-state conditions, the rate of heat removal by the cooled metal mass is equal to the rate of heat collection by the pellet. Constantan wires soldered into both ends of the cylinder AB, form a thermocouple which produces e.m.f. proportional to the energy received by the pellet.

Because of the hemispherical shape of the receiving pellet, the diameter of which is slightly larger than that of the orifice "O", all radiation is received after two reflections at the most from the mirror. The ellipsoidal mirror is made of copper covered with a thin layer of polished gold which has a reflection coefficient very close to unity and which is independent of the angle of incident and the wave length. A current of dry nitrogen (0.8 litre/min flow rate) is injected through two small holes distributed in the plane of the mirror axis of the ellipsoidal to prevent combustion gases condensation and particle deposits on the radiometer mirror.

The ellipsoidal heat flow meter was calibrated by subjecting it to the radiation of a black body of a known temperature. The calibration furnace, shown in Fig. (3.17b), is a spherical black body furnace manufactured by the International Flame Research Foundation (IFRF). It comprises an internal sphere having an internal diameter of 30 cm and 2 cm thickness. It is made of coarse

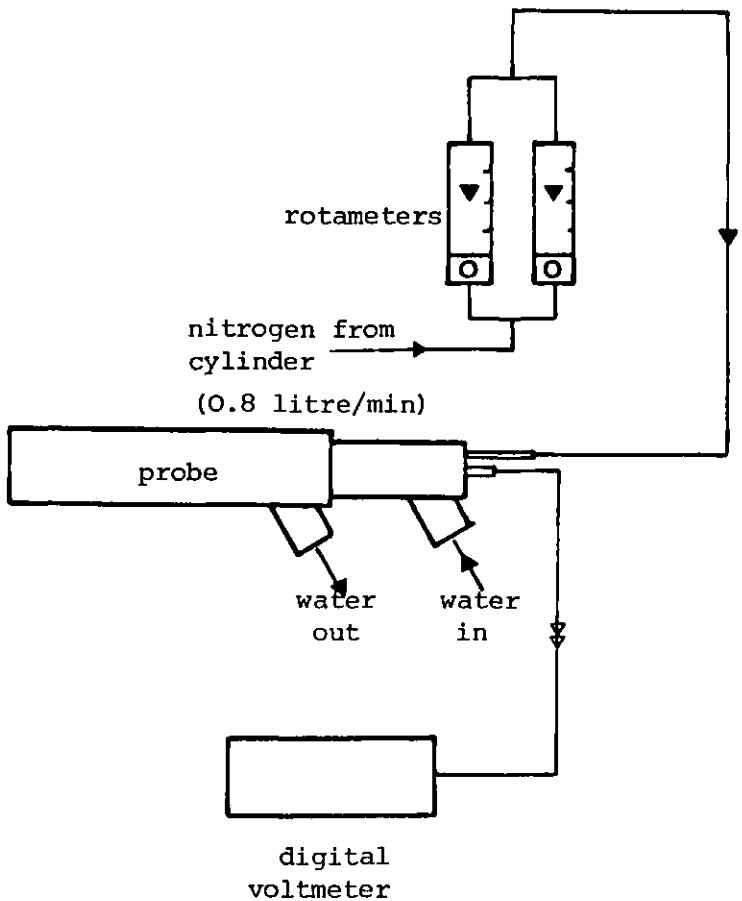

Fig.(3.17a) Instrumentation for incident radiation measurements

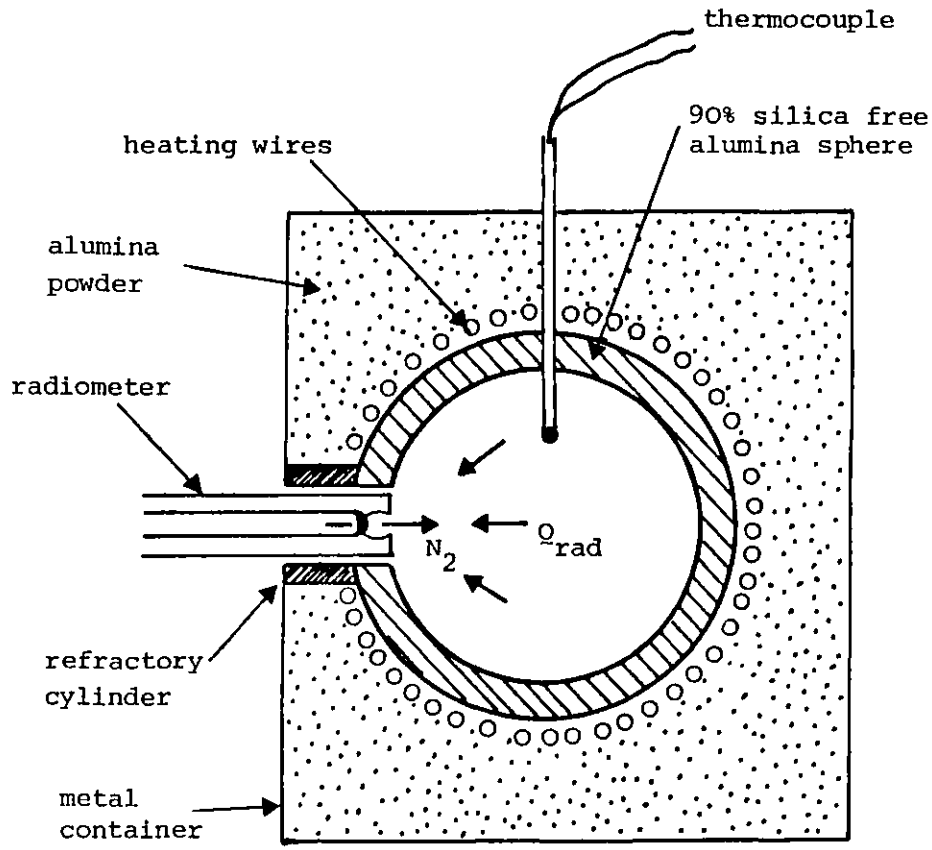

Fig.(3.17b) Ellipsoidal radiometer calibration furnace

grained 90% silica free alumina, and possessing an effective emissivity very close to 0.99. Two heating elements each of approximately 24 ohms resistance, connected in series, are rolled in a spiral form over the internal sphere and embedded in a layer of special cement (Sillimonite Ramming Mix, 5 cm thick). A variac was used to adjust the power to the heating elements. The furnace is placed in alumina powder held in a metal container with the opening extended by a protective refractory cylinder, 65 mm long. A platinum/platinum - 10% rhodium thermocouple protected by a pure calcined alumina sheath, which is inserted about 10 cm into the sphere, serves to measure the furnace equilibrium temperature.

The block diagram of the radiation flux instrumentation is shown in Fig. (3.17a). The response time of the ellipsoidal heat flow meter is of order of one minute and does not therefore follow rapid changes in the flame radiation. The accuracy of the radiation flux measurements depends mainly on the care taken during calibration in the first place, and on the control of the nitrogen flow. According to that, it can be said that the heat flow by radiation was measured to better than 5%.

3.4.3 Concentration Measurement

Samples for the measurements of carbon dioxide, carbon monoxide and oxygen species concentration were withdrawn from different points within the present combustion chamber using a stainless steel water-cooled probe (indirect quenching), panel (a)

of Fig. (3.18). The sampling tube has an inner diameter of 1.2 mm and was surrounded by a water-cooled arrangement comprising two tubes 2.65 mm and 9.53 mm external diameters for water inlet and outlet respectively. The slender-nosed probe tip is of diameter 2.65 mm at the measuring point. The samples were analyzed on-line using calibrated infrared analyzers, Analytic Development Co. type 483 and 336, for CO_2 and CO measurements respectively, and a paramagnetic analyzer (Taylor Servomex type 540A) for O_2 concentration measurements. Figure (3.19) shows a schematic diagram for the sampling system. All components, lines and fittings of the sampling system were teflon to minimize wall absorption of the sample and to diminish catalytic influences. The unburned hydrocarbon vapours and H_2O were condensed and removed from the sampling line and consequently the reported results of the present concentration measurements are based on a dry-analysis.

The factors influencing the accuracy of the concentration measurements can be divided into two groups. The first, includes these resulting from the probe-gas interference, quenching of the sample and catalytic effects within the probe. The second, includes factors associated with the sample handling and analysis. The problem of probe effects on the concentration in laminar flames, where the probe-gas interference can be significant, was investigated theoretically and experimentally by Fristrom and Westenberg (1965), Yanagi (1972, 1977), Tine (1961) and Yanagi and Mimura (1972) for example. Probe effects were mainly related to the probe size and its operating conditions. In turbulent combusting flows, sampling errors, other than those caused by profile distortion due to the probe body and the suction of gases through it, can

Dimensions in mm

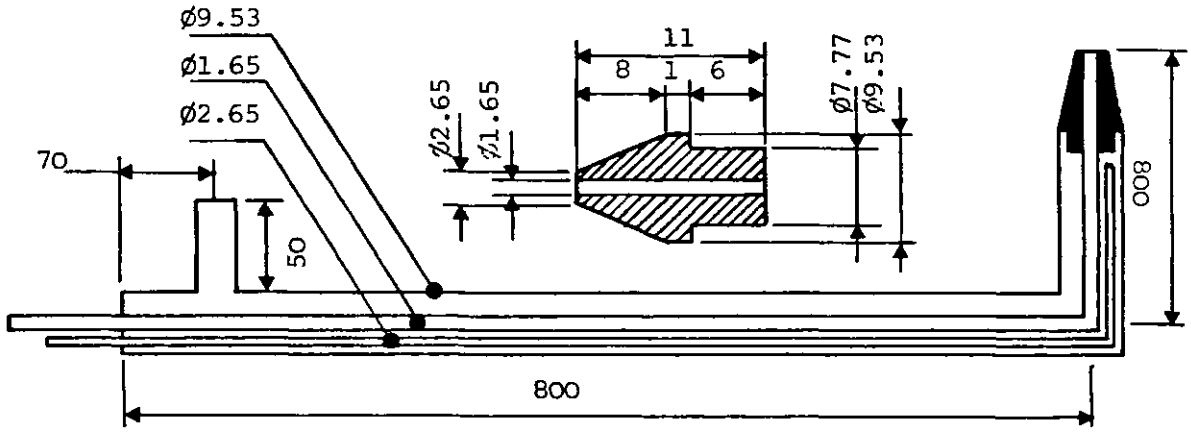

Panel(a) Water-cooled probe

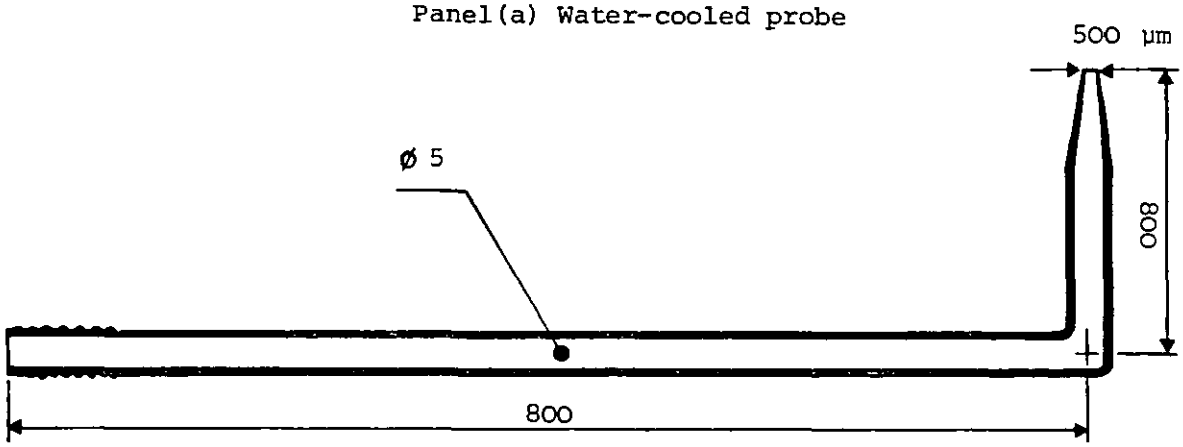

Panel(b) Quartz microprobe

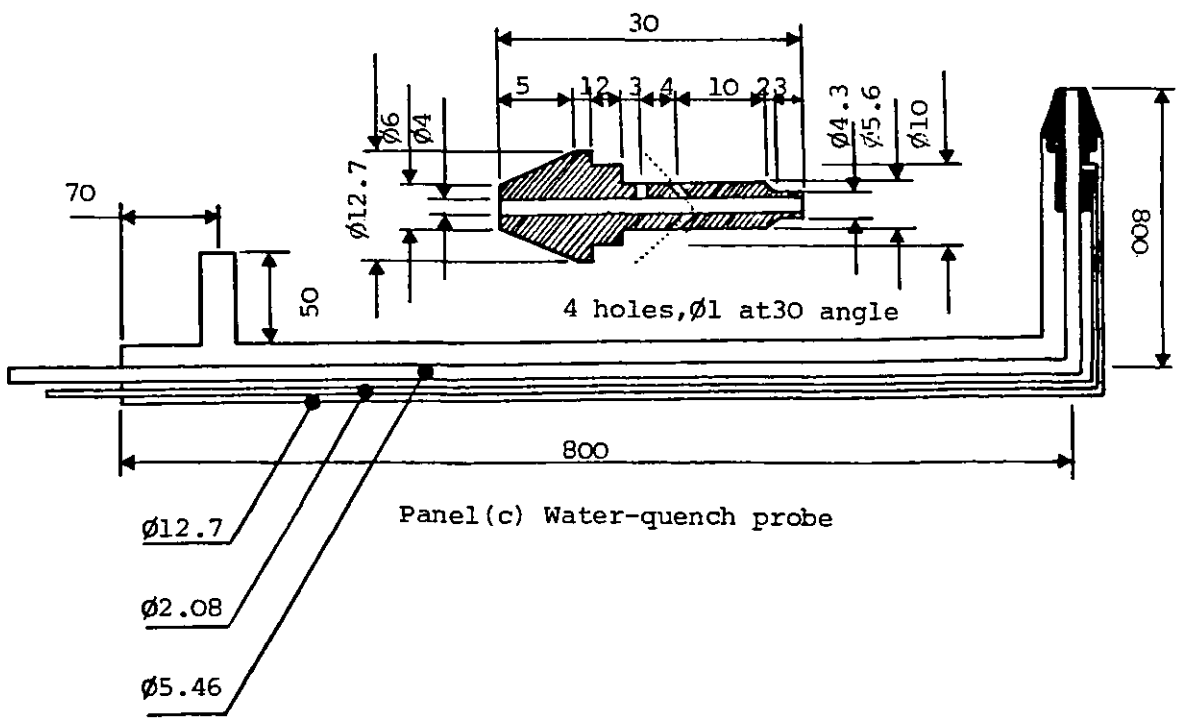

Panel(c) Water-quench probe

Fig.(3.18) Sampling probes

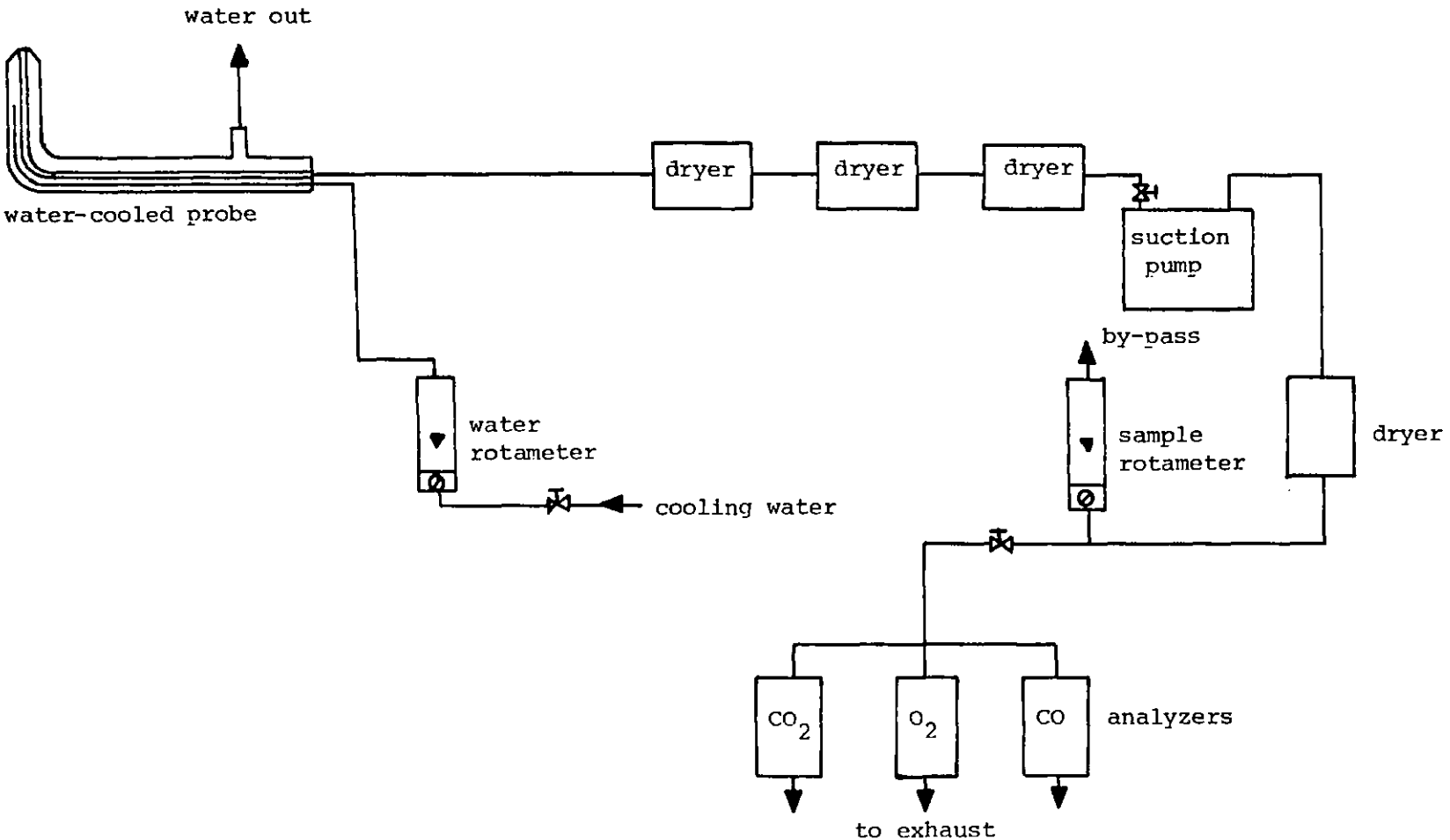

Fig.(3.19) Sketch of sampling system for water-cooled probe

possibly stem from segregation effects especially when sampling under non-isokinetic conditions, Bilger (1977) and Tine (1961). The fluctuating nature of the measured quantities and the large variations in flow conditions from point to point within the turbulent flame, render it difficult to quantify probe interference effects. It should be noted that the interference effects caused by the probe body were minimal due to the small size of the probe (probe to furnace diameter ratio ≈0.03) and the negligible amount of heat transferred to the probe (the maximum rise in the cooling water temperature was less than $5^{o}C$ with water flow rates of less than 1 litre/min).

Sampling probes employing the isokinetic principle (sampling velocity equals gas velocity) were described by Tine (1961), Kent and Bilger (1973b), Vranos et al (1969) and Bowman (1977). They indicated that the sampling error caused by the suction of gases through the probe (profile-distortion and segregation effects in regions of large density fluctuations) can be minimized by keeping the suction velocity equal to that of the gas at the measuring point. However, Tine (1961) had demonstrated large uncertainties in the practical methods used to ensure isokinetic conditions, even in a simple flow configuration. Due to complexity of the aerodynamics of the present flow configuration and the uncertainties associated with achieving isokinetic sampling, non-isokinetic sampling probe (panel (a) of Fig. (3.18)) was used in the present measurements. It is unlikely that sampling errors, induced by catalytic effects of the cool wall of the sample tube, contribute significantly to the overall accuracy of the concentration results, see Tine (1961).

The measured values of species concentrations obtained are subjected to a source of uncertainty which relates to the influence of the fluctuations in the various properties on the type of averaging produced by the probe. During the sampling process, the instantaneous mass conservation of a species i, can be represented by:

$$C_{i_m} \cdot \dot{m}_m = C_{i_t} \cdot \dot{m}_t \tag{3.10}$$

where C_i is the mass concentration of species i, $\dot{m}$ is the mass flow rate of the sample and the subscripts m and t refer to the sample analysis point and the probe tip respectively. By decomposing C_{i_t} and $\dot{m}_t$ to $C_{i_t} = \overline{C}_{i_t} + C'_{i_t}$ and $\dot{m}_t = A(\overline{\rho U_s} + \overline{(\rho U_s)'})$ and taking the average for the above expression, it follows that:

$$\overline{C}_{i_m} \cdot \overline{\rho U}_s = \overline{C}_{i_t} \cdot \overline{\rho U}_s + \overline{C'_{i_t} \cdot (\rho U_s)'} \tag{3.11}$$

i.e.

$$\overline{C}_{i_m} = \overline{C}_{i_t} + \frac{\overline{C'_{i_t} (\rho U_s)'}}{\overline{\rho U}_s} \tag{3.12}$$

which again indicates that the measured mean values are not the true time averaged values at the point of measurement. In effect, the probe produces an averaging according to the expression (3.12). The sampling (suction) velocity can be assumed constant (see Bilger (1975)), the averaging will reduce to the density form usually known as "Favre averaging" i.e.

$$\overline{C}_{i_m} = \overline{C}_{i_t} + \frac{\overline{C'_i \rho'}_t}{\overline{\rho}} \tag{3.13}$$

It is apparent that the difference between the time averaged mass fraction and the measured values is dependent on the density-mass fraction correlation and the gas averaged density. If interest

lies in measuring the time averaged mass fraction the correction term in equation (3.13) represents an error. However, it is clear that assessment of its magnitude is difficult. This point has been recognized by several investigators, see for example Bilger (1977) and Jones (1979). In the present work the measured concentrations are recognized as density-weighted averages and, therefore, errors arising from the fluctuating nature of the present flows do not contribute to the overall accuracy of the measurements.

Comparative species concentration measurements were made using three different probes, utilizing different methods of sample quenching: (i) the water-cooled stainless steel probe, where the sample is quenched by convective heat transfer from it to cold water, (ii) a direct water quench stainless steel probe where the sample is quenched by diluting it with cold water and (iii) a quartz microprobe relying on aerodynamic quenching (sonic expansion of the sample). The water-cooled probe, its sampling system and an assessment of its performance have been given earlier in this subsection. The quartz microprobe is shown in panel (b) of Fig. (3.18) and its sampling system was similar to that given in Fig. (3.19) while its performance and accuracy have been discussed previously in section (2.4).

The water-quench probe was developed originally for gas analysis in particle laden media by Lewis and Smoot (1981) and it was employed here so that its performance may be assessed in less complicated gas flame circumstances before proceeding to ultilize it in the coal-fired conditions. A schematic diagram of the probe tip and the probe is presented in Fig. (3.18) panel (c).

The probe was constructed entirely of stainless steel and permitted the direct quenching of the combustion products by injection of water through small holes near the tip. Some approximation to isokinetic sampling was attempted. The probe contained a small pressure tap near the tip which was used to equilibrate the probe static pressure with the furnace wall pressure at the measurement segment. Control of the probe pressure was achieved by adjusting the water flow rate into the probe. A lower limit of water flow rate was obviously required in order to prevent the probe melting. Difficulties arose in the pressure matching at the hottest location in the furnace ($\bar{T} > 1400^{o}C$) due to boiling at the probe tip impeding the water flow. Concentration data could not be collected in the flame regions near the burner. Later modifications to the probe design (see Chapter 5) proved that a water-cooling jacket should have been incorporated to assess measurements in the hottest regions.

A schematic diagram of the entire quench probe sampling system is shown in Fig. (3.20). All the sampling system components and lines from the probe exit to the analysers were made of teflon. The water and gas were separated by the sampling system downstream of the probe. The sample entered a teflon disengager tangentially which permitted the separation of the gas from the water. A level of water was maintained in the disengager to prevent the gas from exiting with water. The water is then collected in two 10 litres each, pyrex espirators during the sampling time. The gas having been separated from the water, passed through an ice bath to condensate any condensable vapours. The condensate is

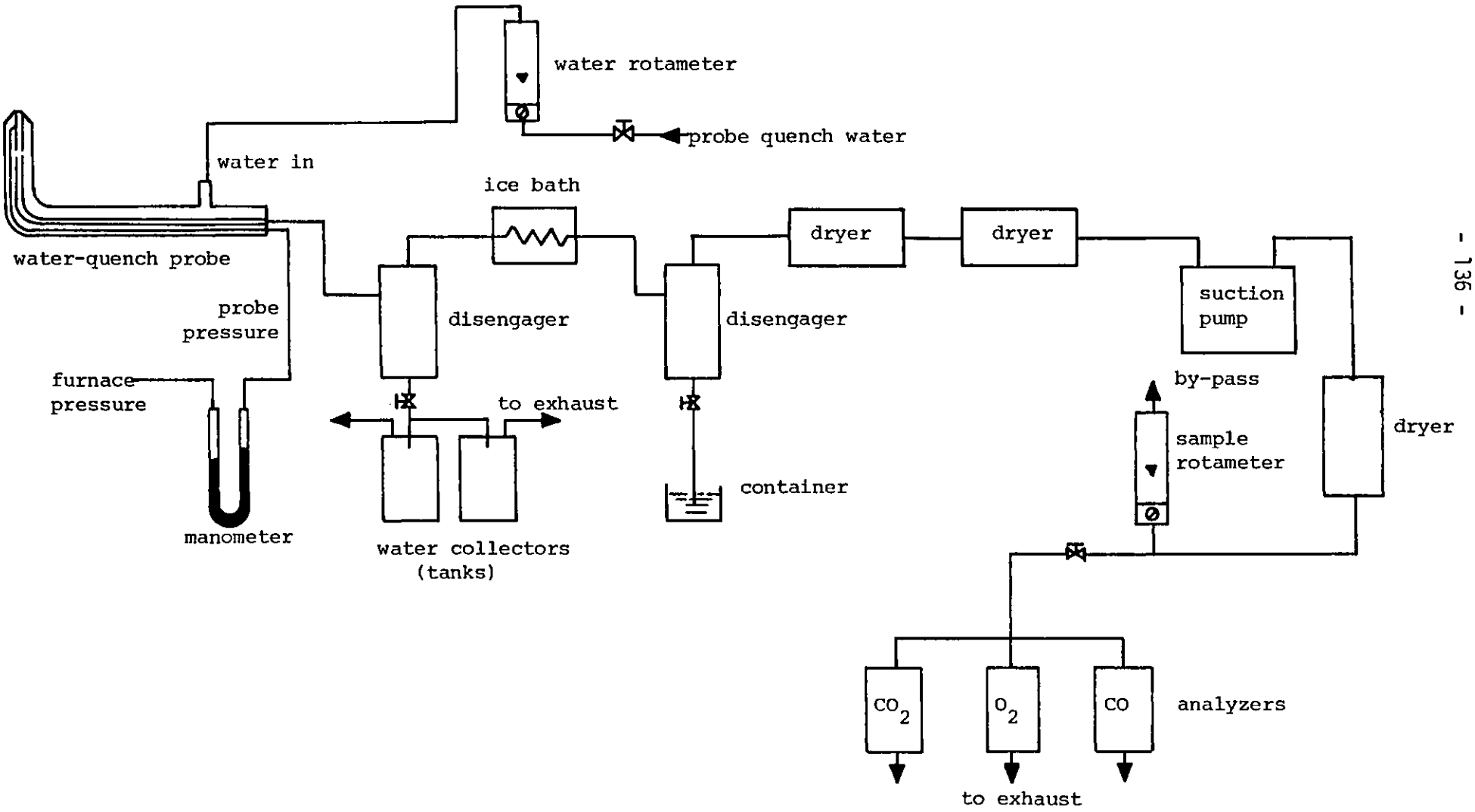

Fig.(3.20) Sketch of sampling system for water-quench probe

then removed and collected in another teflon disengager while the dry gas passed through dryers to eliminate chemically any vapours in the gas. Finally the dry gases are passed through CO, CO_2 and O_2 analysers. It is worth mentioning that the temperature and concentration probes were located quickly, accurately and easily at the desired position within the furnace by a traversing mechanism. At early experiments a manually operated traversing gear was used to move the probe at right angles to the furnace axis (R). Vertical movements were achieved by clamping the probe traverse to the window at the desired axial distance (X). Automation of the probe traverse was successfully accomplished later and this is explained in detail in Chapter (5). A schematic diagram of the traverse can be seen in Fig. (5.8).

3.5 Presentation and Discussion of the Experimental Results

Three experiments summarized in Table (3.1) were conducted. The objectives were: (i) to ensure proper operation of the furnace and its auxillary equipments for gas firing employed in heating up the furnace for coal combustion, (ii) to obtain detailed local measurements of gas species concentrations, temperature and radiation flux for two combustion air swirl numbers and two excess air levels which in total will provide a data base for evaluating predictive computer models, and (iii) to assess the relative performances of the three gas sampling probes discussed earlier in section (3.4).

Table (3.1)

Conditions of experiments[a]

Run	Swirl number (S)	Gas flow rate (litre/min)	Air flow rate (litre/min)	(A/F)[b]	(A/F)*[c]
1	0	211	2550	19.9	19
2	0	211	2410	18.8	17.9
3	0.56	211	2550	19.9	19.0

[a]Gas density = 0.7283 kg/m^3. Air is not preheated; T_{air} = 20^{o}C

[b](A/F) ≡ air-fuel ratio based on input flow measurements.

[c](A/F)* ≡ air-fuel ratio based on gas analysis at the furnace exit.

The furnace inside pressure was maintained very close to atmospheric pressure to minimize possible air leakage. The cooling water flow was kept at 3 litre/min in each of the refractory lined segments and at 6.85 litre/min in the remaining segments. Cooling air to the flame scanners was kept at a minimum of 3 litre/min to minimize aerodynamic disturbances to the flame. The natural gas flow rate was kept constant in all the three experiments at 9.24 kg/hr giving a heat input of 124 kW. Due to the high thermal capacity of the refractory walls, it took three hours to achieve steady state conditions as monitored by steady readings of wall temperatures.

It is an unfortunate fact that the acquisition of sufficient data to assess the physical properties of a flame takes a considerable period of time. In consequence it must be assumed that the input conditions and dependent flame properties remain unchanged throughout the time occupied by the measurements. For the input conditions it is essential not only to be able to set up the independent variables easily and accurately, but to be able to reproduce these settings at a later date. The furnace input conditions can be reproduced with a very good degree of reliability, particularly with respect to air and gas flows, swirl number and cooling water flow rates.

3.5.1 Probe Type

Figure (3.21) and Fig. (3.22) show a comparison of the mean species concentration results for the three different concentration probes at four axial distances in run 3. The quartz microprobe failed to survive in the upstream core of the flame ($X/D < 0.12$) due to the locally very high temperature along the probe length cantilever span. Apart from this, it proved generally delicate for the scale of the present work and so its use was confined only to the early stages of the experimental programme. A comparison of the results of the quartz microprobe with the other two probes in the far downstream region is shown in panel (c) of Fig. (3.22). They differ only by a maximum of about - 0.4% CO_2 and 0.1% O_2 volume fractions compared with those of the water-cooled probe, an encouraging result. The influential parameters; such as spatial resolution, suction velocity, repeatability, segregation, quenching, etc., causing these differences are discussed in section (2.4).

The following conclusion may be drawn when comparing the results of the water-cooled and water-quench probes. Firstly, referring to Fig. (3.21) panels (a) and (b), inside the flame core in the upper stream regions (X/D = 0.1166 and 1.1166, at $0 < R < 120$) where the flow is distinguished by the presence of significant CO, the water-quench probe records lower CO and CO_2 but higher O_2 levels compared to the water-cooled probe. One concludes that the water-cooled probe does not freeze the reaction as rapidly as the quench probe and further reaction takes place in the water-cooled probe; this conclusion was also reported by

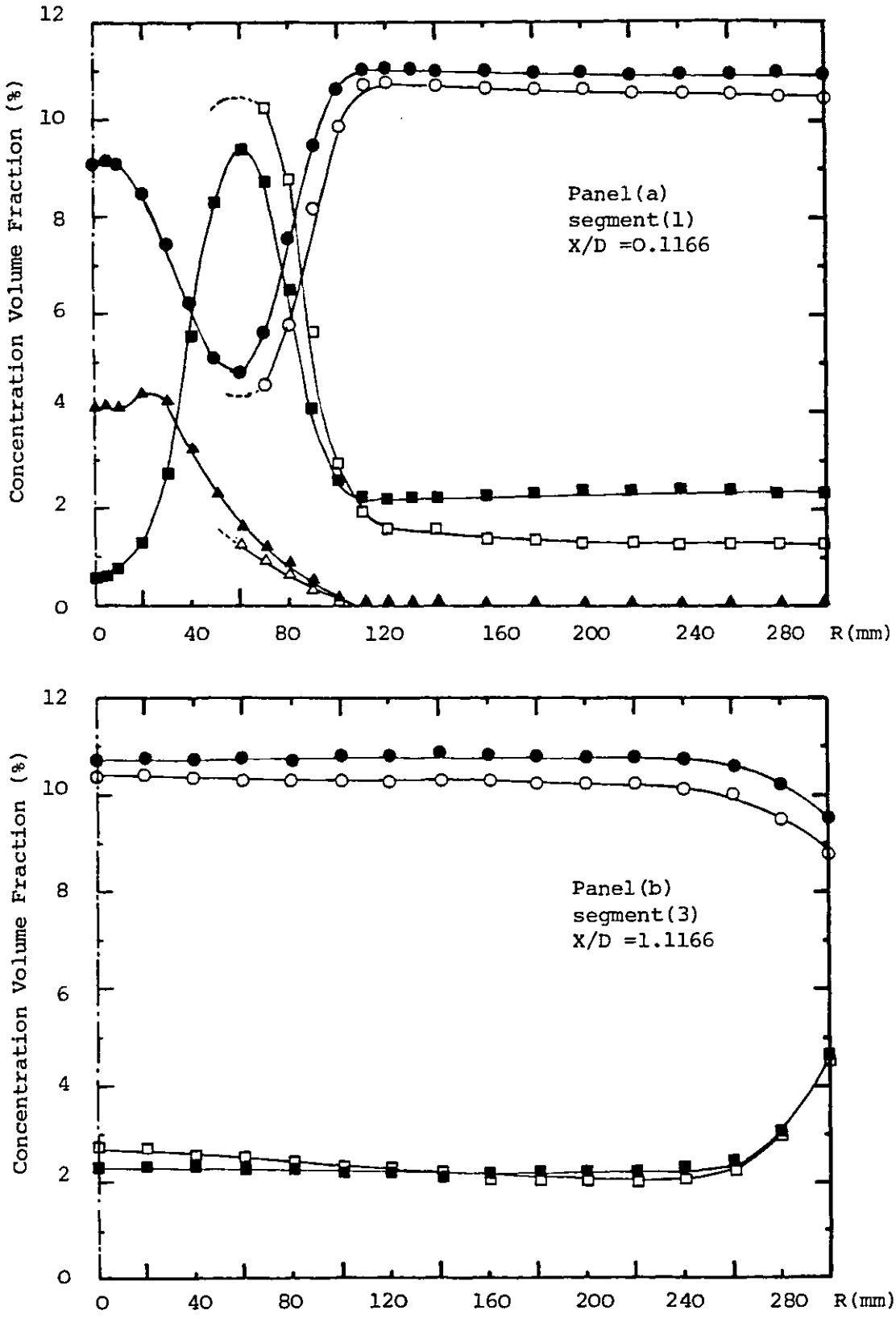

Fig.(3.21) Radial concentration profiles
using different sampling probes,run 3
Water-cooled probe:CO2 ● ,O2 ■ ,CO ▲
Water-quench probe:CO2 ○ ,O2 □ ,CO △

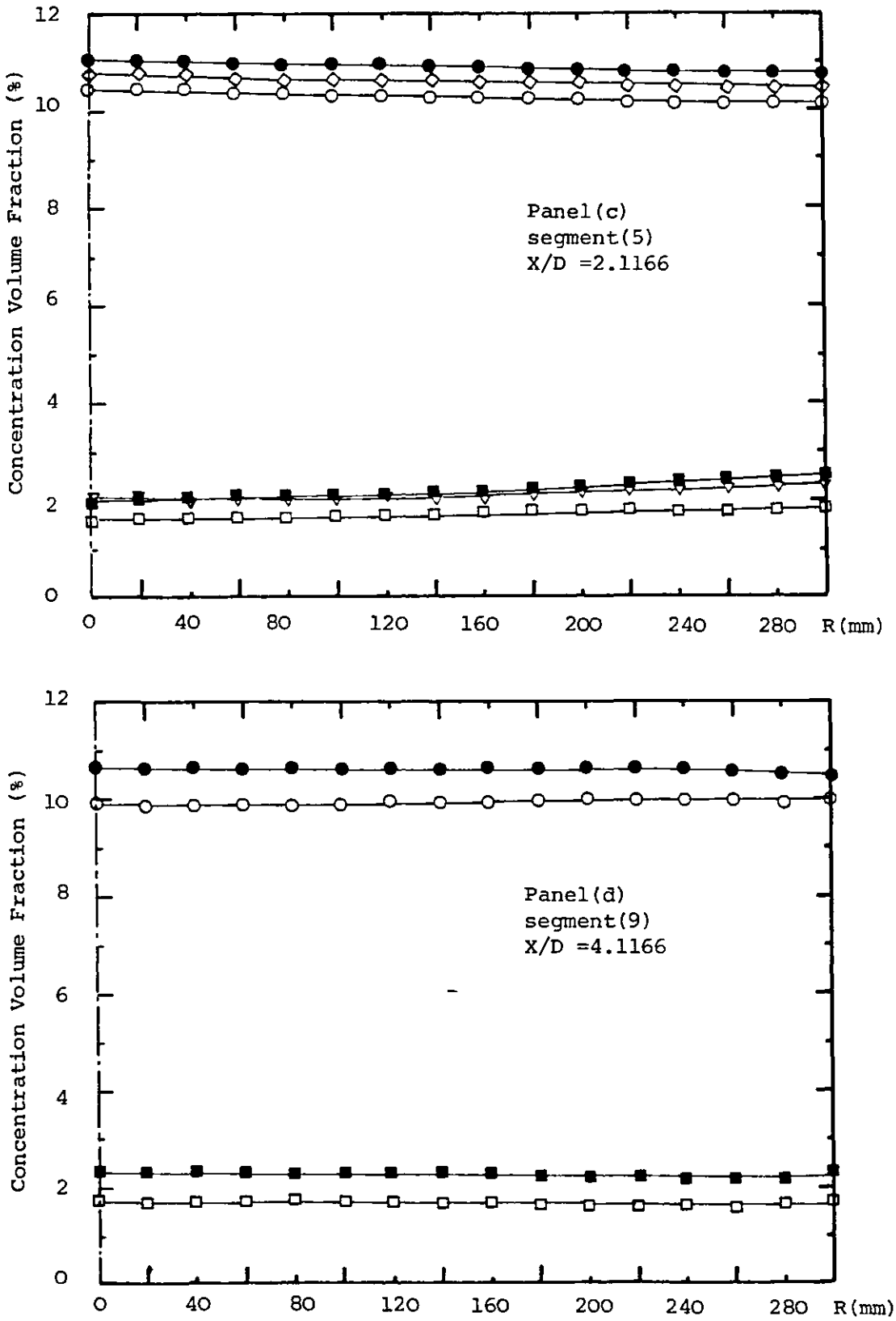

Fig.(3.22) Radial concentration profiles
using different samplig probes,run 3
Water-cooled probe:CO2 ● ,O2 ■
Water-quench probe:CO2 ○ ,O2 □
Quartz microprobe :CO2 ◇ ,O2 ▽

Lewis and Smoot (1981). Secondly, far downstream (X/D = 2.116 and 4.1166), panels (c) and (d) of Fig. (3.22), and also in the outer and upstream regions of the flame (R > 120 mm), see Fig. (3.21) panels (a) and (b), where the chemical reaction is complete the quench probe still produces lower CO_2, however the O_2 concentrations are also now lower. This may be explained by the fact that both carbon dioxide and oxygen dissolve in the quench water of the water-quench probe. It is obviously difficult to quantify exactly the percentage dissolved in the water but, as shown from the results, a maximum of 1% volume fraction seems reasonable. All the subsequent concentration measurements reported in subsection (3.5.3) have been made using the water-cooled probe with an estimated uncertainty not greater than ±1% volume fraction.

3.5.2 Incident Radiation Flux Measurements

Figure (3.23) shows the incident radiation flux to the furnace wall plotted against the dimensionless axial distance X/D. The three experiments demonstrate similar and expected trends. The incident radiation reaches a maximum at about X/D = 0.75 which coincides with the maximum wall temperature shown on Fig. (3.24). The increased swirl, from S = 0 in run 1 to S = 0.56 in run 3, causes increased radiation flux to the furnace wall especially near the burner. The reason for this is, first, the more intensive combustion in the shorter reaction region of the flame caused by an

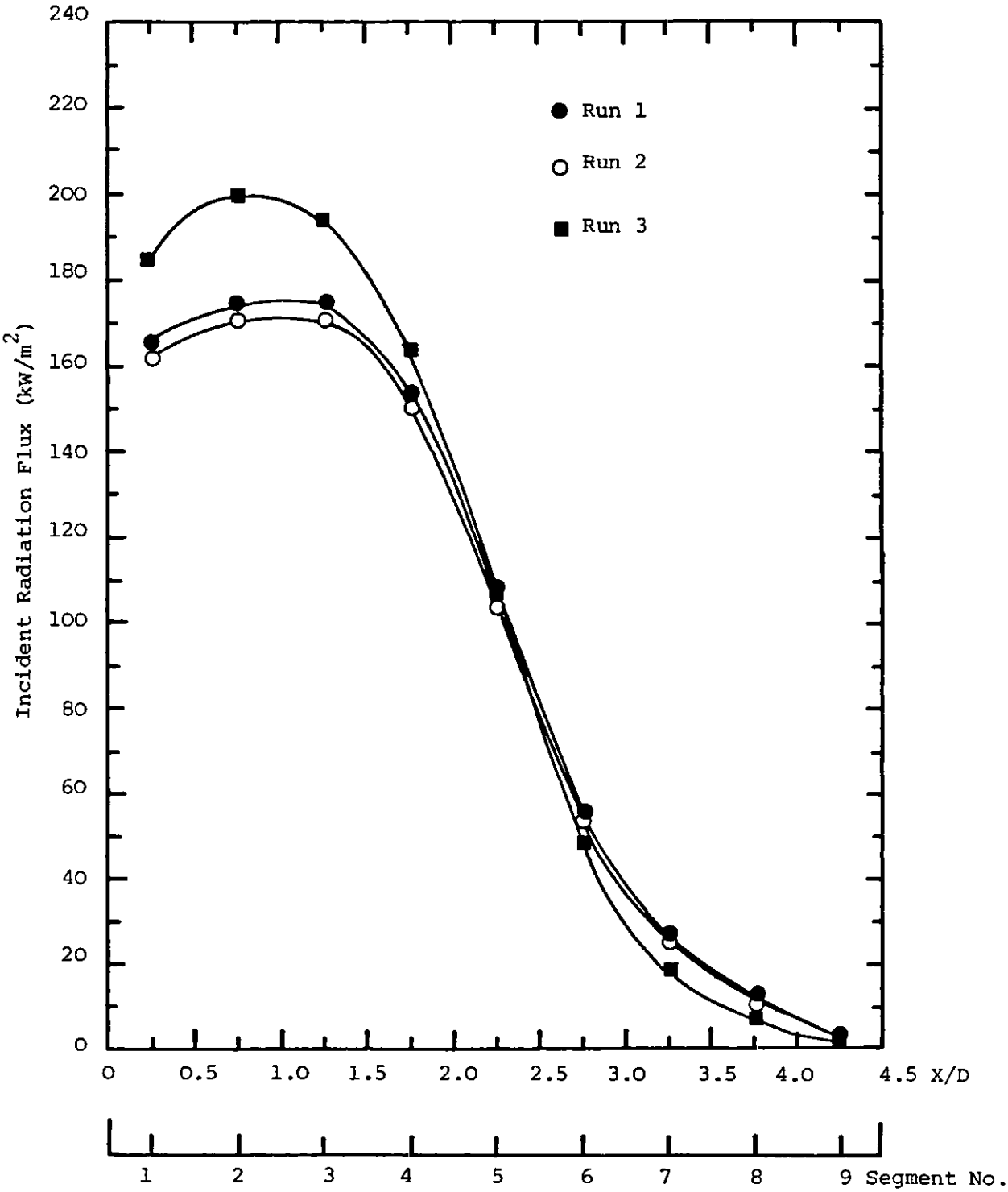

Fig.(3.23) Incident radiation flux to furnace walls

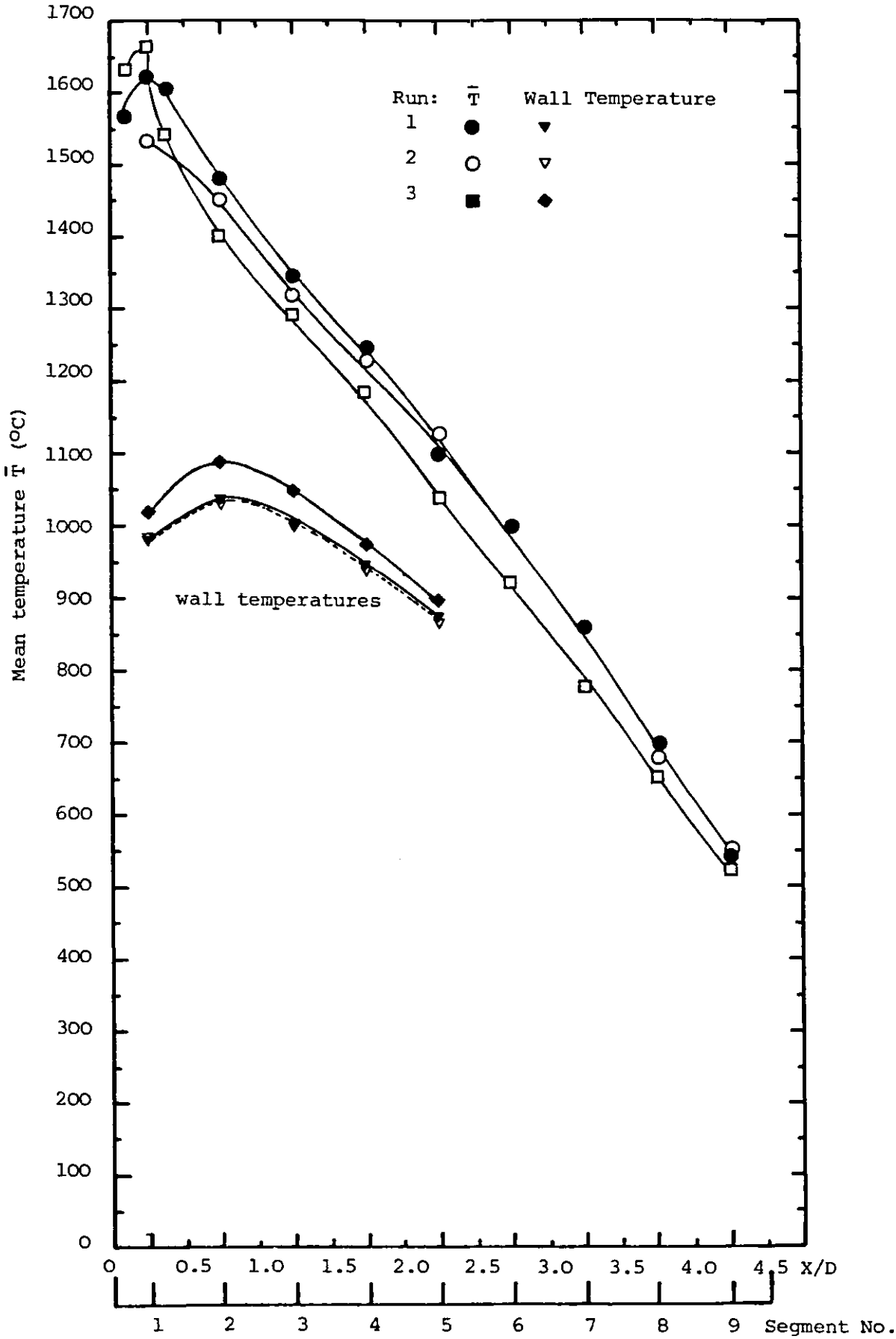

Fig.(3.24) Axial distributions of mean temperature and refractory wall temperature

increased central recirculation zone; second, to the accompanying higher gas velocities along the walls as was concluded by the investigation carried out by Mathur and MacCallum (1967). An impression of the flame length can be seen from Fig. (3.25), in which the cross-sectional averages of CO, CO_2 and O_2 concentrations, as being obtained from the integration of their respective radial profiles, are plotted at various axial distances from the burner. The rapid decay of CO and O_2 for the swirling flame suggests a shorter flame as when compared with the non-swirling flames, see also Khalil et al (1976), Syred and Beér (1974), Lilley (1977) and Lockwood et al (1974).

The variation of the excess air, from 5% in run 2 to 10% in run 1, is seen to have only a slight effect on the incident radiation flux. Possibly the observed differences between run 1 and run 2 are within the ellipsoidal radiometer instrumentation error although several measurement repetitions confirmed the same trend. It can be argued that the lower heat flux at less excess air is due to incomplete mixing which is certainly reflected by the concentration measurements, Fig. (3.26) to (3.28). Since the studied flames only occupied a rather small volume of the furnace (up to $X/D \simeq 1.5$), the rest of the furnace is filled with fairly mixed hot combustion gases and so the incident radiation flux for the three experiments nearly coincide towards the furnace exit ($X/D > 4.5$). This can also be drawn from the mean temperature distribution along the furance axis in Fig. (3.24).

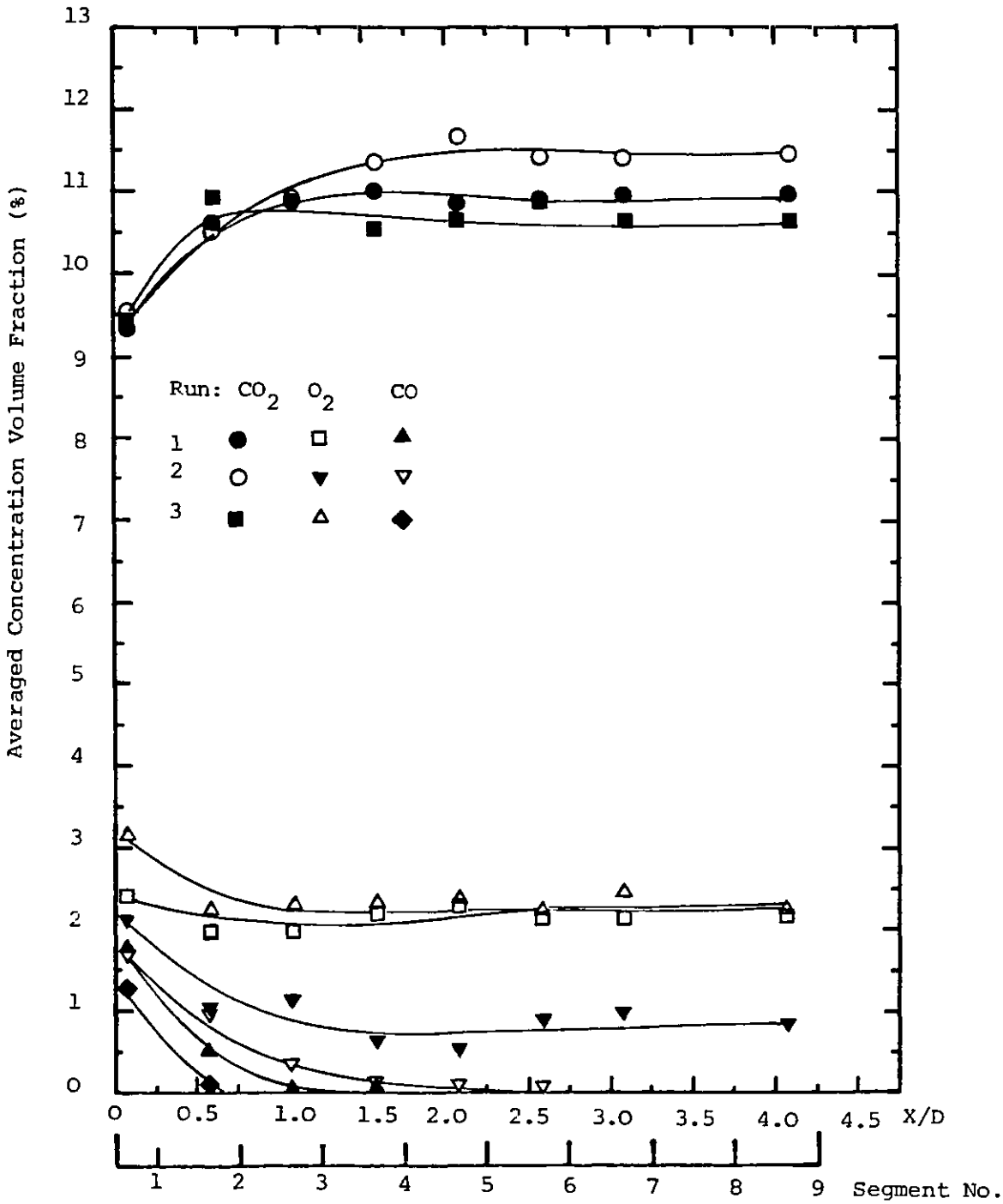

Fig.(3.25) Axial distributions of averaged volume fractions of CO_2,CO and O_2

3.5.3 Concentration and Temperature Measurements

Figure (3.26) to Fig. (3.28) show the effect of a modest change in the excess air (run 1 and run 2) on the radial concentration profiles, while Fig. (3.31) and Fig. (3.32) show the mean temperature distributions for these two experiments. The reaction volume occupies only the upper region of the furnace (up to $X/D \cong 1.6$) as evidence by the steep temperature and concentration gradients. Carbon monoxide concentration levels vanish for $X/D \cong 2$ and both the temperature and concentration variations tend to flat profiles revealing the existence of only hot combustion products.

In the early stages of the flames ($X/D = 0.1166$), Fig. (3.26), two regions may be identified: (i) a central core containing the reaction zone ($a < R < 110$ mm) and (ii) an outer wall recirculation zone ($R > 110$ mm). The central region follows the trends of free jet diffusion flames up to the radial location of minimum carbon dioxide and maximum oxygen concentrations ($R \approx 80$ mm), see Hassan et al (1980) and Chapter (2). The turbulent reaction zone is typically thick indeed, a reaction volume is more appropriately defined. It occupies roughly radial locations $50 < R < 120$ mm. One can note that the levels of carbon dioxide and carbon monoxide measured within the reaction volume and inside the core region exceeded those reported by Hutchinson et al (1975) for stabilized free jet diffusion flames because partial mixing, which is improved by radial injection of gas stream, occurs inside the burner quarl. In the outer region, the finding that carbon dioxide and oxygen and temperature are uniformly distributed, with CO_2 levels being the highest across

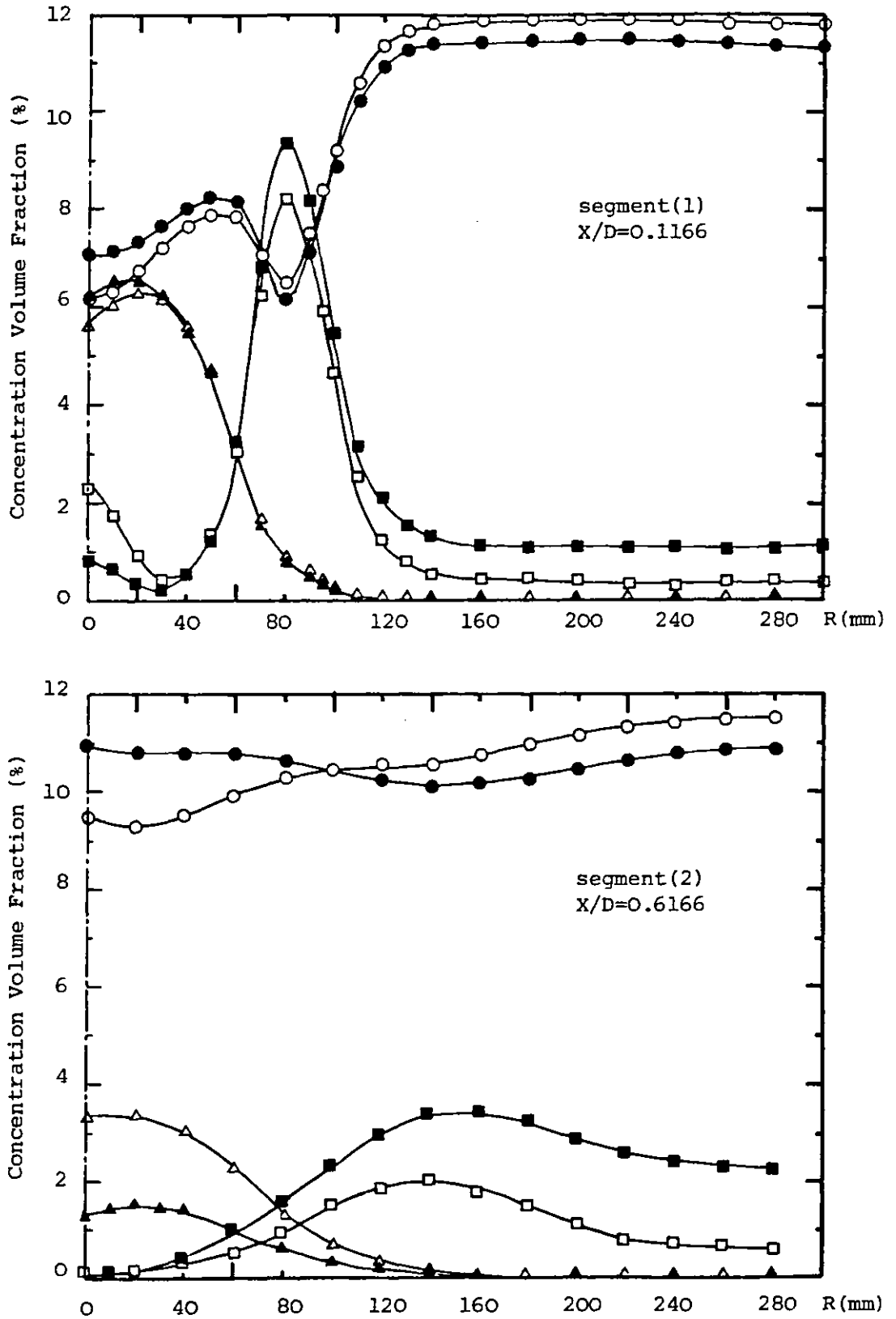

Fig.(3.26) Effect of excess air on the radial concentration profiles
Run 1:CO2 ● ,O2 ■ ,CO ▲
Run 2:CO2 ○ ,O2 □ ,CO △

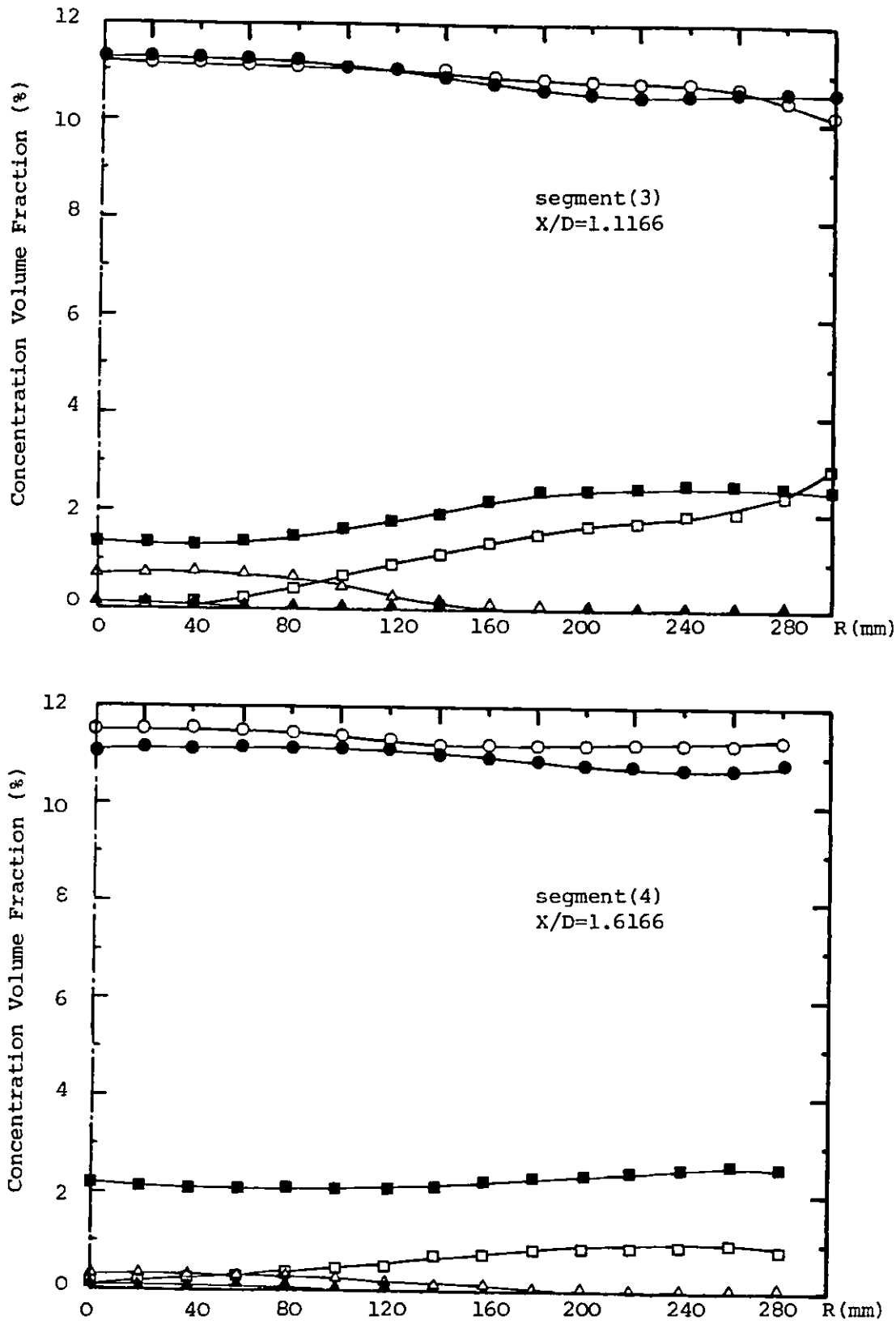

Fig.(3.27) Effect of excess air on the radial concentration profiles
Run 1:CO2 ● ,O2 ■ ,CO ▲
Run 2:CO2 ○ ,O2 □ ,CO △

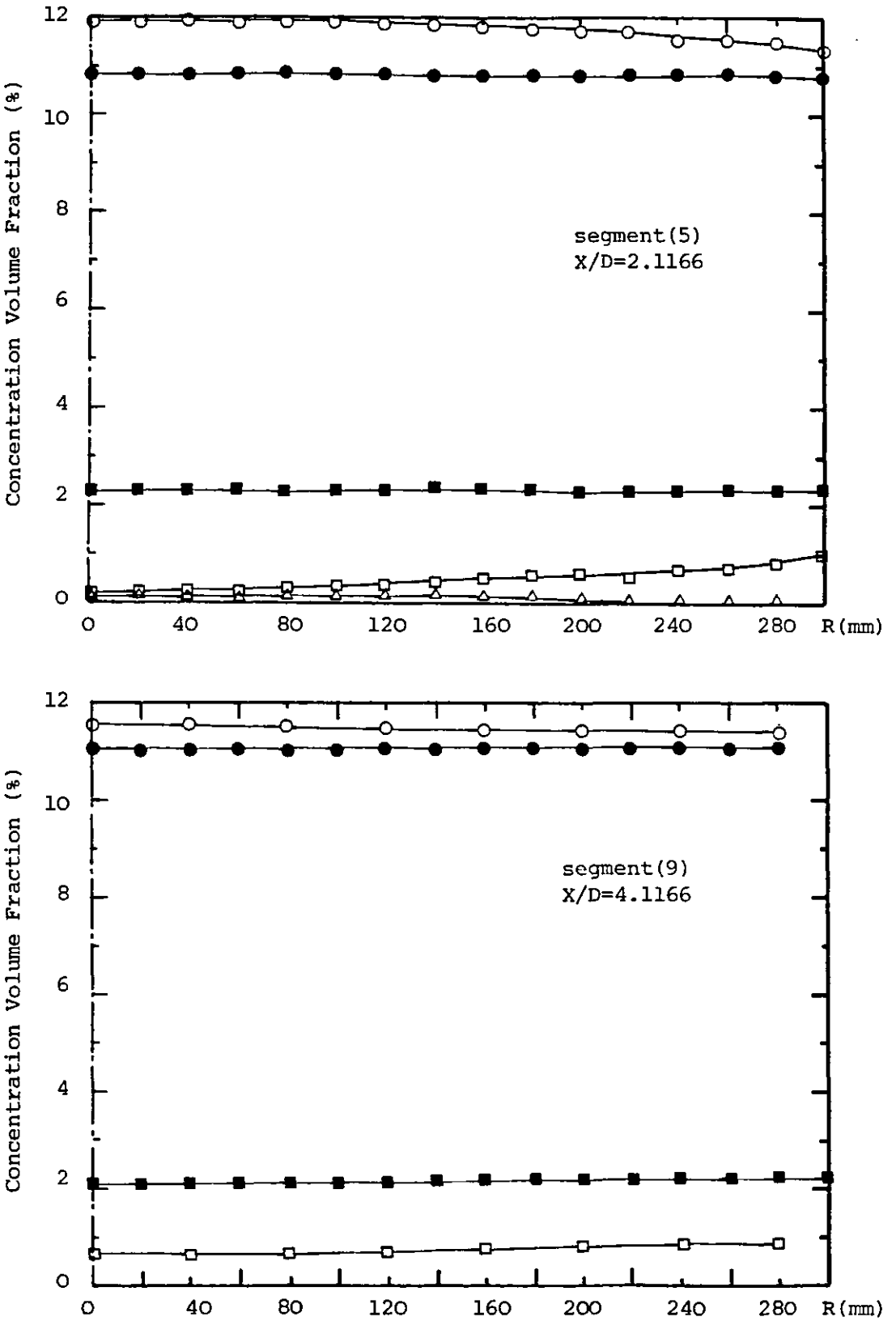

Fig.(3.28) Effect of excess air on the radial oncentration profiles
Run 1:CO2 ● ,O2 ■ ,CO ▲
Run 2:CO2 ○ ,O2 □ ,CO △

the flame zone with the non-existence of CO, reflects the presence of an outer recirculation zone that recirculates well mixed hot chemical species from downstream to upstream. With increasing axial distance (X/D = 0.6166) the carbon dioxide levels inside the flame core dramatically increase due to the slow conversion of carbon monoxide which is also reflected by the rapid consumption of oxygen in this region. The observed differences due to excess air variations are obviously due to the slight differences in the flame length, with the flame in run 1 being more rapidly developed.

Figure (3.29) and Fig. (3.30) show the effect of imparting swirl to secondary air (run 1 at zero swirl and run 3 at swirl number of 0.56) on the radial concentration profiles while Fig. (3.31) and (3.33) show the corresponding mean temperature distributions for runs 1 and 3 respectively. The flow rates of gas and air were kept constant. The additional element here is that more efficient initial mixing occurs at the core of the flame when swirl is imparted (run 3), Lilley (1977), and this is reflected by a higher percentage of CO_2 concentrations and a reduction in the CO levels. Obviously the reason is the existence of a well-stirred central recirculation zone, see Fricker and Leuckel (1976) and Mathur and MacCallum (1967) for example, which also causes a reduction in the reaction zone volume. The swirling flame is also shorter as revealed by the very small percentage of CO at X/D = 0.6166 and by the rapid development of the concentration and temperature profiles.

The temperature radial distribution presented, as an example, in Fig. (3.34) at X/D = 2.25 (run 3) demonstrates the extent

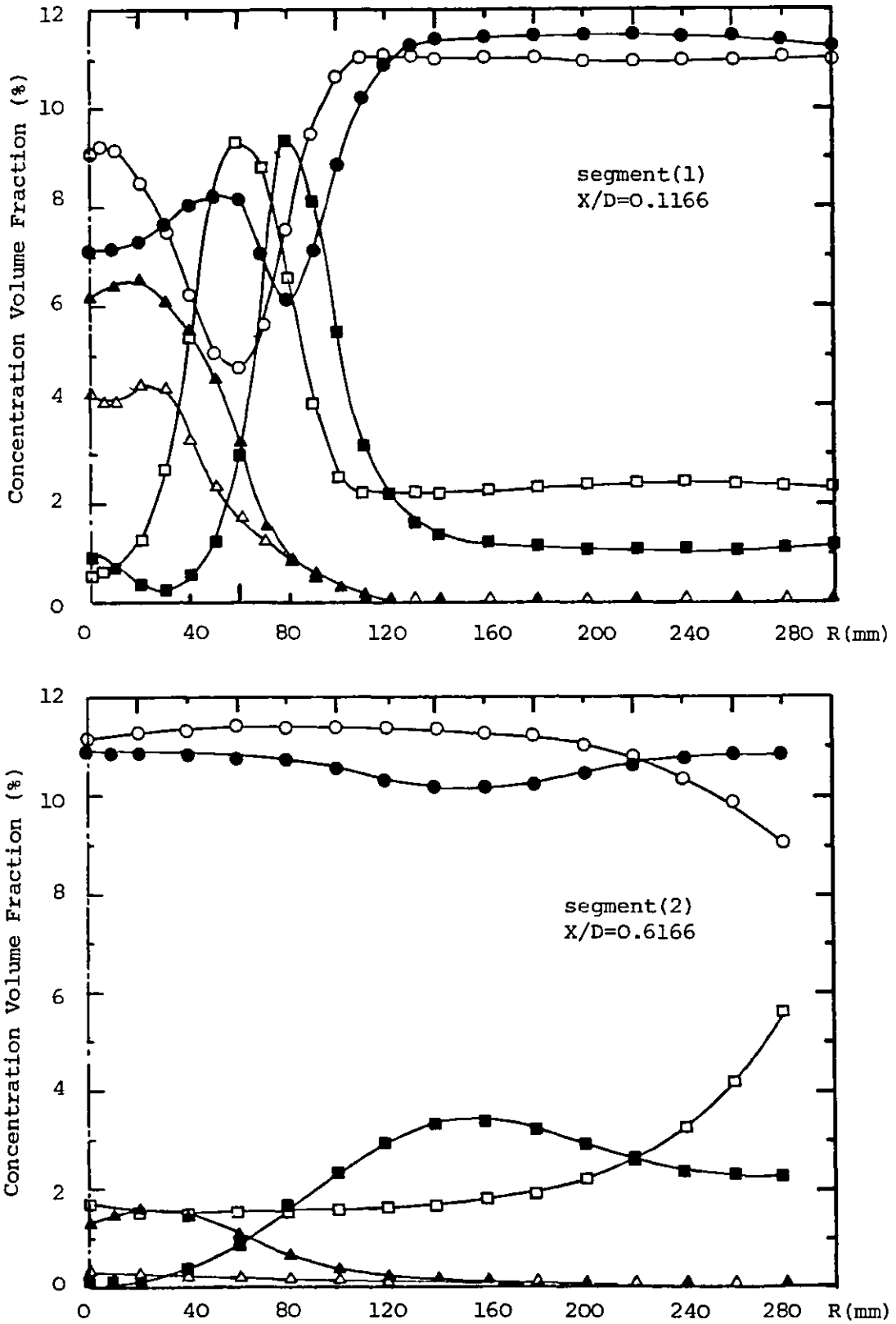

Fig.(3.29) Effect of secondary air swirl on the radial concentration profiles
Run 1:CO2 ● ,O2 ■ ,CO ▲
Run 3:CO2 O ,O2 □ ,CO △

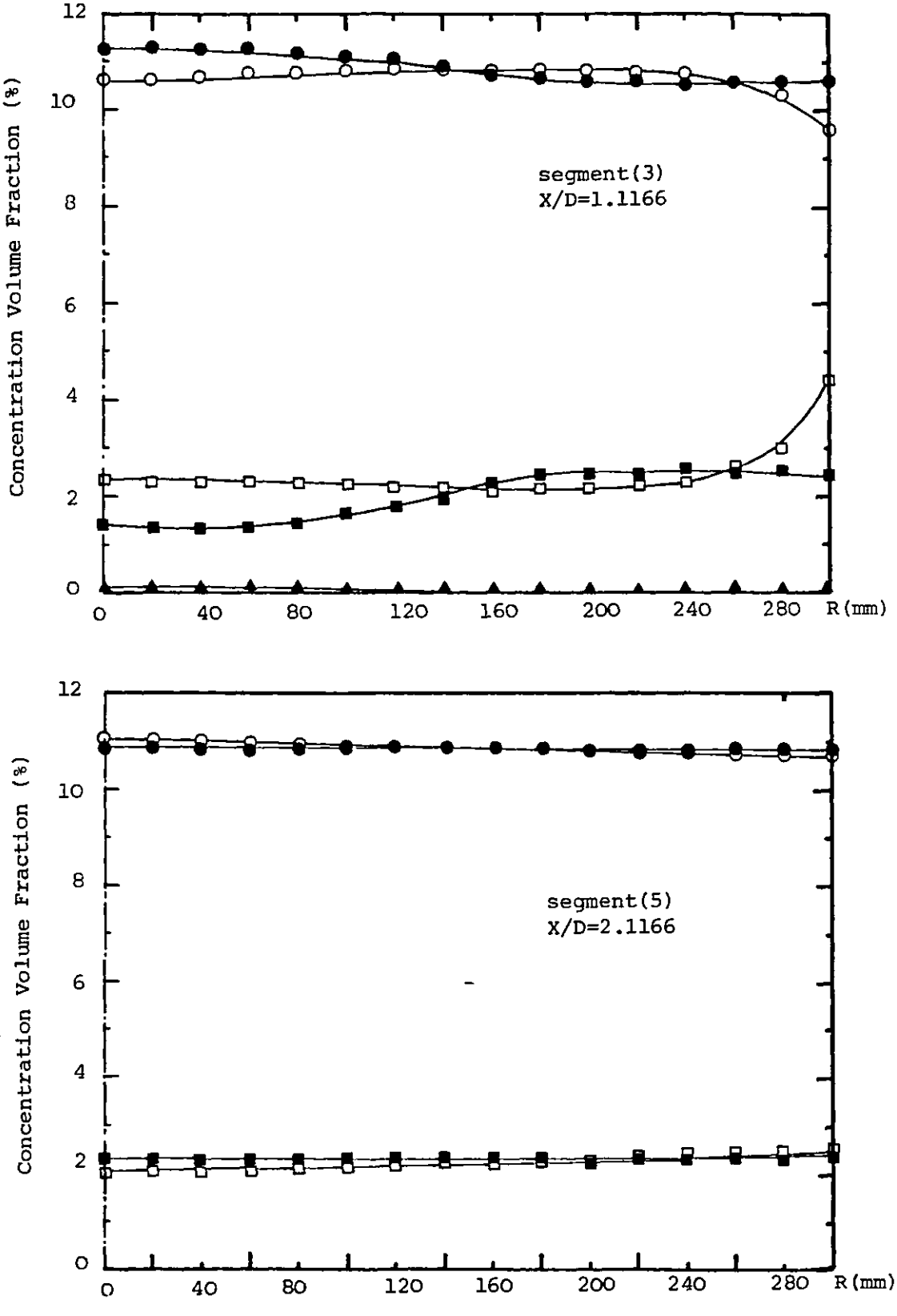

Fig.(3.30) Effect of secondary air swirl
on the radial concentration
Run 1:CO2 ● ,O2 ■ ,CO ▲
Run 3:CO2 ○ ,O2 □ ,CO △

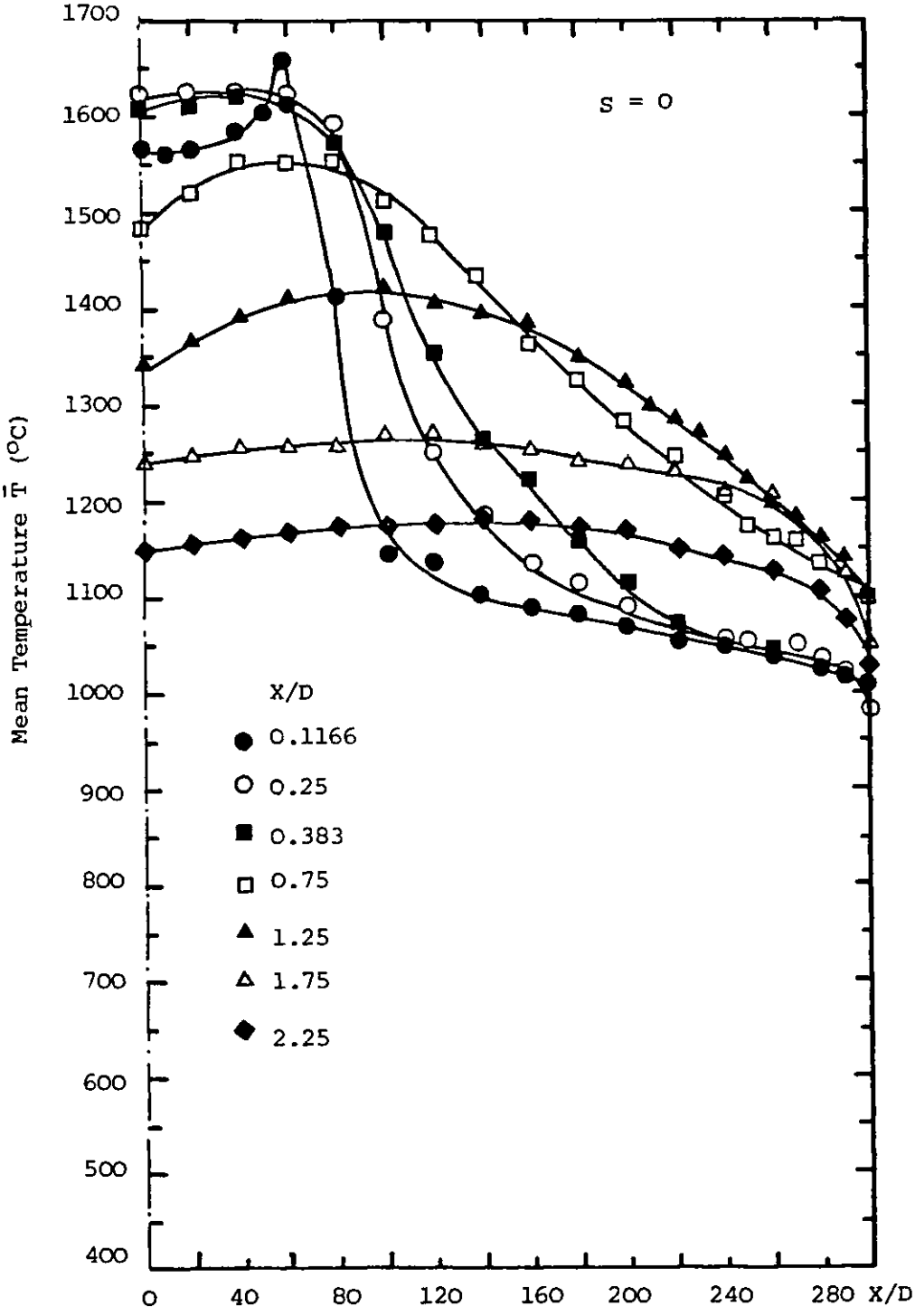

Fig.(3.31) Radial distributions of mean temperature along the furnace,run 1

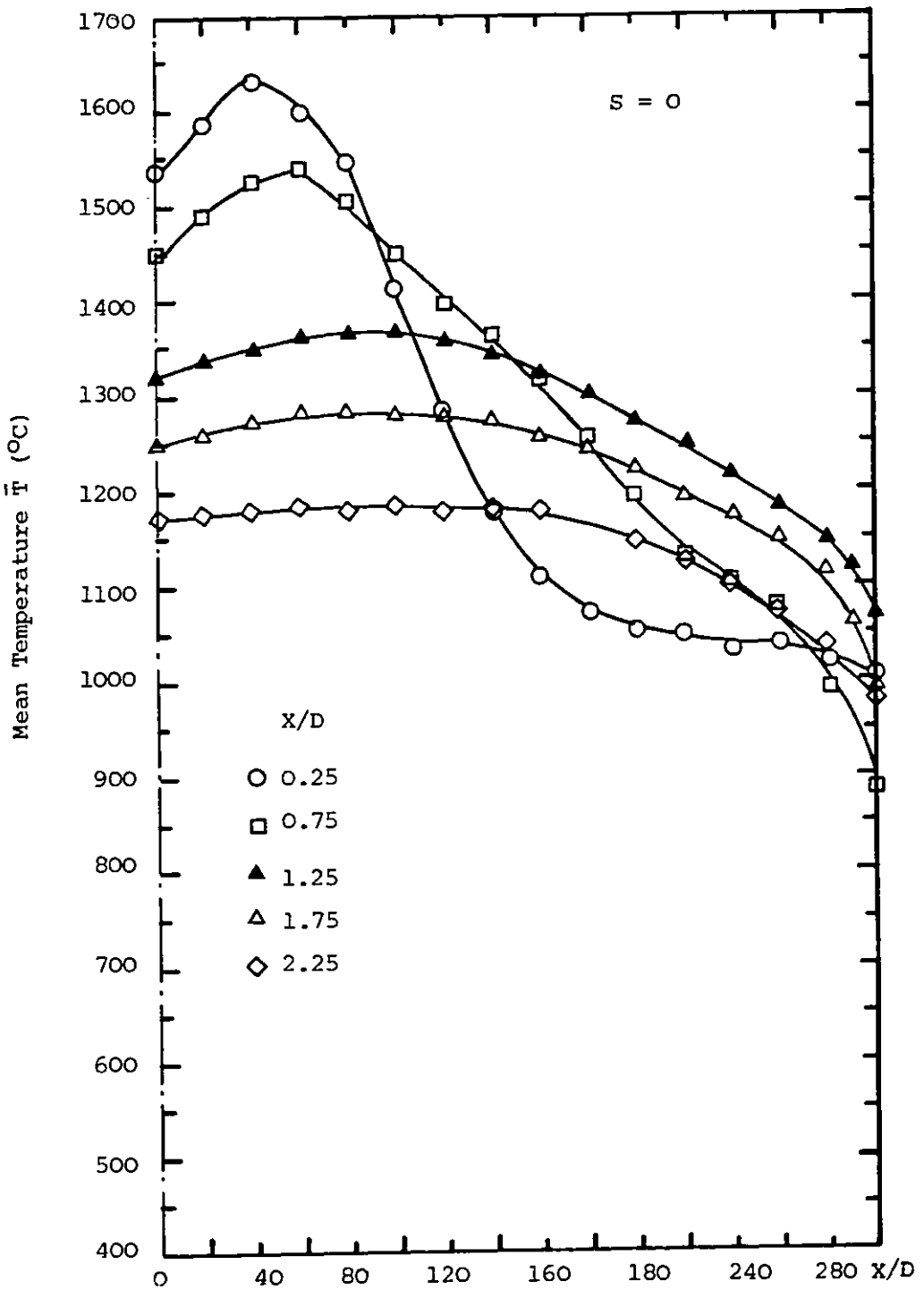

Fig.(3.32) Radial distributions of mean temperature along the furnace,run 2

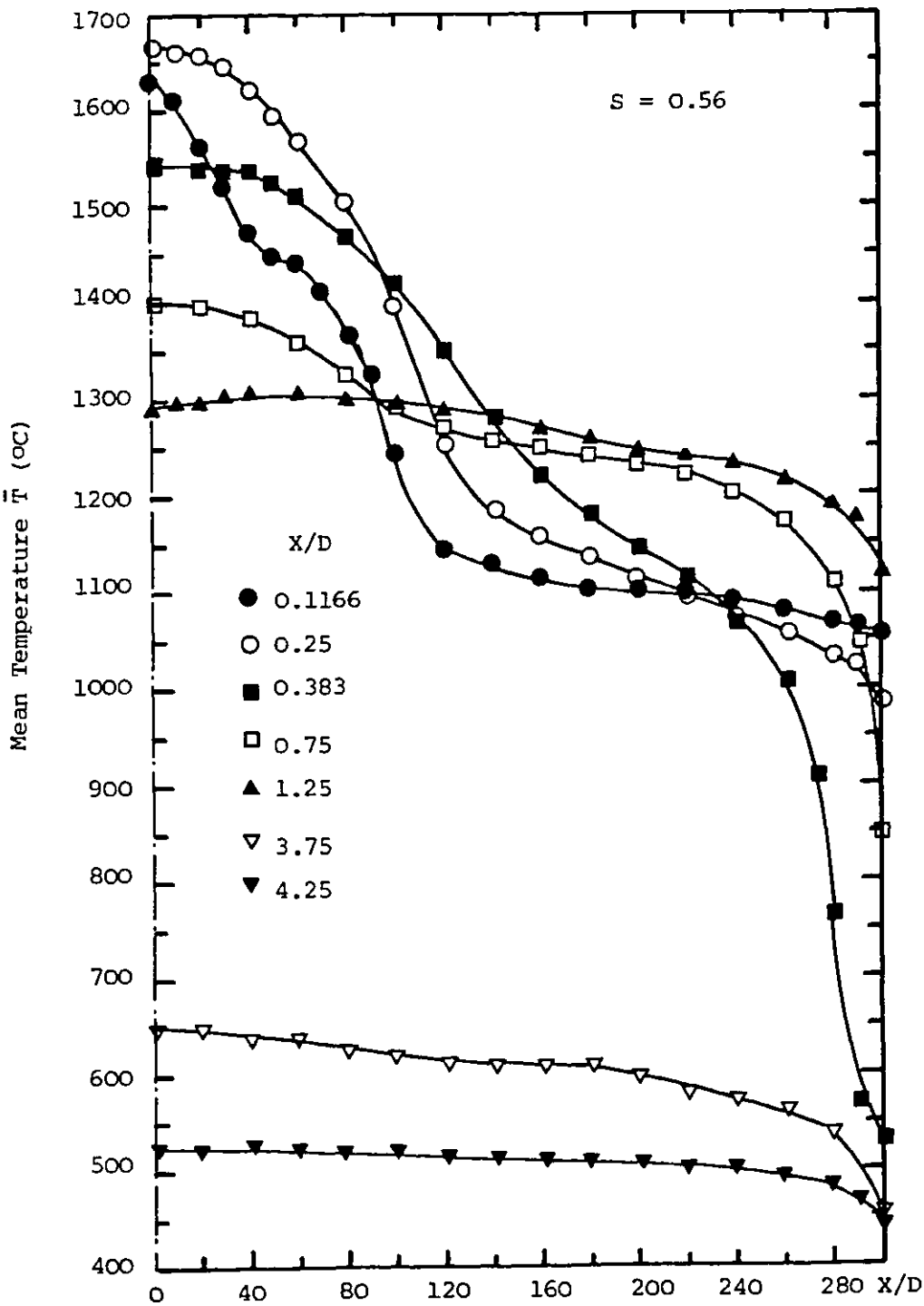

Fig.(3.33) Radial distributions of mean temperature along the furnace, run 3

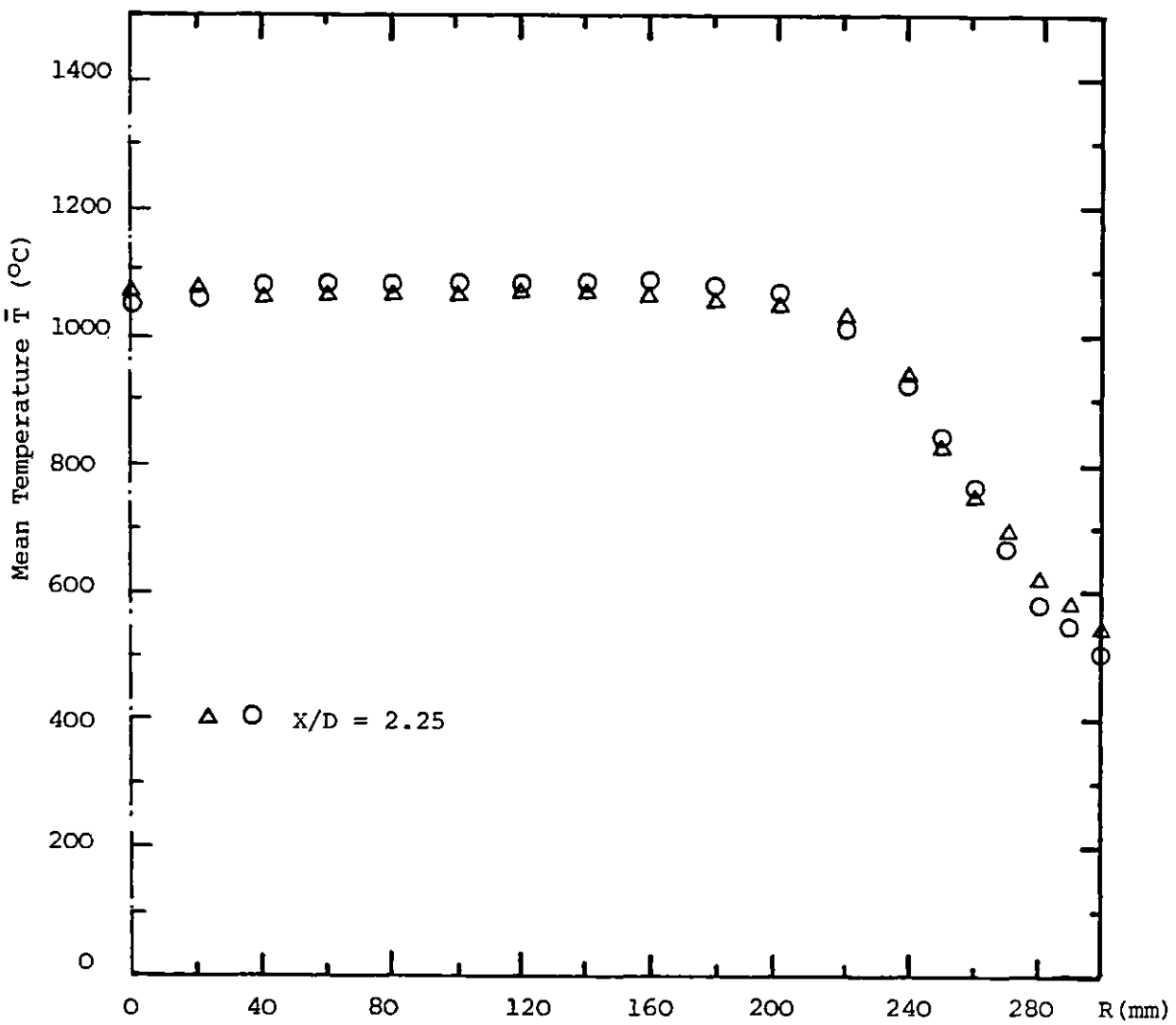

Fig.(3.34) Radial distributions of mean temperature (symmetry check),run 3,X/D=2.25

of possible asymmetry in the radial profiles. Nearly symmetrical distribution is observed; a maximum deviation of only $30^{o}C$ (which is within the repeatability of the measurements) is satisfactory.

CHAPTER 4

A FURNACE FOR RESEARCH INTO COMBUSTION OF PULVERIZED COAL

4.1 Introduction

Pulverized coal research has been of general interest for many years, partly because of its extensive use in the electric power generation industry. Basic or fundamental research in pulverized coal combustion processes, however, has only received significant emphasis during the last 10 to 15 years. Prior to that time, most of the design work was done by trial and error. Such procedures produced the present state-of-the-art knowledge on pulverized coal combustion, but they did not provide a basic understanding of the principles, mechanisms and processes involved. Trial and error approaches are still used simply because of the complex nature of the problems associated with coal combustion. A basic understanding of such processes is nevertheless important. This need is particularly evident in the engineering design of new combustion and gasification processes which will be required to produce large, clean and economical supplies of energy, gas and coal-derived oil products.

This part of the present research effort was undertaken to complete the development of the coal combustion facility which could provide the necessary data and information for determining the rates of various processes (gas and particle mixing, pyrolysis, combustion, etc.) which occur in pulverized coal combustion. Such information would further establish the data base for evaluation

of mathematical models in the prediction procedures and perhaps improve pulverized coal reactor design.

In section (4.2) a description of the preliminary work done on the coal research programme. A two-phase flow jet experiment in which the use of fine wire thermocouples for temperature measurement, in a simulated coal combustion circumstances, was tested. Also, an analytical study of the particle-gas interaction in two-phase flows was carried out. Partial differential equations were derived for the gas and particles turbulence kinetic energies, k_g and k_p respectively, and for the correlation $\overline{v_g' v_p'}$, An effort was made to put these equations in a general solvable form, the difficulties associated with the task are also given. Section (4.3) describes the extension of the gas-fired furnace experiment, dealt with earlier in Chapter (3), for coal firing. Full details of the coal feeding system, primary air and primary stream arrangement, secondary air supply and the gas scrubbing system are given. The safety precautions taken to avoid coal combustion hazards are also reported. Section (4.4) deals with the design of a microprocessor-feedback control system constructed for regulating the coal feed rate supplied to the furnace. This last includes descriptions of the system design, electronic components, the control theory together with the computing software program as well as a discussion of the control system performance.

4.2 The Preliminary Experiment and the Analytical Consideration of the Particle Diffusion

4.2.1 The Preliminary Experiment

A preliminary two-phase flow jet experiment was set up to simulate the main coal combustion experiment. A vertical partially premixed, turbulent diffusion free jet flame, fired vertically downwards, to simulate the furnace burner, was seeded with sand particles of size less than 200 μm. The main objectives of this experiment were to familiarize and gain experience of two-phase flow configurations, feeding systems, their problems and solutions. A more important objective was to test, in a less complicated experimental circumstances, some of the instrumentation which could be used later in the coal experiment data collection

A flow diagram of the experimental arrangement is shown in Fig. (4.1). The burner pipe was stainless steel, thin walled, vertically aligned and 12.7 mm internal diameter. It was long enough to ensure fully-developed flow conditions at the burner exit. The fuel was North Sea natural gas, its physical properties and chemical composition are given in Table (2.1). The gas was supplied from the mains via a water-cooled compressor and its flow rate was measured by a rotameter. The primary air was supplied from a compressed air supply normally at 100 psi, with its flow being monitored by a calibrated orifice plate. The sand particles were supplied by a feeding system which comprised a feed hopper and a screw feeder driven by a variable speed motor. The motor speed (maximum 150 rpm), and hence the sand feed rate, was controlled by an electronic controller. The calibrated feeder was

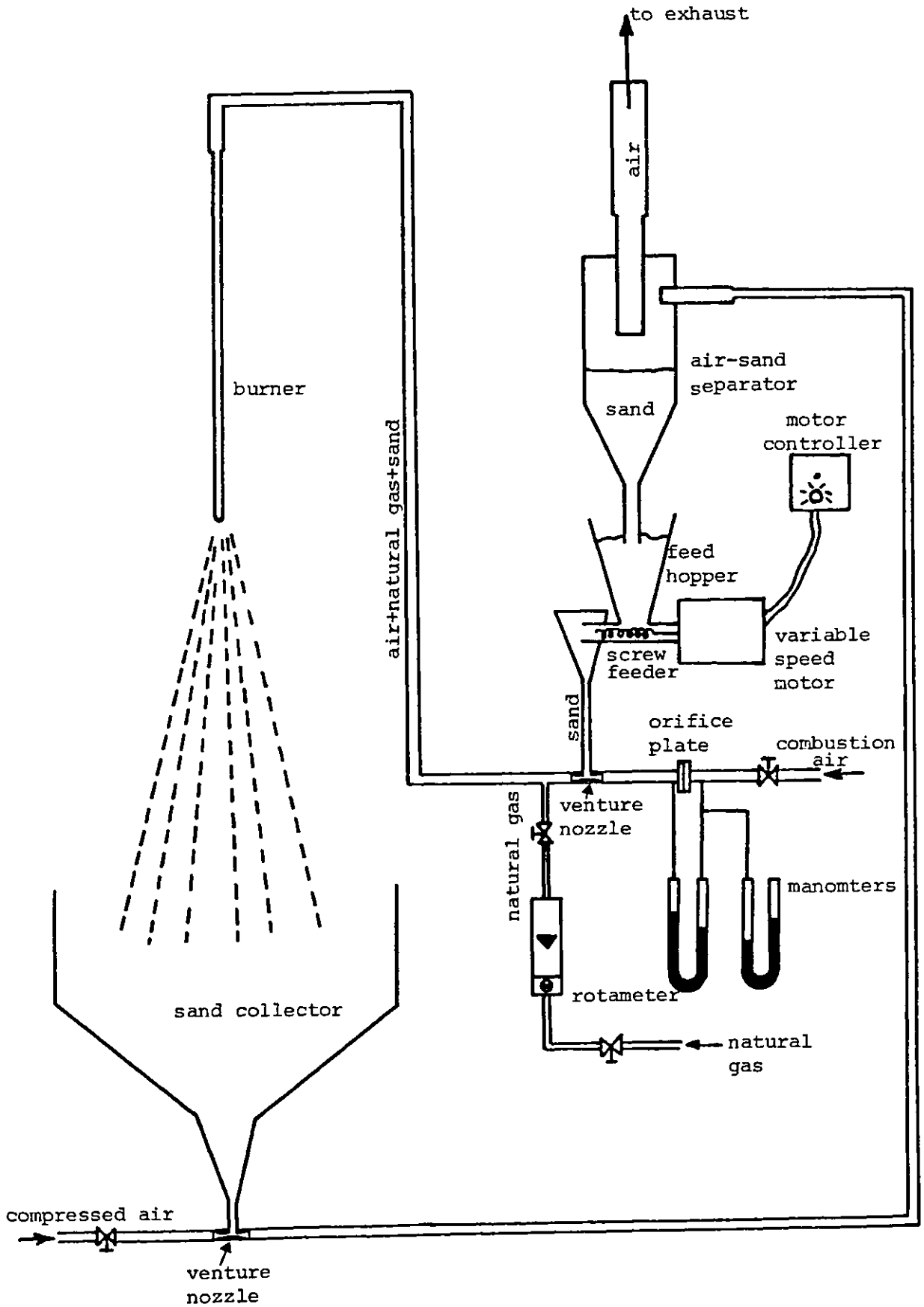

Fig.(4.1) Flow diagram of the preliminary experiment
(two-phase flow free reacting jet)

capable of supplying sand at a rate of 108 kg/hr at full speed. The sand particles were mixed with the primary air in a venturi nozzle. The sand-air stream and the natural gas stream were then mixed prior to the burner entry, far enough in advance to ensure complete mixing. The sand coming out of the flame was collected in a sand-collector, sucked and cooled by an air jet arrangement, mounted at the bottom of the collector. The sand-air mixture was fed to a cyclone separator where the sand was separated from the air and then fed back to the feed hopper to be reused. This closed-loop cycle used only a fixed amount of sand.

Nearly all the previous temperature measurements in powdered coal flames (two-phase flows) had been carried out using different types of suction pyrometers, see Mickel and Payne (1980), Harding (1980) and Graf and Payne (1981) for example. Apart from disturbing the flow because of their bulky size and gas suction, blockage of the pyrometers with fly-ash and unburned particles is a common occurrence. On the other hand, fine wire thermocouples have been used successfully in temperature measurements in gaseous flames, oil flames and inert flows, see for example Lockwood and Odidi (1975), Attaya (1983) and Lockwood and Moneib (1980). Compared to other temperature measuring techniques, the fine wire thermocouple has the superiority of being simple to manufacture, easy to use, compact and therefore causing less thermal and aerodynamic disturbances of the flow field. A discussion of the fine wire thermocouple performance and accuracy in gaseous flame temperature measurements is given in section (3.4).

The opportunity was allowed by the present simple experiment to employ the fine wire thermocouple in simulated coal combustion conditions and to test its merit in the circumstances of particles bombardment. Also to investigate the effect of different probe structures on the measured temperature before attempting to use such a probe in a real coal combustion experiment. Four differently constructed fine wire thermocouples (80 μm diameter, platinum/platinum - 13% rhodium wires), shown in Fig. (4.2), were compared at four axial locations on the centre line of a flame. The sand, primary air and natural gas mass flow rates were 12, 17.1 and 2.2 kg/hr respectively.

The difference in performance among the four probes is shown in Fig. (4.3) panels (a) and (b). The fine wire thermocouple in the horizontal position is the most accurate, see Moneib (1980). The comparison between the probes in horizontal and vertical positions is shown in panel (a) of Fig. (4.3). The vertical orientation results in slightly lower temperatures than the horizontal position. The discrepancies being about 30^{o} maximum. Despite the fact that this difference is within the repeatability of the experiment, it could be due to some loss in the convection heat transfer to the junction when the probe supporting wires are aligned vertically along the flow streams. It should be noted that the vertical orientation is preferred to the horizontal one because the latter was unable to survive the particle bombardment at the junction for more than short periods. Both fine wire probes with a coil around the junction or a shell on top of the junction reduce significantly the convection and radiation heat transferred

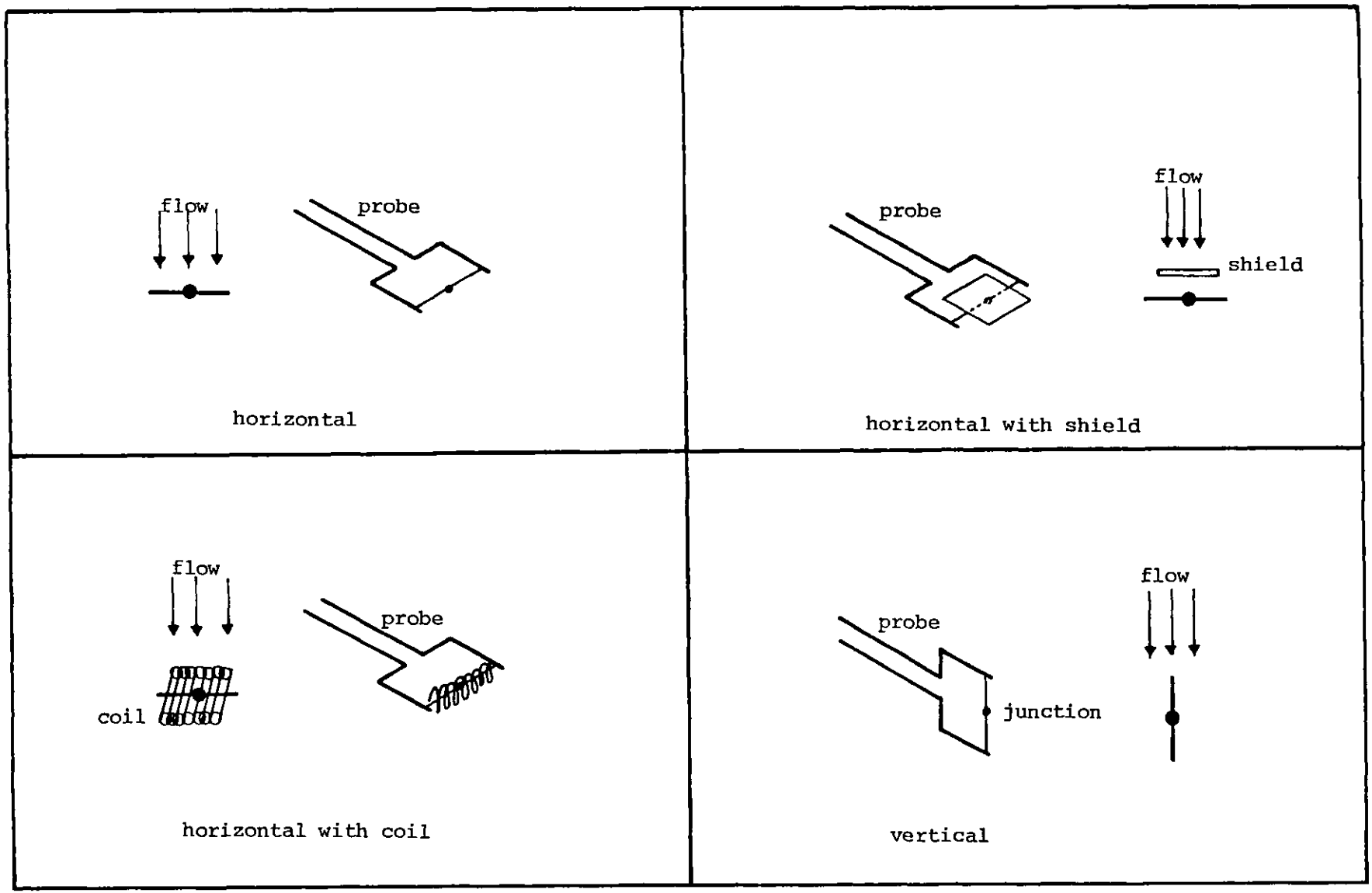

Fig.(4.2) Different designs of fine wire thermocouple probes

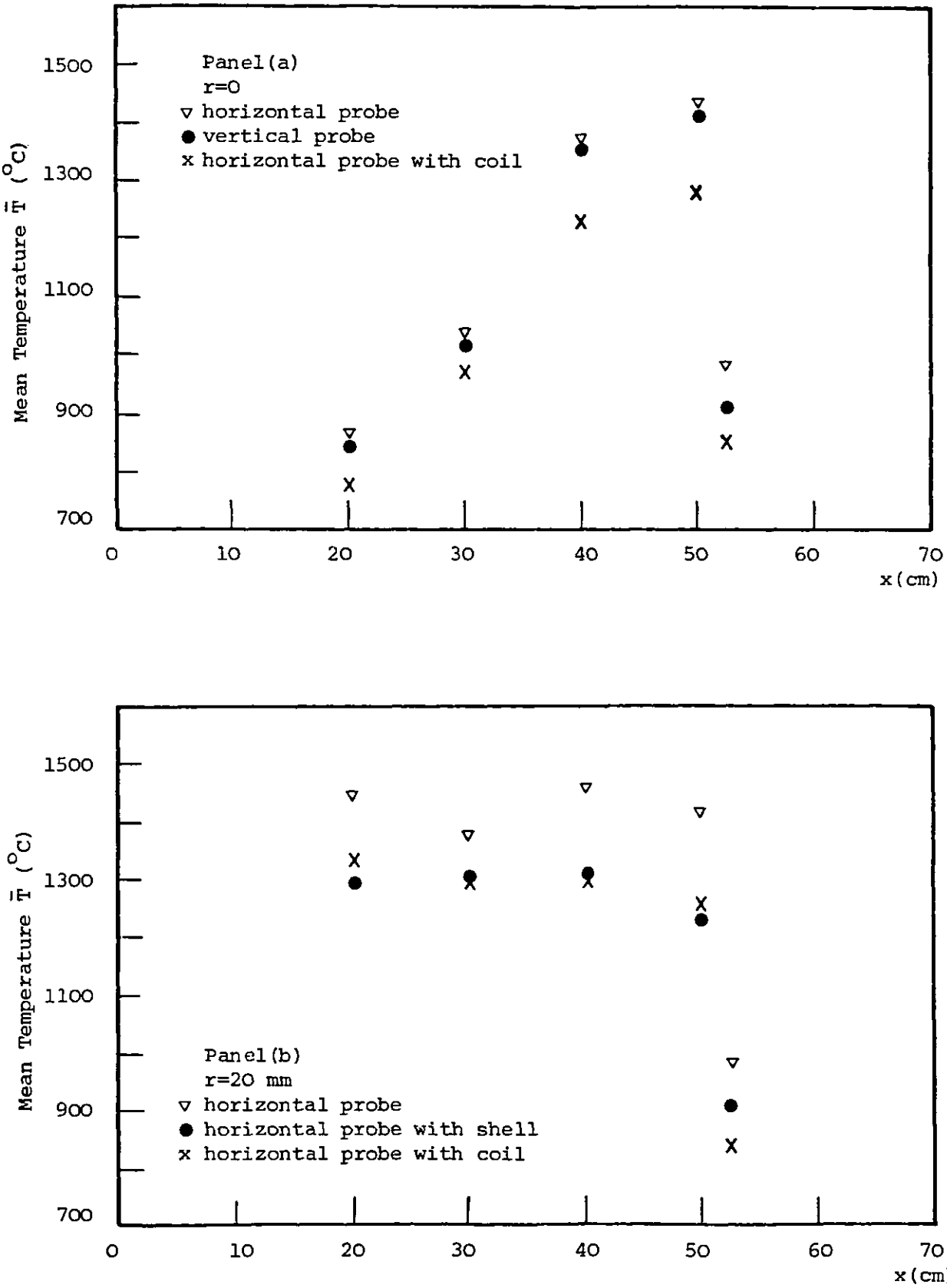

Fig.(4.3) Comparison between different thermocouple probes

to the junction as indicated by the lower temperatures measured by these probes compared to the horizontal one, panel (b) of Fig. (4.3).

It was concluded from these experiments that the fine wire thermocouple in a vertical position can be used successfully to measure a mean temperature between that of the gas and that of the particles in coal flames. Furthermore, it is believed that using the fine wire thermocouple with an adequate electronic and/or computer facilities, it may be possible to differentiate between the temperature of the gas and that of the particles, in a more or less similar manner that has been used successfully by Levy and Lockwood (1980) for the gas and solid particles velocities in a fluidized bed.

4.2.2 Turbulent Diffusion of Particles: Fundamental Consideration of Particle/Turbulence Interaction

The solid particles and the gas in a two-phase gas flow exhibit different concentrations at different locations in the flow domain and move with unequal velocities. For large particle to gas density ratios and moderate accelerations typical for PF combustors, the only important forces acting on the particle, in the absence of gravity, are the inertia and drag forces in which case the equation of motion of a particle can be expressed as, Lockwood et al (1980):

$$\vec{F} = m_p \frac{d\vec{V}_p}{dt} = \frac{C_d}{2} \rho_g A_p (\vec{V}_g - \vec{V}_p) \mid \vec{V}_g - \vec{V}_p \mid \tag{4.1}$$

where m_p and A_p are respectively the particle mass and surface area, $\vec{V}_g$ and $\vec{V}_p$ are the instantaneous gas and particle velocities respectively, ρ_g is the gas density and C_d is the drag coefficient.

The time-dependent velocity ($\vec{V}$) can be replaced by $\vec{V} = \bar{\vec{V}} + \vec{V}'$ where $\overline{V}$ is the time-averaged velocity while V' is its fluctuating velocity component. Substituting in equation (4.1), gives:

$$\bar{\vec{F}} + \vec{F}' = \frac{C_d}{2} \rho_g A_p (\bar{\vec{V}}_g - \bar{\vec{V}}_p)(\bar{\vec{V}}_g - \bar{\vec{V}}_p) + \frac{C_d}{2} \rho_g A_p \left[2(\bar{\vec{V}}_g - \bar{\vec{V}}_p)(\vec{V}_g' - \vec{V}_p') + (\vec{V}_g' - \vec{V}_p')(\vec{V}_g' - \vec{V}_p')\right] \tag{4.2}$$

Equation (4.1) can be written in time-averaged form as:

$$\bar{\vec{F}} = \frac{C_d}{2} \rho_g A_p (\bar{\vec{V}}_g - \bar{\vec{V}}_p)(\bar{\vec{V}}_g - \bar{\vec{V}}_p) \tag{4.3}$$

Subtracting equation (4.3) from equation (4.2), results in the following expression:

$$\vec{F}' = \vec{F} - \bar{\vec{F}} = \frac{C_d}{2} \rho_g A_p \left[2(\bar{\vec{V}}_g - \bar{\vec{V}}_p)(\vec{V}_g' - \vec{V}_p') + (\vec{V}_g' - \vec{V}_p')(\vec{V}_g' - \vec{V}_p')\right] \tag{4.4}$$

For very small particles (diameter <5 μm), which are totally responsive to the gas fluctuations ($\vec{V}_p' = \vec{V}_g'$), $\vec{F}'$ must be summed to zero. For larger particle diameters ($\vec{V}_p' \neq \vec{V}_g'$), $\vec{F}'$ is finite and represents the migration of or diffusion of the particles due to turbulence.

In the prediction procedures applied to particle-laden flow situations, the presence of the particles is usually made known to the gas field through mass, momentum and energy sources appended to the mean equations governing the gas flow. For example, Lockwood et al (1980) and Smoot and Pratt (1979) recognized partially the effect of the turbulence diffusion, represented by $\vec{F}'$ in equation (4.2), by giving the particles a drift velocity component while Abbas et al (1980) and Abbas (1982) simulated the effect of turbulence on particle motion in terms of a diffusion force. However, all the investigators dealing with two-phase flow prediction were using the standard two equation k-ε turbulence model, normally used for non-seeded flow conditions (Launder and Spalding (1972)), for turbulence transport in which the effect of the particle turbulence diffusion on the turbulence kinetic energy equation is not taken into consideration.

In the present work, it was considered that it would prove very useful to derive the exact equations for the correlations $\overline{V_g'^2}$, $\overline{V_p'^2}$ and $\overline{V_g'V_p'}$, which appear in equation (4.4), based on the conventional derivation of the governing equations for non-seeded flow (see for example Frost and Moulden (1977)). This introduces the effect of particle turbulence diffusion into the turbulent kinetic energy equation of the k-ε model when it is used in a particle-laden flow conditions. A summary of some of the difficulties associated with modelling of such equations, especially $\overline{V_g'V_p'}$ equation, is also given.

In order to derive equations for $\overline{V_p'^2}$, $\overline{V_g'^2}$ and $\overline{V_g'V_p'}$, it was assumed that the suspension of particles is sufficiently

dense and the particles are sufficiently small so that a volume may be considered which on one hand is large enough to contain a large number of particles and which on the other hand is small enough for any quantity within the volume to be described as a linear function of the space co-ordinates. So the mathematical implication of the turbulent diffusion of particles is simply expressed within the framework of the continuum approach for both the gaseous and particulate phases, see Hinze (1962). A complete derivation of the turbulent kinetic energy equations of gas and particulate phase and $\overline{V'_g V'_p}$ transport equation is given in Appendix I.

1. Turbulent kinetic energy for the gas phase $k_g (\equiv \sum_i V'^2_{g,i}/2)$

$$\mathrm{div}(\alpha_g \rho_g \vec{V}_g k_g) - \mathrm{div}(\alpha_g \Gamma_{eff,g} \,\mathrm{grad}\, k_g) =$$

$$\alpha_g (G_{k_g} - \rho_g \varepsilon_g) + \sum_i C_d \rho_g A_p (\overline{V}_{g,i} - \overline{V}_{p,i})(\frac{2}{3} k_g - \overline{V'_{g,i} V'_{p,i}}) \qquad (4.6)$$

where α_g is the volume fraction of the gas phase, $\Gamma_{eff,g}$ is the gas diffusion coefficient, G_{k_g} is the production of gas turbulence kinetic energy and ε_g is its dissipation rate.

2. Turbulent kinetic energy for the particulate phase $k_p (\equiv \sum_i V'^2_{p,i}/2)$

$$\mathrm{div}(\alpha_p \rho_p \vec{V}_p k_p) - \mathrm{div}(\alpha_p \Gamma_{eff,p} \,\mathrm{grad}\, k_p)$$

$$\alpha_p G_{k_p} + \sum_i C_d \rho_g A_p (\overline{V}_{g,i} - \overline{V}_{p,i})(\overline{V'_{g,i} V'_{p,i}} - \frac{2}{3} k_p) \qquad (4.7)$$

where α_p is the volume fraction of the particulate phase ($\alpha_p + \alpha_g = 1.0$), $\Gamma_{eff,p}$ is the particulate diffusion coefficient

and G_{k_p} is the production of the turbulence kinetic energy of the particulate phase.

An expression for $\Gamma_{eff,p}$ is required for equation (4.7). The relation between the diffusion coefficients of the gas and the particles is expected to depend on the ratio of the particle dynamic relaxation time (τ_d) to the integral time scale of turbulence (λ), $\psi = \tau_d/\lambda$. For $\psi << 1$ the values of the two diffusion coefficients may be expected to be equal and the ratio between the two coefficients may be expected to diminish with increasing ψ. For ψ of the order of unity, Gudmundsson and Bott (1977) have derived a semi-empirical expression from which the following relation was deduced (Abbas et al (1980)):

$$\frac{\Gamma_{eff,p}}{\Gamma_{eff,g}} = 1 + \psi \tag{4.8}$$

Using the experimental data of Goldschmidt et al (1972) and Lilly (1973), Abbas et al (1980) estimated that this expression (4.8), is valid for values of ψ up to about 2. For $\psi > 2$ the ratio $\Gamma_{eff,p}/\Gamma_{eff,g}$ decreases with increasing ψ, becoming zero for $\psi > \sim 10$. Relation (4.8) is simple because the only turbulence quantity it contains is λ, which can be estimated with the help of the calculated values of k_g and from the following relations, see Launder and Spalding (1972):

$$\lambda = \nu_{eff,g}/\frac{2}{3} k_g \tag{4.9}$$

and knowing that

$$\tau_d = \frac{4}{3} \frac{\rho_p d_p^2}{C_d Re_p \mu} \tag{4.10}$$

where Re_p is Reynolds number ($Re_p = \rho_g d_p |\vec{\bar{V}}_g - \vec{\bar{V}}_p| / \mu_g$), d_p is the particle diameter and $\nu_{eff,g}$ is the gas eddy diffusivity. The gas-particle interaction terms in equations (4.6) and (4.7) contain the correlation $\overline{V'_g V'_p}$ which necessitates the derivation of a third equation for $\overline{V'_g V'_p}$.

3. Transport equation for $\overline{V'_g V'_p}$ ($\equiv \overline{V'_{g,k} V'_{p,k}}$)

$$
\begin{aligned}
&\frac{\partial}{\partial x_k}(\alpha_g \rho_g \bar{V}_{g,k} \overline{V'_{g,i} V'_{p,i}}) + \frac{\partial}{\partial x_k}(\alpha_p \rho_p \bar{V}_{p,k} \overline{V'_{g,i} V'_{p,i}}) = \\
&- \frac{\partial}{\partial x_k}(\alpha_p \rho_p \overline{V'_{p,k} V'_{g,i} V'_{p,i}}) - \frac{\partial}{\partial x_k}(\alpha_g \rho_g \overline{V'_{g,k} V'_{g,i} V'_{p,i}}) \\
&- \alpha_p \frac{\partial \overline{p' V'_{g,k}}}{\partial x_k} - \alpha_g \frac{\partial \overline{p' V'_{p,k}}}{\partial x_k} + \frac{1}{2} \alpha_g \mu \frac{\partial^2 \overline{V'_{g,i} V'_{p,i}}}{\partial x_j \partial x_j} \\
&- \alpha_p \rho_p \overline{V'_{p,k} V'_{g,i}} \frac{\partial \bar{V}_{p,i}}{\partial x_k} - \alpha_g \rho_g \overline{V'_{g,k} V'_{p,i}} \frac{\partial \bar{V}_{g,i}}{\partial x_k} \\
&+ \alpha_g \mu \overline{\frac{\partial V'_{g,i}}{\partial x_j} \frac{\partial V'_{p,i}}{\partial x_j}}
\end{aligned}
\qquad \left.\right\} \text{conventionally modelled generation and destruction terms}
$$

$$
\begin{aligned}
&+ \alpha_p \rho_p \bar{V}_{p,k} \overline{V'_{p,i} \frac{\partial V'_{g,i}}{\partial x_k}} + \alpha_g \rho_g \bar{V}_{g,k} \overline{V'_{g,i} \frac{\partial V'_{p,i}}{\partial x_k}} \\
&+ \alpha_p \rho_p \overline{V'_{p,k} V'_{p,i} \frac{\partial V'_{g,i}}{\partial x_k}} + \alpha_g \rho_g \overline{V'_{g,k} V'_{p,i} \frac{\partial V'_{p,i}}{\partial x_k}} \\
&+ \sum_i 2 C_d \rho_g A_p (\bar{V}_{g,i} - \bar{V}_{p,i}) (\tfrac{1}{3} k_g + \tfrac{1}{3} k_p - \overline{V_{g,i} V'_{p,i}})
\end{aligned}
\qquad \left.\right\} \text{new terms} \qquad (4.11)
$$

It is clear that the modelling of the different terms of equation (4.11) is a very difficult and challenging problem

and no attempt has been made to put this equation in a general form as that done with k_g and k_p and it is a problem for modellers to try and solve it.

4.3 Extension of the Gas-Fired Furnace for Coal Firing

The furnace and its auxiliary equipment described earlier in detail in Chapter (3) was arranged for coal firing. A coal feeding system and a primary air supply were connected to the furnace. A complete diagram for the coal firing arrangement is shown in Fig. (4.4). Pulverized coal is fed into the primary stream by a screw feeder, made by Ajax Equipment (Bolton) Ltd. The feeder is equipped with a 1/4 HP d.c. geared motor, totally enclosed, the speed of which can be varied either manually by a 10-turn precision speed controller or automatically by a microprocessor control system, see section (4.4). The feeder came equipped with a conical feed hopper. Figure (4.5) and panel (4.1) show the coal feeding and primary air arrangement. The discharge rate of the powdered coal leaving the screw feeder tends to be affected by the coal properties, feeder geometry, the helical shape of the screw and its rotational speed. The resulting flow irregularities are accentuated in non-ideal conditions such as when the feed screw is turning at low speed. In order to smooth the flow fluctuations, a cylindrical steel angled chute fitted with a vibrator (eccentric mass rotating by a d.c. motor) is

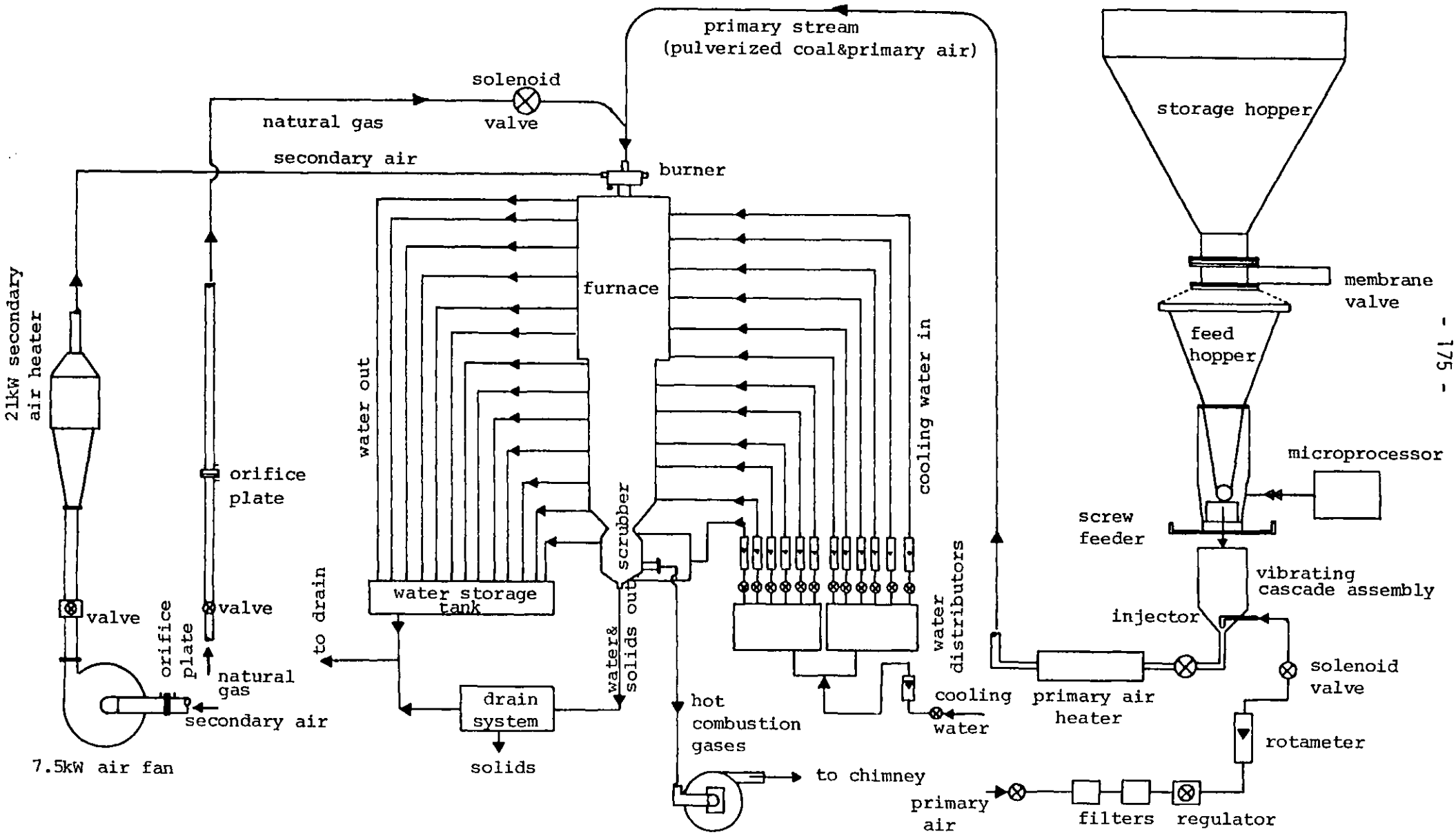

Fig.(4.4) Details of furnace arrangement(coal-firing)

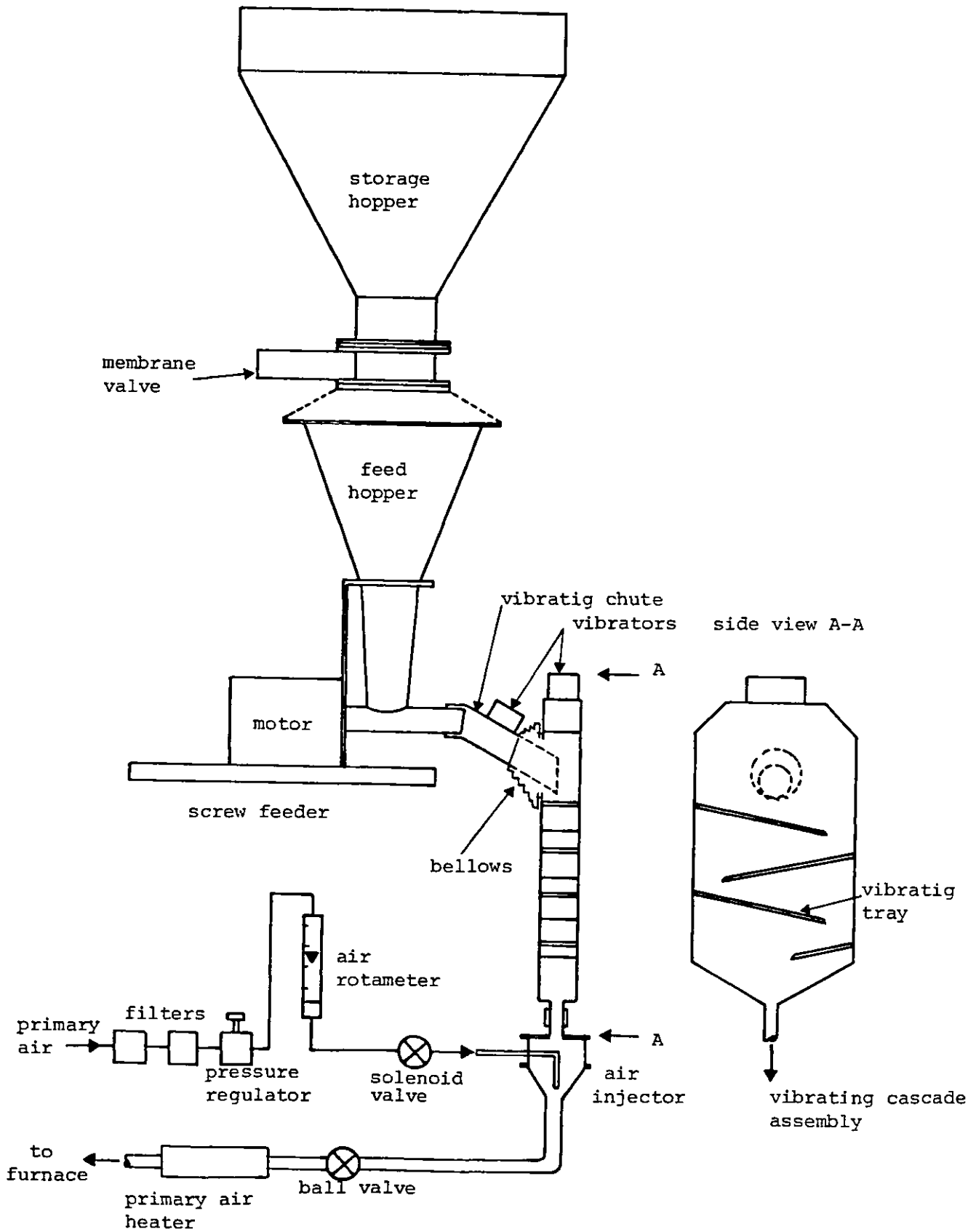

Fig.(4.5) Coal feeding system

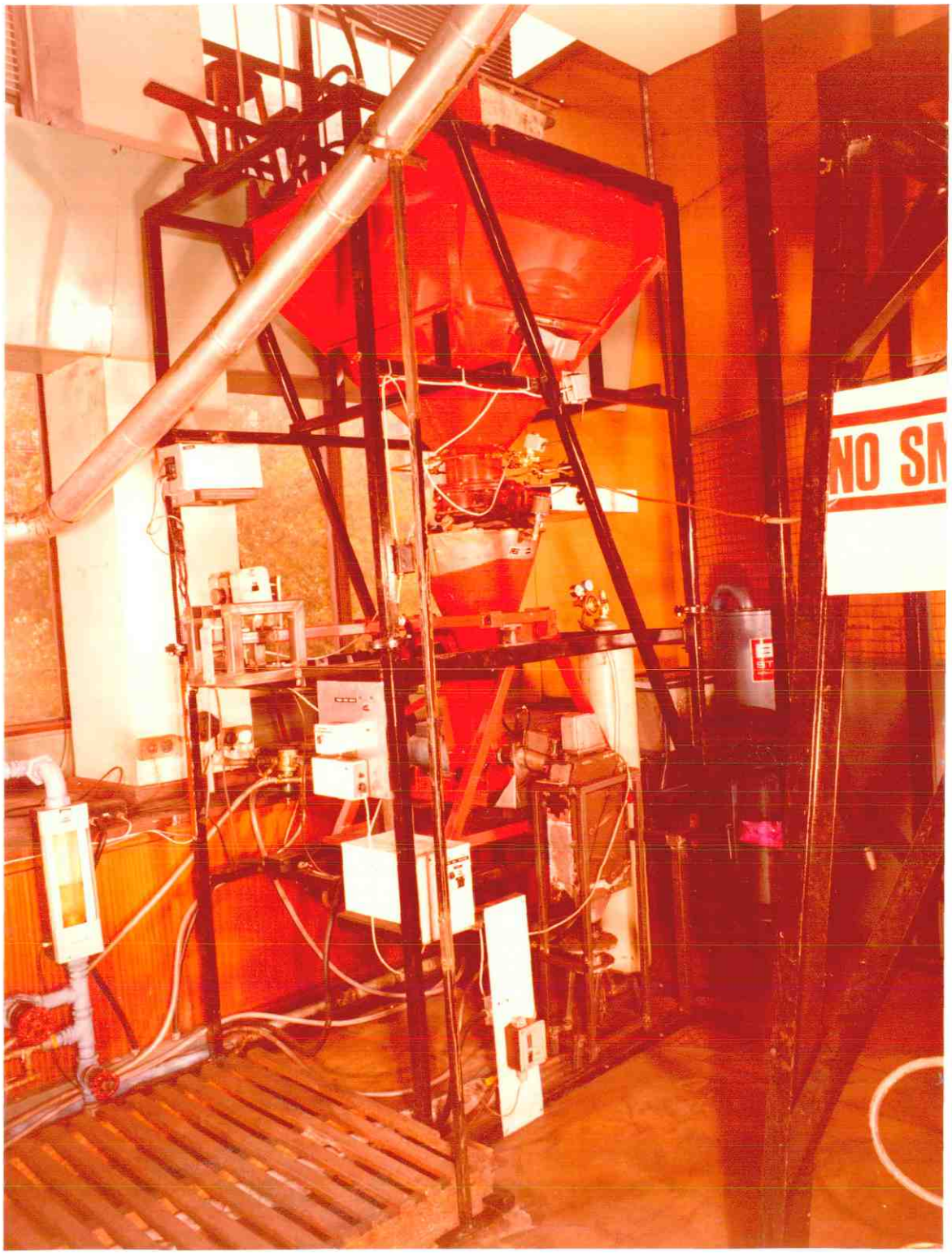

Panel(4.1) Photograph of the coal feed system

placed in the flow path such that the flow of coal powder from the feed screw falls onto this vibrating channel and a smoothing action is effected. The amplitude of the vibration is controlled by changing the vibrator motor speed using a variable power supply (type 430, Weir Electronics Ltd.). The screw feeder, its feed hopper and the vibrating chute are mounted on a weighbridge, see section (4.4). The coal coming from the vibrating chute, is in addition fed to a multi-chute cascade assembly fitted with a vibrator (Eriez Magnetics, type 20N). The cascade assembly has four stainless steel angled chutes, Fig. (4.5), and its main purpose is to apply the maximum possible smoothing action to the coal feed fluctuations before the coal is mixed with the primary air. The vibration is of low amplitude (< 1 mm) and electromagnetically induced at mains frequency of 50 Hz.

The capacity of the feed hopper is quite small (6 Kg) and its coal content is sufficient for a short period of time (about 1/2 hour). In order to keep a continuous feed of coal as long as required for a particular experimentation, refilling of the feed hopper is essential when the weight of the contents drops under a minimum weight limit. A storage hopper, Fig. (4.5), therefore was constructed and placed on the top of the feed hopper. An automatic membrane valve (Bulk United Systems Limited, type AU8) was mounted fully closed on the exit of the storage hopper. Whenever necessary a normally closed solenoid valve is automatically activated, compressed air opens the membrane valve, Fig. (4.15), and the refilling action is carried out until the hopper is filled with a reasonable amount of coal. A temperature control system

was developed and installed on the storage hopper in order to avoid any possibility of fire caused by spontaneous combustion. It comprises, as shown in Fig. (4.6), two temperature sensors covering the temperature range of $70^{o}C$-$100^{o}C$ (thermal switches by RS Components Ltd.) with an electronic circuit which opens a solenoid valve (Dewraswitch Limited) and floods the hopper with nitrogen (from cylinders) through a fluidizing arrangement in the case of any undue rise of temperature of the pulverized coal. This nitrogen purge is discharged from a non-return valve located on the top of the hopper, allowing nitrogen to exit and preventing any air entering. A graduated depth stick was used to measure the coal level in the hopper, see Fig. (4.6).

The coal used was Grimethorpe 250 grade coal dust. It was pulverized and supplied by the Standard Pulverized Fuel Company Limited, in sealed bags each containing 25 Kg . Typical properties and characteristics, as provided by the coal supplier, are shown in Table (4.1). Characterization of this coal is given in Chapter (5). The coal was fed to the storage hopper by a Bivac pump (type CL 3HP, Bivac Stockport) and a cyclone separator arrangement, as shown in Fig. (4.7) panel (b). A size distribution analysis - see Chapter (5) - of coal samples from the bags, coal samples from the storage hopper and samples from the coal trapped in the pump showed that the cyclone was not very efficient and it failed to retain most of the very fine coal particles (less than 50 μm). This together with the fact that the filling of the storage hopper was a time consuming process, the cyclone-pump arrangement was replaced by a steep square ducted angled chute with a one way lid, shown in panel (a) of Fig. (4.7).

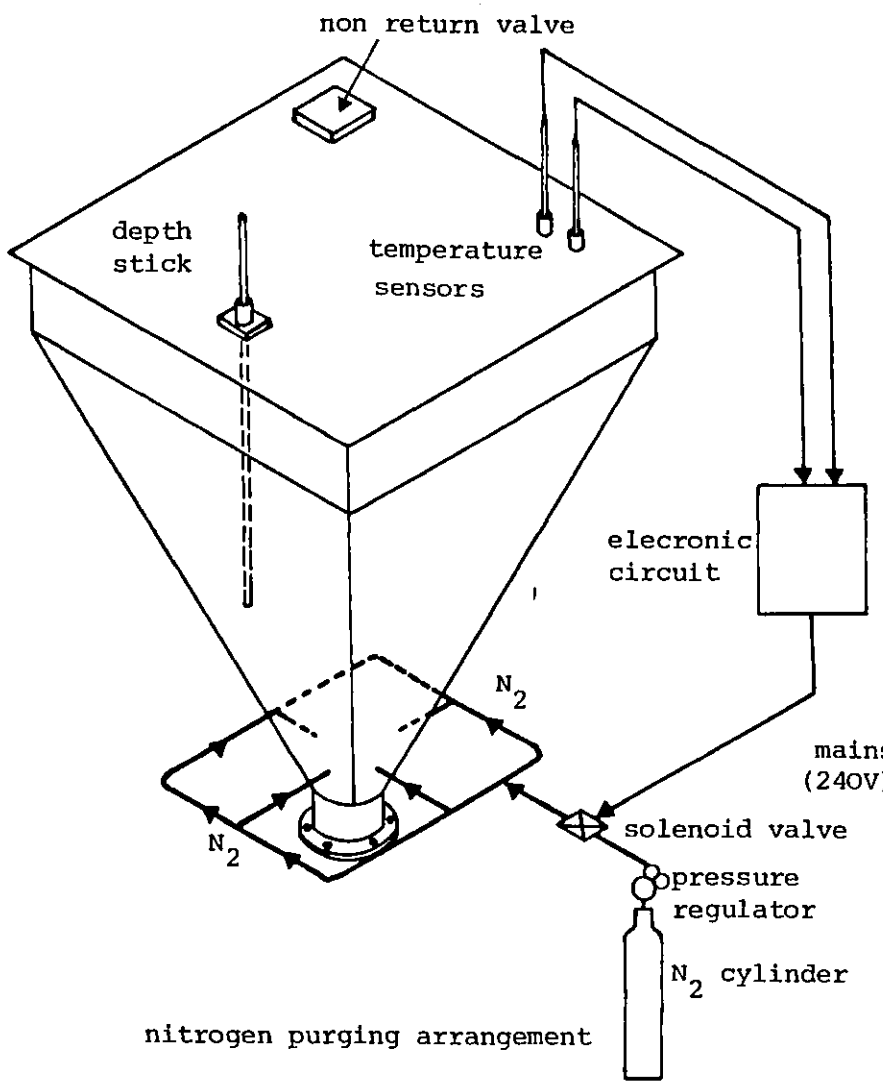

nitrogen purging arrangement

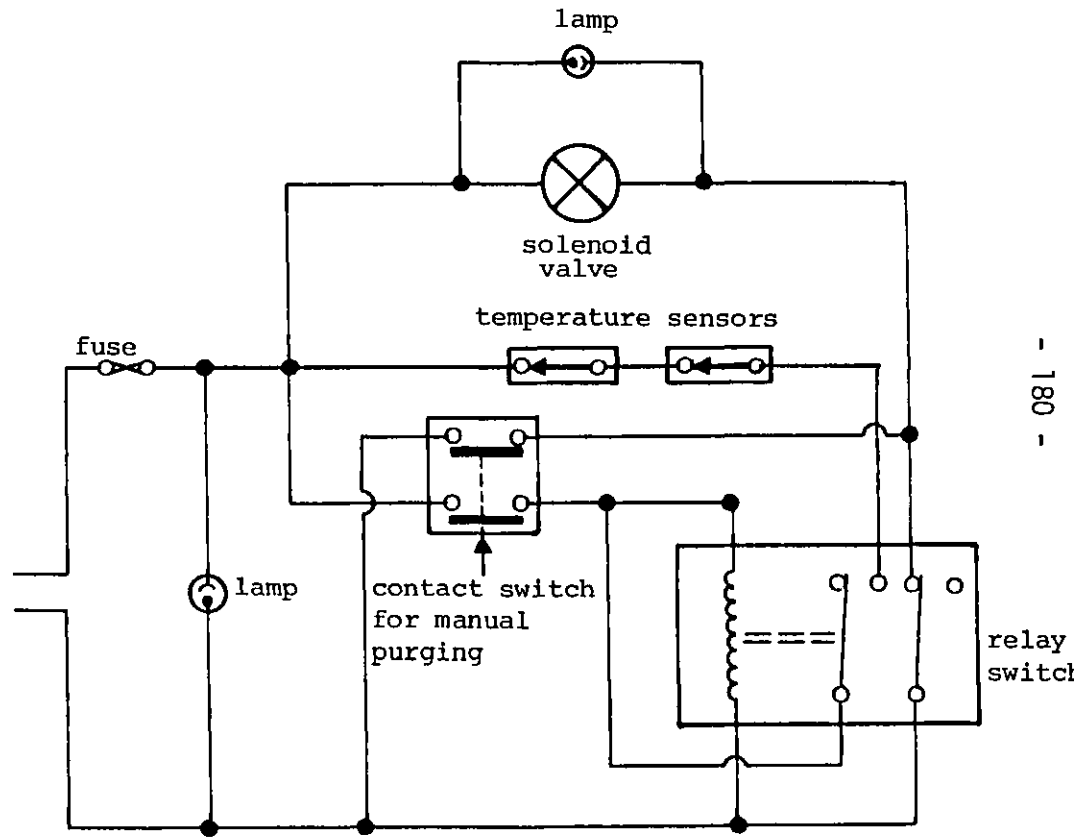

circuit diagram for nitrogen purging system

Fig.(4.6) Temperature control system for the storage hopper

Table (4.1)

Properties and characteristics of the Grimethorpe 250 Grade Coal Dust*

Swell index	4½
Calorific value	14000Btu/lb
Rank	501
Bulk density approx.	35-42 lb/ft^3

Typical Grading

B.S. Sieve	% retained
+ 16	-
+ 30	1
+ 72	2
+ 100	4
+ 200	13
- 200	80

Typical Analysis

Component	% by weight
Ash	5.5
Moisture	3.5
Volatile	33.5
Fixed carbon	57.5
Sulphur	1.5

*These data have been provided by the Standard Pulverized Fuel Co. Ltd.

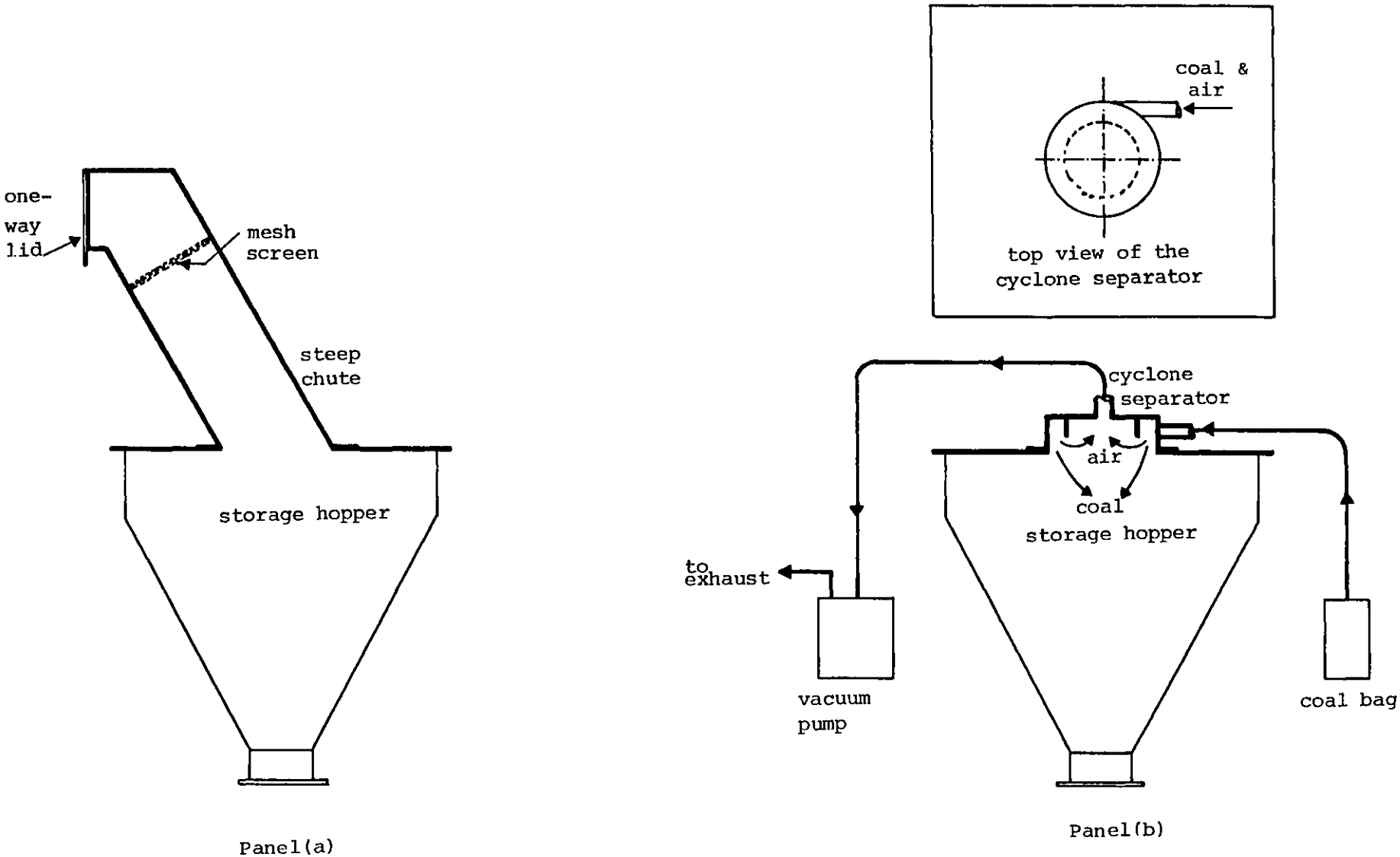

Fig.(4.7) Methods for refilling the storage hopper

Compressed air at 100 psi is used as a primary air supply. The air is filtered and dried by two automatic filters (Norgren, type F13-Ae) connected in series. The air pressure is controlled by a precision pneumatic pressure regulator (Deltech Engineering Limited, series 4000) which provides a uniform output pressure independent of supply pressure variations. The primary air flow rate is monitored by a calibrated rotameter (Fisher Controls Limited, type 2000 TM-35 FM-A). The primary air supply, activated by a normally closed solenoid valve (Dewraswitch Limited), is mixed with the coal powder falling from the vibrating cascade assembly in a nozzle-shaped injector, see Fig. (4.5). This air carries the coal in suspension through a primary line into the furnace. The primary line, made of copper tube (28 mm and 25 mm external and internal diameters respectively), is heated electrically by two type GW heating tapes, 850 watts each (Hotfoil Limited) and controlled by a thermostat. To minimize the heat loss to the atmosphere, the line from the exit of the air injector up to the primary tube of the burner is insulated by a non-combustible rock fibre material (Cape Insulation Limited). The primary stream could be heated up to 80^{o}C and its temperature is monitored by a nickel-chromium/nickel-aluminium thermocouple. The coal-primary air stream is injected into the furnace through a concentric primary tube, Fig. (4.8). The primary tube is a stainless steel straight pipe of 30 mm internal diameter and 35 mm external diameter. This replaced the radial injector used in the gas combustion experiment, see section (3.2).

The secondary air (as shown in Fig. 4.4)) is supplied by a 7.5 kW forced draught fan and controlled by a calibrated orifice

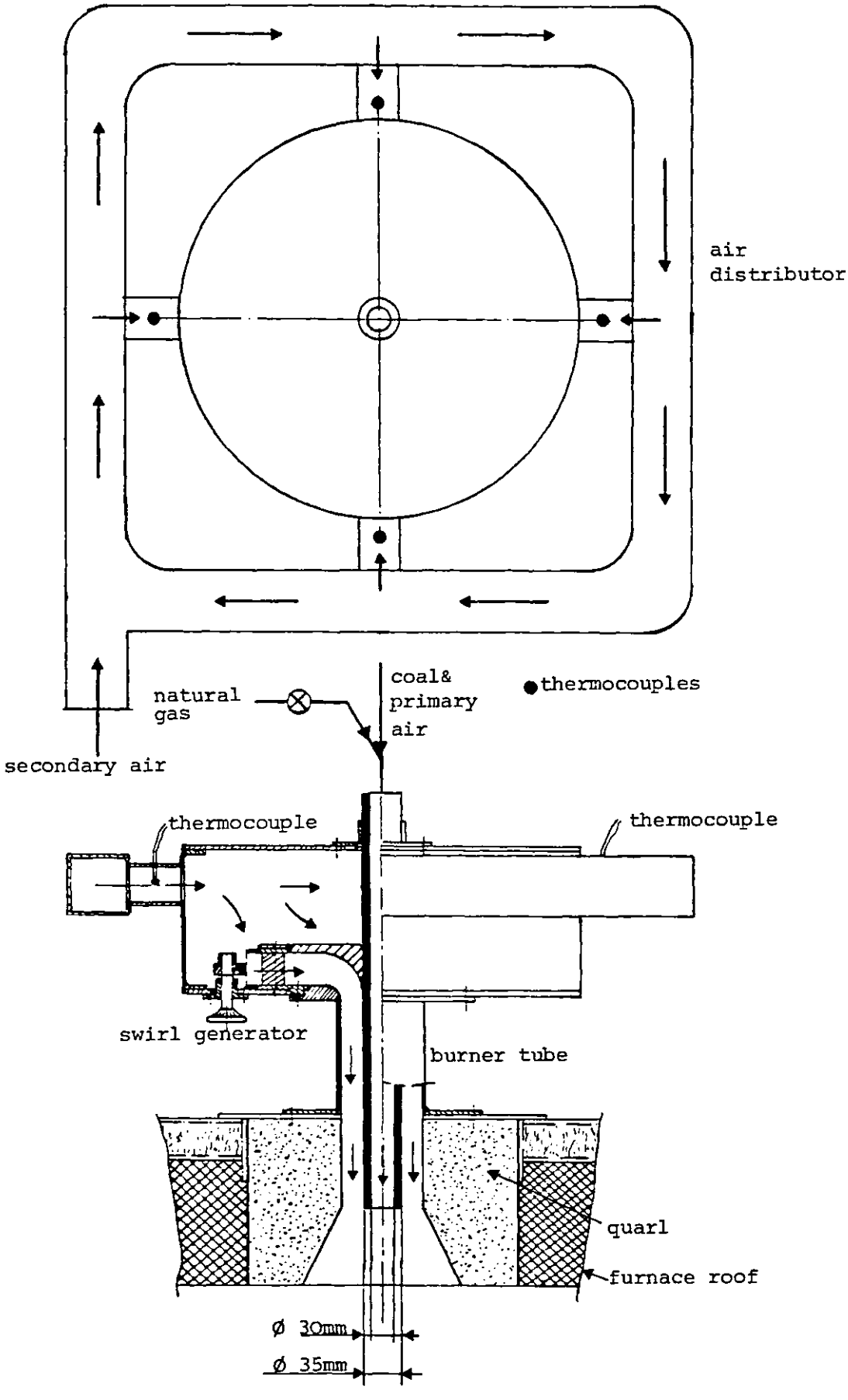

Fig.(4.8) Schematic diagram of coal burner

plate on the inlet side of the fan. An electric heater (Eltron London Limited) rated at 21 kW, controlled by a variac transformer (Zenith Electric Co. Ltd.), is used to preheat the secondary air to 300^{o}C. The secondary air temperature is recorded by a nickel-chromium/nickel-aluminium thermocouple located at the exit of the heater. The air duct from the exit of the heater up to the quarl is completely insulated by Rocksil insulating material manufactured from rock fibre (Cape Insulation Limited). The secondary air temperature is double checked by four nickel-chromium/nickel-aluminium thermocouples located at the four inlet ports of the burner, see Fig. (4.8).

A gas scrubbing system was incorporated into the furnace design to deal with the combustion flue gases and fly-ash particles produced by coal flames. It consists of, as shown in Fig. (4.9), a venturi scrubber with an accompanying cyclone separator, both are cooled by water jackets. The principle behind the venturi scrubbing system is quite simple. The particle-laden gases are forced through a venturi nozzle which greatly increases the gas velocity. At the throat of the nozzle, water is injected by a water spray, in a perpendicular fashion, which traps and decelerates the particles and also reduces the exhaust gas temperature to about 200-300^{o}C. The gas is then separated from the water and solids in the cyclone. Water and solids are discharged from the bottom of the cyclone to a waste system, refer to Fig. (4.10), which consequently precipitates the fly-ash particles using two tanks. A float-lever mechanism in the water tank triggers a water pump on/off depending on the water level. So the water is pumped to the drain while the

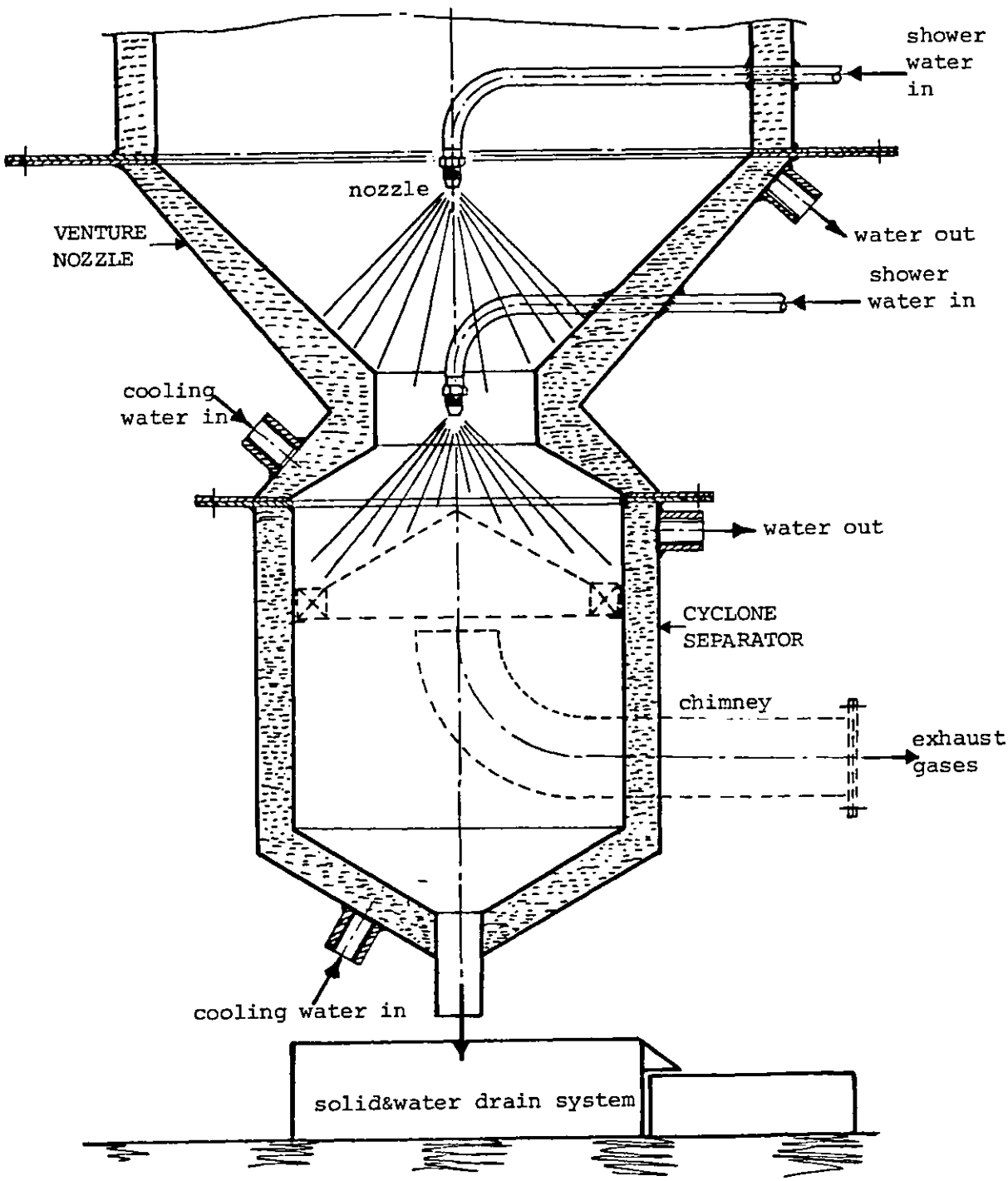

Fig.(4.9) Details of the scrubber

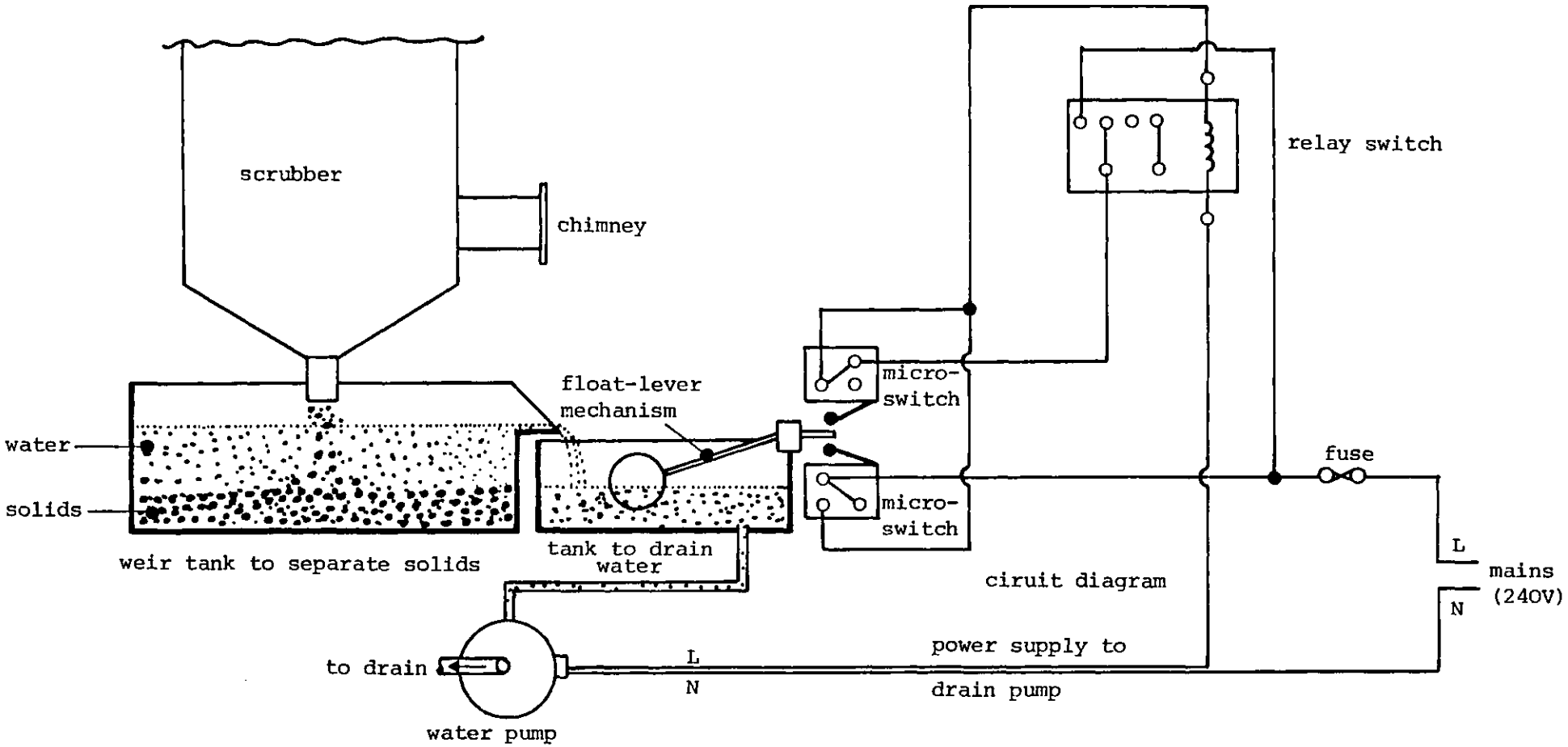

Fig.(4.10) Details of the waste system

solids remaining in the weir tank are cleared manually after each test. The flue gases, the temperature of which is monitored by a plantinum/platinum - 10% rhodium thermocouple,are discharged through an induced draught fan to the laboratory extraction system, Fig. (4.4).

All the test rig components are electrically earthed to minimize the risk of a built-up electro-static charge within the rig which on discharge might ignite a pulverized coal or gas/air mixture and causes an explosion. The explosion vent fitted to the furnace tenth segment is vented via a water trap so that blasts in the case of an explosion are shielded from personnel and atmosphere local to the furnace rig. A ball valve is fitted on the primary line after the air injector to isolate the coal feeding system from the rest of the furnace during light-up on gas to avoid any possibility of flash back. The primary air solenoid valve, coal feed, heaters and vibrating tray and vibrating cascade power supplies are connected into the furnace flame supervision control system which shuts down the coal feed immediately in case of flame failure. Details of the flame supervision system are given in section (3.2); also the complete electric circuit diagram is shown in Fig. (3.12). Slagging of the combustion chamber was unavoidable. Therefore, there was a provision for lifting the top of the furnace for access to the refractory lining and combustion space.

The successful operation of the combustion facility on coal and the collection of data was a time consuming procedure. The basic operation procedure was established through the experience

gained in the series of gas and coal combustion tests. A typical test consists of four main stages: (1) reactor preheat, (2) stabilization of the coal flame, (3) data collection and (4) reactor cool down. Referring to the block diagram in Fig. (4.4), the procedure is commenced by turning on the cooling water to all segments, venturi scrubber and the two water showers and the flame scanners being supplied with the necessary cooling air. The induced draught fan, gas compressor and forced draught fan are switched on. The secondary air flow is adjusted to the desired value and the furnace is purged for about 30 minutes. The igniter burner is then placed correctly in its position in the furnace roof and ignited. The gas control valve is set to produce the desired gas flow rate. The main burner gas solenoid valve is activated and when successful ignition is achieved, a small amount of primary air is admitted to the primary line to prevent the combustion gases from going into the coal feeding system. The reactor is preheated with this natural gas-air flame until an inside refractory wall temperature of $1100^{o}C$ is reached. The primary air heater, vibrating tray, vibrating cascade assembly and screw feeder are switched on. The latter is set to the desired coal feed rate and the primary air flow is increased to the desired flow. When the proper coal feed rate is achieved, the natural gas is shut off, leaving a stabilized coal-air flame. The secondary air flow is adjusted to the required flow rate and the secondary air heater is switched on. The coal-air flame is then allowed to burn for an additional time to establish the required inlet conditions. The pilot flame is switched off and the igniter burner is removed from the furnace and a cover is positioned on its access

tube. After a steady coal flame and nearly steady wall temperatures are attained, data collection procedure is initiated. This is continued until the collection of data is finished. The reactor is shut down and allowed to cool. The total time involved from start up to complete shut down was about eight hours.

4.4 Microprocessor Control of the Pulverized Coal Feed Rate

One of the areas in need of immediate attention in the field of coal combustion is that of feed rate control of the powdered (pulverized) coal entering the combustor. Accurate control of the coal feed rate enhances combustion efficiency and enables pollutant levels to be regulated more easily. In addition, accurate feed rate is a fundamental requirement to obtain reliable data in research experiments, which are usually conducted at nominally constant mass flow rate of fuel. For these reasons it was decided to incorporate some form of feed control into the design of the coal feeding system described earlier in section (4.3).

The present section describes the design of a microprocessor-based feedback control system, relying on the "loss-in-weight" principle, for regulating the mass flow rate of the pulverized coal prior to its entry into the coal experimental furnace. In brief, the system consists of a screw feeder with its feed hopper mounted on a weighing system. The weight of the hopper, coal and the output feeder is applied through a lever system to a load cell. The weight of the hopper and the screw feeder is balanced by a counterbalance

weight and therefore the load cell senses only the weight of coal in the hopper. A spring and airpot dampers are fitted to the lever system to provide preliminary mechanical filtering ahead of the signal conditioning which takes place in the control system. The load cell is attached to the lever system using a tension type spring connection to minimize the effects of side loading. As the coal is fed to the furnace through a primary line, the output signal from the load cell shows a continuously decreasing weight. The load cell signal is amplified and fed to a microprocessor control. The microprocessor detects the difference between the output weight from the load cell and the calculated (theoretical) weight. The resulting error is used to adjust the speed of the feeder motor, thus increasing or decreasing the feed from the hopper. In this way the control system ensures that the weight loss from the hopper is equivalent to a theoretical weight loss calculated from a desired feed rate. When the amount of coal in the loss in weight hopper reaches a preset minimum, it is rapidly replenished from a storage hopper. The programmed outflow rate is not affected by this because a heel of coal always remains in the hopper and the outflow rate is locked on the one prevailing just before refilling. After refilling the loss-in-weight control action takes over again.

4.4.1 The "Loss-in-Weight" Technique

The physical properties of fine powder are such that considerable technical difficulties are encountered in attempting to control its flow behaviour. The occurrence of large variations in local density of a bulk of such fine material is readily apparent. Pressures acting within the bulk are not hydrostatic and may vary widely in both magnitude and direction according to many factors such as container geometry and particle diameter.

Dry granular products which are non-cohesive such as sand, plastic beads, dry crystal and grains are usually free flowing and have stable density. Such products present little difficulty in feeding at controlled rates via calibrated orifices, vibrating feeders or screw or belt feeders which are all essentially constant volume methods of feeding. However, cohesive products, which are generally any material finer than 200 μm, or those with particle adhesive strength due to the presence of surface moisture, presents two main problems. The first is guaranteeing a reliable flow, which is chiefly the problem of hopper design, screw feeder dimensions and the rotational speed of the feed screw. The second is achieving and maintaining a consistent density. Variations of the moisture content and particle size of the product are impossible to accommodate other than by trial and/or by calibration.

The properties of pulverized coal with particle diameters less than 90 μm are such that volumetric feeding proves to be a highly unsatisfactory method of achieving a constant mass flow rate. Apart from the problem of local density variations causing

a fluctuation in the output, the mean bulk density tends to reduce as the level in the feed hopper falls, due to the reduction of the head pressure. Thus it was necessary to include in the flow control technique some means of accounting for density variations. One method of achieving this is to use the so called "loss-in-weight" technique in conjunction with a feedback control system. The rate of weight loss can be determined by measuring the change in the weight of the hopper content over a specific time interval and control over this rate can be achieved by varying the speed of the feeder screw at the base of the hopper. This method is illustrated in Fig. (4.11). A control system operating with the use of feed back is said to be in a closed-loop mode. Feedback control for any control system consists of being able to sense the error which exists between the desired output and the actual output and make adjustments to the system controls to reduce the error. In the present application, the error is the difference between the actual and ideal (theoretical) coal feed rate at any given time and control over the magnitude of the error is obtained by adjusting the rpm of the screw feeder motor accordingly. Thus if the actual weight of the coal is above the desired or ideal value, the speed of the feed screw is temporarily increased and vice versa.

An overall impression of the present control system may be gained by studying the block diagram shown in Fig. (4.12). The weight of the coal in the feed hopper is converted into an electrical signal by means of a strain gauge type load cell transducer. This signal is amplified by a conditioner amplifier to make it

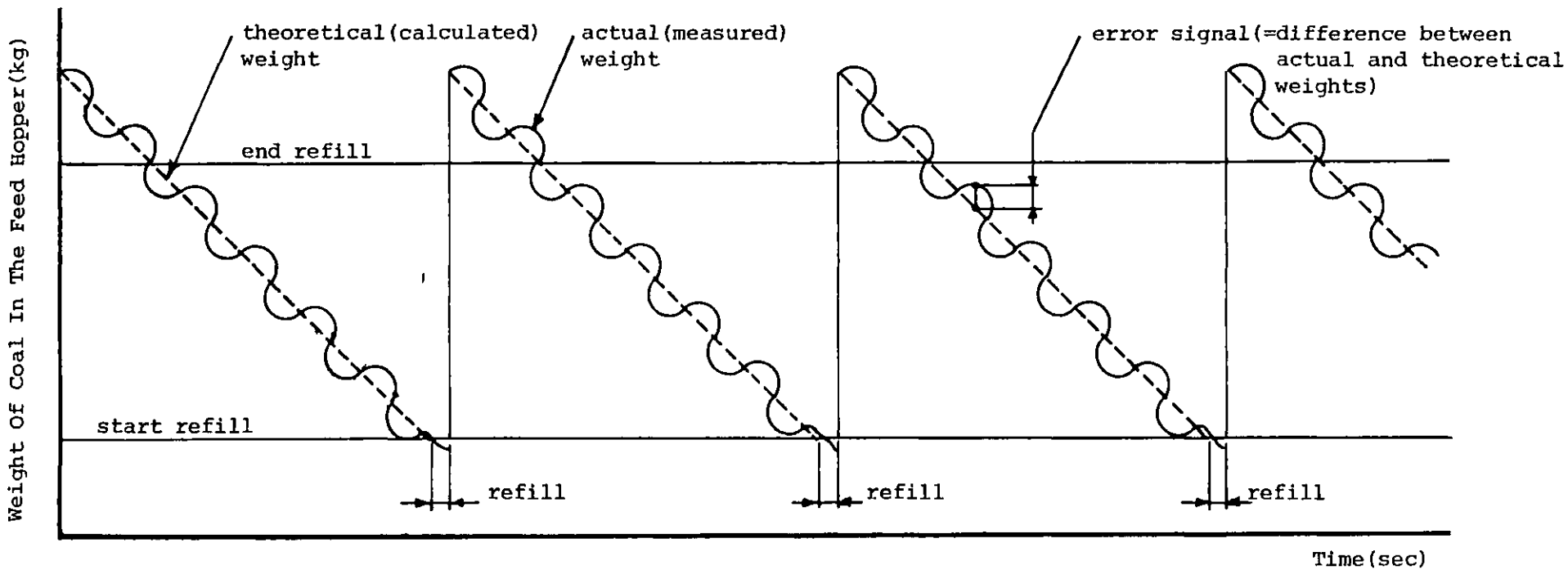

Fig.(4.11) Weight-time graph for the loss-in-weight technique

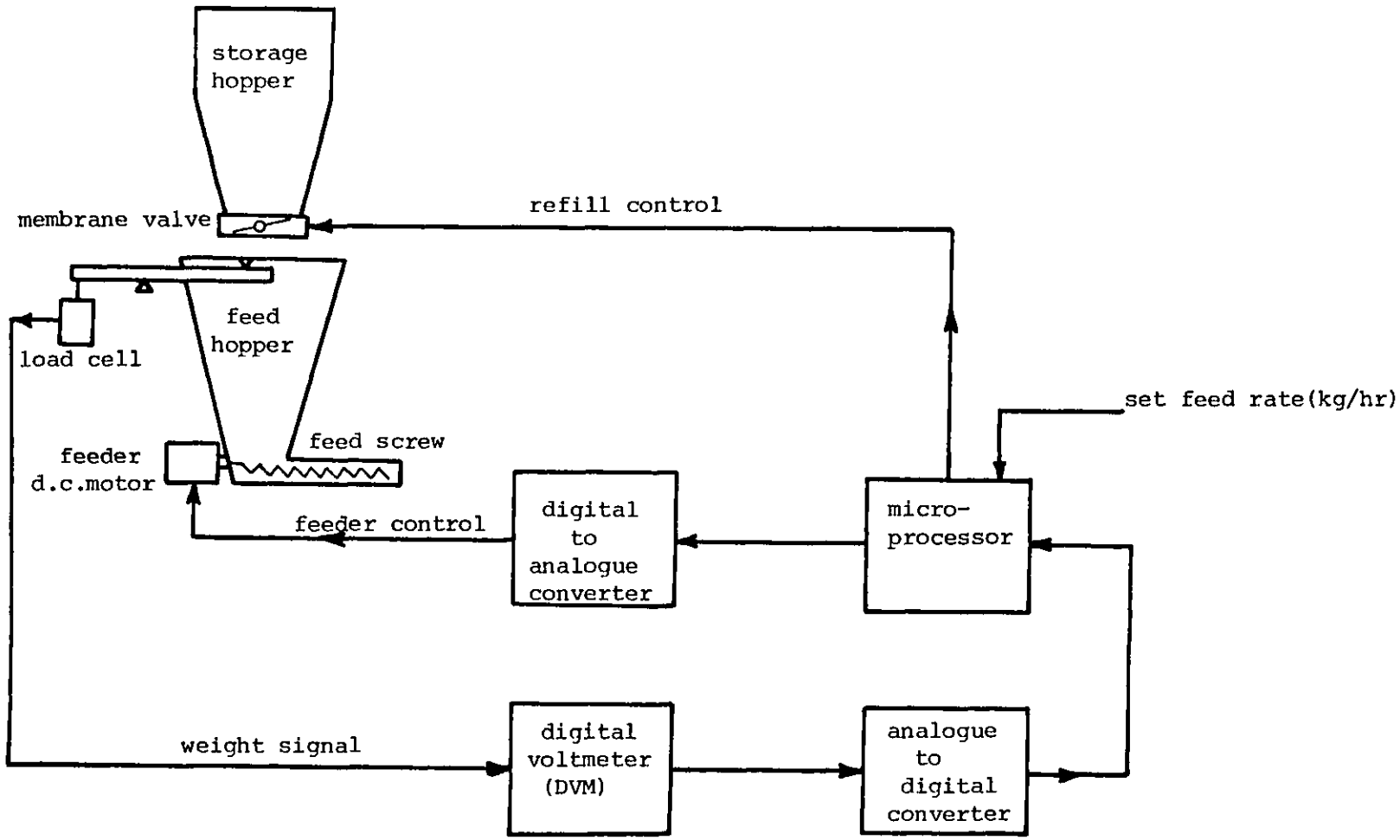

Fig.(4.12) Schematic diagram of the"loss-in-weight"control system

compatible with the digital voltmeter used to display the reading. The conditioned signal which is in an analogue form, is converted into digital form by an analogue to digital converter built in the digital voltemeter. This is a necessary step as the microprocessor can only recognize information in digital form. The signal in digital form is fed into the input port of the microprocessor. The microprocessor then processes the information and checks the weight of the coal in the hopper. The microprocessor evaluates a new screw feeder speed in a digital form. This is converted to an analogue form by a digital to analogue converter to make it compatible with the d.c. motor which drives the feed screw. If the weight of coal in the hopper is less than a lower limit, an analogue signal is sent, from the output port of the microprocessor, to activate a membrane valve mounted between the feed and storage hoppers and a refill operation is initiated until the feed hopper is filled to a preset maximum weight limit.

4.4.2 Design Features of the Weighing Bridge

I. Balance beam method for weight sensing

Traditional practice in weight sensing applications would be to mount the vessel to be weighed on a minimum of three load cells and then take a mean of the three readings to obtain the weight. However, two major disadvantages were apparent

with such a method. Firstly, by measuring gross weight instead of the actual weight of the contents, the effective resolving power would be reduced significantly, and secondly it would be expensive to buy three precision load cells. In order to overcome these disadvantages, a beam and a counterbalance arrangement were adopted as it is shown in Fig. (4.13). This method,which is extremely simple in concept, offers high resolution with the use of only one load cell, and also minimizes the cost. In operation, the position of the counterbalance weight is adjusted by means of a screw adjuster arrangement, so that the collective weights of the feed hopper, feeder screw and its motor on one side of the beam are balanced by the weight of the counterbalance weight on the other side. Now, the addition of coal into the feed hopper causes an out of balance torque to arise. To maintain equilibrium, a reactive torque is supplied by the load cell. Because the strain imposed on the load cell is exactly proportional to the applied torque, the output of the load cell gives a reading proportional to the mass of the coal in the hopper.

If the centre of gravity of the mass of the coal within the hopper shifts in the axial beam direction, the weight sensed by the load cell is no longer the true weight of the coal in the hopper, as the moment arm has been altered. These shifts are caused by the irregular pattern of depletion of coal from the hopper and the unsymmetrical filling of the hopper from the main storage hopper. The screw feeder assembly was mounted on a swing cradle carried by two main knife-edges. This arrangement enables the true weight of the coal to be transmitted (via the knife-edges) to the load cell irrespective of the position of the

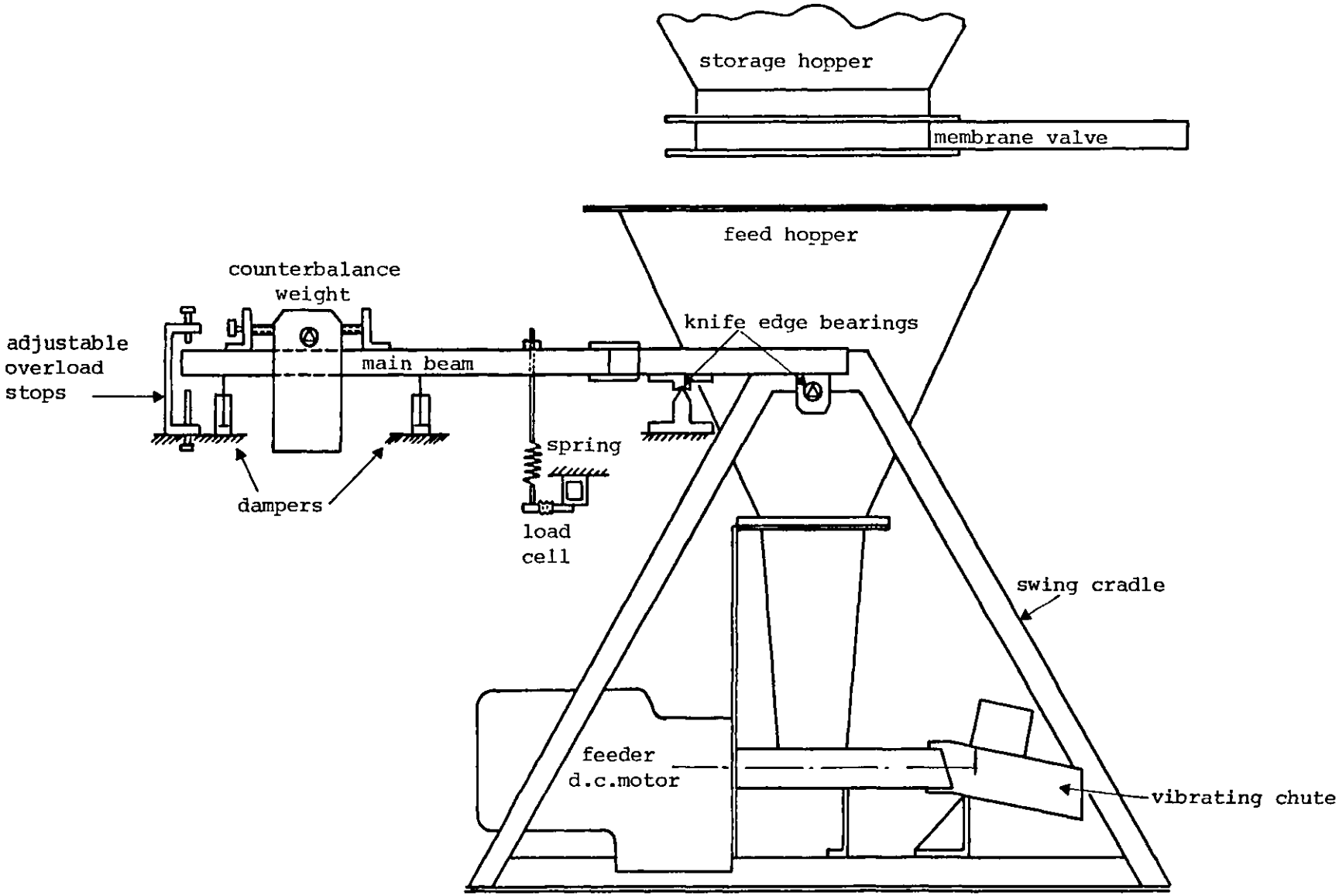

Fig.(4.13) The Weighbridge

centre of gravity of the coal relative to the centre of the feed hopper.

In order to control unwanted oscillations of the main beam and the swing cradle, two adjustable viscous dampers (type Airpot, N.R.G. Engineering Limited) were incorporated into the design. The working fluid in the airpot damper is air so maintenance such as refilling and cleaning is not required. Figure (4.13) shows the locations of the dampers between the main balance beam and two fixed points on the whole assembly frame. For its success the weighbridge design depends on the rotational friction generated at the bearing sites to be kept as small as possible. There are three bearing sites in the design. These are, the main bearings of the balance beam, the secondary bearings for the swing cradle and the bearings from which the counterbalance is suspended. All the bearings are case-hardened ground steel knife-edges which locates into mating vee-grooves thus providing precision balance characteristics with high wear resistance. The knife-edges are situated below the vee-grooves, in order to prevent the coal dust from settling in the grooves.

The weighbridge is linked to the primary stream system by a bellows, as shown in Fig. (4.5). This bellows fufills the following functions: (i) it accommodates the small vertical and swing movements of the weighdeck, (ii) it prevents any unaccounted primary air leaks into the primary system by the vacuum created on the upstream side of the air injector, (iii) it damps some of the oscillations in the weighbridge especially during the refill process and (iv) it acts as an explosion vent in case of a pressure build-up in the primary line.

II. The load cell

The load cell which senses the weight of the coal in the hopper is a Sangamo Transducer D97 series, which has a maximum range of ±500 N at a deflection of ±0.3 mm. Despite its relatively modest size of 32 mm diameter by 115 mm length, its performance characteristics are of a very high order which is very important as far as the overall accuracy is concerned. One of the advantages of this load cell is that it is based on a parallel motion cantilever beam design and thus misalignment errors due to loading induced flexture are avoided. If loads considerably in excess of the design rating were applied to the load cell, permanent damage would be caused to the strain gauges, resulting in the load cell being rendered useless. Such high loads may result from the impulsive surges experienced by the load cell during the refill process or be caused by the accidental dropping of large weights of coal onto the feed hopper. Clearly, some form of overload protection was required. A compression spring was used as an intermediate force transmitting medium between the load cell and the main balance beam, Fig. (4.4). By choosing a suitable spring stiffness it was possible to achieve a main balance beam end deflection of approximately 30 mm. This value was chosen as it would permit easy adjustment, without allowing deflections to be large enough to cause inaccuracies to arise elsewhere in the system. As an extra precaution, the deflection of the end of the main balance beam was restricted by two adjustable screw stoppers.

4.4.3 The Microprocessor Control

As detailed in the overall system description, Fig. (4.12), the main items employed in the control system design were: (1) a microprocessor, (2) a load cell, (3) a digital voltmeter, (4) an analogue to digital converter and a digital to analogue converter, (5) a conditioner amplifier and (6) a membrane valve system. These items and their functions are described in more detail in this subsection.

1. The microprocessor

The microprocessor chosen is the AIM65 model manufactured by Rockwell International Corporation. This microprocessor was chosen in perference to systems currently offered by manufactures such as Apple Computers or Sinclair Electronics, as it was felt that the Rockwell system provides the closest match of computer performance to the control system requirements.

The general specifications of AIM65 microprocessor, see Zaks (1980), includes an R6502 central processor unit (CPU) which operates at 1 MHz frequency giving a minimum instruction execution time of two microseconds. The AIM65 consists of two modules, namely the master module and the keyboard module, which are connected by a short plug-in ribbon cable. It has two kinds of memory: (1) the read only memory (ROM) with 4 K bytes capacity, although this is extendable to 20 K bytes and (2) the random access memory (RAM), capacity is 4 K bytes. The facility for programming in Basic language is provided by an 8 K bytes capacity basic converter which interprets the Basic instructions into

fundamental Machine Code instructions, which are more rapidly executed by the microprocessor. Inputs and outputs are passed to and from the microprocessor via two 8-line input/output ports which are provided specifically for the external devices. Data and program entry is carried out via a standard typewritter keyboard with a small number of special function keys which enables Basic and Assembly language programming instructions to be used. Information is displayed in two ways. A twenty character one line light emitting diode display allows the information to be read at a glance whilst a thermal printer allows hard copies of programs and results to be listed and retained. Further extras includes an audio cassette program storage system to save programs and for rapid program loading. Finally, it is possible to write proven and tested programs into an Eprom (erasable permanent read only memory) chip which will then perform automatically the task for which it has been programmed. This latter facility has been utilized and a well established, satisfactory operating software control program, see subsection (4.4.4), was made as a permanent feature of the microprocessor system.

2. Load cell circuitry

The load cell, as described earlier in subsection (4.4.2), is a high performance parallel motion cantilever beam design. Precision strain gauge load cells based on this design offer high outputs for any given strain level; an output of 3 mv per volt of excitation is achieved at maximum rated load. This high output in effect increases the resolving power of the digital voltmeter

which is used to monitor the output voltage. The load cell is constructed from 17% chromium-4% nickel precipitation hardened stainless steel which offers high strength and hardness combined with excellent corrosion resistance. The total error band, which consists of non-linearity hystresis and repeatability errors, is better than 0.05%. The basic circuitry is that of a Wheatstone bridge configuration. Temperature drifts which are mainly due to the change of modulus of elasticity and to resistivity changes are held to 0.003% per degree C at a rated load of 500 N. Special span correction resistors which are incorporated in the Wheatstone bridge allow accurate operation within a temperature range of $-30^{o}C$ to $70^{o}C$. In addition, the electronics are hermetically sealed allowing safe use in the coal combustion experimental environment.

3. The digital voltmeter (DVM)

The digital voltmeter used is the DM-4100 D model (Datel Intersil) which has a maximum capacity of 1.9999 volts with an accuracy of $\pm$ 0.0001 volts. Figure (4.12) outlines the overall position of the DVM within the control system. In the present mode of use, the DM-1400 D is able to perform three separate tasks simultaneously, and this enables the overall number of components required by the system to be reduced. Firstly, the DM-4100 D provides a visual display of the load cell output to four decimal places. A new reading is displayed once every 0.45 second which enables short term transient effects to be visualized. Secondly, the DM-4100 D is compatible with

the Rockwell AIM65 microprocessor and so the digital voltmeter reading can be fed to the microprocessor at a maximum rate of once every 0.45 seconds. Thus the DM-4100 D fulfils the role of an analogue to digital signal converter. Thirdly, because DM-4100 D transmits data to the microprocessor at regular intervals, the counting of these intervals by the microprocessor enables an accurate time base to be established and used as a reference for the timing of all control actions and motor corrections. In order to fulfill the latter, an electronic circuit,as shown in Fig. (4.14), was developed. It consists of a 3.2768 MHz crystal, 50 Hz time base integrated circuit (RS Components Limited, type M706 B1) and a divider network. The output from the crystal and the time base integrated circuit is 50 pulses per second. These pulses are then modified,to ten pulses over a five seconds period followed by no-action five seconds,by the divider network. The output from the divider network is used to trigger the digital panel meter giving ten readings in five seconds (one every 0.5 of a second) and then the meter holds the last reading for another five seconds; this cycle is repeated every ten seconds.

4. The conditioner amplifer

The maximum output voltage of the load cell is 33 mV at a maximum loading of 500 N. However, the maximum capacity of the digital voltmeter is 1999.9 mV. For optimum resolution it was necessary to make the two values equivalent. This was achieved by the use of a conditioner amplifier, its position within

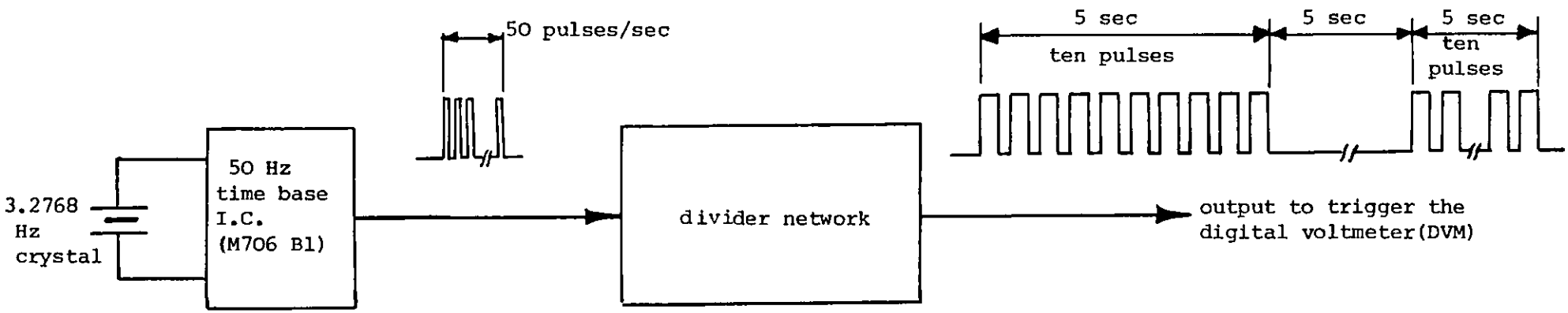

Fig.(4.14) Digital voltmeter time base circuit diagram

the control system is shown in Fig. (4.12). The conditioner, chosen to be compatible with the load cell, was a C30 unit by Sangamo Transducers. Useful features of this conditioner include externally accessible zero and fine gain adjustment points for ease of calibration and maintenance. In operation, the effect of the conditioner amplifier is to multiply the output of the load cell by a gain factor of 60.063.

5. Digital to analogue signal converter

The output voltage from the microprocessor is initially in a digital form. In order to cause speed change for the feed screw motor, the digital speed value must be converted into analogue form. In normal applications an output amplifier would also be required to make the voltages compatible. However, in the present case, the need for an output amplifier is avoided by the use of an external power supply source for the feed screw motor, with the microprocessor output being fed to a digitally controlled potentiometer. This simply replaces the ten-turn manual potentiometer which would be used to alter the speed of the motor if the automatic control is inoperative. The digital to analogue converter used in the control circuit was supplied by Analog Devices, type AD 7525. The manual ten-turn potentiometer was retained on the control box of the feed screw motor. The position of an auto/manual selector switch allows the selection of either modes of operation.

6. The refill circuit

The electronic circuit which controls the refill process is shown in Fig. (4.15). When the coal weight in the feed hopper drops under a minimum weight limit, an address decoded instruction from the Rockwell AIM65 microprocessor is sent to the R6522 VIA which consequently initiates a pulse. This pulse, which lasts for about two microseconds, is extended to approximately one second pulse by a monostable integrated circuit. The output from the solid state relay, which is triggered by the one second pulse, activates a solenoid valve. This solenoid valve controls the operation of the membrane valve mounted in between the storage and feed hoppers, Fig. (4.5). The activated solenoid valve releases the membrane valve open and the coal is dumped into the feed hopper for a period of about one second. This refill cycle is repeated until the hopper is full as indicated when the coal exceeds a maximum weight limit.

4.4.4 Computing, Control Theory and Performance

By software programs, the microprocessor controls the various stages of the coal feed operating cycle. The main control program is written in Basic language. This program is supported by three separate data input and output (interfacing) programs, written in Assembly language for rapid data interfacing. The

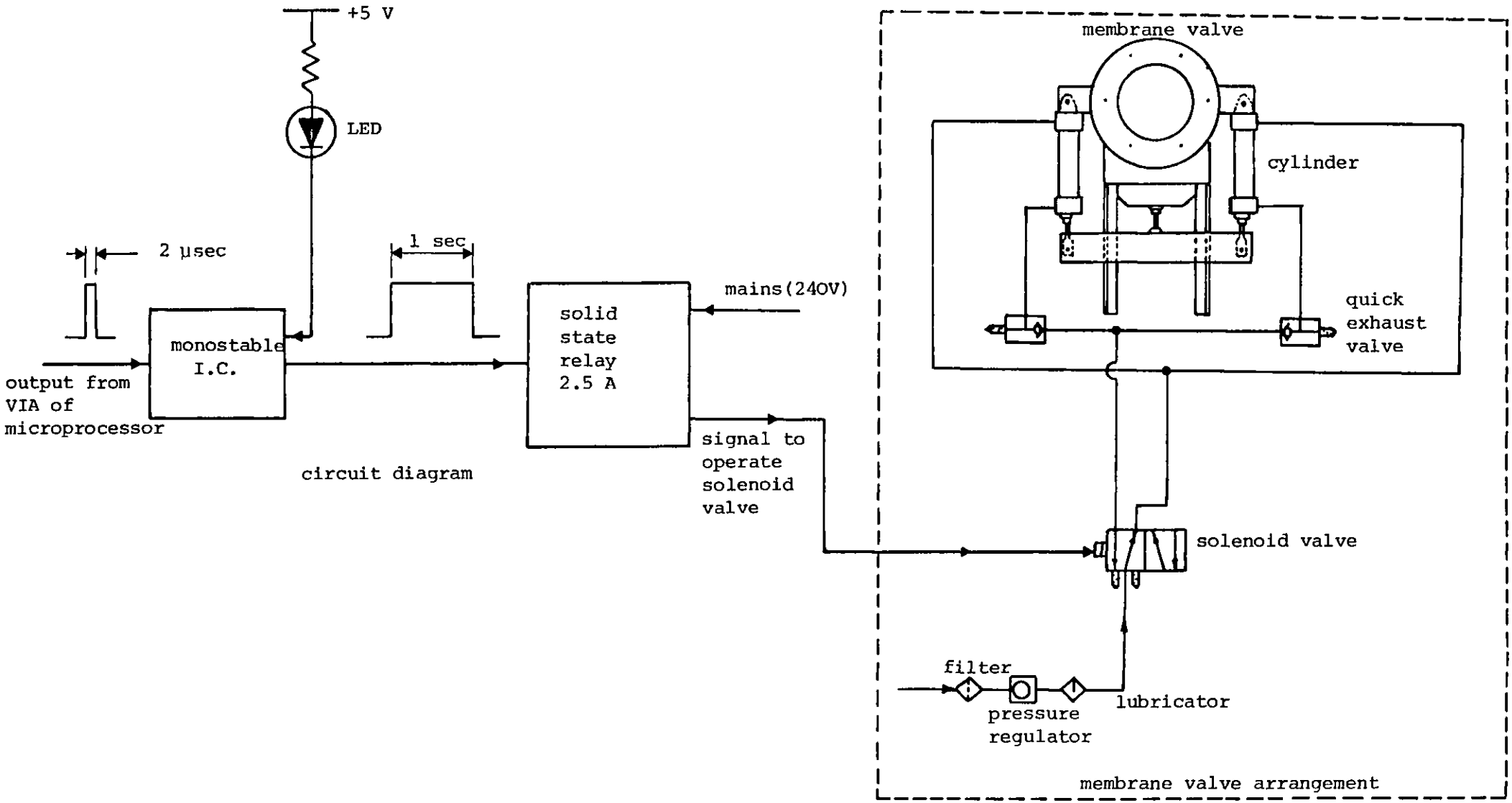

Fig.(4.15) Membrane valve triggering circuit

first interfacing program is used for reading the weight of the coal in the feed hopper as indicated by the load cell output signal, the second is for controlling the rotational speed of the screw feeder motor while the third is for initiating the refill cycle. The block diagram of the Basic control program is shown in Fig. (4.16).

As shown by the dashed line in Fig. (4.17) panel (a), the theoretical weight of the coal in the loss-in-weight (feed) hopper, w_{th}(kg), at any specific time, t (seconds), is computed as follows:

$$w_{th} = w_o - \dot{w}t/3600$$

where w_o is the initial weight of the coal in the feed hopper at t = 0 and $\dot{w}$ is the desired coal feed rate (kg/hr). The theoretical weight loss is calculated as the difference between the theoretical weights at time t_1 and that at time t_2, knowing that $t_2 - t_1$ = 30 sec. The actual weight of the coal in the feed hopper at any time t, solid line in panel (a) of Fig. (4.17), is taken as the average of ten successive weight readings measured by the calibrated load cell, see Fig. (4.14). The actual weight loss, accordingly, in the time period $t_2 - t_1$ is calculated as the difference between the measured weights at t_1 and t_2 respectively. The difference between the output value and the reference value at any particular time is defined as the error in the output of the control system. Figure (4.17) panel (b) shows the block diagram for the present feedback control system where the sole feedback term is the error multiplied by a gain constant, K. This is termed "proportional error feedback". The error in the feed rate, E, according to

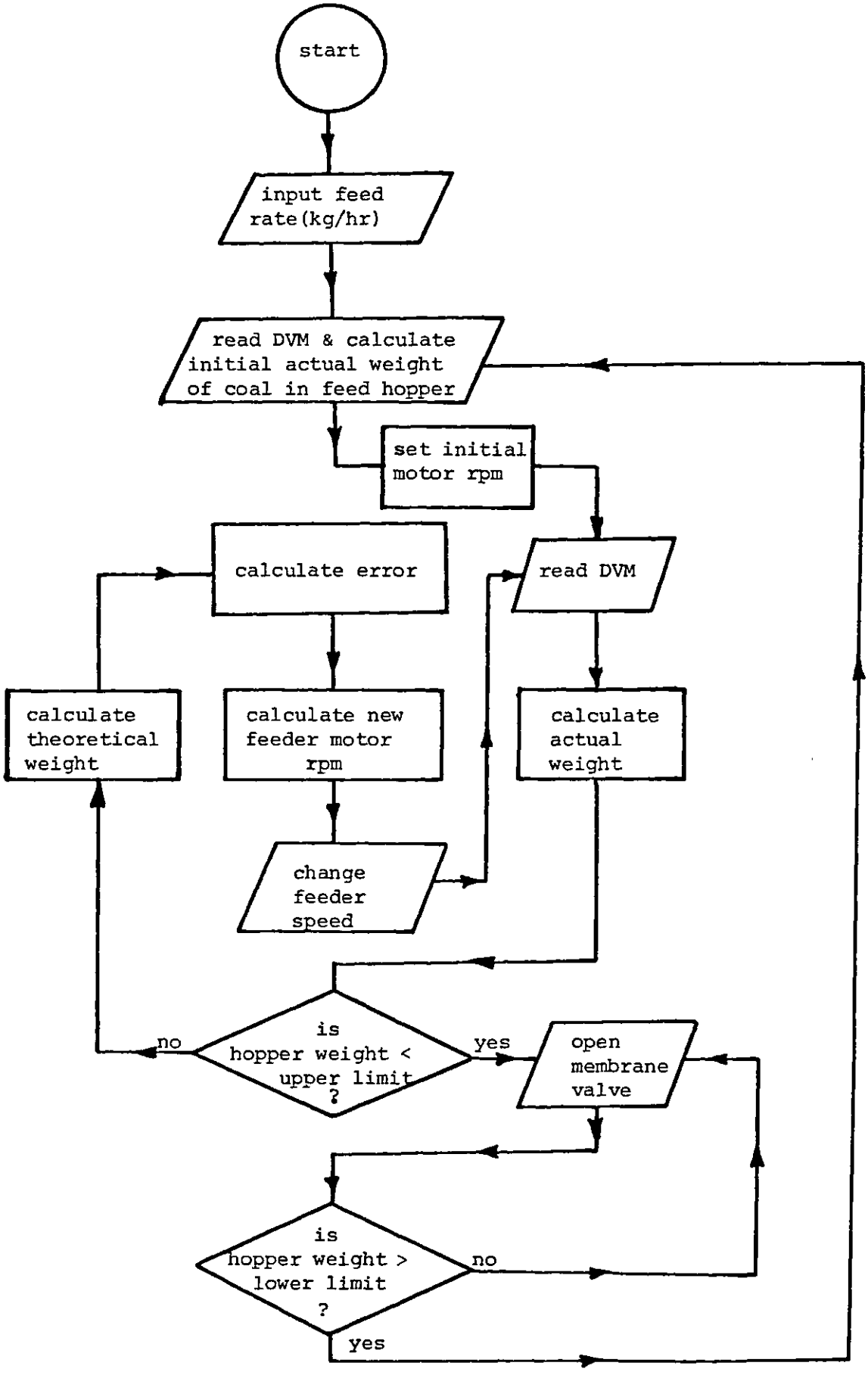

Fig.(4.16) Flow chart of the coal feed control (BASIC) program

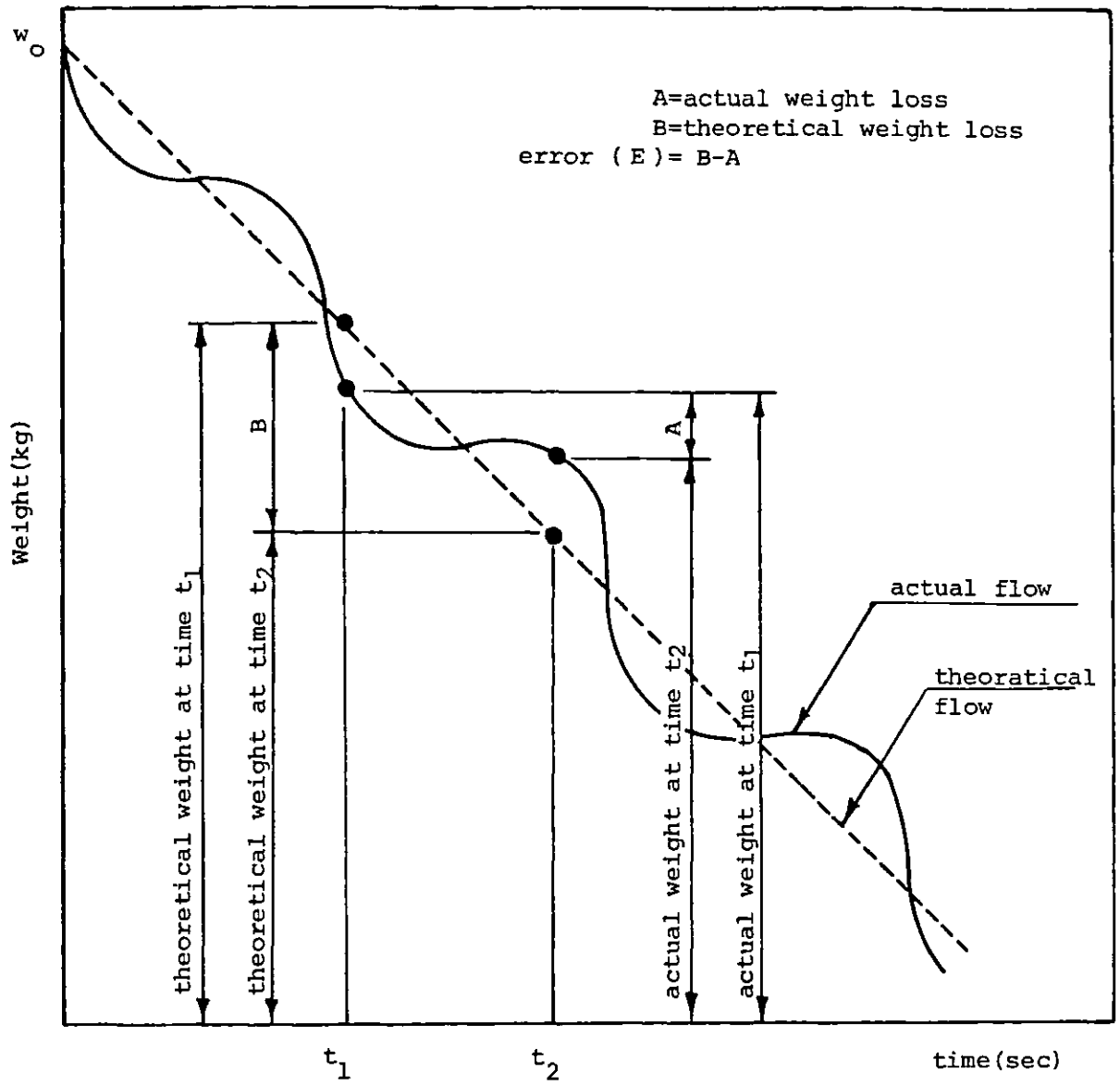

Panel(a)

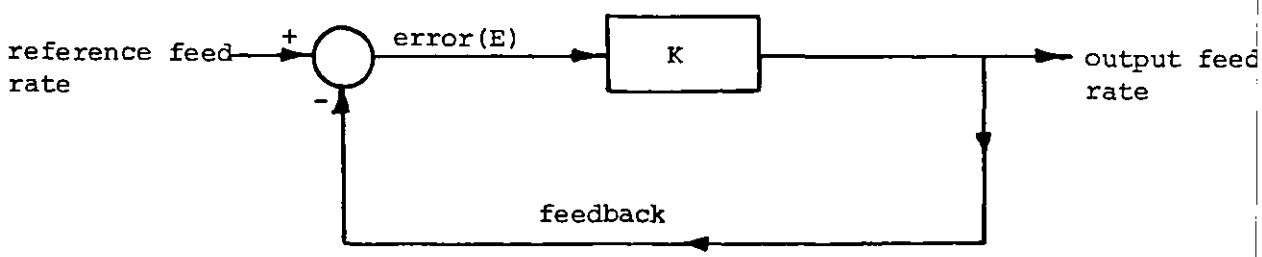

Panel(b)

Fig(4.17) Computing theory of the control system

which the screw rpm is corrected, is calculated as the difference between the theoretical and actual weight losses. The motor speed correction is taken as ±KE where K is the proportional gain factor chosen here to be equal to $10^5|E|$. So, if the theoretical (calculated) weight loss exceeds the actual weight loss (measured), the motor speed is increased to reduce the difference and vice versa. The motor speed is adjusted to a new value every 30 seconds.

Figure (4.18) shows a typical example of the performance of the coal feed system. The decay of the weight of the coal in the feed hopper (as indicated by the calibrated load cell reading) and for a feed rate of 12 kg/hr is drawn as a function of time. The slope of the dashed line in Fig. (4.18) represents the theoretical slope (1/300 in this case) of the ideal (set) coal weight decay. Obviously, the actual feed rate equals the ideal rate when the slopes of the two lines (dotted and dashed lines) are identical.

The deviation of the actual feed rate from the ideal case may be described and judged by the percentage error in the feed rate which is defined as:

$$\% \text{ error} = \left(\frac{\text{actual feed rate-set feed rate}}{\text{set feed rate}}\right) \times 100$$

where the actual feed rate is taken equal to the difference between two coal weight readings divided by their interval time lapse. In the present control system, a reading of the time average weight of coal in the feed hopper is taken every 30 seconds.

Using the above definition for the individual feed error and averaging the errors over many operating periods, a maximum

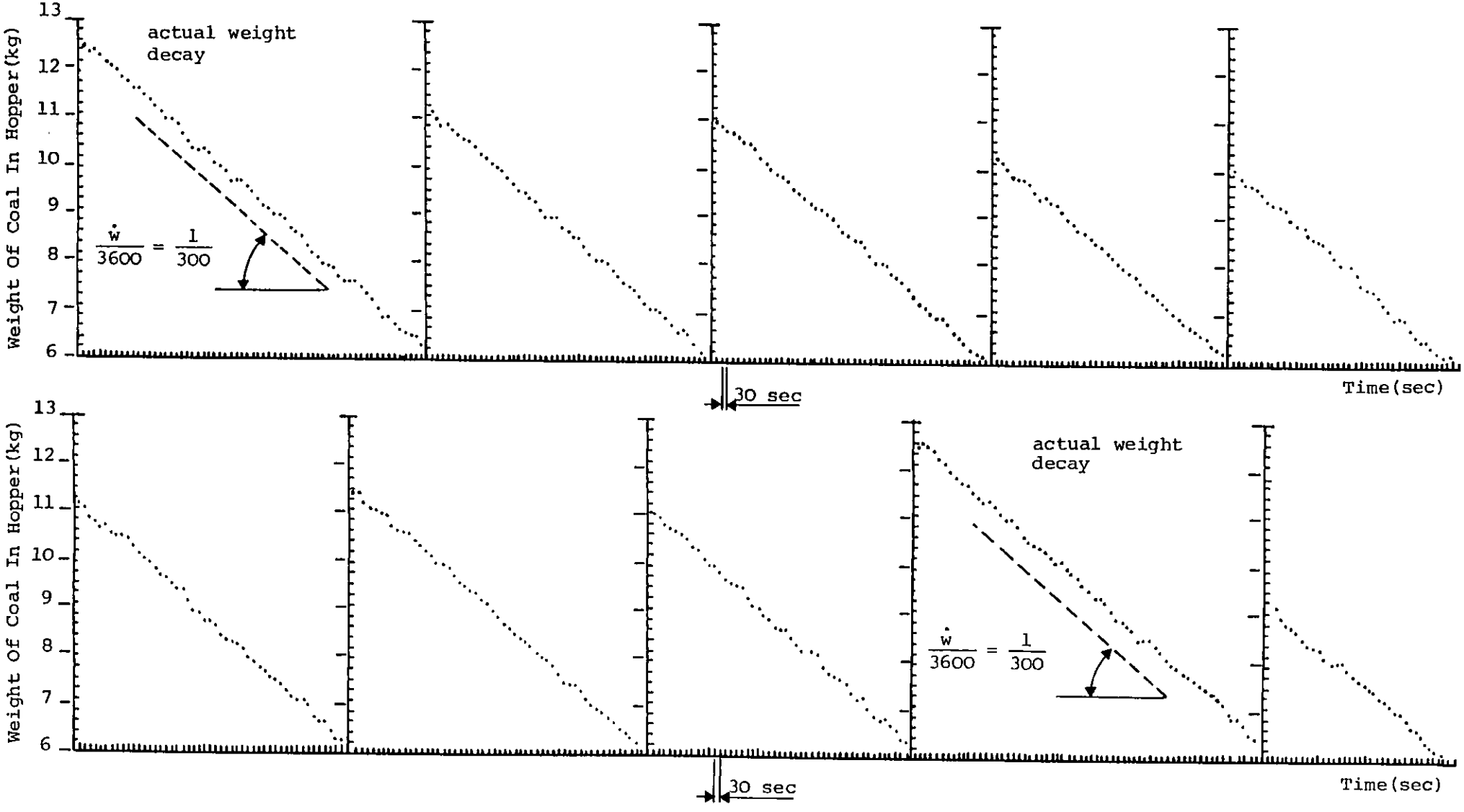

Fig.(4.18) The feed system performance

error of ±2% of the desired feed rate has been found. This error gives an indication of the fairly good performance of the coal feed system.

CHAPTER 5

MEASUREMENTS IN THE COAL-FIRED FURNACE

5.1 Introduction

The scope of the present coal combustion project was to experimentally investigate the effect of the different operating parameters (e.g. coal loading in the primary stream, the primary to secondary velocity ratio, the percentage of excess air, the secondary air temperature, the swirl of the secondary air, the burner geometry and the coal particle size) on the macroscopic structure of the developed flames and the overall performance of the combustor. Such detailed experimental data, obtained under well-defined conditions and in a relatively simple coal-fired configuration, could provide a useful basis for better understanding of the fundamental details of coal combustion and for the validation of the prediction procedures.

The key for the determination of the effect of the different operating parameters and producing well-defined and reliable laboratory data is the ability to obtain - in an easy, simple and accurate manner - measurements of temperature, concentration and ash burnout at various axial and radial locations within a coal-air flame with high time and spatial resolution.

Temperature measurements were obtained using a completely automatic data logging system and a fine wire thermocouple probe. Particle-gas samples were collected with a direct-quench, water-cooled probe and a sampling system which were designed and modified for this specific use. Radial and axial concentrations of carbon

dioxide, carbon monoxide and oxygen in combustion gases were determined from on-line gas analyzers. The particulate material was separated from the gases and the probe quench water and was analyzed to determine the elemental composition; carbon, hydrogen, nitrogen, sulphur and ash (by difference). Ash was used as the key particle tracer. Based upon the ash content in the original coal and that of the collected sample, the local extent of the particle reaction was determined. In addition, the ash content of the char sample was used with its elemental composition to determine the local burnout of nitrogen, carbon, hydrogen and sulphur.

The present chapter represents the closure of the current effort to produce and develop a coal combustion data producing experiment and demonstrate experimentally the capability of different measuring techniques for in-flame measurements. Characterization of the coal in use was also one of the main objectives of this effort. Section (5.2) contains in detail the different analyses currently being used to define and characterize the coal. These include particle sizing, proximate and ultimate analyses. In section (5.3), the description of CO_2, CO and O_2 concentration and burnout measurements is given. It also includes the description of the fine wire thermocouple for flame temperature measurement together with the design features of an automatic data logging system. The accuracy associated with the measurements is also discussed. Section (5.4) contains the restuls obtained for one set of input conditions. These results include mean CO_2, CO and O_2 volume concentrations, ash burnout levels and flame mean bulk temperatures.

5.2 Coal Characterization

Different types of coal exhibit wide variations in composition, volatility, hardness and solubility. Variations in composition such as percent sulphur, percent nitrogen or percent ash can have marked influence on the kinds and amounts of pollutants formed during devolatilization and pyrolysis of coal particles. Therefore, in order to quantify these variables, numerous tests were done to analyze the coal which was used in the present coal firing experimental programme.

5.2.1 Particle Size Distribution

The Grimethorpe 250 grade bituminous coal dust used in the present study, was from Grimethorpe mines in the United Kingdom and bought from the Standard Pulverized Fuel Company Limited. The coal was pulverized by the supplier company to the size of 80% through a 200 mesh screen and it was stored in sealed bags each weighing approximately 25 kg.

To determine the particle size distribution more precisely, a number of samples was obtained from different coal bags in a random basis, each sample weighed about 70 gm. These samples were run through an air jet sieve type 200 LS (Apline Process Technology Limited) to obtain a complete size distribution. This jet sieve is shown schematically in Fig. (5.1a). The coal samples were screened in a series of micro-sieves (Haver and Boecker, Germany) ranging in size from 25 μm to 425 μm. For each particular

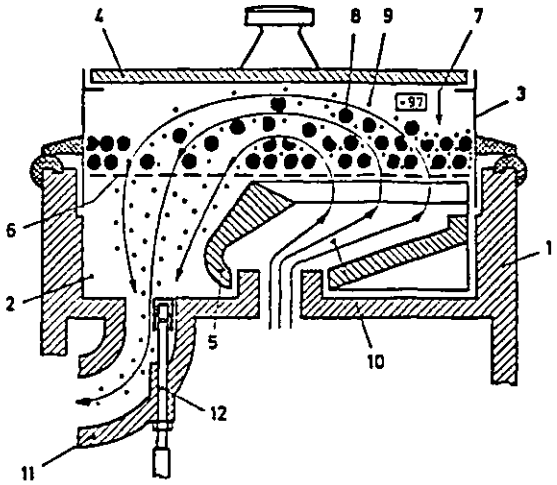

1.housing
2.dish
3.sieve drum
4.lid
5.slit-nozzle
6.gauze
7.layer of coal
8.coarse coal
9.fine coal
10.air jet
11.discharging socket
12.pressure gauge socket with dust hood

Fig.(5.1a) Schematic diagram of the air jet sieve

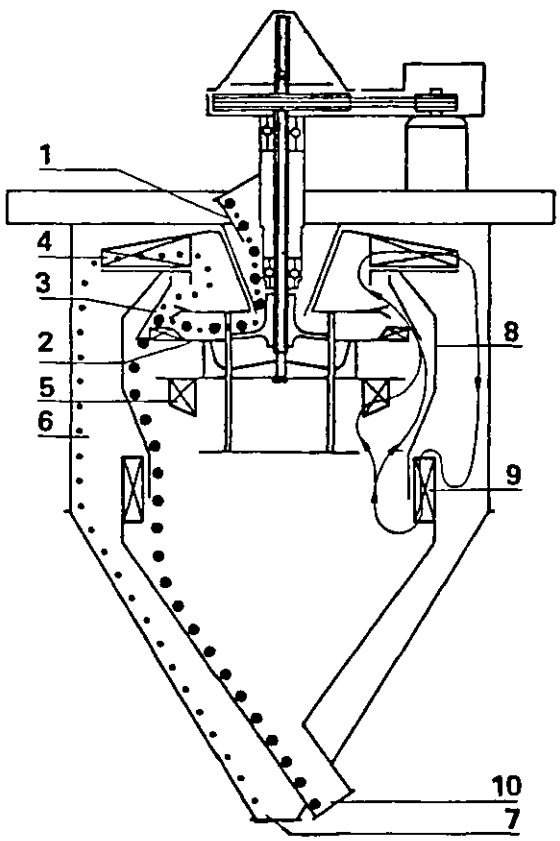

1.inlet funnel
2.strewing plate
3.classifying chamber
4.main fan
5.adjustment fan
6.fines chamber
7.fines output
8.bumper cylinder
9.reverse air blades
10.coarse outlet classifying air stream
●coarse coal
•fine coal

Fig.(5.1b) Schematic diagram of the classifier

sieve, a sample weighing 5 gm was screened. The percentage weight of coal particles passing through that particular sieve was taken equal to an average of three samples. Table (5.1) and Fig. (5.2) represent typical average size distribution of the bituminous pulverized coal used in this study. The weighted-average particle diameter of that coal is 39 μm. That average size distribution represents, in fact, an average of at least 200 coal samples. A complete size distribution of examples of these samples are summarized in Table (5.2).

In order to clean the test sieves after usage without damage, an ultrasonic cleaning device (Sanorex Compact Unit, type RK, Alpine Process Technology Limited) was used. One series of tests may require small particles of a certain size distribution, therefore a classifier (Ventoplex Wind Shifter, Alpine Process Technology Limited) was purchased, see Fig. (5.1b), to fulfill that requirement. The classifier is able to supply coal of varying size distributions.

5.2.2 Proximate Analysis

The proximate analysis is a standard test to determine the moisture content, the fixed carbon, the volatile matter and the amount of ash in a certain coal type. The accepted procedure is that described by British Standard 1016 (1977). Briefly, the procedure begins by placing a 1.0 gm sample of coal in a

Table (5.1)

Average size distribution

Sieve size range µm	% sieve fraction (% by weight)	Nominal aperture size µm	Cumulative under size (% by weight)
> 425	0.4	425	99.6
425 to 25	0.4	250	99.2
250 to 212	0.6	212	98.6
212 to 150	1.0	150	97.6
150 to 125	1.5	125	96.1
125 to 106	2.4	106	93.7
106 to 90	1.9	90	91.8
90 to 75	4.2	75	87.6
75 to 63	4.8	63	82.8
63 to 45	8.1	45	74.7
45 to 40	5.4	40	69.3
40 to 32	7.4	32	61.9
32 to 25	13.3	25	48.6
< 25	48.6		

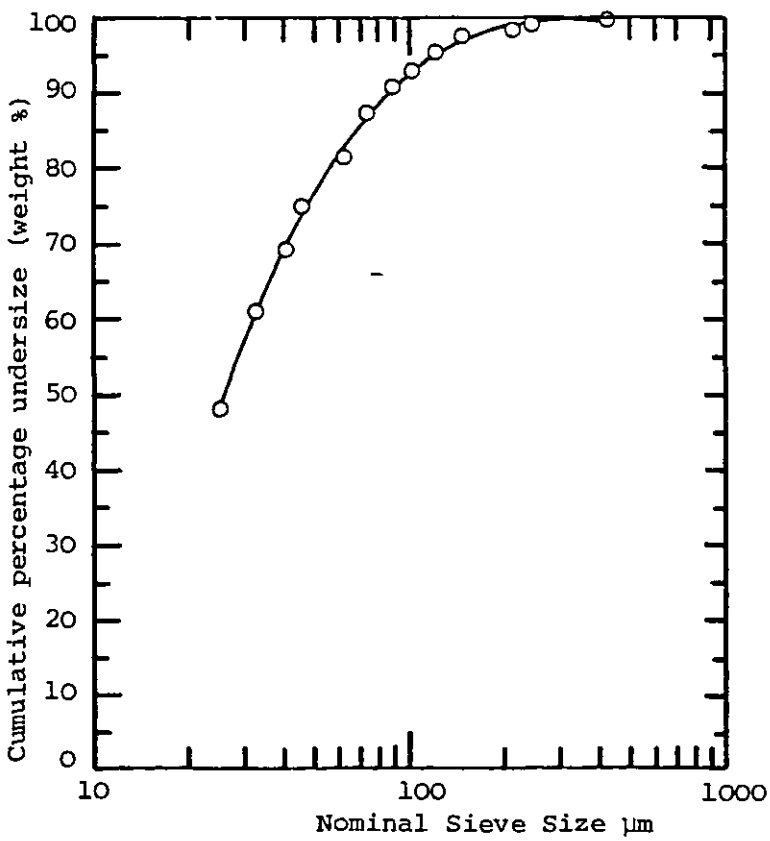

Fig.(5.2) Linear/logarithmic co-ordinate plot of cumulative undersize of average size distribution

Table (5.2)

Coal size characterization for various samples

(% by weight of cumulative under size)*

Nominal sieve size μm	Sample number														
	1	2	3	4	5	6	7	8	9	10	11	12	13	14	15
425	99.5	99.5	99.7	99.8	99.8	99.6	99.6	99.8	99.8	99.8	99.4	99.6	99.6	99.4	99.6
250	99.3	99.2	99.5	99.1	99.4	99.4	99.4	99.6	99.6	99.6	99.4	98.8	99.0	98.4	98.8
212	98.4	98.1	99.0	98.0	98.8	99.2	99.2	99.4	99.4	98.8	98.0	98.2	98.4	97.8	98.0
150	97.5	96.5	97.9	97.4	98.7	97.0	97.4	98.7	99.0	98.0	97.6	98.0	97.4	95.4	97.0
125	95.7	95.0	96.0	97.0	98.3	94.6	95.3	97.0	97.8	97.2	95.0	96.2	97.0	93.4	95.4
106	92.3	90.4	92.5	95.7	96.7	94.0	95.0	95.4	95.6	95.0	92.4	93.6	96.0	90.8	93.4
90	89.5	88.7	91.6	92.9	95.0	90.6	92.2	93.0	94.2	93.4	90.0	91.4	94.9	88.6	91.0
75	85.6	84.0	87.2	90.2	91.4	86.4	88.0	90.0	90.2	88.7	84.0	86.0	93.0	84.0	85.2
63	80.4	79.4	83.1	85.0	86.2	81.5	83.8	85.2	85.0	84.7	79.3	80.9	89.4	77.4	80.8
45	71.7	69.1	73.3	77.4	78.9	73.8	75.8	77.6	78.6	76.4	70.0	71.8	84.4	69.1	73.1
40	65.7	67.6	72.1	72.4	72.4	64.4	69.1	73.0	72.8	70.9	65.4	66.4	79.0	62.7	66.2
32	58.2	55.8	59.9	65.2	65.6	60.0	62.0	65.2	65.9	65.9	58.2	60.0	71.4	55.8	59.4
25	45.9	42.3	46.7	51.9	50.6	47.8	49.8	52.1	52.0	50.5	44.8	46.8	58.8	43.0	46.3

*Average of three samples.

silica crucible, leaving it in a drying oven maintained at 105-110^{o}C in a current of nitrogen for about 60 minutes and measuring the weight loss. This determines the moisture content of the coal. Next, the sample is heated by contact with air in a muffle furnace at 900^{o}C for 7 minutes. The volatile matter in the coal sample is calculated from the loss in weight of the sample (a deduction is made for the loss in weight due to moisture). Finally, the sample is placed in a muffle furnace whose temperature increases with time. The sample is heated in air to 500^{o}C in 30 minutes, from 500^{o}C to 815^{o}C in 60 to 90 minutes and is then kept at 815^{o}C until a constant weight is obtained, usually 45 to 60 minutes. The material remaining is defined as the ash and the material burned off is termed the fixed carbon. Triplicate proximate analyses were run on a composite sample from a selected coal bag. These results were averaged and are reported in Table (5.3).

5.2.3 Ultimate Analysis

Another analysis extremely useful and fundamental for the characterization of coal is an ultimate or elemental analysis, wherein the precent carbon (C), hydrogen (H), nitrogen (N), sulphur (S) and ash are determined. In the present work, the elemental analysis for C, H, N and S, was obtained using the Carlo Erba Strumentazione automatic analyzer CHN-O-S model 1106, fitted with two automatic samplers (type AS50). The percentage of oxygen and ash was determined by difference.

Table (5.3)

Summary of proximate analysis

Component	Weight percent
Moisture	3.2
Volatiles	30.8
Fixed carbon	58.2
Ash	7.8

Table (5.4)

Average ultimate analysis

Element	Weight percent
Hydrogen	4.9
Carbon	75.9
Nitrogen	1.6
Sulphur	1.4
(Oxygen + ash)*	16.2

*Calculated by difference

In the elemental analyzer, see its block diagram in Fig. (5.3), a coal sample is weighed in a special tin capsule, using a micro-balance, the sample container is then placed in the automatic sampler which takes up to 50 samples. At a preset time the sample container drops into a quartz vertical reactor, which is packed with selected catalysts and heated up to 1000^{o}C, through which a constant flow of helium is maintained. Oxidation is ensured by enriching the carrier gas (helium) with pure oxygen, timed to coincide with the tin capsule dropping into the reactor. This results in flash combustion, lasting a few seconds, producing a temperature of 1800-2000^{o}C. The quantitative oxidation phase is followed by a catalytic phase during which oxidation of the gases is completed. The mixture of combustion gases is then carried out by the helium flow to a chromatographic column heated to 100^{o}C where N_2, CO_2 and H_2O are separated in that order and detected by a hot wire detector. The detector signal is visualized on a potentiometric recorder and the areas under the respective peaks are measured by an electronic peak integrator (SP4100 Computing Integrator, Spectra Physics). The area integration values are subsequently used to calculate the corresponding percentages. The total time required for one CHN analysis is about 10 minutes. Sulphur is analyzed in the same oxidative conditions as for CHN, but the combustion tube and the chromatographic column are substituted and a signal proportional to the SO_2 generated is obtained. Each analysis for sulphur takes about 8 minutes. No analysis has been done for oxygen percentage. For conditioning and calibrating the instrument, micro-analytical standards were used: Cyclohexanone 2,4 Dinitrophenylhydrazone (51.79% C, 5.07% H, 20.14%N) for CHN and Sulfanilamide(18.62% S) for S.

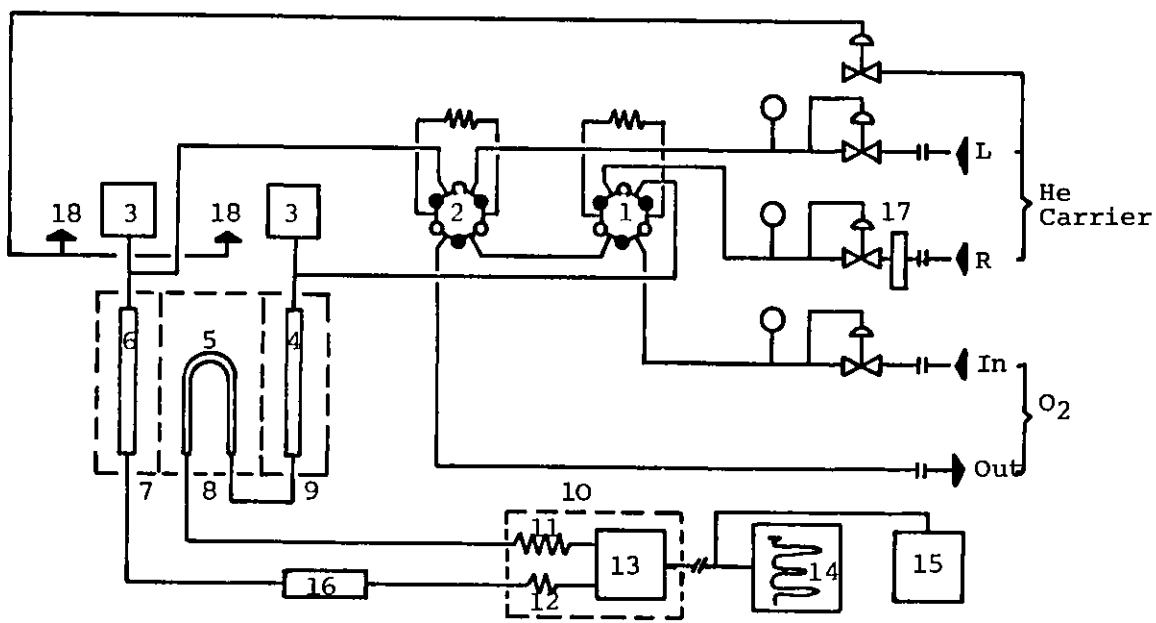

1.oxygen injection valve(CHN)
2.oxygen injection valve(S)
3.samplers
4.combustion reactor(CHN)
5.reduction reactor(CHN)
6.pyrolysis/combustion reactor(O/S)
7.pyrolysis/combustion furnace(O/S)
8.reduction furnace(CHN)
9.combustion furnace(CHN)
10.thermostated oven
11.chromatographic column(CHN)
12.chromatographic column(O/S)
13.detector
14.recorder
15.integrator
16.trap
17.doping system
18.purge

Fig.(5.3) Block diagram of the elemental analyzer

The accuracy of the analytical results is closely related to the sample weight. So the delicate weighing operation was performed using a reliable electronic micro-balancewith a digital readout (model 4431 Ultramicro-balance, 0.1 microgram sensitivity, Sartorious Instruments Limited).

A number of samples from different coal bags were chosen on a random basis to determine the coal ultimate analysis. An average of carbon, hydrogen, nitrogen and sulphur percentage is given in Table (5.4) while a list of some results is given in Table (5.5). These results show that the coal seems to have quite uniform composition. The percentages, listed in Table (5.4), were accepted as the coal composition in order to determine the theoretical amount of air required for complete combustion for a certain coal feed rate.

5.3 Measurements and Instrumentation

This section provides a description of the measurement techniques used for data collection in coal flames. Emphasis is given to the reasons for the choice of each particular technique and the assessment of its accuracy under the present experimental conditions. The measurements made use of a water-cooled shower sampling probe for concentration and ash burnout measurements and a fine wire thermocouple probe for in-flame temperature measurements. These instruments are described in detail in the following subsections.

Table (5.5)

Ultimate analysis of different samples (weight percent)*

Element	Sample number														
	1	2	3	4	5	6	7	8	9	10	11	12	13	14	15
Hydrogen	5.0	5.0	4.8	4.9	4.8	4.8	4.8	4.8	4.8	4.8	4.9	5.0	5.0	5.0	5.0
Carbon	76.7	76.1	75.5	75.9	75.5	75.3	74.8	75.1	74.9	74.9	74.9	76.9	78.2	77.1	77.4
Nitrogen	1.7	1.7	1.6	1.6	1.5	1.5	1.5	1.5	1.5	1.5	1.5	1.6	1.6	1.6	1.6
Sulphur	1.4	1.5	1.4	1.5	1.5	1.5	1.4	1.6	1.5	1.4	1.5	1.5	1.3	1.3	1.3
(Oxygen and Ash)**	15.2	15.7	16.7	16.1	16.7	16.9	17.5	17.0	17.3	17.4	17.2	15.0	13.9	15.0	14.7

*Average of fine samples.
**Determined by difference.

5.3.1 Concentration Measurement

In order to obtain gas-particle samples from the coal flames, a direct water-quench (shower), water-cooled sampling probe was designed and fabricated. The probe was constructed entirely of stainless steel and permitted the direct quenching of combustion products by injection of water through small holes near the probe tip. Schematic diagrams of the probe and its tip are shown in Fig. (5.4). The quench water was introduced to the probe at a flow rate of approximately 0.4 - 0.6 litre/min. The quench water served to prevent blockage, quench the sample effectively, keep the probe clean and it helped to carry the particulates through the sampling train.

A water-quench probe was tested for use in a gas firing experiment, see section (3.4). The probe, as was concluded from the discussion in section (3.5), was found to function well in sections of the combustor where the temperature was not high ($<1400^{o}C$). At the higher temperatures - especially when most of the probe span lies in the flame zone - the injected water in the probe would flash, stopping any further probe cooling and the probe would be damaged. That probe was also tested in a coal flame and it proved to be worse due to the presence of the particles and its operation became very difficult. Two possible ways seem evident to overcome this problem. The first one is to increase the quench water flow rate to the higher possible limit while the second alternative, was to use minimum possible quench water flow for quenching and to separately cool the probe using a cooling water jacket. The former alternative proves unfeasible since

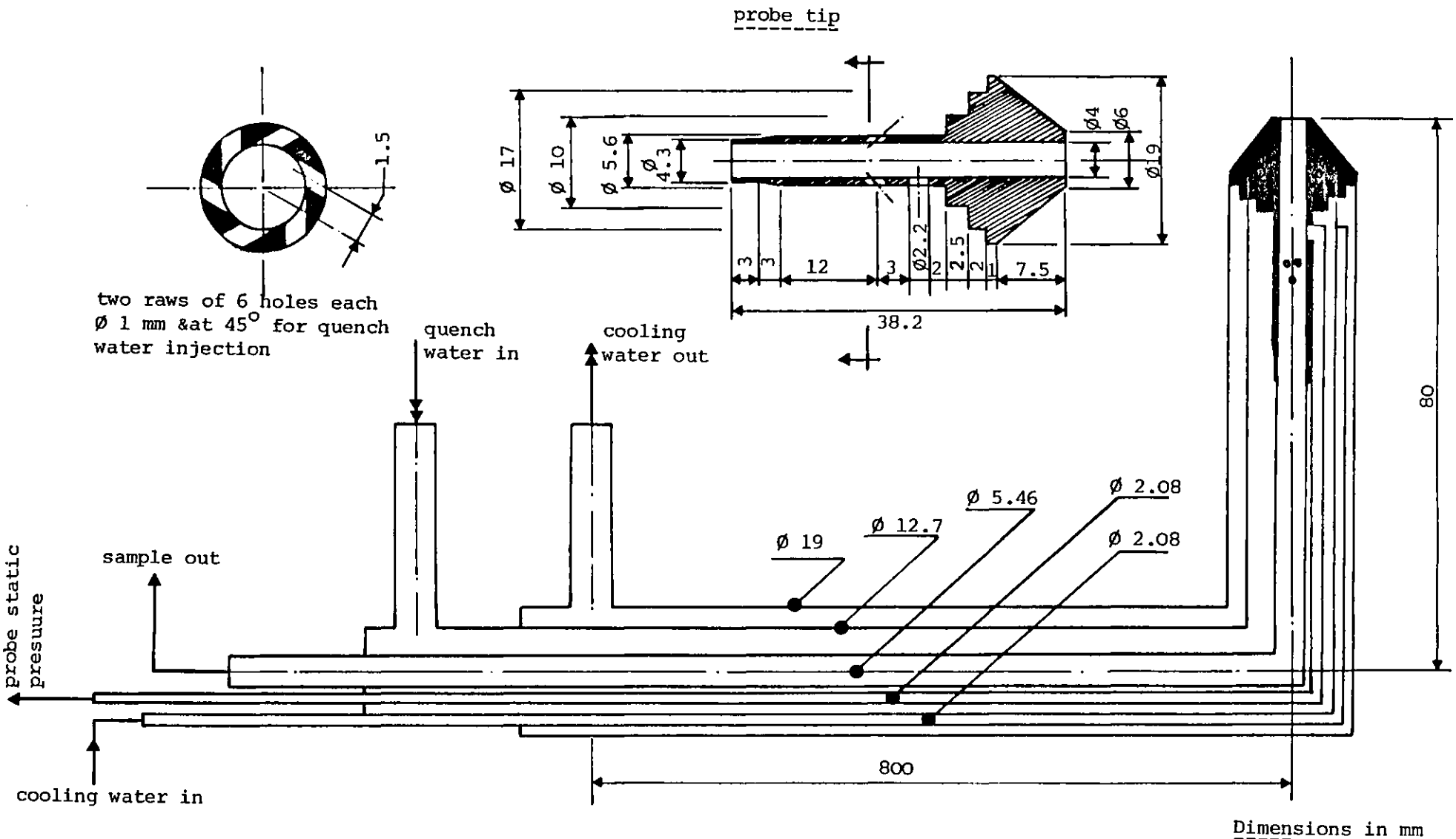

Fig.(5.4) Schematic diagram of the water-cooled, direct water-quench probe

it causes a decrease and in some circumstances nearly diminish samples well below what is required by the on-line analyzers. This is subsequently coupled with a lengthy analysis time. The second alternative has the advantages of an adequate sample flow for analysis and the ability to change quench water flow rate in order to achieve isokinetic sampling but it has the disadvantage of a bulkier probe size. The second alternative was chosen and a water-cooled, water-quench probe (Fig. (5.4)) proved to work successfully in all parts of the furnace.

Goulard et al (1976) and Bilger (1977) indicate that isokinetic sampling has little meaning in turbulent combustion flows due to the random turbulent fluctuations in the mean flow and the presence of reverse flow zones where recirculations occur. Isokinetic sampling in recirculation regions is not meaningful, however, in other regions isokinetic sampling is considered the best available method for obtaining a representative sample. Although random flow fluctuations are certainly present, they will be averaged out if the sample is taken over a sufficiently long period of time. Therefore, an effort was made to approach isokinetic sampling with sampling times averaging from three to five minutes. To achieve that objective, the probe contained a small static pressure tap near the tip, see Fig. (5.4), which was used to equilibrate the probe static pressure with the static pressure at the same axial location in the reactor as measured from the pressure tap located at the furnace wall. Some control of the probe pressure was achieved by adjustment of the quench water flow rate. If a greater pressure was observed in the probe tip than in the reactor, a lowering of the water flow rate tended to reduce the

probe pressure. A lower limit (≈ 0.2 litre/min) of water flow rate was required in order to prevent clogging of the probe with particles. The probe was mounted on a traversing mechanism which permitted a radial mapping at specific axial locations. The traversing gear is similar to that shown in Fig. (5.8).

One of the most important aspects of the test program is the proper handling of the probe samples. For this reason, great care was taken to collect efficiently and accurately samples for analysis. Due to the three phase sample (gas, particles and water) collected by the water-quench probe, a special sampling train was designed and developed to separate the three phases and facilitate their analysis. A schematic diagram of the entire sample collection system is shown in Fig. (5.5). All lines, fittings and components from the probe exit to the analyzers were teflon for minimum catalytic effects and minimum sample absorption by the walls.

Due to the presence of the water in the sample, it has to be separated from the gas. Therefore, as the sample stream came from the probe, it entered a disengager which permitted separation of the gas from the solid/liquid sample. A level of water was maintained mechanically in the disengager using a float-valve arrangement, see Fig. (5.6), to prevent gas from exiting with the water/particulate sample. The liquid was then either by-passed into a sintered glass filter to screen the solid particles for ash burnout measurement or it is discharged to the drain. The sampling suction pump created a vacuum force on the top surface of the liquid accumulated in the disengager.

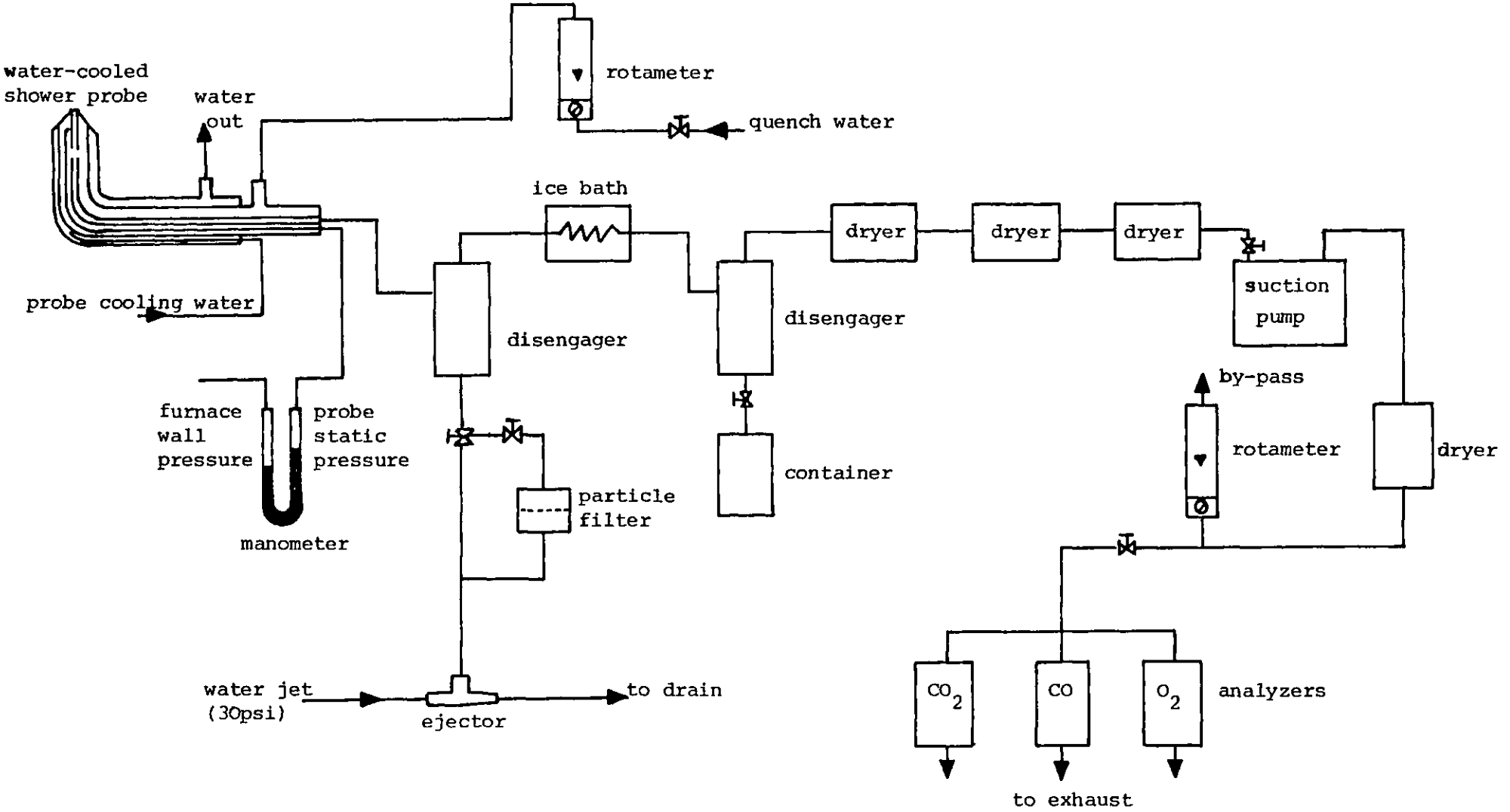

Fig.(5.5) Schematic diagram of the sampling system

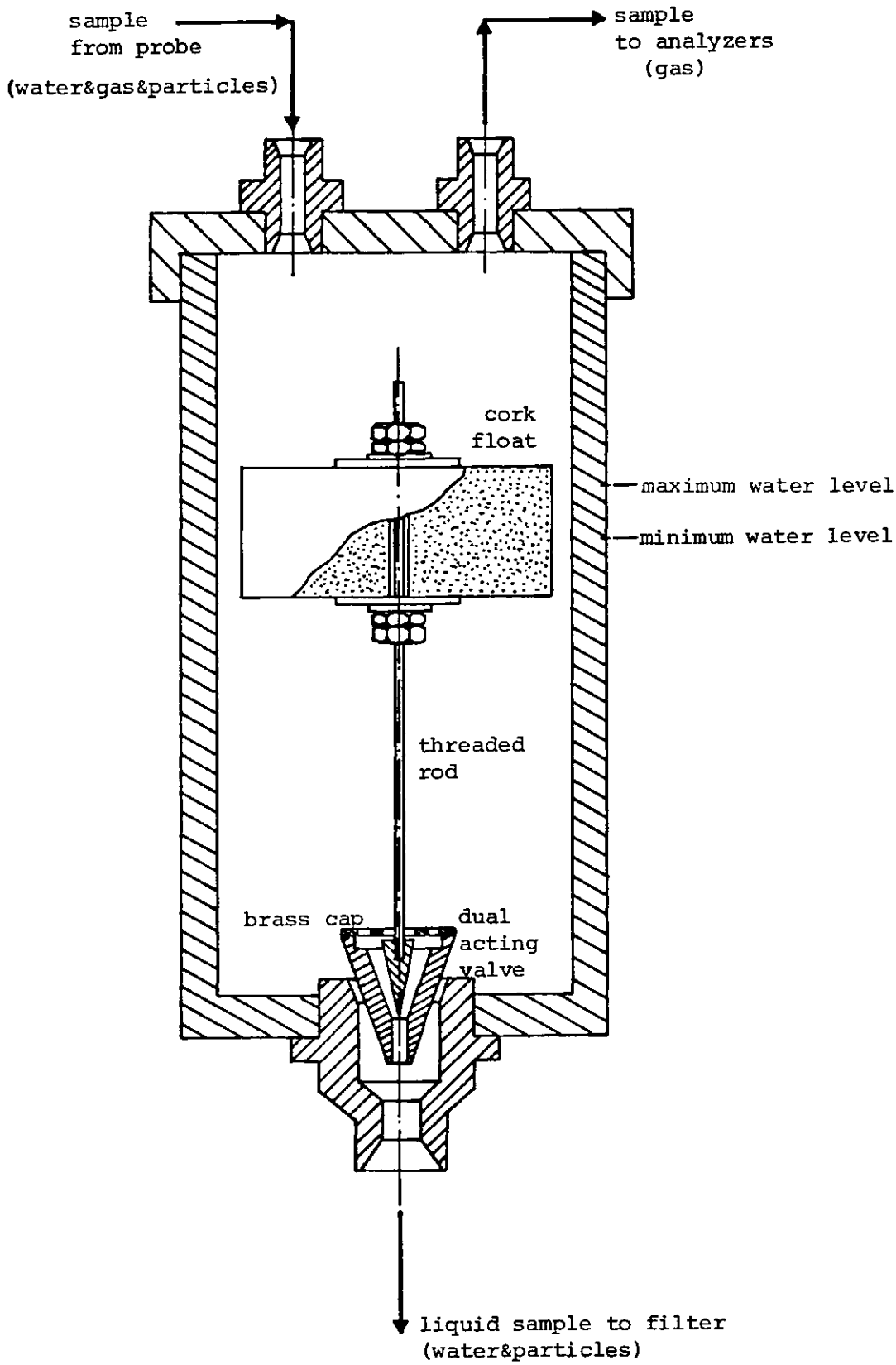

Fig.(5.6) disengager with constant water level arrangement

In order to discharge that liquid, a water ejector was fitted at the bottom of the disengager, see Fig. (5.5). The ejector supplied with a 30 psi water jet and placed a few metres below the disengager level was able to apply enough differential pressure for the withdrawal of the liquid from the disengager.

The gas, having been separated from the liquid, was passed through an ice bath to eliminate any condensable material. Any condensate was then collected in another teflon disengager while the gas passed through dryers stuffed with absorbant cotton wool and calcium chloride for drying and cleaning the gas. The gas sample finally passed through ADC types 483 and 336 CO_2 and CO infrared analyzers respectively and Taylor Servomex type 540 A oxygen analyzer. These on-line instruments were zeroed with pure nitrogen and then standardized with calibrated gases of composition (by volume): 12% CO_2 in nitrogen for carbon dioxide analyzer, 1.5% CO in nitrogen for carbon monoxide analyzer while dry air (21% O_2) was used to standardized oxygen analyzer.

5.3.2 Burnout Measurement

The liquid stream (quench water and solid particles) which remained in the disengager was passed out of the disengager and filtered, Fig. (5.5). Care was taken to collect as much of the solid particles as possible so as to enable an accurate solid analysis. The filter used was a 5-15 μm sintered glass

plate (40 mm diameter) and it was held in a leak-proof teflon filter holder. That filter type was chosen, after several attempts to use different types of filters because: (i) it proved able to trap most of the particulates, (ii) it was easy to obtain the solid sample from the filter for analysis by oven drying up to 110^{o}C and (iii) it was easily cleaned for reuse. Where possible, at least five analysis were done on each char sample. On all samples, an ultimate analysis was done on the Carlo Erba elemental analyzer model 1106 to determine the percentage of hydrogen, carbon, nitrogen and sulphur. The sum of oxygen and ash was determined by difference.

A complete description of the operational procedure for analyzing the solid samples on the Carlo Erba elemental analyzer was given in section (5.2). Briefly, the elemental analyzer is standardized with analytical standards of known hydrogen, nitrogen, carbon and sulphur. Several blank samples (tin containers) are also analyzed to quantify the background levels of H, C, N and S. Char samples from the furnace are then analyzed, with blanks analyzed every five samples.

The extent of the coal burnout was calculated from ash levels measured on each reactor char sample. The residue remaining after analysis of hydrogen, carbon, nitrogen and sulphur is defined as ash. The ash fraction was used in determining the extent of the particle burnout of an individual char sample. Knowing the fraction of ash in the input raw coal and the sample, the burnout levels on an ash-free basis (ψ) was calculated as follows, see Harding (1980):

$$\psi = \frac{1 - (\omega_{\alpha k}/\omega_{\alpha x})}{1 - \omega_{\alpha k}} \tag{5.1}$$

where ω is the weight fraction and the subscript α refers to ash in the original coal (k) or the char sample (x). A dry, ash-free basis was used to report the burnout data since each char sample was dried before ash measurements were performed. Thus dividing by the weight fraction of non-ash material in the original coal $(1 - \omega_{\alpha k})$ normalizes the range of the burnout between 0 and 100%.

Use of particle tracer component was essential in the determination of the particle burnout. Several coal components were considered for use as a particle tracer including iron, aluminium and the coal ash. Ash was the logic choice due to the simple nature of its analysis. However, recent work by Padia (1976) showed that some of the ash components are volatile at combustion heating rates and temperatures. An investigation of the use of ash as a tracer was made by Harding (1980). Harding was not only agreed with Padia but also found the ash to be somewhat soluble in the water. The combined effects of ash volatility and its solubility in the quench water of the sampling probe indicate that the measured ash values are probably low by a maximum of 10%. Because there was relatively few samples analyzed herein for ash, a definite accuracy level was not determined. However, it was felt that the burnout levels calculated using the ash as the particle tracer had an error of about 5-10%.

Finally, the component release percentage of hydrogen, carbon, nitrogen and sulphur were also calculated from the following equation, see Michel and Payne (1980) and Skinner (1980):

$$\% \text{ released} = \left(1 - \frac{\omega_{ix}\,\omega_{\alpha k}}{\omega_{ik}\,\omega_{\alpha x}}\right) \times 100 \qquad (5.2)$$

where ω is the weight percentage and the subscripts i and α stand for the species of interest and ash measured in the sample (x) or the raw coal (k) respectively.

5.3.3 Flame Temperature Measurement

In pratical combustors, the suction pyrometer is most commonly used, in which the thermocouple bead is covered with ceramic sheath for protection and surrounded by ceramic shields to reduce radiative heat transfer. The hot gases are withdrawn under suction from the flame and convective heat transfer is expected to be sufficiently good so that, over a period of minutes, the thermocouple measures the mean gas temperature. A suction pyrometer becomes clogged in dense particle regions but measurements can be made in less dense regions. The sheathing and shielding of the thermocouple results in a very large increase in the volume of the probe and the frequency response is reduced to a very low level.

Non-intrusive optical techniques such as the two-colour pyrometer, see Mitchell and McLean (1982) for measuring particles temperature, hold-out promise but they are not sufficiently developed for use in the difficult environment of pulverized coal combustors. Also the task of traversing the relatively large volume of the present furnace is a major one.

The fine wire thermocouple has a long history of usage for temperature measurements in gaseous flames but in the past it has been considered unsuitable for measurements in particle-laden flames. The first requirement for the use of such thermocouples with particulate flows is that it should be able to survive the direct impact of the solid particles, the selection of the minimum wire diameter is governed by this criterion. In the present study, a 40 μm fine wire thermocouple probe has been used directly in coal flames. It survived and proved the possibility of making accurate temperature measurements with a high degree of both time and spatial resolution. The decision to use the fine wire thermocouple technique was taken according to the conclusion obtained from the preliminary experiment, the two-phase flow jet flame, reported in section (4.2). In regions of high particulate concentrations, there is a high possibility of particles hitting the thermocouple bead, where they can cause an instantaneous variation in temperature and may remain on the bead forming a layer. So the measured local mean temperature reported herein denotes a mixed temperature between the local gas temperature and the temperature of the particles.

The thermocouple was manufactured from platinum/platinum - 13% rhodium wires of 40 μm diameter. The unshielded junction has a diameter of about 50 μm and was supported on 500 μm diameter wires of the same material. The supporting wires were enclosed in a twin-bore alumina sheath with an external diameter of 4 mm which in turn was encased in a stainless steel tube (5 mm diameter) for mechanical strength. Figure (3.13a) showed the probe construction. The probe supporting wires were oriented vertically across the flow

to reduce the particle impact with the junction. A block diagram of the temperature instrumentation is shown in Fig. (5.7). The thermocouple signal was magnified by a factor of 100 and then fed to an automatic data logging system, which is described in detail in subsection (5.3.4). This system enables the automatic measurement of the local bulk mean temperature at different locations across and along the furnace.

Under conditions typical of those encountered in flames, the radiation and conduction heat losses from the thermocouple represent the main error sources associated with temperature measurement by fine wire thermocouple. The true flame temperature can, in principle, be obtained by correcting the measured values either through experimental techniques similar to those used by Odidi (1974), Holderness et al (1969) and Attya (1983) for example, or through the simultaenous solution of equations describing heat transfer modes between the thermocouple bead and surroundings, see Sato et al (1975), Bradley and Mathews (1968) and Glawe et al (1956). Apart from the practical difficulties associated with such techniques, they are subjected to uncertainties relating to the calculation of the heat transfer coefficient and the calculation of the radiant heat transfer (wire emissivity, local mixture properties, etc.), see for example Chedaille and Braud (1972), Khalil (1975) and Moffat (1962).

As an effort to assess the temperature measurements accuracy, the following simplified analysis is used. It allows the quantification of the error associated with the radiation between the junction and the refractory walls of the furnace. Figure (3.13b) showed the heat transfer modes associated with

fine wire thermocouple. The energy balance for the junction can be written as follows:

$$hA_j(T_g - T_t) = \varepsilon_t \varepsilon_w \sigma A_j(T_t^4 - T_w^4) + \text{conduction} \qquad (5.3)$$

The temperature error, can be then written as:

$$T_g - T_t = \frac{\sigma \varepsilon_t \varepsilon_w}{h} (T_t^4 - T_w^4) + \text{conduction error} \qquad (5.4)$$

So,

$$\text{the radiation error} = \frac{\sigma \varepsilon_t \varepsilon_w}{h} (T_t^4 - T_w^4) \qquad (5.5)$$

Available data for platinum/platinum - rhodium thermocouples, Moffat (1962) and Sato et al (1975), indicates that clean wire emissivity, ε_t, is in the order of 0.18 - 0.55 with its thermal conductivity ranges from 40 to 60 Kcal/hr m^oC. Emissivities of refractory wall and particle layer deposited on the thermocouple bead were considered equal to 0.6 and 0.4 respectively, Shah (1983). The convection heat transfer coefficient, h, was calculated from the following correlation for the heat transfer to the thermocouple bead, see Bradley and Mathews (1968):

$$Nu = 0.42\ Pr^{0.2} + 0.57\ Pr^{0.33}\ Re^{0.5} \qquad (5.6)$$

where

$$Nu = \frac{hd_j}{k_g}, \quad Re = \frac{\rho_g d_j U_g}{\mu_g} \quad \text{and} \quad Pr = \frac{C_p \mu}{k_g}$$

Gas flow properties (k, ρ, μ and C_p) appear in equation (5.6) were evaluated at the measured thermocouple temperature using the measured concentration data which are reported in section (5.4). Theoretical data on properties of gas mixtures at high temperatures given by Svehla (1962) have been used in conjunction with expressions

of Brokaw (1961) for mixtures viscosity and thermal conductivity. The radiation error was calculated for a clean 40 μm thermocouple junction and it was found to be about 15^{o}K at 1500^{o}K. But once the thermocouple probe was placed in the coal flame, especially in regions of high particle concentration, some of the ash particles deposited on the probe junction forming a layer and increase the junction diameter accordingly up to 800 μm at most. Recalculation of the radiation error, based on this fact and taking the particles emissivity into consideration indicates that the radiation error is of the order of 110^{o}K at 1500^{o}K for a junction of 800 μm diameter and 50^{o}K for 200 μm diameter. The radiation error is negligible at 1100^{o}K. These values give an approximate magnitude of the radiation error associated with the use of fine wire thermocouples in coal flames and it is unlikely that large modifications to that error can result from the uncertainties in the presumed mixture property values and the heat transfer coefficient correlation. Using a suction pyrometer for temperature measurements in coal flames, Wendt et al (1979) and Harding (1980) estimated an error correction of 20-200^{o}K in the temperature range of 1100^{o}K-1500^{o}K.

On the other hand, the results of Bradley and Mathews (1968) and Sato et al (1975) indicate that the conduction error can be minimized by keeping the temperature of the thermocouple wires adjacent to the juction as high as possible i.e. small temperature gradients must be assured close to the junction. In the present study, the probe was not water-cooled and a reasonably long portion of the supporting wires was exposed to the flame hot gases at temperatures very close to that at the junction. Therefore, it is expected that the contribution of the conduction losses on the

accuracy of the present temperature measurements is relatively very small.

5.3.4 An Automatic Data Logging System

The original method of collecting temperature data from the furnace, which depended mainly on the manual operation of a traverse mechanism carrying a thermocouple probe, was very time consuming and laborious. In order to reduce furnace operating costs, labour and personal errors and increase furnace utilization, productivity and accuracy, an automatic data logging system - based on an ITT microcomputer - was designed and developed for temperature measurements. Temperature was measured by a thermocouple probe which is moved in and out across the furnace by a traverse mechanism. This mechanism is driven automatically by an electric motor controlled by a microcomputer. At each measuring station, data is collected by the computer, converted to an adequate form and stored in a floppy disk. When all the data has been logged, the computer retrieves it from the disk and then prints the results in a tabulated form.

In order to achieve a solution to the design of such a system, the problem was split into several areas. The first area was that of moving the probe in and out of the furnace segment. The second area was the control of the movement of the probe so that its exact position was always known. Finally, the output from the

thermocouple probe has to be collected and stored in a usable form for later analysis. The stored data then has to be reassessed and presented in a hard copy form. All the above has to be controlled by a main program which encompasses all the variations that might be needed on a run. In order to achieve all the system requirements mentioned above, the system components were finalized as shown by the block diagram in Fig. (5.7). The system consists of an ITT microcomputer with its auxiliary equipment; a parallel interface, an analogue to digital converter, a control box containing ancillary electronics and the traverse mechanism with its drive motor and limit switches. Details of each of these components are given as follows:

I. Main system

An ITT computer system was chosen. It consists of an ITT 2020 48 K microcomputer, an Hitachi video monitor, a silentype thermal printer and 116 K byte disk drive. The computer has two functions. Firstly,it controls the probe movement and secondly,it converts and records the measured data.

II. Interfaces

To enable the computer to perform its functions, two different interfaces were needed. For controlling the probe motor, a peripheral adaptor PIA (California Computer Systems, parallel interface model 7720) was used to form a two byte parallel port. This is a device which converts a number written to a memory location in the computer into a set of potentials on eight lines

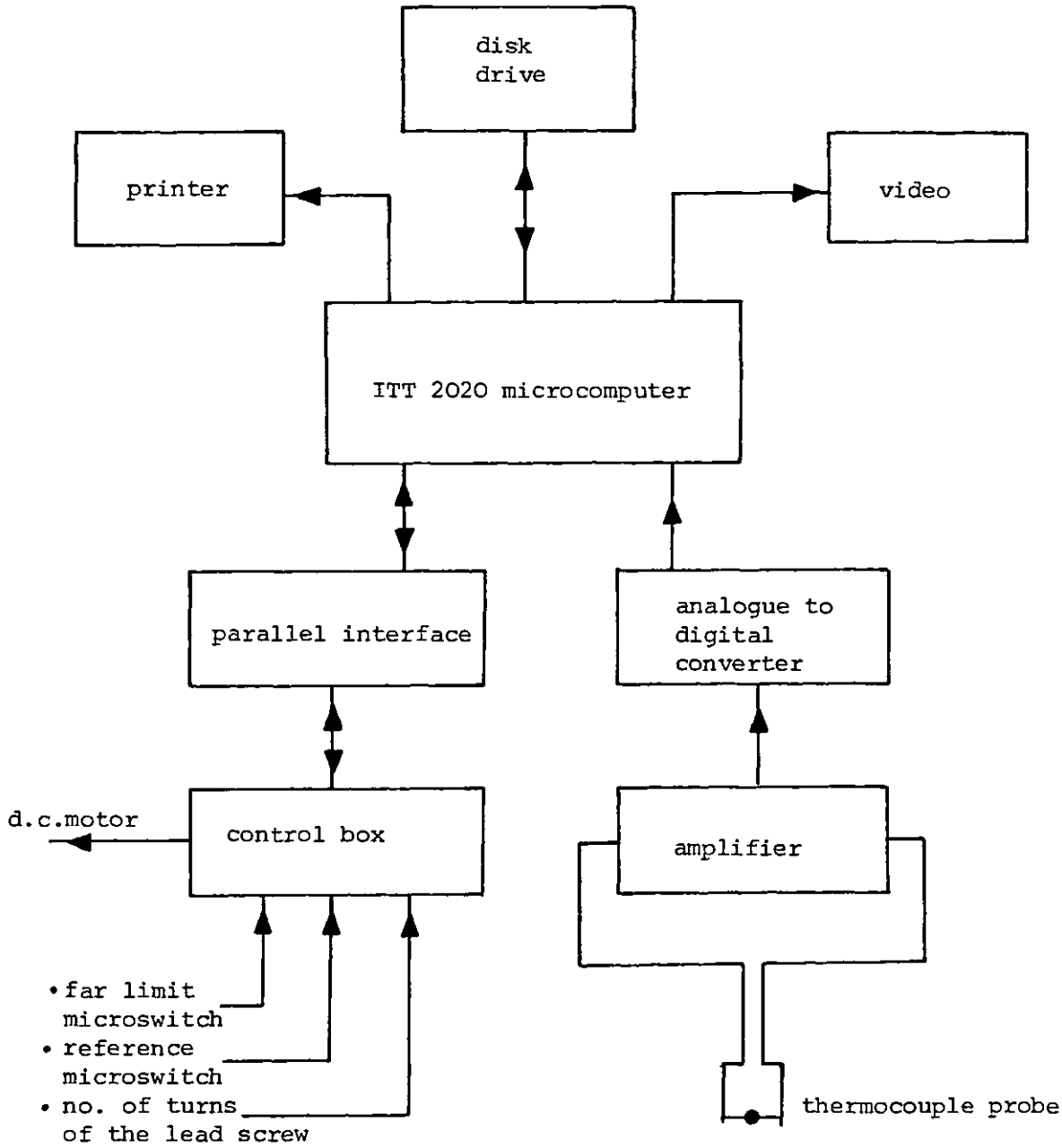

Fig.(5.7) Block diagram of the temperature automatic data logging system

leaving the computer. The PIA parallel interface acts as a form of communication with the traverse arrangement in an on/off mode.

Connecting the variable thermocouple output emf to the computer necessitates the need for an analogue to digital converter. This is a device which converts a voltage into a number in a specific memory location in the computer. In order to choose a suitable analogue to digital converter, two basics have to be determined. Firstly the speed at which sampling has to take place, and secondly the accuracy needed on the measurements taken. Analogue to digital converters usually come in 8, 12 or 16 bit resolutions. This means that there are 2^n-1 steps between the highest reading and the lowest reading where n is the number of bits. Accordingly, the sensitivities of 8, 12 and 16 bit converters are approximately 16 mV/step, 1 mV/step and 0.06 mV/step respectively. In the existing combustion experiment, the flame temperature is in the range of approximately 500-1500^{o}C. This gives a resolution of 11-15^{o}C for the 8 bit, 1^{o}C for the 12 bit and better than 0.1^{o}C for the 16 bit. It was decided that the resolution given by the 12 bit converter would be more than sufficient. The rate of conversion (sampling speed) is only critical when fluctuations are being measured, see Bendat and Piersol (1971). At the present application, only mean temperatures are measured, so sampling rate is not critical as long as the measurement time is sufficiently long to ensure representative sampling. The analogue to digital converter chosen was the CCS model 7470 A (California Computer Systems) with a 12 bit resolution and a sampling speed of 300 ms. This analogue to digital converter reads and converts

potentials between 0 and 4 volts. The thermocouple signal (few millivolts) was multiplied by a factor of 100 using a differential amplifier OP-07 giving an emf in the range of 0-2 volts.

III. The traverse mechanism

The traverse mechanism, shown schematically in Fig. (5.8), provides horizontal radial movement across the furnace at a certain vertical distance along the furnace. The traverse consists of a frame on which a moveable saddle is mounted. The probe is then mounted up on the saddle so that as the saddle is moved along the guides, the probe moves in and out the furnace. The saddle is propelled by a long lead screw (1 revolution = 2 mm travel). This lead screw is driven by an electric motor. At this point there was a choice of whether to use a stepper motor system or a standard direct current (d.c.) motor. A stepper motor had the advantages of being very accurate, but a relatively large motor is needed for small torque. Stepper motors also need a large amount of ancillary equipment such as drive boards in order to operate them. A d.c. motor offered less precision but was a lot simpler and much cheaper. Therefore, it was decided to use a d.c. motor as the accuracy of the motor system would be acceptable. The motor was AM4003, 12 volts d.c. motor with a 25:2 reduction gear box (McLennan Servo Supplies Limited).

Fixed to the lead screw is an eccentric cam which upon revolution depresses and releases a microswitch and this enables the computer counting the number of revolutions of the lead screw and hence the distance the probe has travelled. Two microswitches

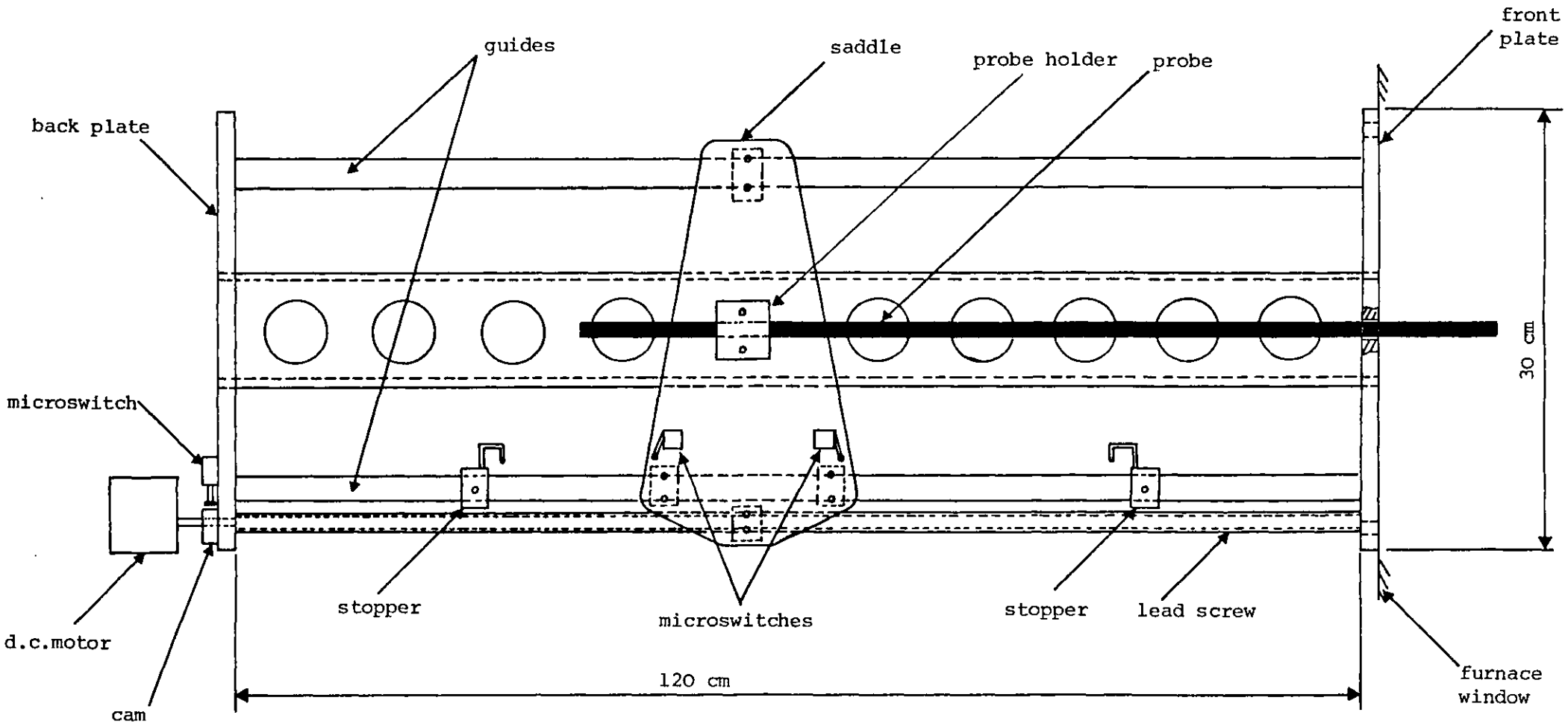

Fig.(5.8) Schematic diagram of the traversing mechanism

were fixed to the saddle so that they make first contact with any object that gets in their way. Mounted on the lower guide are two adjustable stoppers. These can be moved to provide with the two microswitches, the back reference point (start point) for the probe and the position of dangerous excess travel.

IV. Control box (Ancillary electronics)

A complete electronic circuit of the control box is shown in Fig. (5.9). Once a potential has been obtained from the computer, it has to be converted into a usable form. The potential from the computer has a value of either 5 V or 0 V and with power insufficient to drive the d.c. motor. So in order to drive the traverse motor, a power supply was constructed. This consists of a transformer and a relay circuit. The transformer was connected via fuse, isolating switch to the main supply (240 V). The secondary side of the transformer has two 4.5 V 1.3 A outputs, which were connected in series to give a 9V 1.3 A output. The output is then connected to a 1 A rectifier producing a 12 V d.c. supply which is smoothed by a 100 μF capacitor. A light emitting diode (LED) was connected at the output terminals of the transformer circuit to indicate whether the power is on or off.

The power supply (12 V) is then fed to the motor via two miniature relays. Depending on which way the relays are powered up, the motor will be driven either forwards, backwards or the terminals will be shorted to stop the motor. In order to control these relays, the power from the computer has to be transformed into a usable form. This was done by the aid of "pull up resistors"

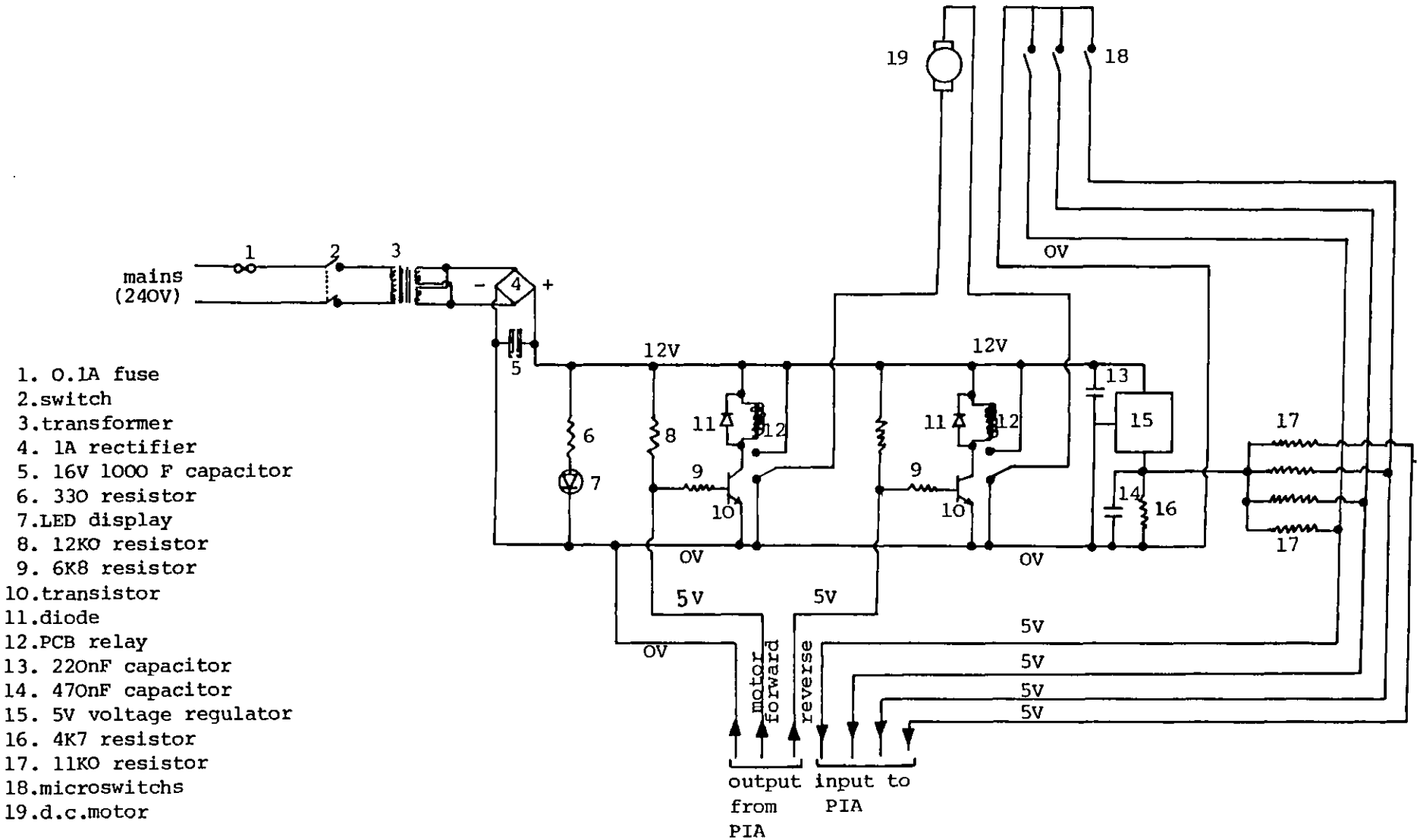

1. 0.1A fuse
2. switch
3. transformer
4. 1A rectifier
5. 16V 1000 F capacitor
6. 330 resistor
7. LED display
8. 12K0 resistor
9. 6K8 resistor
10. transistor
11. diode
12. PCB relay
13. 220nF capacitor
14. 470nF capacitor
15. 5V voltage regulator
16. 4K7 resistor
17. 11K0 resistor
18. microswitchs
19. d.c. motor

Fig.(5.9) Circuit diagram of the control box

driving transistors which power the relays. The 12 V supply is connected via the relay coil to the collector of the transistor emitter is then connected to the ground. When the transistor base is fed a current, this is amplified and a large current flows from the 12 V supply through the relay coil and the transistor to the ground. This causes the relay to switch over and the circuit to be made. When no current is fed to the transistor no current flows through the relay coil and the motor circuit is broken. To protect the circuit from the induced voltage when the coil flux breaks down, a diode was connected across the relay coil. Two relay circuits were used, giving a complete line of communication between the computer software and the motor. When a certain number is written in a specified memory location, one relay will be excited and the motor moves in a set direction. If a different number is written in the motor memory location, the other relay will be excited then the motor will reverse, and when both are excited or both are off, the motor terminals are shorted and it halts.

The second line of communication to the computer is from the microswitches. The three microswitches shown in Fig. (5.8), are used to detect: (1) the reference point which is used as a reference for all the travel across the furnace, (2) the far limit of travel which represents the maximum desirable distance to be travelled by the probe and (3) the number of turns the lead screw has made. These microswitches form a feedback to the computer to tell it what the probe is doing and enable the computer to switch off the motor in the event of failure in the

system. The microswitch system has to present potential of 0 V or 5 V as appropriate at PIA parallel interface. The switches were driven by a "pull up resistor" circuit. This regulating circuit is supplied by a 12 V input and provides a 5 V output which is fed to the microswitches. The computer is then fed a 5 V potential through resistors. When a microswitch is closed, the system is earthed and the potentials presented to the computer becomes 0 V. All the current coming through the resistor passes through a microswitch to earth.

V. Control of the system

A Basic computer program was designed to control the data logging operation. The objectives of this program were to make the probe traverse the furnace, taking a preset number of readings at preset stations across the furnace. This information is then accumulated and a hard copy of the results is produced at the end of the run. The main flow diagram of the control program is shown in Fig. (5.10).

5.4 Presentation of the Experimental Results

Only one coal test experiment has been conducted in this part of the research programme. Its main objectives were to check out the measuring instrumentation and to verify their ability to conduct easily a complete set of temperature, concentration and burnout measurements. This data set would also assist the validation of the computer prediction procedures. A summary of the test conditions for this experiment is given in Table (5.6).

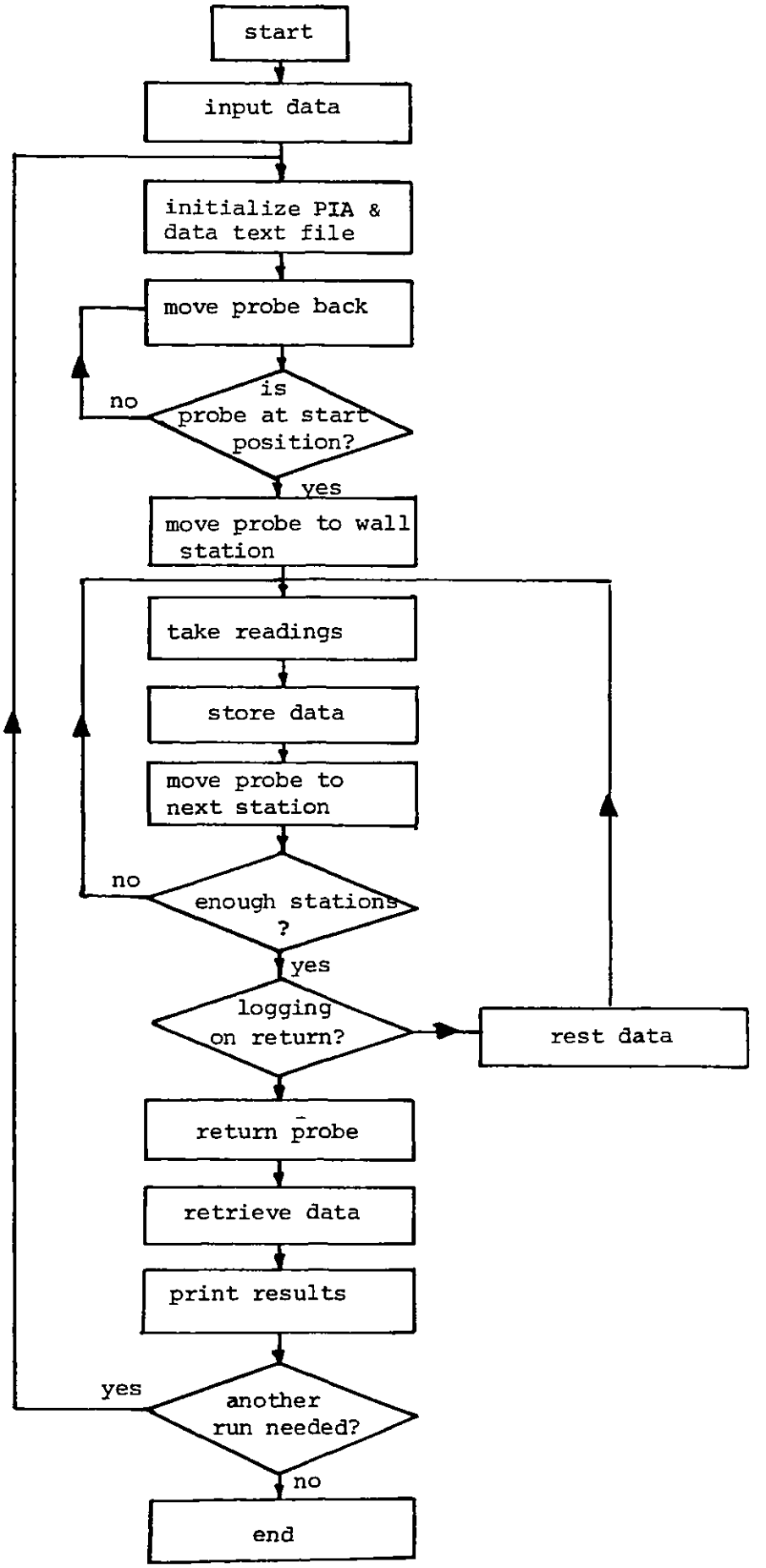

Fig.(5.10) Flow chart of the temperature data (BASIC) program

Table (5.6)

Conditions used in the experiment

Variable	Value
Coal feed rate, kg/hr	12
Primary air mass flow rate, kg/hr	25.7
Secondary air mass flow rate, kg/hr	115.5
Excess air, %	15.5
Stoichiometric air requirement, kg/kg of coal	10.184
Mean particle diameter, μm	39
Solid loading, %	32
Secondary swirl number	0.8
Primary preheat temperature, ^{o}C	50
Secondary preheat temperature, ^{o}C	300

The furnace pressure was adjusted and maintained within a few millimeters of water below the atmospheric pressure to prevent any possibility of air leakage. The cooling water was kept at a flow rate of 5 litre/min in all segments. Flame scanners cooling air was kept at a minimum flow rate of 3 litre/min to avoid aerodynamic flame disturbances. Due to the disturbances created by the feed hopper refill operation, no measurements were conducted during the refill period and a sufficiently long time was allowed after the refill for the flame to return to the steady state conditions before the measurements could be continued.

Radial profiles of various gas species concentrations (carbon dioxide, carbon monoxide and oxygen) and temperature were measured at several axial locations during this test. Because the sampling probe tip is 8 cm upstream from the probe axis, see Fig. (5.4), temperature and sample collection could not be done at the same axial location. Therefore, the reported temperature profiles are at a position 8 cm further downstream of the species concentration profiles. For burnout, centre line solid samples were collected using the shower probe at axial locations of $\bar{X}/D$ = 0.1166 and 0.6166. Also, a liquid sample was collected at the exit of the scrubber and filtered to give an indication of the chimney burnout or combustion efficiency. Burnout of coal and percentage release of carbon, hydrogen, nitrogen and sulphur have been calculated from the analysis of collected solid char samples and the average input coal analysis.

Figures (5.11) to (5.13) show the radial profiles of CO_2, CO and O_2 percentage volume fraction (on dry basis) as a function of the radial distance, measured at three axial distances of

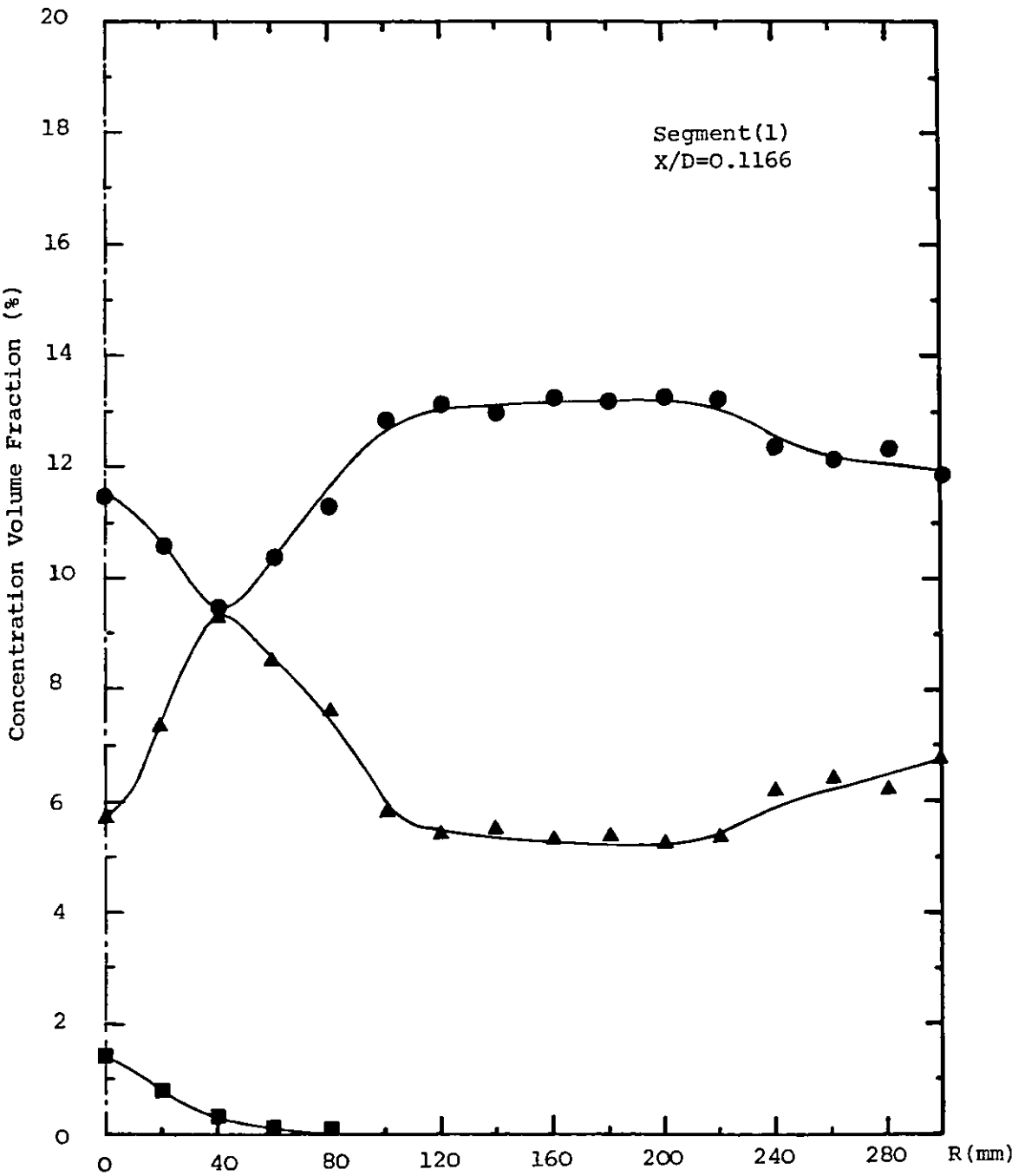

Fig.(5.11) Radial concentration profiles : ● CO_2, ■ CO, ▲ O_2

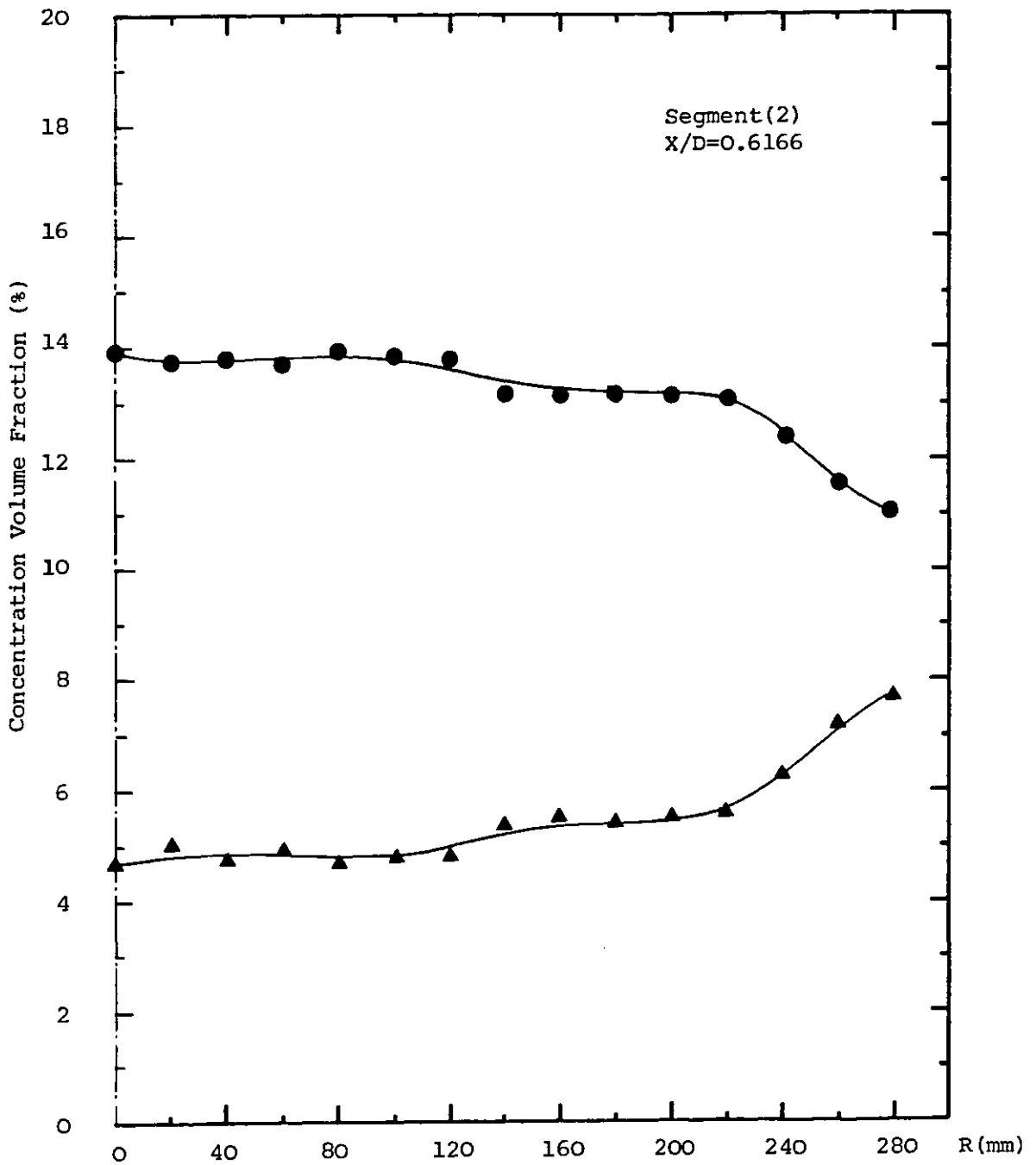

Fig.(5.12) Radial concentration profiles : ● CO_2, ■ CO, ▲ O_2

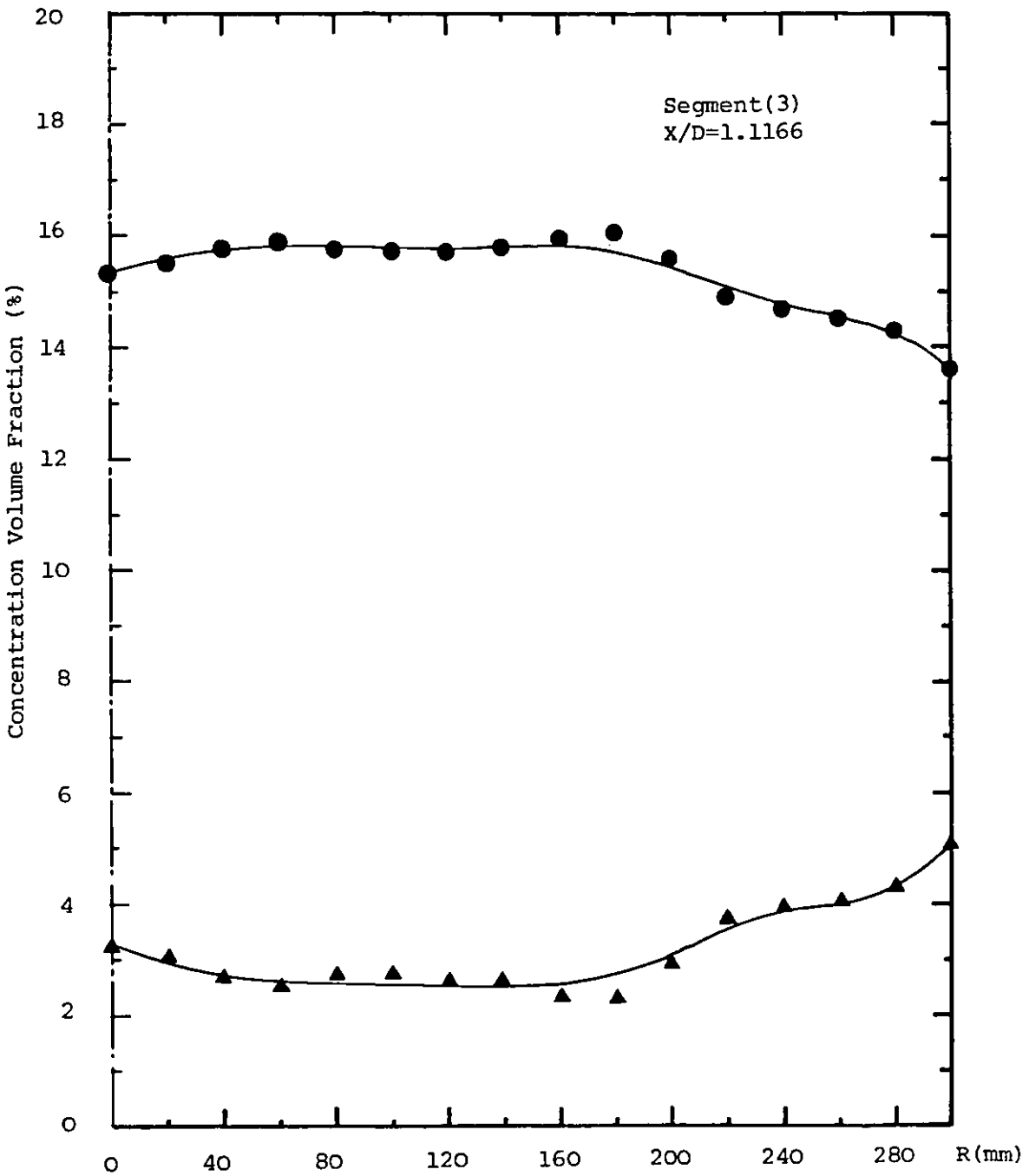

Fig.(5.13) Radial concentration profiles : ● CO_2, ■ CO, ▲ O_2

X/D = 0.1166, 0.6166 and 1.1166 from the burner exit. Temperature profiles are shown in Fig. (5.14) to Fig. (5.16) at axial locations of X/D = 0.1166, 0.125, 0.383, 0.75, 1.25 and 2.25. Table (5.7) shows the burnout levels and the percentage release of carbon, nitrogen, hydrogen and sulphur as a function of the axial distance.

At first glance, the results, in particular for segment (2) (X/D = 0.75), show a very short flame. This is clearly evidenced by the flat profiles of carbon dioxide and oxygen concentrations with the absence of carbon monoxide (Fig. (5.12), X/D = 0.6166) and also indicated by the flat temperature distribution at X/D = 0.75 (Fig. (5.15)). These flat profiles reveal the existence of only hot combustion gases. The coal burnout at centre line (X/D = 0.6166) was about 90%, Table (5.7), and this indicates that the reaction volume occupies only a very small volume of the furnace top. This short flame was a result of the low primary velocity (about 7 m/sec) and the high swirl number of 0.8.

At X/D = 0.1166, Fig. (5.11), the radial profiles of CO_2, CO and O_2 concentrations show increasing O_2 from the centre line to about 40 mm off centre line where it peaks. These values then decrease and show a quite flat profile as the wall is approached. Carbon dioxide on the other hand has a higher value in the centre line than 40 mm from the centre line, it then rapidly rises to form a nearly flat profile in the outer region near to the wall. Carbon monoxide shows a peak value at the centre line and drops to zero at radial distance of 60 mm. By X/D = 0.6166 (Fig. (5.12)) the species profiles appear quite flat with the vanish of carbon monoxide concentration. Figure (5.13), X/D = 1.1166, shows also flat distributions. Temperature profiles show more or less similar trends, see Fig. (5.14) to Fig. (5.16). A maximum temperature of

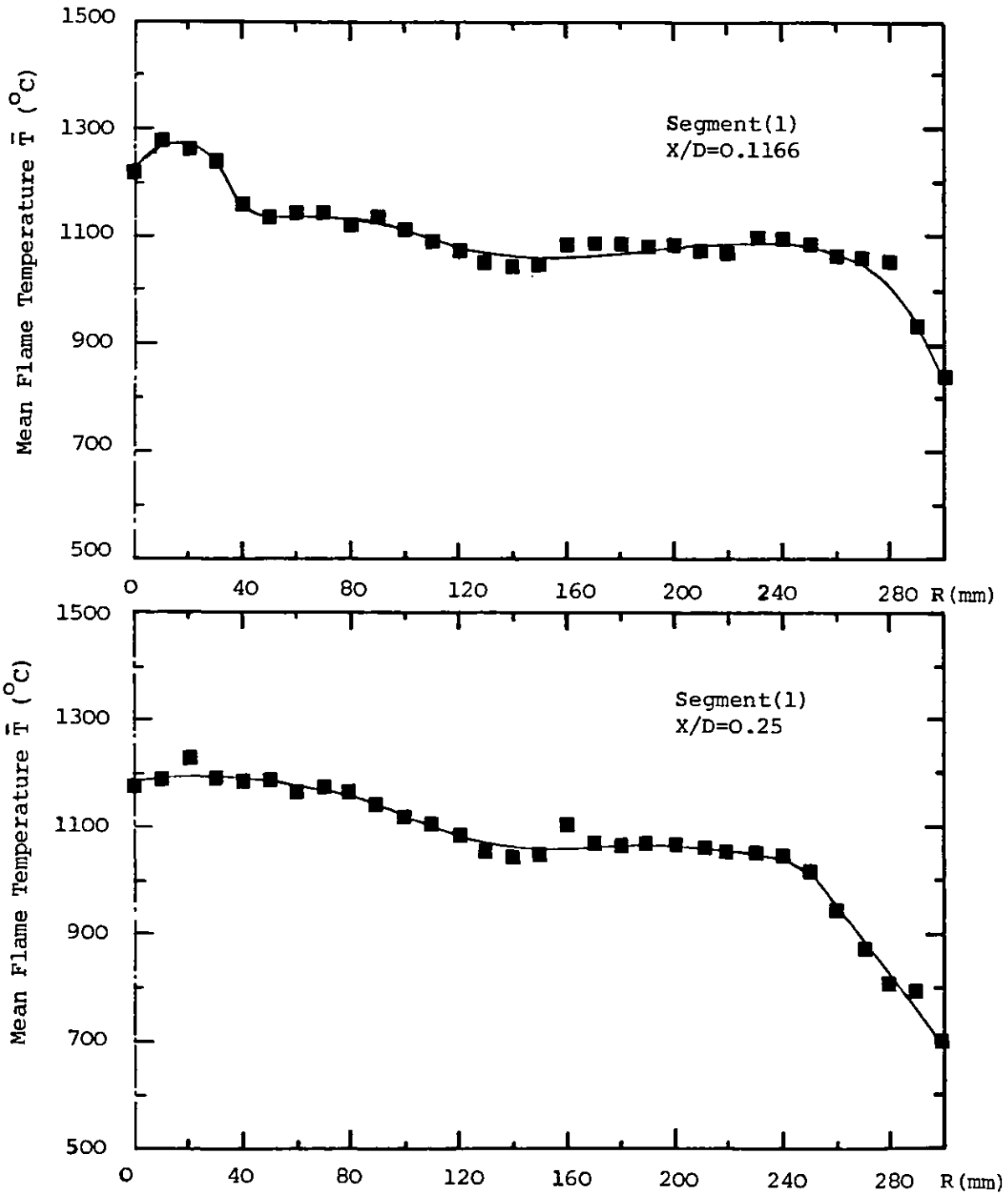

Fig.(5.14) Radial distributions of mean flame temperature along the furnace

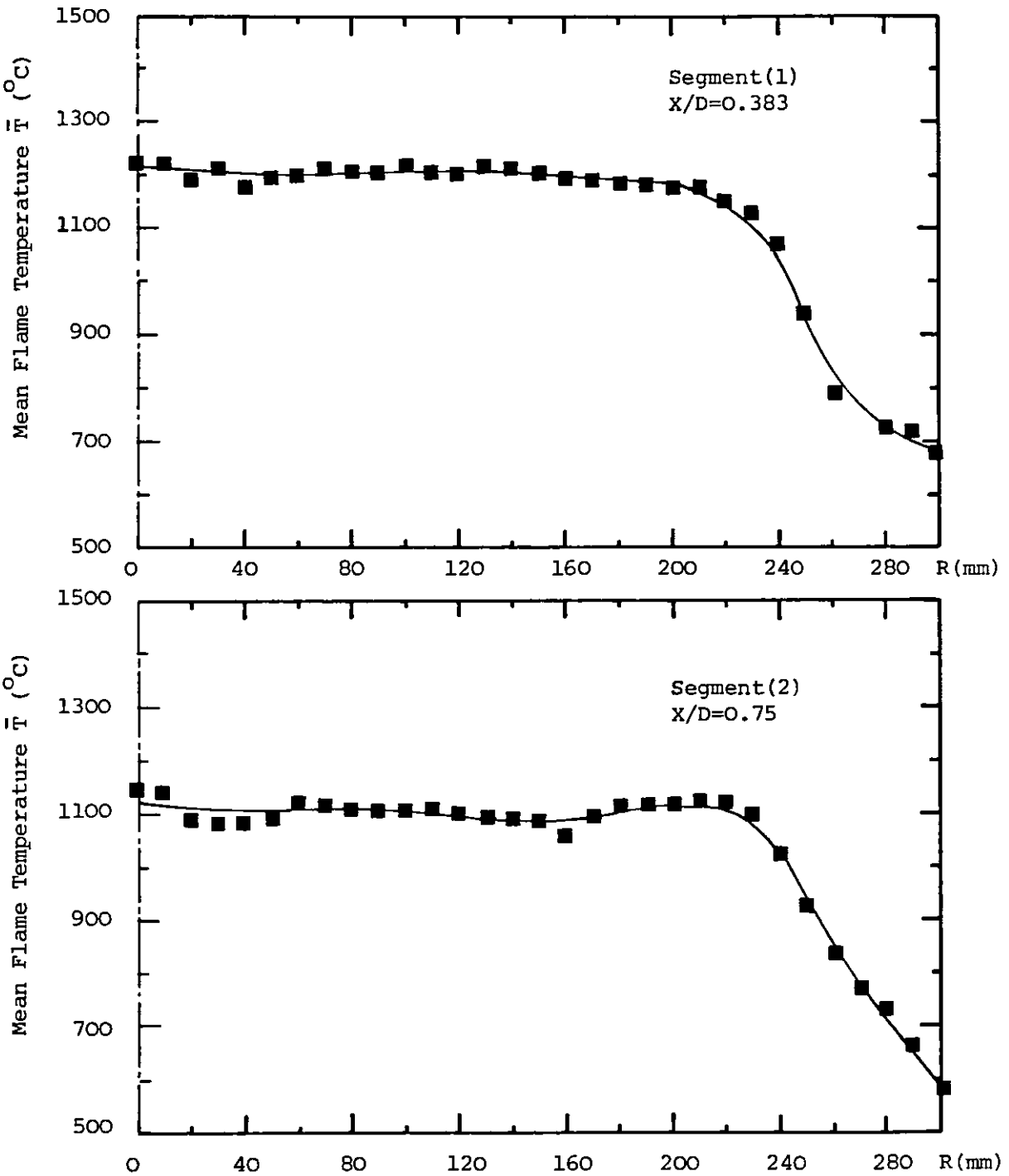

Fig.(5.15) Radial distributions of mean flame temperature along the furnace

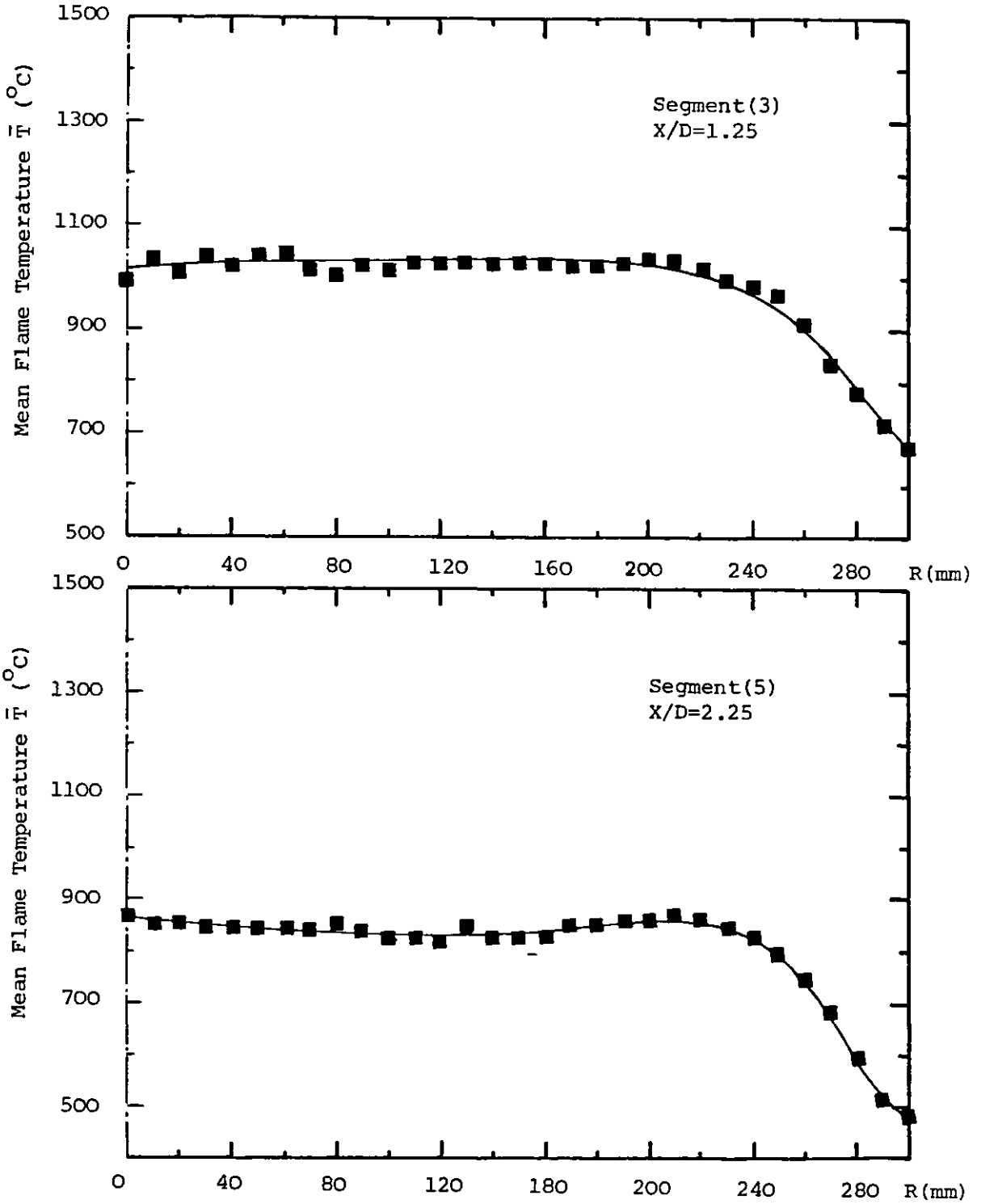

Fig.(5.16) Radial distributions of mean flame temperature along the furnace

Table (5.7)

Summary of the char burnout results

Axial Location X/D	Ultimate Analysis of the Char Sample					Coal burnout	% carbon released	% hydrogen released	% nitrogen released	% sulphur released
	% C	% H	% N	% S	% Ash*					
0.1166 Segment (1)	41.35	1.31	0.72	0.96	55.66	85	84.2	92.2	86.5	80.6
0.6166 Segment (2)	34.65	0.22	0.51	0.32	64.31	89	88.5	98.9	91.8	94.4
4.5 Furnace Chimney	13.08	0.08	0.17	0	86.67	97.8	96.8	99.7	98.0	100.0

*Percentage ash is calculated by difference.

1300^{o}C, (uncorrected for radiation loss), was recorded. In general, the recorded temperatures are in the same range as those reported by Harding (1980) for similar coal flames. Approximately the same temperature levels exist to about X/D = 0.383 where more than 85% of coal has been burned, see Table (5.7). This is followed by a gradual decrease in the temperature towards the furnace exit.

From these data, there appears to be a hot, fuel-rich core, produced by the swirl, in the centre of the reactor surrounded by a flame located initially (Fig. (5.11)) at 40 mm radially and approximately 60 mm thick. The trends within this central core are similar to those for free jet diffusion flame, see section (2.5). The presence of an outer recirculation zone, in the region of R > 120 mm, is reflected by the uniformly distributed carbon dioxide, oxygen and temperature with CO_2 levels being the highest across the flame zone and with the non-existence of CO. Further downstream from that location the flame becomes broader. It is noted that the carbon dioxide levels recorded in the central core and in the outer recirculation zone exceeded those reported for the natural gas confined flames, see section (3.5). This is because the carbon content in the coal is higher than that of the natural gas.

As can be seen from Table (5.7), the total burnout is found to be about 90% at the visible flame length (X/D = 0.6166). There is little evolution after this point and up to the 97% burnout recorded at the entrance of the chimney. It is interesting to note, from the same table, that carbon tends to be released at the same rate as the coal is burned, which is not surprising

since at least 75% of the coal is carbon. This suggests that carbon can be used to represent the coal burnout.

CHAPTER 6

SUMMARY AND CONCLUSIONS

6.1 Summary

The first objective of the research programme of this thesis was to provide and extend the experimental data in reacting turbulent diffusion jets. The local mean concentration and velocity fields were studied. Such data, apart from providing many details of the physical processes encountered, are relevant to the modification and/or the development of turbulence and combustion models.

An axial free vertical jet geometry has been utilized because it is simple and well defined. The experimental programme encompassed extensive and detailed measurements of the mean species concentrations and mean, fluctuation and turbulence intensity of axial velocity. The concentration measurements have been obtained using a quartz microprobe while laser-Doppler anemometer technique has been used to obtain velocity measurements.

A wide range of flame types were considered including both stabilized and lifted natural gas diffusion flames. Different fuel types of lower calorific values have been simulated by adding nitrogen to the combustible gas while keeping the input Reynolds number constant. A complete set of measured quantities has been obtained for one of each of the flame types. The influence of Reynolds number on the axial distribution of the mean concentration has been determined for all the flames studied.

The second objective of this research effort was to build and develop a research combustor facility capable of providing the

necessary data and information concerning the processes associated with pulverized coal combustion. These data can be used in computer prediction procedures. Also, they can be used to improve pulverized coal reactor design and performance.

A new cylindrical, axisymmetric and vertical laboratory furnace composed of water-cooled and refractory-lined segments has been constructed and commissioned. The large size of the furnace (diameter = 0.6 m, height ≡ 4 m) renders significant the role of thermal radiation from the walls and ensures fully developed turbulent flows. An industrial type double concentric burner with a calibrated swirl generator and a quarl was used. The three-dimensional effects were minimized by orienting the furnace vertically. The furnace was fired from its top end to facilitate fly-ash particle removal. Exhaust gases exit via an axial port at its bottom end to preserve the axial symmetry throughout the combustor. An electronic flame supervision system incorporating different types of safety features was used to control the ignition sequence and the continuous operation of the furnace.

To assist the validation of the combustion prediction procedures in furnaces and to check out the proper operation of the experimental arrangement before running up to coal firing, data for gaseous turbulent diffusion flames have been collected from the combustor using a radial natural gas injection burner configuration. The experiments covered the effect of excess air level and swirl number on gas temperature, species concentration and incident radiation flux. Comparative concentration measurements have been made using different types of sampling probes. A fine wire thermocouple

probe was used to map the temperature. Incident radiation flux to the walls was obtained by an ellipsoidal radiometer.

For coal firing, a complete pulverized coal feeding arrangement was designed and constructed. A microprocessor feedback control system, based on the "loss-in-weight" principle was developed and incorporated in the feeding system. It controlled the speed of the screw feeder in order to regulate the coal feed rates within reasonable tolerances and ensure continuous pulverized coal feeding to the combustor. An accurate coal feed rate was a fundamental requirement to obtain reliable data from the coal combustion experiment.

Particular attention was given to the measuring techniques in order to collect reliable data at various locations within a coal air flame. A considerable effort was made to develop a reliable sample handling system and to automate the data acquisition. Temperature measurements were obtained by a fine wire thermocouple probe coupled to an automatic data logging system. Particle-gas samples were collected with a water-cooled shower probe. Different gaseous concentrations were determined from on-line gas analyzers. The particulate material was separated from the gas and the quench water and was analyzed to determine the ash burnout levels.

The remainder of the present chapter contains a summary of the main conclusions, section (6.2), and some recommendations for future work, section (6.3). Section (6.2) is divided into three parts: subsection (6.2.1) provides the main conclusions regarding the experimental results in the turbulent free diffusion flames whereas subsection (6.2.2) and (6.2.3) include respectively

the main conclusions of the experimental results in the gas-fired and coal-fired furnace.

6.2 Conclusions

6.2.1 Experimental Results in the Turbulent Free Jet Diffusion Flames

1. Concentration and velocity measurements are presented for a well defined turbulent free jet natural gas flame, which, because such data are suprisingly few, will prove useful for validating mathematical models. Indeed, the data has already been employed by Liew et al (1981), Godoy (1982) and Lockwood and Stolakis (1983) to validate their prediction techniques.
2. Vertical free flames are greatly affected by the Froude number.
3. The measurements in burner stabilized flame reveal typical diffusion flame behaviour. The measurements also suggested that finite rate kinetic effects are responsible for the unexpected finite oxygen concentration that appears upstream in the main flame region. As interesting as this is in its own right the effect would not seem large enough to be of much importance to mathematical simulation intended for most engineering applications.
4. The unburned hydrocarbon concentration vanishes at nearly the same axial location at which the carbon dioxide concentration attains its maximum. The maximum CO_2 and CO peaks on the

flame axis are augmented and flattened as the role of buoyancy is decreased with the increase of Reynolds number.

5. The basic structure of lifted flames comprised two main zones: (i) an upstream zone which exhibits an initial steep rise in CO and CO_2 concentrations due to the burning of the partially premixed mixture as indicated by steep reduction in unburned hydrocarbon and oxygen concentrations and (ii) a diffusion zone in which the flame behaviour is similar to that of the stabilized flame cases.
6. The increase in Reynolds number is shown to be associated with an increase in the length of the premixed region and in the on-axis CO_2 and CO levels reached at the end of this zone. Also increasing the Reynolds number augments the oxygen peaks and decrease its minima.
7. In the stabilized nitrogen-diluted flames (of the same input Reynolds number) the increase in the percentage of nitrogen shortens the flame and causes a reduction in both the levels of unburned hydrocarbon and maximum levels of both carbon dioxide and carbon monoxide.
8. Velocity measurements suggest that the onset of the reaction is the reason of the different behaviour of turbulence intensity in both the stabilized and lifted flame.
9. The turbulence intensities for the stabilized flame are considerably less than those for an inert jet. Suppression of turbulence by combustion is argued to be due to dilation effects. This is evidence by the fact that the turbulence intensity is slightly higher in the cooler nitrogen-diluted

flames than those of stablized flame, while the onset of the partially premixed combustion in the lifted flame causes a dramatic reduction in turbulence intensity.

10. The present results are more extensive, in terms of types of flames studied and the number of measured quantities, than any previous work. The use of quartz microprobe for gas sampling and laser Doppler anemometry for velocity measurements allowed an increase of accuracy of the present results.

6.2.2 Experimental Results in the Gas-Fired Cylindrical Furnace

1. The present experiment is distinguished by the care which has been taken in the design and setting up of the furnace to ensure axisymmetric flow conditions, the rather large size of the furnace which renders significant the role of thermal radiation and ensures fully turbulent Reynolds numbers and the use of an industrial type of burner.
2. Three experiments have been conducted to assess the relative performance of three gas sampling probes and to report data, for two excess air levels and two air swirl numbers, mainly intended to assist mathematical modellers.
3. Comparative concentration measurements have been performed using three different sampling probes utilizing different methods of sample quenching: quartz microprobe, water-cooled stainless steel probe and a water-quench (shower) probe. The discrepancy between the three probe types is not excessive.

The results indicate that the water-cooled probe does not freeze the reaction as rapidly as the shower probe but the latter has the disadvantage of dissolving some carbon dioxide and oxygen, in the gas sample, in its quenching water.

4. The quartz microprobe, which proved to be generally delicate for the scale of the present experiments, failed to survive in the upstream core of the flame due to the high temperature gradients on its lengthy cantilever span.
5. In the case of the water quench probe, difficulties arose in the pressure matching at the hottest locations in the furnace due to boiling at the probe tip which impeded the quench water flow.
6. Precise measurements of incident radiation flux to the furnace walls were obtained by an ellipsoidal radiometer and a 40 μm fine wire thermocouple probe was used to accurately map gas temperatures.
7. Concentration measurements, obtained using the water-cooled probe, and temperature measurements revealed that in the early stages of flames, two regions may be identified: (i) central core containing the reaction zone and (ii) an outer wall recirculation zone. The central region follows the trends of free jet flames up to the radial location of maximum oxygen concentrations and minimum carbon dioxide concentrations. In the outer region, CO_2 and O_2 concentrations and temperature are uniformly distributed. The high CO_2 levels together with the non existance of CO reflects the existance of a strong recirculation zone.

8. Imparting swirl to the secondary air has the effect of increasing the radiation fluxes near the burner zone and making the reaction zone more compact. Variations in excess air from 5 to 10% has only a slight effect on the incident radiation fluxes.

6.2.3 Coal Firing Experiment

1. The development of a data producing test facility for the study of pulverized coal combustion has been completed and it is successfully operational.
2. The microprocessor-controlled pulverized coal feeding system operated satisfactorily and the coal feed rate was maintained at the set value with an error of ±2%.
3. A water-quench sampling probe with a cooling water jacket was found to solve the problem of boiling or flashing of the probe quench water at the hottest flow regions. It was very efficient in collecting gas and particle samples at any point in the coal-air flame.
4. The concentration sampling system handled well the three phase samples (water, gas and particles). The system manipulation was minimized by using a float-valve arrangement to maintain the liquid level constant in the first disengager and by the use of a water ejector to discharge the excess liquid out of that disengager.

5. The analytical equipment used in gas and particle analyses and in coal particle sizing (the CO_2, CO and O_2 gas analyzers, the elemental analyzer and air jet sieve) were very satisfactory and produced reliable results.
6. The 40 μm fine wire thermocouple probe, used to measure mean flame temperature, survived particle impact and its temperature data are probably more accurate than those of a suction pyrometer which suffers immediate blockage problems and causes flow disturbances.
7. The automatic data logging system for temperature measurements is a success and it helps to reduce time and effort needed for a temperature set of data. Automation of the concentration data collection has been successfully completed as well and it is already in use, see Hirji (1983).
8. A set of experimental data was provided for the British bituminous pulverized coal to assist computer prediction procedures validation and to demonstrate the satisfactory operation of both the test facility and the data collection systems. The data includes flame temperatures, gas concentrations and burnout levels.
9. Particle sizing of the Grimethorpe pulverized coal used in this study showed that at least 80% of the coal particles are less than 60 μm and the particles mean diameter is 39 μm. The ultimate analyses indicated that more than 75% (by weight) of the coal is carbon while sulphur, nitrogen and hydrogen represent only a small percentage (8% by weight). It was found from the proximate analyses that about 7% of coal weight is ash, the volatile matter is about 30% and 3% moisture content.

10. The concentration, temperature and burnout results showed that the studied coal flame behaves in its central, hot and fuel-rich core as a free jet flame up to the radial locations where CO_2 and O_2 attain their minima and maxima respectively. This central zone is surrounded by a quite thick flame envelope. An outer recirculation zone exists and contains only well mixed hot combustion products.

6.3 Recommendations for future work

1. The immediate need is to investigate the effect of different operating conditions: swirl number, primary air velocity, solid loading, primary and secondary air preheat and coal type and size on coal burnout, temperature and gaseous species concentrations.
2. The rate of release of the individual coal components under various operating conditions has to be determined.
3. The study of coal flame stability under different combustor conditions is of immediate interest.
4. Tests should be conducted to study the effect of operating parameters on nitrogen pollution evolution and sulphur pollutant species.
5. The laser Doppler anemometer technique has to be developed and then applied to get both gas and particle velocity distributions in the combustor under variable operating conditions.

6. The emissivity of the fine wire thermocouple after particle deposition on the junction should be measured for accurate estimation of the radiation error.
7. Better configurated viewing ports would aid in flame visualization studies.
8. A permanent exhaust pipe probe collection system needs to be designed so as to ensure continuous quantification of exhaust stream concentration.
9. Means for reducing or eliminating the disturbances in the combustor created during the refill process of the feed hopper should be developed. It is suggested that an inverted cone may be placed in the hopper to act as a damping buffer.

REFERENCES

ABBAS, A.S. (1982)

Predicting the performance of heavy oil-fired combustors.

Ph.D. Thesis, University of London.

ABBAS, A.S., KOUSSA, S.S. and LOCKWOOD, F.C. (1980)

The prediction of particle laden gas flows.

18th Symp. (Int.) on Combustion, pp. 1427-1438

ABBOTT,S.W., SMOOT, L.D. and SCHADOW, K. (1974)

Direct mixing and combustion efficiency measurements in a ducted, partile-laden jets.

AIAA J., Vol. 12, No. 3, pp. 275-282.

AHLHEIM, M. and GÜNTHER, R. (1980)

Investigation of turbulent reaction fields by ionization measurements.

AIAA 18th Aerospace Science Meeting, Pasadena, California, Paper-80-0283.

ALPERN, B., COURBON, P., PLATEAN, J. and TISSANDIER, G. (1960)

Microscopic examination of sample taken from a pulverized-fuel flame.

J. Inst. Fuel, Vol. 33, pp. 399-402.

ASALOR, J.O. and WHITELAW, J.H. (1974)

The design and performance of across flow particle generator for use in laser-Doppler anemometry.

Mech. Eng. Dept., Imperial College, Report No. HTS/74/25.

ATTYA, A.M. (1983)

Kerosene spray flames.

Ph.D. Thesis, University of London.

ATTYA, A.M. and WHITELAW, J.H. (1981)

Velocity, temperature and species concentration in unconfined kerosene spray flames.

ASME Winter Annual Meeting, Nov., Paper No. 81-WA/HT-47.

BAKER, P.C., BARKER, M.H., LOVERIDGE, D.J., THURLOW, G.G. and WINGFIELD, G.J. (1969)

A furnace for research into the combustion of pulverized coal.

J. Inst. Fuel, Vol. 42, pp. 371-377.

BAKER, R.J., HUTCHINSON, P., KHALIL, E.E. and WHITELAW, J.H. (1975)

Measurements of three velocity components in a model furnace with and without combustion.

15th Symp. (Int.) on Combustion, pp. 553-559.

BALLANTYNE, A., BOON, D.J. and MOSS, J.B. (1976)

Measurements of fluctuating temperature in open diffusion flames employing fine wire thermocouples.

Dept. of Aeronautics and Astronautics, University of Southampton, AASU Memo. No. 36/3.

BALLANTYNE, A. and MOSS, J.B. (1977)

Fine wire thermocouple measurements of fluctuating temperature.

Comb. Sci. Tech., Vol. 17, pp. 63-72.

BANDYOPADHYAY, S. and BHADURI, D. (1971)

Effect of particle size and distribution on the combustion of coal dust.

J. Inst. Fuel, Vol. 44, pp. 337-380.

BECKER, H.A. and BROWN, A.P.G. (1969)

Velocity fluctuations in turbulent jets and flames.

12th Symp. (Int.) on Combustion, pp. 1059-1068.

BECKER, H.A., HOTTEL, H.C. and WILLIAM, G.C. (1963)

Concentration fluctuations in ducted turbulent jets.

9th Symp. (Int.) on Combustion, pp. 7-30.

BECKER, H.A., HOTTEL, H.C. and WILLIAMS, G.C. (1967)

Mixing and flow in ducted turbulent jets.

11th Symp. (Int.) on Combustion, pp. 791-798.

BECKER, H.A. and LIANG, D. (1978)

Visible length of vertical free turbulent diffusion flames.

Comb. and Flame, Vol. 32, pp. 115-137.

BECKER, H.A. and YAMAZAKI, S. (1978)

Entrainment, momentum flux and temperature in vertical turbulent diffusion flames.

Comb. and Flame, Vol. 33, pp. 123-149.

BEÉR, J.M. and CHIGIER, N.A. (1969)

Stability and combustion intensity of pulverized-coal flames - effect of swirl and impingement.

J. Inst. Fuel, Vol. 42, pp. 443-450.

BEÉR, J.M. and CHIGIER, N.A. (1972)

Combustion aerodynamics.

Applied Science Publishers Inc., London.

BEÉR, J.M., CHIGIER, N.A. and LEE, K.B. (1962)

Modelling of double concentric burning jets.

9th Symp. (Int.) on Combustion, pp. 892-900.

BELTAGUI, S.A. and MACCALLUM, N.R.L. (1973)

Aerodynamic of swirling flames, vane generated type.

Comb. Institute European Symp., pp. 559-564.

BENAT, J.S. and PIERSOL, A.G. (1971)

Random data: analysis and measurement procedures.

John Wiley & Sons Inc., London.

BIARSKI, A.A., BARNES, R.H. and KIRCHER, J.F. (1978)

Flame measurements utilizing Raman scattering.

Comb. and Flame, Vol. 32, pp. 111-114.

BILGER, R.W. (1975)

A note on Favre averaging in variable density flows.

Comb. Sci. Tech., Vol. 11, pp. 215-217.

BILGER, R.W. (1977)

Probe measurements in turbulent combustion.

AIAA Prog. in Astronautics and Aeronautics, Vol. 53, pp. 333-351.

BILGER, R.W. and BECK, R.W. (1975)

Further experiments on turbulent jet diffusion flames.

15th Symp. (Int.) on Combustion, pp. 541-552.

BOWMAN, C.T. (1977)

Probe measurements in flames.

AIAA Prog. in Astronautics and Aeronautics, Vol. 53, pp. 3-24.

BRADLEY, D. and MATHEWS, K.J. (1968)

Measurement of high gas temperatures with fine wire thermocouples.

J. Mech. Eng. Sci., Vol. 10, No. 4, pp. 299-305.

BRAY, K.N.C. (1974)

Kinetic energy of turbulence in flames.

Dept. of Aeronautics and Astronautics, University of Southampton,

AASU Report No. 332.

BRITISH STANDARD 1106 (1977)

Methods for analysis and testing of coal and coke.

Part 3: Proximate analysis of coal.

BROKAW, R.S. (1961)

Alignment charts for transport properties: viscosity, thermal conductivity and diffusion coefficients for non-polar gas mixtures at low densities.

NASA TR-R81.

BULAU, J.R. and KASKAN, W.E. (1975)

Radial overshoot and dissociation in methane/air flames.

J. Chemical Physics, Vol. 62, No. 9, pp. 3605-3608.

CERNASKY, N.P. and SAWYER, R.F. (1975)

NO and NO_x formation in turbulent hydrocarbon/air diffusion flame.

15th Symp. (Int.) on Combustion, pp. 1039-1050.

CHEDAILLE, J. and BRAUD, Y. (1972)

Measurements in flames.

Industrial Flames, Vol. 1, Edward Arnold Publishers, London.

CHEN, S.L., HEAP, M.P., PERSHING, D.W. and MARTIN, G.B. (1982)

Influence of coal composition on the fate of volatile and char nitrogen during combustion.

19th Symp. (Int.) on Combustion, pp. 1271-1280.

CHIGIER, N.A. and YULE, A.J. (1979)

The structure of eddies in turbulent flame - I.

A Project Squid Technical Report, Dept. of Chemical Eng. and Fuel Tech., University of Sheffield.

CLAYPOLE, T.C. and SYRED, N. (1981)

The effect of swirl burner aerodynamic on NO_x formation.

18th Symp. (Int.) on Combustion, pp. 81-89.

CLIFFORD, W.C., HOLDERNESS, F.H. and STONER, J.R. (1977)

Spatial contours of chemical composition and gas velocity in a model combustor.

NGTE Note No. 1089.

COLKET, M.B., CHIAPPETTA, L., GUILE, R.N., ZABIELSKI, M.F. and SEERY, D.J. (1982)

Internal aerodynamics of gas sampling probes.

Comb. and Flame, Vol. 44, pp. 3-14.

DIBBLE, R.W. and HOLLENBACH, R.E. (1981)

Laser Rayleigh thermometry in turbulent flames.

18th Symp. (Int.) on Combustion, pp. 1489-1499.

DIMOTAKIS, P.E. (1976)

Single scattering particle laser Doppler measurements of turbulence. AGARD Conference Proceedings No. 193, Applications of Non-Intrusive Instrumentation in Fluid Flow Research, Paper 10.

DRAKE, M.C., LAPP, M., PENNEY, C.M., WARSHAW, S. and GERHOLD, B.W. (1981)

Measurements of temperature and concentration fluctuations in turbulent diffusion flames using pulsed Raman spectroscopy. 18th Symp. (Int.) on Combustion, Combustion Institute, pp. 1521-1531.

DRISCOLL, J.F., SCHEFER, R.W. and DIBBLE, R.W. (1982)

Mass fluxes $\overline{\rho' u'}$ and $\overline{\rho' v'}$ measured in a turbulent non-premixed flames. 19th Symp. (Int.) on Combustion, pp. 477-485.

DURÃO, D.F. (1976)

The application of laser anemometry to free jets and flames with and without recirculation. Ph.D. Thesis, University of London.

DURÃO, D.F.G., LAKER, J. and WHITELAW, J.H. (1978)

A microprocessor controlled frequency analyzer for laser-Doppler anemometry. Mech. Eng. Dept., Imperial College, Report No. FS/78/21.

DURÃO, D.F.G., LAKER, J. and WHITELAW, J.H. (1980)

Bias effects of laser-Doppler anemometry. J. Phys. E: Sci. Instruments, Vol. 13, pp. 442-445.

DURÃO, D.F.G. and WHITELAW, J.H. (1975)

The performance of acousto-optic cell for laser-Doppler anemometry. J. Phys. E: Sci. Instruments, Vol. 8, pp. 776-780.

EBRAHIMI, I. and KLEINE, R. (1977)

The nozzle fluid concentration fluctuation field in round turbulent free jets and jet diffusion flames.

16th Symp. (Int.) on Combustion, pp. 1711-1723.

EICKHOFF, H. (1982)

Turbulent hydrocarbon jet flames.

Prog. Energy Comb. Sci., Vol. 8, pp. 159-168.

EICKHOFF, H. and SCHODL, R. (1980)

Velocity and turbulence measurements in turbulent flames using the L2F technique.

AGARD Conference Proceedings No. 281, Paper 11.

EL-BANHAWY, Y.H. (1979)

Open and confined spray flames.

Ph.D. Thesis, University of London.

ELGHOBASHI, S.E. and PUN, W.M. (1975)

Theoretical and experimental study of turbulent diffusion flames in cylindrical furnaces.

15th Symp. (Int.) on Combustion, pp. 1353-1365.

FLORIS, F. (1981)

The effect of vitiated air on the combustion of pulverized coal for applications to coal fired combined cycle steam generators.

18th Symp. (Int.) on Combustion, pp. 1313-1320.

FRICKER, N. and LEUCKEL, W. (1976)

The characteristics of swirl-stabilized natural gas flames.

Part 3: The effect of swirl and burner mouth geometry on flame stability.

J. Inst. Fuel, Vol. 49, pp. 152-158.

FRISTROM, R.M., PRESCOTT, R. and GRUNFELDER, C. (1957)
Flame zone studies. III - Techniques for the determination of composition profiles of flame fronts.
Comb. and Flame, Vol. 1, pp. 102-113.

FRISTROM, R.M. and WESTENBERG, A.A. (1965)
Flame structure.
McGraw Hill, New York.

FROST, W. and MOULDEN, T.H. (1977)
Handbook of turbulence.
Plenum Press.

GAYDON, A.G. and WOLFHARD, H.G. (1970)
Flames: their structure, radiation and temperature.
Chapman and Hall Ltd., London.

GLASS, M. and BILGER, R.W. (1978)
The turbulent jet diffusion flame in a co-flowing stream - some velocity measurements.
Comb. Sci. Tech., Vol. 18, pp. 165-177.

GLASS, J.W. and WENDT, J.O.L. (1982)
Mechanisms governing the destruction of nitrogeneous species during the fuel rich combustion of pulverized coal.
19th Symp. (Int.) on Combustion, pp. 1243-1251.

GLAWE, G.E., SIMMON, F.S. and STICKNEY, T.M. (1956)
Radiation and recovery corrections and time constants of several chromel-alumel thermocouple probes in high temperature, high velocity gas streams.
NASA TN3766.

GODOY, S. (1982)
Turbulent diffusion flames.
Ph.D. Thesis, University of London.

GOLDSCHMIDT, T.W., AHMADI, G., HOUSHOLDER, M.K. and CHUNG, S.C. (1972)
Turbulent diffusion of small particles suspended in turbulent jets.
Prog. Heat Mass Trans., Vol. 6, pp. 487-491.

GOSMAN, A.D. and LOCKWOOD, F.C. (1973)
Prediction of the influence of turbulent fluctuations on flow and heat transfer in furnaces.
Mech. Eng. Dept., Imperial College, Report No. HTS/73/52.

GOULARD, R., MELLER, A.M. and BILGER, R.W. (1976)
Combustion measurements in air breathing propulsion engines.
Comb. Sci. Tech., Vol. 14, pp. 195-219.

GRAF, R. and PAYNE, R. (1981)
A preliminary study of boiler type and cement kiln type burner arrangement firing both low and high ash coals.
Int. Flame Research Foundation, Ijmuiden, Doc. No. F32/a/42.

GUDMUNDSSON, J.S. and BOTT, T.R. (1977)
Particle diffusivity in turbulent pipe flow.
J. Aerosol. Sci., Vol. 8, pp. 317-319.

GÜNTHER, R. (1970)
Measurements of flame turbulence: aims, methods and results.
J. Inst. Fuel, Vol. 43, pp. 187-192.

GÜNTHER, R. and SIMON, H. (1969)
Turbulence intensity, spectral density functions, and Eulerian scales of emission in turbulent diffusion flames.
12th Symp. (Int.) on Combustion, pp. 1069-1079.

GÜNTHER, R. and WITTMER, V. (1981)
The turbulent reaction field in a concentric diffusion flame.
18th Symp. (Int.) on Combustion, pp. 961-967.

GUPTA, A.K., SYRED, N. and BEER, J.M. (1975)

Fluctuating temperature and pressure effects on the noise output of swirl burners.

15th Symp. (Int.) on Combustion, pp. 1367-1377.

HALL, R.J. (1979)

CARS spectra of combustion gases.

Comb. and Flame, Vol. 35, pp. 47-60.

HARDING, N.S. (1980)

Effects of secondary swirl and other burner parameters on nitrogen pollution formation in a pulverized-coal combustor.

Ph.D. Dissertation, Dept. of Chemical Eng., Brigham Young University, Provo, Utah.

HASSAN, M.M.A., LOCKWOOD, F.C. and MONEIB, H.A. (1980)

Fluctuating temperature and mean concentration measurements in a vertical turbulent free jet diffusion flame.

Paper presented at the "Italian Flame Days", Milano, Vol. 34, pp. 357-372.

HAYWOOD, R.W. (1972)

Thermodynamic tables in SI (metric) units.

Engineering Laboratory, University of Cambridge.

HEDMAN, P.O. and SMOOT, L.D. (1975)

Particle-gas dispersion effects in confined co-axial jets.

J. Am. Inst. Chem. Eng., Vol. 21, No. 2, pp. 372-379.

HINZE, J.O. (1962)

Momentum and mechanical energy balance equations for a flowing homogeneous suspension with slip between the two phases.

Appl. Sci. Res., Section A, Vol. 11, pp. 33-46.

HINZE, J.O. (1975)

Turbulence.

2nd Ed., McGraw Hill.

HIRJI, K. (1983)

Private communication.

Mech. Eng. Dept., Imperial College.

HOLDERNESS, F.H., TILSTON, J.R. and MACFARLANE, J. (1969)

Electrical compensation for radiation loss in thermocouples.

NGTE Note No. 758.

HUBBARD, E.H. (1957)

Effect of preheat combustion air.

J. Inst. Fuel, Vol. 30, pp. 564-576.

HUBBARD, E.H. (1960)

Research on pulverized co-fuel flames by IFRF. The first performance trial and first combustion mechanism trial with pulverized coal.

J. Inst. Fuel, Vol. 33, pp. 386-399.

HUTCHINSON, P., KHALIL, E.E., WHITELAW, J.H. and WIGLEY, G. (1975)

The calculation of furnace flow properties and their experimental verification.

ASME, Paper No. 75-HT-8.

JENG, S.M., CHEN, L.D. and FAETH, G.M. (1982)

The structure of buoyant methane and propane diffusion flames.

19th Symp. (Int.) on Combustion, pp. 349-358.

JONES, W.P. (1979)

Models for turbulent flows with variable density and combustion.

Von Karman Institute for Fluid Dynamics, Lecture Series 1979-2,

Prediction Methods for Turbulent Flows.

JONES, W.P. (1982)

Private communication.

Chem. Eng. Dept., Imperial College.

JONES, W.P. and WHITELAW, J.H. (1981)

Calculation methods for reacting turbulent flows.

Invited Paper, ASME Symp. on Combustion, Boulder Co.

KENNEDY, I.M. and KENT, J.H. (1979)

Measurements of a conserved scalar in turbulent jet diffusion flames.

17th Symp. (Int.) on Combustion, pp. 279-287.

KENT, J.H. (1970)

A noncatalytic coating for platinum-rhodium thermocouples.

Comb. and Flame, Vol. 14, pp. 279-282.

KENT, J.H. and BILGER, R.W. (1973a)

Turbulent diffusion flames.

14th Symp. (Int.) on Combustion, pp. 615-625.

KENT, J.H. and BILGER, R.W. (1973b)

Measurement techniques in turbulent diffusion flames.

First Australian Conference on Heat and Mass Transfer,

Monash University, Melbourne, Australia, Sec. 4.4, pp. 39-46.

KHALIL, E.E. (1976)

Flow and combustion in axisymmetric furnaces.

Ph.D. Thesis, University of London.

KHALIL, M.B. (1975)

Analysis of the different factors affecting the accuracy of

temperature measurements in flames.

M.Sc. Thesis, Mech. Eng. Dept., Faculty of Engineering, Cairo University.

KHALIL, K.H., EL-MAHALLAWY, F.M. and MONEIB, H.A. (1976)
Effect of combustion air swirl on the flow pattern in a cylindrical oil-fired furnace.
16th Symp. (Int.) on Combustion, pp. 135-143.

KOWALIK, R.M. and KRUGGER, C.H. (1979)
Laser fluorescence temperature measurements.
Comb. and Flame, Vol. 34, pp. 135-140.

LAPP, M. and HARTLEY, D.L. (1976)
Raman scattering studies of combustion.
Comb. Sci. Tech., Vol. 13, pp. 199-210.

LAUNDER, B.E. and SPALDING, D.B. (1972)
Mathematical models of turbulence.
Academic Press, London and New York.

LEESLEY, M.E. and HEDLEY, A.B. (1972)
The effect of particle size distribution on the combustion rate of a pulverized anthracite dust cloud.
J. Inst. Fuel, Vol. 45, pp. 224-230.

LENZ, W. and GÜNTHER, R. (1980)
Measurements of fluctuating temperature in a free-jet diffusion flame.
Comb. and Flame, Vol. 37, pp. 63-70.

LENZE, B. (1982)
The influence of recirculation and excess air on enclosed turbulent diffusion flames.
19th Symp.(Int.) on Combustion, pp. 565-572.

LEUCKEL, W. and FRICKER, N. (1976)

The characteristics of swirl-stabilized natural gas flames. Part 1: different flame types and their relation to flow and mixing patterns.

J. Inst. Fuel, Vol. 49, pp. 103-112.

LEVY, Y. and LOCKWOOD, F.C. (1980)

Two phase flow measurements in the board of a fluidized bed using LDA.

Mech. Eng. Dept., Imperial College, Report No. FS/80/7.

LEWIS, M.H. and SMOOT, L.D. (1981)

Turbulent gaseous combustion. Part I: local species concentration measurements.

Comb. and Flame, Vol. 42, pp. 183-196.

LIEW, S.K., BRAY, K.N.C. and MOSS, J.B. (1981)

A flamelet model of turbulent non-premixed combustion.

Comb. Sci. Tech., Vol. 27, pp. 69-73.

LILLEY, D.G. (1977)

Swirl flow in combustion: a review.

AIAA J., Vol. 15, pp. 1063-1078.

LILLY, G.P. (1973)

Effect of particle size on particle eddy diffusivity.

Ind. Eng. Chem. Fundamentals, Vol. 12, pp. 268-275.

LOCKWOOD, F.C., EL-MAHALLAWY, F.M. and SPALDING, D.B. (1974)

An experimental and theoretical investigation of turbulent mixing in a cylindrical furnace.

Comb. and Flame, Vol. 23, pp. 283-293.

LOCKWOOD, F.C. and MEGAHED, I.E.A. (1978)
Extinction in turbulent reacting flows.
Comb. Sci. Tech., Vol. 19, pp. 77-80.

LOCKWOOD, F.C. and MONEIB, H.A. (1982)
Fluctuating temperature measurements in turbulent jet diffusion flame.
Comb. and Flame, Vol. 47, pp. 291-314.

LOCKWOOD, F.C. and ODIDI, A.O.O. (1975)
Measurements of mean and fluctuating temperature and ion concentration in round free-jet turbulent diffusion and premixed flames.
15th Symp. (Int.) on Combustion, pp. 561-571.

LOCKWOOD, F.C., SALOOJA, A.P. and SYED, S.A. (1980)
The prediction of coal fired flames.
Comb. and Flame, Vol. 38, pp. 1-15.

LOCKWOOD, F.C. and STOLAKIS, P. (1983)
Assessment of various turbulence models for turbulent round diffusion jets with combustion.
Paper to be presented at the 14th Symp. on Turbulent Shear Flows.

LOISON, R. and KISSEL, R.R. (1962)
Observation on experiments carried out on the combustion of pulverized fuel.
J. Inst. Fuel, Vol. 35, pp. 60-73.

LYON, T.F., COLLEY, W.C., KENWORTHY, M.J. and BAHR, D.W. (1975)
Development of emission measurement techniques for after-burning turbine engines.
General Electric Company, Air Craft Engine Group, Cincinnati, Ohio, Report No. AFAPL-TR-75-52.

MATHUR, M.L. and MACCALLUM, N.R.L. (1967)

Swirling air jets issuing from vane swirlers. Part 2: enclosed jets.

J. Inst. Fuel, Vol. 40, pp. 238-245.

MAYER, G.H. (1957)

Description of the new experimental furnace. Its control and instrumentation.

J. Inst. Fuel, Vol. 30, pp. 561-564.

MCLAUGHIN, D.K. and TIEDERMAN, W.G. (1973)

Biasing correction for individual realization of laser anemometer measurements in turbulent flows.

Physics of Fluids, Vol. 16, No. 12, pp. 2082-2088.

MEMMOTT, V. (1977)

Rates of mixing of particles and gases in confined jets.

M.Sc. Thesis, Dept. of Chemical Eng., Brigham Young University, Provo, Utah.

MICHEL, J.B. and PAYNE, R. (1980)

Detailed measurement of long pulverized coal flames for the characterization of pollutant formation.

Int. Flame Research Foundation, Ijmuiden, Doc. No. FO 9/a/23.

MITCHELL, R.E. and McLEAN, W.J. (1982)

On the temperature and reaction rate of burning pulverized fuels.

19th Symp. (Int.) on Combustion, pp. 1113-1122.

MOFFAT, R.J. (1962)

Gas temperature measurements.

Temperature: Its Measurement and Control in Science and Industry.

Vol. 3, Part 2, Paper 52, pp. 553-571.

Reinhold Publishing Co.

MONEIB, H.A. (1980)

Experimental study of the fluctuating temperature in inert and reacting turbulent jets.

Ph.D. Thesis, University of London.

ODIDI, A.O.O. (1974)

The influence of turbulence on the time-mean rate of chemical reaction.

Ph.D. Thesis, University of London.

ONUMA, Y. and OGASAWARA, M. (1977)

An approach to the theoretical description of turbulent jet diffusion flames. Part I: Combustion model and calculation.

Comb. and Flame, Vol. 30, pp. 163-176.

PADIA, A.S. (1976)

The behaviour of ash in pulverized coal under simulated combustion conditions.

SC.D. Thesis, Massachussetts Institute of Technology, Cambridge.

PAAUW, T.T.A., STROO, A.J., VAN KOPPEN, C.W.J. (1979)

An effective probabilistic simulation of the turbulent flow and combustion in axisymmetric furnaces.

Presented at 54th AGARD-PEP Congress on Advanced Control Systems for Aircraft. AGARD Conference Pre-print No. 275, Cologne.

PATANKAR, S.V. and SPALDING, D.B. (1973)

A computer model for three-dimensional flow in furnaces.

14th Symp. (Int.) on Combustion, pp. 606-614.

PETERS, N. and DONNERHACK, S. (1981)

Structure and similarity of nitric oxide production in turbulent diffusion flames.

18th Symp. (Int.) on Combustion, pp. 33-42.

RAGLAND, K.W., JEHN, T.C. and YANG, J.T. (1981)

Coal combustion at high Reynolds number.

18th Symp. (Int.) on Combustion, pp. 1295-1305.

RAMSDEN, A.R. (1968)

Application of electron microscopy to the study of pulverized-coal combustion and fly-ash formation.

J. Inst. Fuel, Vol. 41, pp. 451-453.

RAWE, R. and KREMER, H. (1981)

Stability limits of natural gas diffusion flames with swirl.

18th Symp. (Int.) on Combustion, pp. 667-677.

REES, D.P. (1980)

Local nitrogen pollutant formation measurements in a pulverized coal combustor.

Ph.D. Dissertation, Brigham Young University, Provo, Utah.

REES, D.P., SMOOT, L.D. and HEADMAN, P.O. (1981)

Nitrogen oxide formation inside a laboratory pulverized coal combustor.

18th Symp. (Int.) on Combustion, pp. 1305-1311.

RICOU, F.P. and SPALDING, D.B. (1961)

Measurements of entrainment by axisymmetrical turbulent jets.

J. Fluid Mech., Vol. 11, pp. 21-32.

ROBERTS, P.T. and MOSS, J.B. (1981)

A wrinkled flame interpretation of the open turbulent diffusion flame.

18th Symp. (Int.) on Combustion, pp. 941-950.

RODI, W. (1978)

Turbulence models and their applications in hydraulics.

A state of the Art Review,

University of Karlsruhe, FSB 80/T/127.

SATO, A., HASHIBA, K., HASATANI, M., SUGIYAMA, S. and KIMURA, J. (1975)

A correctional calculation method for thermocouple measurements of temperature in flames.

Comb. and Flame, Vol. 24, pp. 35-41.

SCHOENUNG, S.M. and HANSON, R.K. (1981)

CO and temperature measurements in a flat flame by laser absorption spectroscopy and probe techniques.

Comb. Sci. Tech., Vol. 24, pp. 227-237.

SCHOENUNG, S.M. and HANSON, R.K. (1982)

Temporally and spatially resolved measurements of fuel mole fraction in a turbulent CO diffusion flame.

19th Symp. (Int.) on Combustion, pp. 449-458.

SCHOENUNG, S.M. and MITCHELL, R.E. (1979)

Comparison of Raman and thermocouple temperature measurements in flames.

Comb. and Flame, Vol. 35, pp. 207-211.

SHAH, N.G. (1983)

Private communication.

Mech. Eng. Dept., Imperial College.

SHET, U.S.P., SPIRAMULU, V., PRITCHARD, R. and GUPTA, M.C. (1978)

Stability studies of piloted burner flames.

J. Inst. Fuel, Vol. 51, pp. 191-194.

SHOFFSTALL, D.R. and LARSON, D.H. (1975)

Aerodynamic characteristics and pollution emission from scaled industrial burners.

AICHE Symposium Series 71, No. 148.

SKINNER, F.D. (1980)

Mixing and gasification of pulverized coal.

Ph.D. Disseration, Brigham Young University, Provo, Utah.

SMOOT, D.L. and PRATT, D.T. (1979)

Pulverized-coal combustion and gasification.

Plenum Press.

SOCHET, L.R., LUCQUIN, M., BRIDOUX, M., CRAS, M.C., GRASE, F. and DELHAYE, M. (1979)

Use of multichannel pulsed Raman spectroscopy as a diagnostic technique in flames.

Comb. and Flame, Vol. 36, pp. 109-116.

STARNER, S.H. and BILGER, R.W. (1981)

Measurements of scalar velocity correlations in a turbulent diffusion flame.

18th Symp. (Int.) on Combustion, pp. 921-930.

STOLAKIS, P. (1983)

Private communication.

Mech. Eng. Dept., Imperial College.

SUNAVALA, P.D. (1968)

Mixing and combustion in pulverized-coal flames.

J. Inst. Fuel, Vol. 41, pp. 477-483.

SUNAVALA, P.D. (1973)

Mixing and combustion in swirling and impinging jet high volatile pulverized-coal flames.

J. Inst. Fuel, Vol. 46, pp. 30-38.

SVEHLA, R.A. (1962)

Estimated viscosities and thermal conductivities of gases at high temperatures.

NASA TR-R132.

SYRED, N. and BEÉR, J.M. (1974)

Combustion in swirling flows: A review.

Comb. and Flame, Vol. 23, pp. 143-201.

TAKAGI, T., OGASAWARA, M., FUJII, K. and DAIZO, M. (1975)

A study on nitric oxide formation in turbulent diffusion flames.

15th Symp. (Int.) on Combustion, pp. 1051-1059.

THRING, M.W. and NEWBY, M.P. (1953)

Combustion length of enclosed turbulent jet flames.

4th Symp. (Int.) on Combustion, pp. 789-796.

THURGOOD, J.R., SMOOT, L.D. and HEADMAN, P.O. (1980)

Rate measurement in a laboratory-scale pulverized coal combustor.

Comb. Sci. Tech., Vol. 21, pp. 213-223.

THURLOW, G.G. (1960)

Research on pulverized-fuel flames by the International Flame Research Foundation. 1. Summary of work carried out.

J. Inst. Fuel, Vol. 33, pp. 366-376.

TICE, C.L. (1977)

Particle and gas mixing rates in confined co-axial jets with recirculation.

M.Sc. Thesis, Dept. of Chemical Eng., Brigham Young University, Provo, Utah.

TINE, G. (1961)

Gas sampling and chemical analysis in combustion processes.

Pergamon Press, New York.

TISSANDIER, G. (1960)

Two cold aerodynamic trials on a fifth-scale model of the Ijmuiden pulverized-fuel furnace.

J. Inst. Fuel, Vol. 33, pp. 377-385.

TORAL, H. and WHITELAW, J.H. (1982)

Velocity and scalar characteristics of the isothermal and combusting flows in a combustor sector rig.

Comb. and Flame, Vol. 45, pp. 251-272.

TRUELOVE, J.S., WALL, T.F., DIXON, T.F. and STEWART, I.M. (1982)

Flow, mixing and combustion within the quarl of a swirled, pulverized-coal burner.

19th Symp. (Int.) on Combustion, pp. 1181-1187.

VANQUICKENBORNE, L. and TIGGELEN, V.A. (1966)

The stabilization mechanism of lifted diffusion flames.

Comb. and Flame, Vol. 10, pp. 59-69.

VENTURA, J.M.P., SUZUKI, T., YULE, A.J., RALPH, S. and CHIGIER, N.A. (1981)

The investigation of time dependent flame structure by ionization probes.

18th Symp. (Int.) on Combustion, pp. 1543-1551.

VENTURA, J.M.P., YULE, A.J. and CHIGIER, N.A. (1982)

The investigation and concentration measurements in the transitional region of partially premixed flames.

19th Symp. (Int.) on Combustion, pp. 469-475.

VRANOS, A., FAUCHER, J.E. and CURTIS, W.E. (1969)

Turbulent mass transfer and rates of reaction in confined hydrogen-air diffusion flame.

12th Symp. (Int.) on Combustion, pp. 1051-1058.

WENDT, J.O.L., PERSHING, D.W., LEE, J.W. and GLASS, J.W. (1979)

Pulverized coal combustion: NO_x formation mechanisms under fuel rich and staged combustion conditions.

17th Symp. (Int.) on Combustion, pp. 77-87.

WITTMER, V. and GÜNTHER, R. (1980)

Correlation measurement of velocity and temperature fluctuations in a free jet diffusion flame.

AGARD Conference Proceedings No. 281, Paper 10.

WU, L. (1969)

Comparison of the performance of natural gas and oil flames in a cylindrical furnace.

J. Inst. Fuel, Vol. 42, pp. 316-322.

WU, H.L. and FRICKER, N. (1976)

The characteristics of swirl-stabilized natural gas flames.

Part 2: the behaviour of swirling jet flames in a narrow cylindrical furnace.

J. Inst. Fuel, Vol. 49, pp. 144-151.

WYGNANSKI, I. and FIEDLER, H. (1969)

Some measurements in the self-preserving jet.

J. Fluid Mech., Vol. 38, Part 3, pp. 577-612.

YANAGI, T. (1972)

Effect of concentration gradient on composition of sampled gas.

II. Experimental verification.

Comb. and Flame, Vol. 19, pp. 1-9.

YANAGI, T. (1977)

Effect of probe sampling rates on sample composition.

Comb. and Flame, Vol. 28, pp. 33-44.

YANAGI, T. and MIMURA, Y. (1972)

Effect of concentration gradient on composition of sampled gas.

I: Theoretical analysis.

Comb. and Flame, Vol. 18, pp. 347-355.

YANTA, W.J. (1973)

Turbulence measurements with a laser velocimeter.

Naval Ordnance Laboratory, Silver Spring, Maryland, Report No. TR-73-94.

YOU, H.Z. and FAETH, G.M. (1982)

Buoyant axisymmetric turbulent diffusion flames in still air.

Comb. and Flame, Vol. 14, pp. 261-275.

ZAKS, R. (1980)

Programming the 6502.

Sybex Inc., U.S.A.

APPENDIX I

DERIVATION OF GASEOUS AND PARTICULATE TURBULENCE KINETIC ENERGY EQUATIONS

In order to make the derivation of the equations not too complicated the following assumptions are made: (1) constant fluid properties, (2) the correlation products containing turbulence fluctuations of the gas and particles volume fractions are small and can be neglected and (3) steady state condition and isotropic turbulence for both the gas and particulate phases.

I.1 Gas phase turbulence kinetic energy equation

The balance of forces in the fluid phase, in the i-direction, reads:

$$\alpha_g \rho_g \frac{dV_{g,i}}{dt} = \frac{\partial}{\partial x_j}(\alpha_g \sigma_{ji}) - F_i \qquad (I.1)$$

where F_i is the force exerted by the fluid on the suspended particles in the i-direction.

Since $\frac{d}{dt} = V_{g,k} \frac{\partial}{\partial x_k}$ and $\sigma_{ji} = - p + \mu(\frac{\partial V_{g,i}}{\partial x_j} + \frac{\partial V_{g,i}}{\partial x_j})$, equation (I.1) can be written as:

$$\frac{\partial}{\partial x_k}(\alpha_g \rho_g V_{g,k} V_{g,i}) = - \alpha_g \frac{\partial p}{\partial x_i} + \alpha_g \mu \frac{\partial^2 V_{g,i}}{\partial x_j \partial x_j} - F_i \qquad (I.2)$$

By taking the same statistical approach as that used by Hinze (1975), the instantaneous values of the velocity, force and pressure are separated into mean and fluctuating quantities

$$V_g = \overline{V}_g + V'_g, \quad p = \overline{p} + p', \quad F = \overline{F} + F'$$

Since the continuity equation for the fluid phase is

$$\frac{\partial}{\partial x_k}(\alpha_g \rho_g V_{g,k}) = 0$$

equation (I.2) then becomes after time-averaging:

$$\frac{\partial}{\partial x_k}(\alpha_g \rho_g \overline{V}_{g,k} \overline{V}_{g,i}) + \frac{\partial}{\partial x_k}(\alpha_g \rho_g \overline{V'_{g,k} V'_{g,i}}) = - \alpha_g \frac{\partial \overline{p}}{\partial x_i} + \alpha_g \mu \frac{\partial^2 \overline{V}_{g,i}}{\partial x_j \partial x_j} - \overline{F}_i \tag{I.3}$$

multiplying equation (I.3) by $\overline{V}_{g,i}$, it becomes:

$$\frac{\partial}{\partial x_k}[\alpha_g \rho_g \overline{V}_{g,k} (\overline{V}^2_{g,i}/2)] = - \alpha_g \overline{V}_{g,i} \frac{\partial \overline{p}}{\partial x_i} + \alpha_g \mu \frac{\partial (\overline{V^2_{g,i}}/2)}{\partial x_j \partial x_j}$$

$$- \overline{V}_{g,i} \overline{F}_i - \overline{V}_{g,i} \frac{\partial}{\partial x_k}(\alpha_g \rho_g \overline{V'_{g,k} V'_{g,i}}) \tag{I.4}$$

multiplying equation (I.2) by $V_{g,i}$ and time-averaging, it becomes:

$$\frac{\partial}{\partial x_k}[\alpha_g \rho_g \overline{V}_{g,k} (\overline{V^2_{g,i}}/2)] + \frac{\partial}{\partial x_k} [\alpha_g \rho_g \overline{V}_{g,k} (\overline{V'^2_{g,i}}/2)]$$

$$+ \frac{\partial}{\partial x_k}(\alpha_g \rho_g \overline{V}_{g,k} \overline{V'_{g,k} V'_{g,i}}) + \frac{\partial}{\partial x_k} [\alpha_g \rho_g V'_{g,k} (\overline{V'^2_{g,i}}/2)] =$$

$$- \alpha_g \overline{V}_{g,i} \frac{\partial \overline{p}}{\partial x_i} - \alpha_g \overline{V'_{g,i} \frac{\partial p'}{\partial x_i}} + \alpha_g \mu \frac{\partial^2 (\overline{V'^2_{g,i}}/2)}{\partial x_j \partial x_j}$$

$$- \alpha_g \mu \frac{\partial \overline{V}_{g,i}}{\partial x_j} \frac{\partial \overline{V}_{g,i}}{\partial x_j} - \alpha_g \mu \overline{\frac{\partial V'_{g,i}}{\partial x_j} \frac{\partial V'_{g,i}}{\partial x_j}}$$

$$- \overline{V}_{g,i} \overline{F}_i - \overline{V'_{g,i} F'_i} \tag{I.5}$$

Subtracting equation (I.4) from equation (I.5), yields:

$$\frac{\partial}{\partial x_k}\left[\alpha_g \rho_g \overline{V}_{g,k}\left(\overline{V'^2_{g,i}}/2\right)\right] + \frac{\partial}{\partial x_k}\left[\alpha_g \rho_g \overline{V'_{g,k}\left(V'^2_{g,i}/2\right)}\right] + \alpha_g \rho_g \overline{V'_{g,k} V'_{g,i}} \frac{\partial \overline{V}_{g,i}}{\partial x_k} =$$

$$- \alpha_g \overline{V'_{g,i} \frac{\partial p'}{\partial x_i}} + \alpha_g \mu \frac{\partial^2 \left(\overline{V'^2_{g,i}}/2\right)}{\partial x_j \partial x_j} - \alpha_g \mu \overline{\frac{\partial V'_{g,i}}{\partial x_j} \frac{\partial V'_{g,i}}{\partial x_j}}$$

$$- \overline{V'_{g,i} F'_i} \qquad \text{(I.6)}$$

Summing up to this equation, similar equations in the other two directions, gives:

$$\underbrace{\frac{\partial}{\partial x_k}\left(\alpha_g \rho_g \overline{V}_{g,k} k_g\right)}_{\text{convection term}} = \underbrace{- \frac{\partial}{\partial x_k}\left(\alpha_g \rho_g \overline{V'_{g,k} k_g}\right) - \alpha_g \frac{\partial \overline{p' V'_{g,k}}}{\partial x_k} + \alpha_g \mu \frac{\partial^2 k_g}{\partial x_k \partial x_k}}_{\text{diffusion term}}$$

$$\underbrace{- \alpha_g \rho_g \overline{V'_{g,k} V'_{g,i}} \frac{\partial \overline{V}_{g,i}}{\partial x_k}}_{\text{production term}}$$

$$\underbrace{- \alpha_g \mu \overline{\frac{\partial V'_{g,i}}{\partial x_j} \frac{\partial V'_{g,i}}{\partial x_j}}}_{\text{dissipation term}}$$

$$\underbrace{- \sum_i \overline{V'_{g,i} F'_i}}_{\text{interaction term}} \qquad \text{(I.7)}$$

Applying a similar simulation procedure for the different terms of equation (I.7) as that used for the non-seeded gas flows, see

Launder and Spalding (1972), the turbulent kinetic energy equation of the gas phase reads:

$$\mathrm{div}(\alpha_g \rho_g \vec{\bar{V}}_g k_g) - \mathrm{div}(\alpha_g \Gamma_{\mathrm{eff},g} \,\mathrm{grad}\, k_g)$$

$$= \alpha_g (G_{k_g} - \rho_g \varepsilon_g) + \sum_i C_d \rho_g A_p (\bar{V}_{g,i} - \bar{V}_{p,i})(\tfrac{2}{3} k_g - \overline{V'_{g,i} V'_{p,i}}) \qquad (I.8)$$

I.2 Particulate phase turbulence kinetic energy equation

The balance of forces acting on the particles can be written as:

$$\alpha_p \rho_p \frac{dV_{p,i}}{dt} = - \alpha_p \frac{\partial p}{\partial x_i} + F_i \qquad (I.9)$$

which can be rewritten as:

$$\frac{\partial}{\partial x_k}(\alpha_p \rho_p V_{p,k} V_{p,i}) = - \alpha_p \frac{\partial p}{\partial x_i} + F_i \qquad (I.10)$$

Applying Reynolds' averaging (Hinze (1975)) to equation (I.10) and multiplying both sides of the resultant equation by $\bar{V}_{p,i}$, it becomes:

$$\frac{\partial}{\partial x_k} [\alpha_p \rho_p \bar{V}_{p,k} (\overline{V^2_{p,i}}/2)] + \bar{V}_{p,i} \frac{\partial}{\partial x_k}(\alpha_p \rho_p \overline{V'_{p,k} V'_{p,i}}) =$$

$$- \alpha_p \bar{V}_{p,i} \frac{\partial \bar{p}}{\partial x_i} + \bar{V}_{p,i} \bar{F}_i \qquad (I.11)$$

Multiplying equation (I.10) by $V_{p,i}$, applying Reynolds' averaging yields:

$$\frac{\partial}{\partial x_k}\left[\alpha_p \rho_p \overline{V}_{p,k}(\overline{V^2_{p,i}}/2)\right] + \frac{\partial}{\partial x_k}\left[\alpha_p \rho_p \overline{V}_{p,k}(\overline{V'^2_{p,i}}/2)\right]$$

$$+ \frac{\partial}{\partial x_k}(\alpha_p \rho_p \overline{V}_{p,i}\ \overline{V'_{p,k} V'_{p,i}}) + \frac{\partial}{\partial x_k}\left[\alpha_p \rho_p \overline{V'_{p,k}(V'^2_{p,i}/2)}\right]$$

$$= -\alpha_p \overline{V}_{p,i} \frac{\partial \overline{p}}{\partial x_i} - \alpha_p \overline{V'_{p,i} \frac{\partial p'}{\partial x_i}} + \overline{V}_{p,i} \overline{F}_i + \overline{V'_{p,i} F'_i} \qquad \text{(I.12)}$$

Subtracting equation (I.11) from equation (I.12), results:

$$\frac{\partial}{\partial x_k}\left[\alpha_p \rho_p \overline{V}_{p,k}(\overline{V'^2_{p,i}}/2)\right] + \frac{\partial}{\partial x_k}\left[\alpha_p \rho_p \overline{V'_{p,k}(V'^2_{p,i}/2)}\right]$$

$$+ \alpha_p \rho_p \overline{V'_{p,k} V'_{p,i}} \frac{\partial \overline{V}_{p,i}}{\partial x_k} = -\alpha_p \overline{V'_{p,i} \frac{\partial p'}{\partial x_i}} - \overline{V'_{p,i} F'_i} \qquad \text{(I.13)}$$

adding to equation (I.13), the similar two equations in the other two directions, gives:

$$\underbrace{\frac{\partial}{\partial x_k}(\alpha_p \rho_p \overline{V}_{p,k} k_p)}_{\text{convection term}} = \underbrace{-\frac{\partial}{\partial x_k}\left[\alpha_p \overline{V'_{p,k}(p' + \rho_p k_p)}\right]}_{\text{diffusion term}}$$

$$\underbrace{-\alpha_p \rho_p \overline{V'_{p,k} V'_{p,i}} \frac{\partial \overline{V}_{p,i}}{\partial x_k}}_{\text{production term}}$$

$$\underbrace{+ \overline{V'_{p,i} F'_i}}_{\text{interaction term}} \qquad \text{(I.14)}$$

Applying a similar simulation technique as that applied to the gas-phase, equation (I.14) can be written in a general form as:

$$\mathrm{div}(\alpha_p \rho_p \vec{\bar{V}}_p k_p) - \mathrm{div}(\alpha_p \Gamma_{\mathrm{eff},p} \ \mathrm{grad}\ k_p)$$

$$= \alpha_p G_{k_p} + \sum_i C_d \rho_g A_p (\bar{V}_{g,i} - \bar{V}_{p,i})(\overline{V'_{g,i} V'_{p,i}} - \frac{2}{3} k_p) \qquad (I.15)$$

I.3 Transport equation for $\overline{V'_g V'_p}$ ($\equiv \overline{V'_{g,k} V'_{p,k}}$)

Applying Reynolds' procedure to the gas phase momentum equation (I.2) and subtracting from the resultant equation its mean values, yields:

$$\frac{\partial}{\partial x_k}(\alpha_g \rho_g \bar{V}_{g,k} V'_{g,i}) + \alpha_g \rho_g V'_{g,k} \frac{\partial \bar{V}_{g,i}}{\partial x_k} + \frac{\partial}{\partial x_k}(\alpha_g \rho_g V'_{g,k} V'_{g,i})$$

$$= - \alpha_g \frac{\partial p'}{\partial x_i} + \alpha_g \mu \frac{\partial^2 V'_{g,i}}{\partial x_j \partial x_j} - F'_i \qquad (I.16)$$

multiplying both sides by $V'_{p,i}$ and time-averaging, gives:

$$\begin{aligned}
\frac{\partial}{\partial x_k}(\alpha_g \rho_g \bar{V}_{g,k} \overline{V'_{g,i} V'_{p,i}}) = & - \frac{\partial}{\partial x_k}(\alpha_g \rho_g \overline{V'_{g,k} V'_{g,i} V'_{p,i}}) \\
& - \alpha_g \frac{\overline{\partial p' V'_{p,i}}}{\partial x_i} + \frac{1}{2} \alpha_g \mu \frac{\partial^2 \overline{V'_{g,i} V'_{p,i}}}{\partial x_j \partial x_j} \\
& - \alpha_g \rho_g \overline{V'_{g,k} V'_{p,i}} \frac{\partial \bar{V}_{g,i}}{\partial x_k} \\
& + \alpha_g \overline{p' \frac{\partial V'_{p,i}}{\partial x_i}} \\
& - \alpha_g \mu \overline{\frac{\partial V'_{g,i}}{\partial x_j} \frac{\partial V'_{p,i}}{\partial x_j}} - \overline{V'_{p,i} F'} \\
& + \alpha_g \rho_g \bar{V}_{g,k} \overline{V'_{g,i} \frac{\partial V'_{p,i}}{\partial x_k}} + \alpha_g \rho_g \overline{V'_{g,k} V'_{g,i} \frac{\partial V'_{p,i}}{\partial x_k}}
\end{aligned} \qquad (I.17)$$

Applying a similar sequence of operations on the particulate phase momentum equation (I.10), yields:

$$\frac{\partial}{\partial x_k}(\alpha_p \rho_p \overline{V}_{p,k} \overline{V'_{g,i} V'_{p,i}}) = -\frac{\partial}{\partial x_k}(\alpha_p \rho_p \overline{V'_{p,k} V'_{g,i} V'_{p,i}})$$

$$- \alpha_p \frac{\partial \overline{p' V'_{p,k}}}{\partial x_k} - \alpha_p \rho_p \overline{V'_{p,k} V'_{g,i}} \frac{\partial \overline{V}_{p,i}}{\partial x_k}$$

$$+ \alpha_p \overline{p' \frac{\partial V'_{g,i}}{\partial x_i}} + \overline{V'_{g,i} F'}$$

$$+ \alpha_p \rho_p \overline{V}_{p,k} \overline{p',i \frac{\partial V'_{g,i}}{\partial x_k}}$$

$$+ \alpha_p \rho_p \overline{V'_{p,k} V'_{p,i} \frac{\partial V'_{g,i}}{\partial x_k}} \qquad \text{(I.18)}$$

adding equation (I.17) to equation (I.18):

$$\frac{\partial}{\partial x_k}(\alpha_g \rho_g \overline{V}_{g,k} \overline{V'_{g,i} V'_{p,i}}) + \frac{\partial}{\partial x_k}(\alpha_p \rho_p \overline{V}_{p,k} \overline{V'_{g,i} V'_{p,i}})$$

$$= -\frac{\partial}{\partial x_k}(\alpha_p \rho_p \overline{V'_{p,k} V'_{g,k} V'_{p,i}}) - \frac{\partial}{\partial x_k}(\alpha_g \rho_g \overline{V'_{g,k} V'_{g,i} V'_{p,i}})$$

$$- \alpha_p \frac{\partial \overline{p' V'_{g,k}}}{\partial x_k} - \alpha_g \frac{\partial \overline{p' V'_{p,k}}}{\partial x_k} + \frac{1}{2} \alpha_g \mu \frac{\partial^2 \overline{V'_{g,i} V'_{p,i}}}{\partial x_j \partial x_j}$$

$$- \alpha_p \rho_p \overline{V'_{p,k} V'_{g,i}} \frac{\partial \overline{V}_{p,i}}{\partial x_k} - \alpha_g \rho_g \overline{V'_{g,k} V'_{p,i}} \frac{\partial \overline{V}_{g,i}}{\partial x_k}$$

$$+ \alpha_p \overline{p' \frac{\partial V'_{g,i}}{\partial x_i}} + \alpha_g \overline{p' \frac{\partial V'_{p,i}}{\partial x_i}} - \alpha_g \overline{p' \frac{\partial V'_{p,i}}{\partial x_i}}$$

$$- \alpha_g \mu \overline{\frac{\partial V'_{g,i}}{\partial x_j} \frac{\partial V'_{p,i}}{\partial x_j}} + \alpha_p \rho_p \overline{V}_{p,k} \overline{V'_{p,i} \frac{\partial V'_{g,i}}{\partial x_k}}$$

$$+ \alpha_g \rho_g \overline{V}_{g,k} \overline{V'_{g,i} \frac{\partial V'_{\rho,i}}{\partial x_k}} + \alpha_p \rho_p \overline{V'_{p,k} V'_{p,i} \frac{\partial V'_{g,i}}{\partial x_k}}$$

$$+ \alpha_g \rho_g \overline{V'_{g,k} V'_{g,i} \frac{\partial V'_{p,i}}{\partial x_k}}$$

$$+ \sum_i 2 C_d \rho_g A_p (\overline{V}_{g,i} - \overline{V}_{p,i}) (\frac{1}{3} k_g + \frac{1}{3} k_p - \overline{V'_{g,i} V'_{p,i}}) \qquad (I.19)$$